Comparative Life Cycle Assessment of Novel Environmentally Friendly Brake Rotors

Matthew Currie

Submitted in accordance with the requirements for degree of

Doctor of Philosophy

The University of Leeds

School of Mechanical Engineering

March 2025

Intellectual Property and Publication Statements

The Candidate confirms that the work submitted is his own, except where work which has formed part of jointly authored publications has been included. His contribution and the other authors to this work has been explicitly indicated below. The candidate confirms that appropriate credit has been given within the thesis where reference has been made to the work of others.

The work in Chapters 3 and 6 of this thesis has appeared in the publication:
Currie M., Barton D., Huang Y., Brooks P., Shrestha S., "Comparative Life Cycle Assessment (LCA) of Lightweight Novel Environmentally Friendly Brake Rotors" Eurobrake 2023 Conference Proceedings, Fisita, 2023, doi: 10.46720/EB2023-EFA-004.

The work in Chapters 6 and 7 of this thesis has appeared in the publication:
Currie M., Huang Y., Brooks P., Shrestha S., Barton D., "Life Cycle Assessment of Plasma Electrolytic Oxidation Treated Aluminium Alloy Brake Rotors" Eurobrake 2024 Conference Proceedings, Fisita, 2024, https://www.fisita.org/library/eb2024-efa-009.

The work in Chapter 4 of this thesis has been accepted for the following publication:
Currie M., Limmer F., Huang Y., Brooks P., Barton D., "Friction Performance and Wear Emissions from a Laser-Clad Brake Rotor in Comparison with Uncoated Grey Cast Iron" Eurobrake 2025 Conference Proceedings, Fisita, 2025

The Candidate was responsible for Majority of the work presented in these published papers, such as development of the methodology, building the model and presenting the results. The co-authors contributed to the work by reviewing publications and providing valuable advice. The exception to this is for the publication based on Chapter 4, where the testing rig and uncoated grey cast iron emissions data were designed and gathered by Limmer [1].

Acknowledgements

I would like to thank my supervisors David Barton, Yue Huang and Peter Brooks for their continued support and guidance throughout my postgraduate research. Their friendly approach made my research journey an enjoyable experience.

I would like to thank Fabian Limmer, Ishmaeel Ghouri and Joshua Armitage with their kind support throughout conducting the experimental work required for my PhD.

I would like to thank Curtiss-Wright Keronite, especially Suman Shrestha for his support surrounding the Plasma Electrolytic Oxidation process. I would also like to thank Cummins Meritor, TWI and Fabian Limmer for their guidance and support surrounding data collection for my LCA study.

Finally, I would like to thank my parents, Alan and Ann for their continued financial support throughout my research, without whom this project would not have been possible. Also, to Laura for her continued moral support, and belief in my academic abilities to undertake a postgraduate research project.

Abstract

This work focussed on conducting a comparative life cycle assessment (LCA) of novel environmentally friendly brake rotors for automotive application. The purpose for this research was to investigate alternative brake rotor solutions to reduce the wear, emissions and environmental impact from the current uncoated grey cast iron (GCI) rotor, throughout the whole life cycle, from 'cradle-to-grave'. The less frequent use of friction brakes within electric vehicles and more stringent legislation have increased the demand for wear and corrosion resistant materials.

The LCA methodology used the ReCiPe 2016 impact approach with a hierarchist analysis, including endpoint impact scores for a broader overview of the environmental and human health impacts. The Structured Analysis and Design Technique notation was adapted for LCA applications, simplifying complex systems. A custom Python model was developed to assess the environmental impact of four brake rotor materials: a laser-clad GCI, a Plasma Electrolytic Oxidation (PEO) treated wrought Al, a PEO treated cast Al, and an uncoated GCI rotor as a baseline. All rotors were paired with low-metallic friction materials.

Emission data was collected using a previously developed small-scale test rig operating under WLTP (worldwide harmonised light-vehicle test procedure) cycle conditions. These data were scaled to compare to the impending Euro 7 emission standards, revealing that only coated rotors are likely to meet the new limits. Additional life cycle phase data was collected from industry collaborations and secondary sources. The comparative LCA was streamlined through the omission of identical parts for the different rotor materials.

The study found that coatings or surface treatments can significantly reduce environmental and human health impacts due to their recoating potential and reduced wear rate. Lightweight rotors also offered benefits of reduced fuel consumption and CO_2 emissions. Laser-clad GCI, wrought PEO-Al and cast PEO-Al were found to reduce the average endpoint impacts by 37%, 39% and 43%, respectively, compared to the uncoated GCI.

Contents

List of Figures

List of Tables

List of Equations

$\mathbf{A}_{rotor}$	-	friction surface area of rotor.
$\mathbf{A}_{pad}$	-	friction surface area of pad.
$\mathbf{R}_A$	-	The ratio of the friction surface area of the rotor to the pad.
$\mathbf{R}_v$	-	Sliding velocity gradient along the friction radius.
$\mathbf{R}_{pad}$	-	Pad aspect ratio, defined as the ratio of width to length.
$\mathbf{f}$	-	Scaling factor for small-scale test rig.
$\mathbf{Q}_{exhaust}$	-	Volumetric flow rate of exhaust duct.
$\mathbf{Q}_{dekati}$	-	Volumetric flow rate of dekati sampling.
$\Delta\mathbf{H}$	-	Latent heat of fusion.
$\mathbf{C}_{p_s}$	-	Specific heat, solid.
$\mathbf{C}_{p_l}$	-	Specific heat, liquid.
$\mathbf{T}_0$	-	Initial temperature.
$\mathbf{T}_s$	-	Solidus temperature.
$\mathbf{T}_l$	-	Liquidus temperature.

Nomenclature

APS	-	Atmospheric Plasma Spray
BEV	-	Battery Electric Vehicle
CAD	-	Computer Aided Design
CF	-	Characterisation Factor
CGDS	-	Cold Gas Dynamic Spray
CMC	-	Ceramic Matrix Composite
CoF	-	Coefficient of Friction
COPD	-	Chronic Obstructive Pulmonary Disease
CVI	-	Chemical Vapor Infiltration
DALY	-	Disability-Adjusted Life Year
EE	-	Exhaust Emissions
EHLA	-	Extreme High speed Laser Cladding
EPD	-	Environmental Product Declaration
FC	-	Fuel Consumption
FCF	-	Fuel Consumption Factor
FEA	-	Finite Element Analysis
FU	-	Functional Unit
GCI	-	Grey Cast Iron
GHG	-	Greenhouse Gases
GUI	-	General User Interface
HEPA	-	High Efficiency Particulate Air
HGV	-	Heavy Goods Vehicle
HVAF	-	High Velocity Air Fuel
HVOF	-	High Velocity Oxygen Fuel
IBT	-	Initial Brake Temperature
ICEV	-	Internal Combustion Engine Vehicle
IDEF0	-	Integrated Definition for Function Modelling
ILCD	-	International Life Cycle Data System
IPCC	-	Intergovernmental Panel on Climate Change
ISO	-	International Organisation for Standardisation
LC	-	Laser-Cladding
LCA	-	Life Cycle Assessment
LCC	-	Life Cycle Costing

LM	-	Low-Metallic
MMC	-	Metal Matrix Composite
NAO	-	Non-Asbestos Organic
NEE	-	Non-Exhaust Emissions
NF	-	Normalisation Factor
NVH	-	Noise, Vibration and Harshness
PEF	-	Product Environmental Footprint
PEO	-	Plasma Electrolytic Oxidation
PM	-	Particulate Matter
PM$_x$	-	Particulate Matter of less than X μm equivalent diameter
PTA	-	Plasma Transferred Arc
ReCiPe	-	Developed by RIVM, CML amd Pré Consultants
SADT	-	Structured Analysis and Design Technique
SETAC	-	Society of Environmental Toxicology and Chemistry
SPS	-	Suspension Plasma Spray
TWI	-	The Welding Institute
UMT	-	Universal Mechanical Tester
WLTP	-	World harmonised Light vehicle Test Procedure

List of Chemical Symbols

1,4-DCB	-	1,4-Dichlorobenzene
Al	-	Aluminium
CCl_4	-	Carbon tetrachloride
Cd	-	Cadmium
CeGd	-	Cerium Gadolinium
CFC_{11}	-	Trichlorofluoromethane
CH_3Cl	-	Methyl chloride
CH_4	-	Methane
CO	-	Carbon monoxide
CO_2	-	Carbon dioxide
COD	-	Chemical oxygen demand
Cr	-	Chromium
Cr(VI)	-	Hexavalent Chromium
Cu	-	Copper
Fe	-	Iron
HC	-	Hydrocarbons
Mg	-	Magnesium
N_2O	-	Nitrous oxide
Nd	-	Neodynium
NH_3	-	Ammonia
Ni	-	Nickel
NMVOC	-	Non-methane volatile organic compound
NO_2	-	Nitrogen dioxide
NO_x	-	Nitrogen oxides
P	-	Phosphorus
Si	-	Silicon
SO_2	-	Sulphur dioxide
Ti	-	Titanium
Y	-	Yttrium

Chapter 1

Introduction

1.1 Introduction

Chapter 1 provides an introduction to the research topic and describes the motivation behind why this postgraduate research is required. A brief introduction into the modelling technique known as life cycle assessment (LCA) is outlined, and why such a technique is required within the braking industry.

1.2 Background

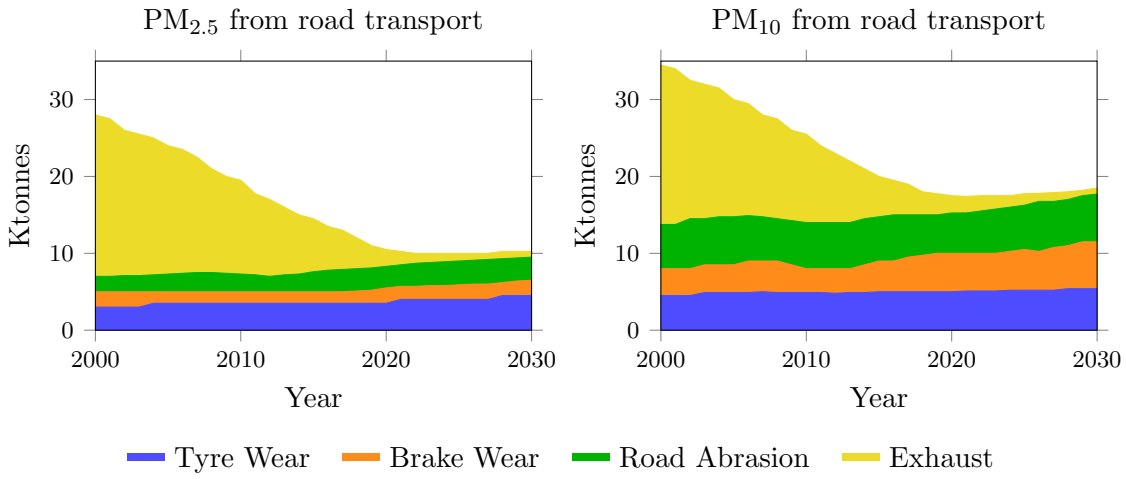

Figure 1.1: Particulate matter (PM) trends from road transport (2000-2030) [2].

In efforts to combat air pollution from land transport, research on reducing emissions has become a major focus. In 2019 the transport industry was one of the largest emitters of greenhouse gases (GHG), contributing 27% to the total within the UK [3]. The particles emitted by road vehicles can be categorised according to their source. Exhaust emissions (EE) are the result of the combustion process within internal combustion engine vehicles (ICEVs). On the other hand, non-exhaust emissions (NEE) refer to particles released from brake and tyre wear, as well as those already deposited in the environment being resuspended by road traffic [4]. These resuspended particles include any road surface abrasion emissions created by the impact of road vehicles. Due to legislation and the introduction of battery electric vehicles (BEVs) [5], particulate matter (PM) of less than 10 µm equivalent diameter (PM_{10}) from exhausts has become less of a contributor to total emissions, compared to tyres, brakes, and road abrasion – – the so-called non-exhaust

emissions (NEE). The total mass of NEE exceeded those of the exhaust PM_{10} emissions in about 2012 for the UK, while occurring slightly later for $PM_{2.5}$ emissions, as indicated in Figure 1.1 [2].

Approximately a third of the total NEE originate from the brakes, mainly due to the poor wear and corrosion resistance of the current grey cast iron (GCI) rotors. These PM emissions from brake wear are detrimental to human health because they are deposited in the respiratory system. Coarse particles end up in the nose and throat, meanwhile ultrafine particles can go deep into the lungs, even occasionally entering the blood stream [4]. Human health can be at risk from these deposited particles, with the possible causation of inheritable mutations, premature births, and birth defects [6]. Such emissions have also been associated with Alzheimer's disease, increased heart rate variability, and reduced lung function, such as asthma [7].

While these health concerns underline the urgency of reduced brake related emissions, it is crucial to also consider how evolving vehicle technologies, such as BEVs are influencing brake system design and usage. The number of BEVs is expected to increase considerably as a result of the UK government's goal of decarbonising transport by eliminating ICEVs by 2050 [3]. BEVs cause a change in the priority for material characteristics within the friction braking system due to changes in operating conditions. To improve their efficiency, the traction motors within BEVs are implemented as generators. This means that they have the ability to receive a negative torque from the wheels, recovering the kinetic energy of the vehicle during braking to charge the battery — a process called regenerative braking [8]. Despite the benefits, this new regenerative system still has limitations. Firstly, the motor generators have maximum torque capabilities, and secondly kinetic energy can only be recovered providing the battery is not fully charged. Therefore, to overcome such limitations and for safety requirements, the friction brake is still a necessary component, except that it is now used less frequently. This reduced frequency of use has implications, causing corrosion products to remain on friction surfaces in many driving scenarios, making good corrosion resistance a more vital property of the material [9, 10].

The rate of corrosion depends on parameters such as the acidity of the rainwater and the levels of salts (sodium/magnesium/calcium chloride) added to the roads. Corrosion can cause surface degradation to the brake rotor leading to increased wear and PM emissions. The crumbly nature of surface degradation can lead to a reduced coefficient of friction (CoF), reducing the performance of the braking system. Even after the initial corrosion

products have been removed, the remaining surface still has a higher surface roughness than the uncorroded rotor. This increased roughness can increase pad wear and prohibit the effective formation of a stable tribolayer [11]. A tribolayer is a thin layer made up of a combination of particles from the brake rotor and pad that form a film on the surface of the rotor. These corrosion effects are one of the driving forces in the search for replacements of the current GCI rotor. GCI has poor corrosion resistance, with the corrosion products mainly being iron oxides. Iron oxide particles are associated with potential human health risks such as inflammation, fibrosis, extrapulmonary effects, and even potentially Alzheimer's diseases [12].

The reduction of emissions and the accompanying corrosion effects are currently a large topic of investigation. The most researched solution is to apply a coating to the current GCI, as this allows for the utilisation of the manufacturing processes already in place. Specific coating techniques and methodologies are discussed in Chapter 2 (Section 2.4). In summary, these coatings can offer improved wear and corrosion resistance, reducing PM emissions and maintenance requirements during use. Alternatively, lightweight materials such as light metal composites or metal alloys can be investigated, as discussed in Section 2.4.2. The weight reduction can offer energy savings during transportation, as well as reduced fuel consumption and impact on the road surface during use due to reductions in the unsprung mass of the vehicle. The unsprung mass refers to the components of the vehicle that are not supported by the suspension system.

1.3 Life Cycle Assessment (LCA) Framework

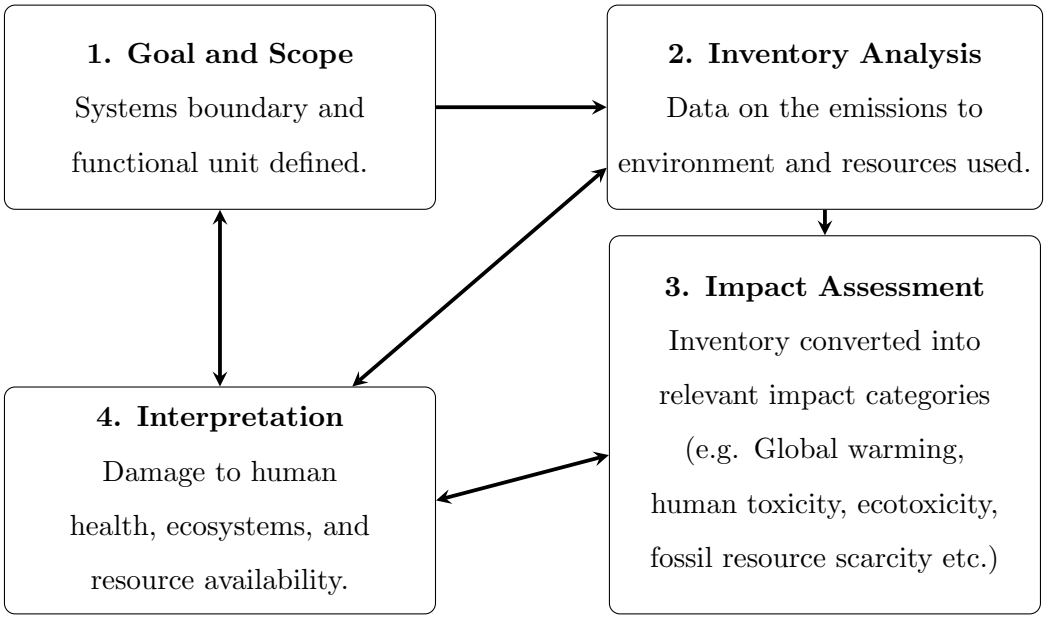

Figure 1.2: Iterative approach to LCA outlining the four-stage process.

LCA is a methodology used to identify, quantify, and assess the impacts involved in the life cycle of a product or service [13]. This technique is an iterative 'cradle-to-grave' process that analyses the full life cycle of a product system within the four main stages of any LCA: goal and scope, inventory analysis, impact assessment, and interpretation. Initial results can offer feedback and possibly force alterations to the methodological choices made during the goal and scope phase, ensuring a robust study. Figure 1.2 outlines this process. During inventory analysis, data are collected based on the resources used and emissions released from any given section of the life cycle [14]. These data can be difficult to interpret. Therefore, it is crucial for the inventory to be mapped onto impact categories, clearly identifying how different aspects of human health, the ecosystem, and resource availability are affected. Primary and secondary sources (from companies and online databases, respectively) are used for the data collection process, although in some cases estimations are required. The data that are required to be collected is greatly affected by the defined system boundary — a crucial methodological choice of the goal and scope phase. This choice influences the accuracy of the results. If the system boundary is too large, it can lead to an LCA study becoming too time-intensive, making it impossible to gather all the required data. However, if the boundary is too small, the results can be misleading. For a fair comparison between each brake rotor, a functional unit is defined. In the case of a braking system, this would specify the braking conditions and the required vehicle lifetime.

1.3.1 Requirement for LCA Techniques

Most emissions-based research only focusses on the use phase of a component because it is the phase of the life cycle that legislation, such as Euro 7, typically restricts. However, superficially attractive brake rotor materials may have hidden environmental impacts associated with their manufacture or disposal processes that outweigh the benefits provided during use. Therefore, it is crucial to conduct a complete and transparent study, comparing the full life cycle of each material. This is where a cradle-to-grave technique, such as LCA, can be implemented. The interpretation of results provided by such a technique can also be applied by companies to ensure that environmental impact reductions outweigh the inevitable cost increase associated with investing in alternative materials.

Within LCA, the term 'trade-off' is typically used. This term refers to a situation where there is an increase in impacts associated with one phase of the life cycle to allow for a decrease in another. An example of this would be if a new brake rotor material

offered reduced emissions during use but required more energy to manufacture. When comparing new rotor materials and coating techniques, there are three main trade-offs to consider.

First, a product having high initial impacts, such as energy demands within manufacture but lower maintenance requirements. This phenomenon was demonstrated by Iraldo et al. [15], who conducted a study on how the durability of a product affects the environmental impact and economic efficiency of that product. It was found that improving durability, thus increasing the useful life of a product and reducing maintenance requirements, offers reductions in both the cost to the consumer and the environmental impact.

Second, a desirable characteristic for reducing the emissions from the braking system is to improve the resistance to wear and corrosion. In the case of a coated GCI rotor, this could increase the overall weight, affecting the total unsprung mass. This can therefore affect the impact forces on the road made by the tyre and potentially influence road abrasion emissions. This trade-off is difficult to quantify because most brake tests are conducted within enclosed dynamometers with no road or tyre present. However, it is possible to calculate the effect an increase in unsprung mass has on range and fuel consumption, but this would add complexity to the model. Gradin and Åström [16] conducted a study that demonstrated the environmental benefits of coating a GCI rotor, finding that the effect on fuel consumption to be minimal between rotors.

Third, efforts to reduce environmental impacts come with an increased cost associated with more expensive materials and initial investment. This trade-off is potentially the most important issue for many companies. An example of this would be a material such as a carbon-carbon composite, which offers excellent weight reduction and corrosion resistance. However, as a result of its high cost, it is only implemented in racing series such as Formula 1, where every gram of weight matters.

1.4 Legislation and Standardisation

The decrease in exhaust emissions shown in Figure 1.1 is mainly due to the increased stringency of legislation, ranging from Euro 1 to Euro 6. Euro 1, introduced in 1992, made catalytic converters a mandatory component of a vehicle's exhaust system, thus limiting CO, NO_x and PM emissions. The limits on the amount of emissions released have become more stringent over the years, leading to the current legislation of Euro 6. Euro 1 limited

PM_{10} emissions to 0.14 g/km for diesel cars, with no limit on petrol. However, Euro 6 now implements limits of 0.005 g/km for both types of fuel [17]. When Euro 7 legislation is brought in, this will for the first time place restrictions on brake PM emissions. PM_{10} released from the braking system will be required to be less than 7 mg/km for ICEVs and less than 3 mg/km for BEVs under a standard driving cycle. The World Harmonised Light Vehicle Test Procedure (WLTP) outlines a process of 303 unique brake events to model such a standard driving cycle for ICEVs (Appendix A) [18].

ISO (International Organisation for Standardisation) 14040 and 14044 outline standard procedures that should apply to all LCA studies. This ensures accurate results that are comparable and repeatable. Therefore, these standards must be fully understood and adhered to during the course of the present research.

1.5 Aim and Objectives

The aim of this research was to develop an LCA methodology tailored to brake system applications, enabling the evaluation of environmental and human health impacts of automotive brakes throughout their entire life cycle.

The following objectives were established to realise the overall aim of this work:

- To review literature relating to LCA, brake emissions, and alternative rotor materials.
- To identify relevant LCA software tools and determine their strength and weakness in relation to this study. This includes an assessment of a novel hierarchical diagrammatic representation of an LCA using the well established Structured Analysis and Design Technique (SADT).
- To determine the methodological choices for the LCA comparative study, specific to a friction brake application. These include the functional unit, system boundary, and allocation methods.
- To generate an LCA model specific to a friction brake system that can be used in the future for new potential materials, as well as those considered in this study.
- To generate the necessary data on the PM emissions from coated brake rotors when such data are not available in the literature.

- To conduct an LCA case study on a laser-clad GCI brake rotor, using uncoated GCI as a baseline for the comparison.

- To conduct a further LCA case study on a light Al alloy brake rotor with a hard alumina coating applied by plasma electrolytic oxidation (PEO), again using uncoated GCI as a baseline for the comparison.

- To interpret the LCA results and to compare the different rotors considered in order to make recommendations as to the most environmentally friendly alternatives to the current uncoated GCI rotor.

- To archive the outcome of the research in the form of interim reports, journal articles, and/or conference papers, as well as within this thesis.

1.6 Thesis Structure

Chapter 1 - Provides an outline for the motivation behind the research topic and the requirement for LCA techniques within the brake industry.

Chapter 2 - Existing literature is reviewed, investigating how emissions from brakes affect human health and how various alternative brake rotors can improve both emissions and wear, with the potential to offer weight reductions. Provides an overview of current literature on LCA applications and their relevant methodological choices.

Chapter 3 - Outlines the development of the LCA methodology for brake rotor applications. This includes the key methodological choices, adaptation of the SADT diagram notation, and the selection of the brake rotor materials for the case studies.

Chapter 4 - Initially this chapter details the methodology for small-scale testing, developed by Limmer [1], before presenting the emissions results from the laser-clad GCI conducted as part of the present research.

Chapter 5 - Provides the results for case study I on GCI rotor, both uncoated and coated. This involves flow diagrams utilising the adapted SADT notation, data collection and calculation, and both midpoint and endpoint impact results.

Chapter 6 - Provides the results for case study II on PEO-Al rotors, both wrought and cast, demonstrating the benefits of lightweight alternative materials. This involves flow diagrams utilising the adapted SADT notation, data collection and calculation, and both midpoint and endpoint impact results.

Chapter 7 - This chapter discusses the methodological choices made and compares the results from both case studies, detailing the key novel aspects of the research. Several sensitivity studies are outlined, detailing the effects of certain methodological choices on the end results.

Chapter 8 - Conclusions from the research are drawn and recommendations for future work are made.

Chapter 2

Literature Review

2.1 Introduction

As discussed in Chapter 1, it is unlikely that emissions levels released by the uncoated GCI rotors will be able to meet the limits outlined by the impending Euro 7 legislation [18]. Therefore, new materials, coatings, and surface treatments are being investigated. When determining the most suitable alternative, aforementioned trade-offs need to be considered. For example, a coated GCI rotor will likely reduce emissions during the use phase, but with the addition of a manufacturing process that will come with its own environmental burdens. LCA can be used to ensure that the life cycle as a whole offers an improvement. Chapter 2 provides an in-depth review of the existing relevant literature. The key technical requirements of the braking system, potential new materials, brake testing methods, and past LCA methodological choices are reviewed in the following sections.

2.2 Fundamentals of Brake Systems

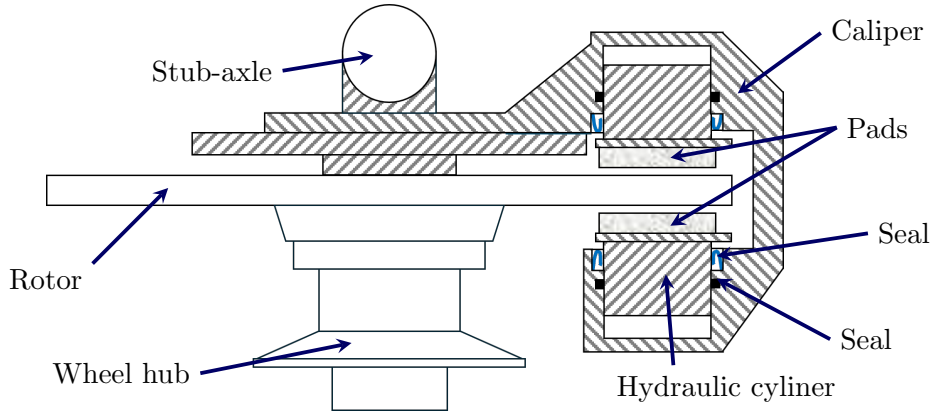

Figure 2.1: Brake assembly schematic of a standard hydraulic disc brake system.

Figure 2.1 details a disc brake design. The rotor (or disc) is directly bolted to the wheel hub, therefore, the brake torque within such a design is directly transferred into the wheel. A calliper, attached to the outboard structure of the car suspension, houses two brake pads positioned on either side of the rotor. As a force is applied to the brake pedal, the fluid flows through pressurised lines, resulting in the application of proportional forces to the two opposing pistons. Each piston pushes the brake pads into frictional contact with the rotor. This braking action is proportional to the pedal force applied, with no axial thrust on the rotor due to the cancellation of the equal opposing forces of each pad [19].

There are two types of system used to connect the brake pedal to the brake pads, hydraulic brakes, and air brakes. The air brakes are activated at zero or low air pressure, only to be released when the air pressure is increased. In contrast, hydraulic brakes are not engaged until pressure increases through an applied force to the brake pedal. Air brakes are therefore considered to have a built-in safety feature, where if a leak occurs within the brake lines, the brakes remain engaged. However, the drawback of air brakes is the necessity for additional components, such as air compressors, causing these systems to become more expensive. Therefore, the convention is to utilise air brakes on large heavy goods vehicles (HGVs), where such a safety feature is more crucial, while hydraulic systems can be implemented in smaller vehicles, such as passenger cars [20].

2.2.1 Technical Requirements of Brake Systems

The technical requirements of any brake system are good wear and corrosion resistance, excellent thermophysical properties, and high damping capabilities. The friction braking event will cause wear to the rotor and pads over time, releasing PM emissions. Good wear resistance not only reduces these emissions but also prolongs the life of the components, thus reducing maintenance requirements. The friction event generates a large amount of heat, leading to high operating temperatures. Therefore, it is important for a material to possess excellent thermophysical properties to withstand such high temperatures without mechanical property degradation. When a vehicle brakes, load transfer occurs onto the front axial, resulting in the front brakes generating ~70% of the braking power. The front brake rotors and friction material therefore undergo faster wear, theoretically releasing more emissions. As a consequence of this increased wear, the front brakes will also require more frequent maintenance [4]. Such an uneven power distribution can lead to a technical requirement for a greater level of stability in the CoF, as well as increased thermophysical properties, due to the higher brake temperatures seen within the front brake system. A higher stability in CoF will also lead to increased ride comfort. In addition, ride comfort can be improved by a material that has high damping capability, reducing vehicle noise, vibration, and harshness (NVH). Uncoated GCI has been the dominant choice within the vehicle industry due to meeting all of these technical requirements. They also offer additional benefits, such as low material cost and good machinability and castability [21].

In recent years, the increase in BEVs has caused a shift in the level of importance of each technical requirement. The introduction of regenerative braking has caused less frequent application of friction brakes, resulting in prolonged exposure to corrosive environments. The friction brakes are only applied when the torque limit of the traction

motor is exceeded or an emergency stop is required. This has limited their use, leading to fewer opportunities for wet brakes to dry out under the heat generated by friction, therefore increasing corrosion. This phenomenon has caused the poor corrosion resistance of uncoated GCI to become a worrying factor, with corroded rotors leading to premature brake failure [11]. An additional concern with uncoated GCI is also the high wear rate, which releases large amounts of PM emissions, correlating to a detrimental impact on human health and the environment.

2.2.2 Friction Materials

The braking performance is largely dependent on the frictional interface between the pad and the rotor. This interface can be heavily influenced by a change in the roughness of the material or surface of either component. The selection of pad composition is critical to ensure that the performance criteria of the braking system are met. Such criteria include safety and durability under a range of operating conditions (pressure and temperature changes in the rotor, operating speed, and environmental aspects). The brake pad is made up of multiple components as shown in Figure 2.2 [1].

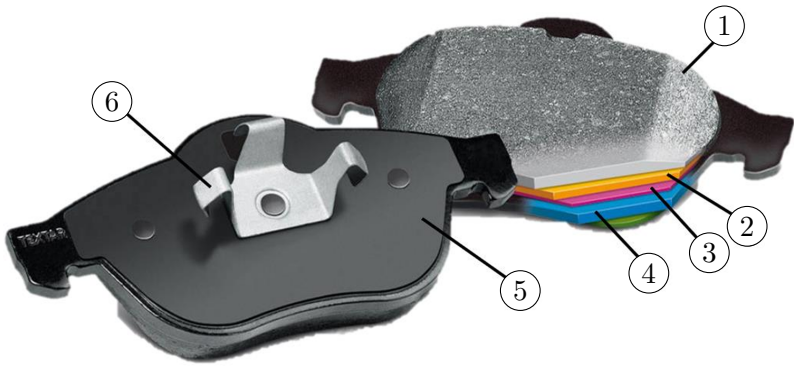

1. Friction material
2. Underlayer
3. Glue
4. Back plate
5. Shim
6. Clip

Figure 2.2: Components of an automotive brake pad [1, 22].

The friction material can be categorised into three main groups, non-asbestos organic (NAO), ceramic, and metallic [4]. NAO friction materials are typically softer and have no steel fibres or powders. They tend to possess a relatively low CoF (μ=0.3-0.4), and so are classed as a low performance material, being better suited for softer rotor materials such as aluminium to limit excessive wear [4, 1, 23]. Ceramic materials were derived to work against ceramic counterparts. They possess a higher CoF, with a more aggressive nature, typically used within the racing industry due to their high performance. The elevated brake temperatures of racing also alleviate their disadvantage compared to other materials, being more susceptible to brake fading at low temperatures [1, 24]. Metallic friction materials can be divided into subgroups according to the wt% of the metal content. Friction materials

with a metal content of 50 wt% or higher are classified as semi-metallic. Similarly to NAO, semi-metallic friction materials tend to posses low CoF values (μ=0.25-0.35), limiting their application. On the other hand, friction materials with a metal content less than 20% by weight display some of the highest CoF values (μ=0.35-0.5). These are classified as low-metallic (LM) and are very popular within the European market [1, 23, 25].

Table 2.1: Typical compositions and component roles of friction materials.

Brake Pad Component	Role	Proportion of Pad (by mass)
Binders	Holds other components together, ensuring structural integrity under mechanical and thermal stresses.	20-40%
Fibres	Reinforce the pad providing mechanical strength and structure. (Usually metallic, mineral, ceramic or organic)	6-35%
Fillers	Improve thermal properties, reduce noise, and lower manufacturing cost. (Usually inorganic compounds, silicates, ground slag, stone and metal powders)	15-70%
Frictional additives/ lubricants	Alters wear characteristics. (Inorganic, metallic or organic)	5-29%
Abrasives	Increases friction and limits transfer layer build up. (Al_2O_3, Fe_2O_3, SiO_2 and $ZrSiO_4$)	10%

Table 2.1 summarises the role and typical mass percentage of the five main constituents of a friction material on the market today [26, 27, 28]. The composition of such constituents is highly complex and typically very confidential to a brake pad manufacturer. Traditionally, the volume and type of ingredients used within a friction material is determined through empirical analysis and experience; however, often a certain proportion of trial and error is required. The frictional characteristics are largely affected by the binder resin and the reinforcing fibres. The binder (e.g. phenolic resin) type is typically referred to by the term organic, with organic friction materials used in a large proportion of passenger vehicles [29]. The type of binder depends on the operating temperatures. If incorrectly selected, the frictional heat generated has the potential to exceed the glass transition temperature of the resin, causing abrupt changes in frictional behaviour during a braking event.

2.2.3 Friction and Wear Mechanisms

Figure 2.3 displays a schematic diagram of a standard tribological system, where the wear of two contacting bodies forms a transfer film. The term tribology refers to principles such as friction, wear, and lubrication between interacting surfaces in relative motion [1, 30].

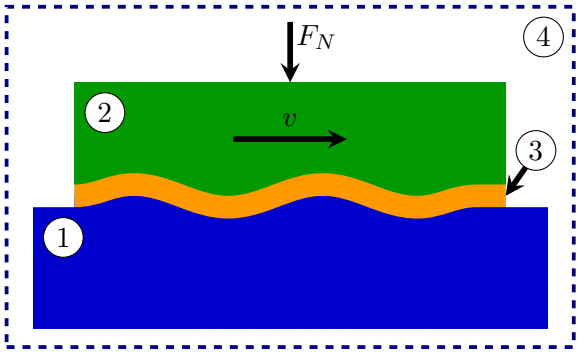

1. Base body - pad/rotor
2. Counter body - pad/rotor
3. Intermediate (third body) – transfer film (tribolayer)
4. Ambient medium – surrounding air

Figure 2.3: Schematic diagram of tribological system [1].

The body whose wear is currently under consideration is referred to as the base body. The transfer film, also called the tribolayer, forms through material being transferred between the pad and the rotor as the temperature of the brake system increases. The wear of both components is critical for the formation of such a film. The formation of this tribolayer can effectively decrease the wear rate [31]. A lower wear rate can improve durability, thus reducing maintenance requirements [32]. For consistent braking performance, a stable CoF is required. Therefore, a brake rotor will typically undergo several bedding-in cycles to ensure sufficient formation of this tribolayer before being used. The frictional behaviour and stability are strongly influenced by the surface roughness of each component. As the roughness increases, a higher CoF is generally generated, which increases the amount of wear under the same braking pressure. The added crevices of a rougher surface can also prohibit sufficient formation of a tribolayer, therefore indirectly impacting the wear rate [11]. The characteristics of the formed tribolayer can affect braking performance and are heavily influenced by surface temperature, normal pressure, and sliding speed [33]. A good balance is required when considering the desired CoF of the system between high and low surface roughness. As explained, a CoF that is too high increases the wear rate with prohibited tribolayer formation. On the other hand, if the CoF is too low, there will be no sufficient braking performance. A typical value of 0.3-0.4 should be aimed for [11].

Friction and wear can occur through different mechanisms. The mechanism that occurs depends on the current conditions of the system. There are four conditions under which frictional interfaces can exist. Dry friction is the absence of any lubrication, which means that two solid bodies are in direct contact. A subset of dry friction is boundary friction,

where a protective layer, such as an oxide film, has formed on one or both of the solid bodies. When lubrication is added to a system, the mechanism is referred to as fluid friction. Finally, mixed friction refers to a combination of boundary and fluid friction mechanisms, where a protective layer and lubricant are present [1].

During any braking event, the two friction mechanisms that are considered are dry and boundary friction. The mechanisms behind the frictional forces generated are adhesion and ploughing. Adhesion occurs because the initial points of contact between two surfaces (asperities) form chemical bonds that hold the bodies together. Therefore, the adhesion mechanism occurs at an interatomic level. When considering two metals, the strength of the adhesion depends on the solubility of the metals. Two metals with high solubility would be considered incompatible due to higher frictional forces and therefore higher wear rates [1, 34]. Ploughing can occur when the contact points interlock, deforming either elastically or plastically. This arises when one material has a significantly higher hardness than the other.

Frictional mechanisms are directly related to wear mechanisms that can occur. Wear is defined as the damage to a material, typically through progressive material loss due to two contacting surfaces [35]. The wear of this material can influence the conditions of the friction mechanism. An example of this is with boundary friction, where surface wear could remove a materials oxide layer, therefore converting the process into dry friction. Within the braking industry, there are three wear mechanisms to consider [1, 36, 37]. Abrasion results from a ploughing friction mechanism, where material loss can occur through the following methods:

- Cutting – material is removed from the softer body through a shear force.
- Fracture – if the wearing body is brittle, cracks can propagate, creating wear debris.
- Fatigue – the wearing body is ductile, causing deformation. Sideways material displacement occurs, leading to fatigue rather than shearing.
- Detaching grains – low bonding strength between grains in materials such as ceramics can cause whole grains to become loose and dislodged.

When the adhesive bond between two materials exceeds the cohesive strength of one material, adhesion can occur. The asperities deform, causing ductile or brittle fracture [38]. During adhesion, material loss occurs through:

- Scuffing – material is transferred between the two surfaces, forming grooves in the sliding direction [39].
- Scoring – similar to scuffing, except that it occurs after the transfer of material rather than because of.
- Galling – large particles are torn from the surface, leading to protrusions [40].
- Seizing – abrupt failure of the system due to large areas joining, typically as a result of galling [41, 42].

Finally, chemical reactions can occur between the surfaces of both materials, leading to tribochemical reactions. This tribochemical wear mechanism can typically be accelerated by increasing the temperature of the friction event. Usually for braking systems, this is an oxidation reaction due to the surrounding air. The removal and formation of the oxide layer through friction and oxidation can lead to a varying CoF (low with oxide layer and high without) [1].

2.2.4 Effects of Corrosion

Corrosion effects have been found to increase both the number and mass of PM emissions released during brakes. Furthermore, a corroded part can lead to reduced friction levels, which inhibits brake performance [11]. In extreme cases, the mechanical properties of each material can be detrimentally impacted to catastrophic premature brake failure due to corrosion effects. With the rise of BEVs and the introduction of regenerative braking, which prolongs the exposure of components to corrosive environments, high corrosion resistance becomes a more sought-after material property. The rate of corrosion is exasperated by the level of rainfall and its acidity. Freezing conditions also have an indirect impact since more salts (sodium chloride, magnesium chloride, calcium chloride) are used to defrost the roads [43]. Ghouri et al. [11] conducted tests on corroded and uncorroded uncoated GCI rotors. The corrosion process was carried out by exposing the rotor to a 5 wt% salt fog ASTM B117 for a duration of 96 hours. It was found that with a drag braking pressure of 5 bar, the levels of $PM_{2.5}$ and PM_{10} for the corroded rotor were double that of the uncorroded counterpart. When repeating the test at 10 bar, these effects were found to increase significantly up to 30 times the amount. This increase was linked to the corroded surface being mainly iron oxide particles, which have a weaker bonding strength than iron ions, leading to easier removal. Furthermore, after this initial layer was removed, the remaining surface of the corroded rotor was rougher (0.719 µm compared to 0.587 µm) leading to increased pad wear through abrasion. A secondary

observation was an increase in the number of cracks and crevices on the rotor surface, due to weaker mechanical properties. These cracks could lead to premature brake failure, as well as prohibit a stable tribolayer from forming.

The benefits of a material with superior corrosion resistance to uncoated GCI were demonstrated through further tests conducted by Ghouri et al. [44, 11, 45]. Both an Al metal matrix composite (MMC) rotor and a plasma electrolytic oxidation (PEO) treated wrought Al alloy rotor were tested. For Al MMC, it was shown that at 10 bar drag braking pressure, the mass of $PM_{2.5}$ decreased, while PM_{10} remained stable from the uncorroded to the corroded rotor. This was a significant improvement compared to the uncoated GCI, where approximately 30 times the mass of $PM_{2.5}$ and approximately 17 times the mass of PM_{10} were found for the corroded rotor compared to the uncorroded counterpart. However, the PEO-Al rotor was more promising, outperforming the uncoated GCI at all three brake line pressures (5 bar, 7.5 bar and 10 bar) for both particle sizes.

2.3 Environmental and Health Impacts

There are two main elements of environmental impacts within the brake industry. First, the energy used to transport and manufacture the components (including raw material extraction), and second, the emissions and waste released during such processes. Typically, global warming and CO_2 production are the main concern within product systems, with energy consumption being a reasonable indicator of these impacts. Within the brake industry, PM formation is an additional consideration, including its effects on human health and the requirements to meet the impending Euro 7 legislation.

2.3.1 Energy Use, Emissions and Recyclability

Energy consumption largely promotes the production of carbon emissions, with legislation being introduced to try to constrain the increase in these emissions. A significant impactor on this relationship is the electricity mix used, with renewable sources of energy production producing fewer carbon-related emissions. A study by Stamford et al. [46] found that a mix containing 75% fossil fuels reduces the impact of global warming by 25% compared to a mix containing 85%. A secondary method of reducing carbon emissions is through the use of recycled materials. The energy required to manufacture a material can be significantly reduced by using recycled materials instead of extracting new raw materials. A material, such as aluminium, has a high energy demand during smelting, leading to a higher impact on global warming. However, if recycled aluminium can instead be used,

the energy required for primary aluminium production can be reduced by up to 95% [47]. These potential reductions in the use of recycled materials are more pronounced in countries where electrical power is mainly generated from fossil fuels than those with high levels of renewable sources [48].

Emissions released during the lifetime of a product can have environmental and health impacts other than a detrimental effect on global warming. When copper (a toxic metal) was used more commonly, it was estimated that the traffic industry represented one of the largest contributors to the copper load in Europe. The associated emissions from brake wear were estimated to contribute up to 75% (2.4 kT per year) of the copper input into the North Sea. Copper-containing water can greatly impact aquatic life, potentially causing chemosensory deprivation (loss of senses). Chemosensory deprivation can affect the ability to sense nearby predators, thus increasing mortality rates [7]. Emissions released during use of a standard uncoated GCI rotor will typically comprise Fe, Si, Cr, Cu, and Mg, depending on the partnering friction material. Heavy metals, such as Fe, Cu, and Cr, can disrupt cellular function by binding to parts of cells, damaging organs. Therefore, such metals can have an impact on both aquatic and human life, directly affecting both ecotoxicity and human toxicity [49]. Other impact categories that can be affected by the release of emissions are acidification and eutrophication. Eutrophication occurs when an environment becomes enriched with nutrients, leading to excessive growth of plants and algae. Blooms of mucus-forming harmful algae were found in European waters as a direct result of an increase in the nitrate content. Excess plant growth has also been associated with oxygen depletion in certain areas [50, 51]. Sulphur and nitrogen-based compounds are a direct cause of both eutrophication and acidification by altering the chemical composition of soils and water after their deposition.

2.3.2 Impacts on Human Health

The main concern surrounding brake emissions and the driving factor for the introduction of legislation, such as Euro 7, is their impact on human health. The nature and severity of such impacts are dependent on the size, concentration, and chemical composition of the particles [52]. Many premature deaths in Europe can be related to the air pollution generated by road transport [53]. PM is deposited within the human body to different extremities depending on the shape and size of the particles. Coarse particles (PM_{10}) typically deposit in the nose and throat, while finer particles ($PM_{2.5}$) can enter the lungs and ultrafine particles (PM_1) can even enter the bloodstream. $PM_{2.5}$ can lead to reduced lung function through inheritable mutations, as well as weakening pulmonary

antimicrobial immune defence. In essence, the lungs become significantly more prone to harmful effects of inhaled microorganisms [54]. $PM_{2.5}$ is believed to be responsible for deleterious effects on the lungs and a possible cause of chronic obstructive pulmonary disease (COPD) [7].

Ultrafine particles (PM_1) that enter the bloodstream can be found to directly impact the heart and can cause increased heart rate variability [55]. Linked to this, serum protein levels associated with inflammation, homeostasis, and thrombosis are altered. As Peikertova and Filip [7] have stated, such an increase in heart rate variability can increase the frequency of premature supraventricular beats and elicit pro-inflammatory and prothrombotic responses, which is particularly harmful to young men. Another dangerous result of ultrafine metals entering the bloodstream is a possible correlation with ischemic heart disease. This association comes from inflammation triggered by the formation of reactive oxygen species, with damage to the junction between cells (tight junction).

More generally, metal pollution associated with brake wear is a potential causation of an increased risk of cancer. Although typically below the safety limits for human intake, metal pollution can be harmful in the long term. In extreme cases, bioavailable fractions of metals such as Cd, Cr, and Ni exceeded the standard limits of cancer risk in an urban site in Pune, India. High concentrations in the soluble fraction of toxic metals such as Cd and Pb were also discovered [56].

2.4 Emission Reduction Methods

Several alternative materials and surface coating techniques have been investigated to reduce the drawbacks of an uncoated GCI rotor. Such drawbacks include low corrosion and wear resistance.

2.4.1 Surface Coatings for GCI

The most widely researched solution to reduce the detrimental effects of the current uncoated GCI braking system is the application of a surface coating to the rotor. This solution offers a key advantage of using the manufacturing infrastructure already in place. Such coatings can improve both wear and corrosion resistance, thus reducing the PM emissions released, whilst increasing the lifespan of the rotor and reducing maintenance demands. In addition, coated rotors offer recoatability potential, creating a form of

closed-loop recycling where the coating can be reapplied at the end of life to allow the GCI rotor to be used again.

When coating techniques and materials are considered, heavy metals such as copper and nickel should be avoided. The reason for this is that the fine particles of both metals are toxic and can cause severe health risks [21]. Therefore, any coating techniques that rely on metallurgical bonding with these heavy metals are not suitable for brake rotor applications. Such coatings include plasma transferred arc (PTA) and traditional laser-cladding (LC) (with certain feedstock powders).

To overcome the restrictions presented by traditional laser cladding, extreme high-speed laser cladding (EHLA) has been developed. EHLA offers a coating that is superior to traditional LC with a more efficient application and a denser microstructure. These coatings tend to use titanium or tungsten carbide feedstocks with materials such as stainless steel as the matrix. Compared to traditional LC, a thinner coating can also be achieved, thus reducing the amount of feedstock required. The Welding Institute (TWI) has developed an EHLA process that uses an 80/20 wt% powder/substrate split compared to the typical 20/80 wt% found with the traditional method. The theory behind this change was that the substrate was the main cause for poor coating deposition. TWI's method removes graphite from the rotors surface through CO_2 laser melting, resulting in an improved surface roughness and no visible porosity between the coating and the substrate [57].

A hard chrome coating also has a dense microstructure. They have a low oxide inclusion that provides an improved corrosion resistance in harsh environments, as well as an increased fracture toughness [58]. Balamurugan et al. [59] demonstrated the high potential of such a coating technique by testing a chrome plated stainless steel rotor. Superior wear resistance was demonstrated at high and low temperatures compared to the uncoated counterpart. However, a separate study by Krelling et al. [60] found contradictory results. Numerous cracks and microcracks were found on the surface of the coated steel rotor. Despite these contradictory results, further investigation is unlikely within the brake industry. The plating bath contains hexavalent chromium, Cr(VI), thus producing a toxic carcinogenic mist [61, 62].

High velocity oxygen fuel (HVOF) was also found to apply dense coatings to GCI. This technique injects a stream of fine powder into a high temperature supersonic gas

stream. The high flame temperature is typically produced through the combustion of propane, generating temperatures of around 3000 degrees Celsius [21]. Porsche has already implemented HVOF, applying a hard tungsten carbide coating to a standard GCI rotor [63]. A potential limitation of this technique is the reduced coefficient of friction, which increases the chance of slip during braking. A study by Standford et al. [64] demonstrated this lower friction level with a GCI rotor coated with stellite alloy powder. However, it was found that despite the lower level of friction, the frictional behaviour remained stable. To reduce weight loss due to wear during dry operation, higher carbide content coatings would be required (80/20 wt% compared to 75/25 wt%) [21].

High velocity air fuel (HVAF) attempts to overcome the potential restrictions of HVOF, such as carbide dissolution and brittle phase formation. This process differs from HVOF by using air as a fuel source instead of oxygen. A convergent-divergent (de Laval) nozzle is used to produce velocities higher than those found in HVOF, mitigating the decarburisation issues and reducing operational and production costs. These higher velocities result in extremely dense coatings with excellent cohesion and adhesive strength [21].

2.4.2 Alternative Lightweight Solutions

An alternative solution to coating the current GCI rotors is to use lightweight materials. These offer the advantage of reducing the mass of the braking system while simultaneously improving resistance to wear and corrosion.

2.4.2.1 Benefits of Weight Reduction

The braking system contributes to the unsprung mass of a vehicle. Therefore, reduced rotational inertia from a lighter rotor can reduce fuel consumption (or for an electric vehicle, increase its range), thus indirectly reducing CO_2 emissions [65]. Furthermore, a reduction in rotational inertia could lead to a reduced road impact, lowering the emissions associated with road abrasion. A further benefit can include energy savings during transportation of the manufactured rotors to different processing plants and vehicle assembly factories.

2.4.2.2 Lightweight Metal Alloys

Lightweight metal alloys offer the possibility of a cheap and lightweight rotor, with good manufacturability. The three main alloys worth investigating are aluminium, titanium, and magnesium.

Aluminium alloys offer a low weight solution with good mechanical properties [66]. Typically, such alloys possess good corrosion resistance, unless cracks start to form. A natural oxide layer forms on the surface of the alloy, preventing further oxidation and therefore corrosion. The level of corrosion resistance depends on the type of alloy selected. Silicon and magnesium-based alloys show good corrosion resistance in all environments. Copper-based alloys, on the other hand, have significantly decreased corrosion resistance in marine environments. At elevated surface temperatures of braking systems, corrosion is found to propagate further into the metal with an increased film thickness [67]. Aluminium alloys can also suffer from property degradation at temperatures as low as 150 °C and at around 275 °C the yield strength is halved [68]. With the high operating temperatures of braking systems ranging from 300 °C to 800 °C this material degradation becomes a concerning problem. Even with a well-ventilated rotor, temperatures can reach around 350 °C [69], thus prohibiting the uptake of untreated aluminium alloys as brake rotors.

Although heavier than aluminium, titanium alloys still offer a lightweight solution compared to coated GCI rotors. Specifically, the alloy Ti-6Al-4V can offer a significant weight reduction compared to GCI (4.4 g/cm^3 compared to 7.2 g/cm^3). Despite the increased weight compared to aluminium, titanium alloys possess a superior strength to weight ratio, with greater temperature and corrosion resistance. However, prohibitive factors in the uptake of titanium alloys are their inferior tribological properties, lower wear resistance, and low load bearing capacity compared to uncoated GCI [70]. Further research is required to investigate the potential to overcome such drawbacks through surface modification.

A third low density, lightweight solution is magnesium alloys. Although they are more expensive than aluminium, they have inferior mechanical properties such as yield strength. To improve mechanical properties, magnesium alloys can be combined with elements such as CeGd, Nd, and Y (cerium gadolinium, neodynium, and yttrium). However, these alterations come with an increased cost, making such alloys a less favourable option for automotive applications [71]. The biggest restriction to uptake within the braking system is the potential risks of ignition and flammability at elevated temperatures [72].

All three metal alloys share the same drawback of poor temperature resistance. This is a significant factor when considering the high operating temperatures reached during braking events of up 800 °C [69]. Once safety factors are incorporated, the required operating temperature without material property degradation becomes even higher. There

are two options to overcome this issue; the alloy can be reinforced throughout to form a metal matrix composite (MMC), or alternatively a coating or surface treatment can be applied to the surface.

2.4.2.3 Lightweight Composites

Composites are reinforced throughout the material, reducing detrimental effects on the mechanical properties of the alloy at high operating temperatures, while offering the same lightweight benefits. However, this reinforcement will typically add cost to the manufacturing process of such materials.

A commonly adopted material that is used within aircrafts and high-end sports cars is carbon-carbon. This composite is made from a matrix of graphite, reinforced with carbon fibres. Carbon-carbon possesses a high strength to weight ratio, offering extremely lightweight solutions [73]. However, the material properties can vary depending on fibre orientation. Hutton et al. [74] investigated how the orientation of the fibre within the matrix can affect the wear mechanism and the tribological behaviour. It was discovered that the qualitative features of the wear mechanism were unchanged; however, the wear rate and the development of the friction film were affected. When a friction film forms, overtime it will start to delaminate, partially being recycled into a new friction film. This process will repeat in a constant cycle. There were two orientations of fibres that were investigated. The first of which looked at the fibres within the matrix being placed parallel to the wear face. The second orientation had the fibres perpendicular to the wear face, with the fibre ends emerging at the surface. In parallel, shear deformation of the graphitic chemical vapour infiltration (CVI) matrix sheaths surrounding the fibres led to easy formation of a friction film and a lower wear rate. The perpendicular orientation led to higher wear rates due to microfractures of the fibre ends contributing to particulate debris. This higher wear rate was found to inhibit the formation of friction films until higher rotational speeds were reached. Speeds and temperatures exceeding than 1800 rpm and 140 °C were required before a friction film could occur [75]. Due to a high cost and low wear resistance, carbon-carbon has typically been limited to aeronautical and race car applications. In racing conditions, such as in Formula 1, the weight reduction becomes a more significant deciding factor over wear rate and cost, due to the high budgets and the ability to replace the rotors after each race weekend. Carbon-carbon also requires high temperatures to produce good braking performance, so at lower operating temperatures of passenger cars they would not operate as effectively [74].

Alternatively, carbon-carbon are ceramic matrix composites (CMC). CMCs were developed as a more roadworthy alternative to carbon-carbon. CMCs can offer higher wear resistance and better frictional stability at the lower temperatures of passenger vehicles [76]. Replacement of the carbon-carbon graphite matrix with silicon carbide was investigated by Renz et al. [76]. Carbon fibre reinforced silicon carbide was found to have high fading stability with significant weight reductions similar to those of carbon carbon ($\sim$ 50% compared to an equivalent uncoated GCI rotor). This fading stability ensures constant performance even after many harsh braking events, with a low required pedal force due to a high coefficient of friction. CMC brake rotors have been found to withstand temperatures of up to 800 °C without irreversible distortion, demonstrating outstanding thermal stability up to 1300 °C [21]. Due to a low thermal expansion and high wear resistance, judder issues are minimised. Despite all the promising characteristics of CMCs and their price reduction compared to carbon-carbon they are still typically too expensive for passenger cars. This is due to a complex manufacturing process and high raw material costs [76]. Therefore, similar to carbon-carbon, CMCs are also likely limited to racing and luxury car applications.

An attractive alternative to both carbon-carbon and CMCs that offers a cost reduction are metal matrix composites (MMCs). The conventional method for production of MMC rotors is by casting processes such as semipermanent gravity casting. Typically, MMCs offer good mechanical behaviour and physical properties, although with a major drawback of low ductility. MMCs have been used commercially in the automotive market for 30 years and are implemented for brake components on the Toyota RAV4 and Ford Prodigy. MMC brake rotor designs typically offer a weight reduction of 50-60% when compared to an equivalent uncoated GCI, improving fuel efficiency and reducing road impact [77]. Although uncoated GCI rotors being cheaper, they are outperformed by MMC components on performance, marketability, and environmental impact.

Aluminium is typically a favoured matrix material due to its low density and high electrical and thermal conductivity. When properly manipulated, aluminium can be sufficiently strengthened for brake rotor applications. This strengthening is done through precipitation hardening (heat treatment) and the resulting material can offer superior corrosion and wear resistance compared to uncoated GCI [77]. Judder issues are reduced through the high damping capability of aluminium MMCs. However, similar to aluminium alloys, they also suffer from low melting points due to the aluminium alloy being still exposed on the surface of the brake rotor [77, 78]. An aluminium MMC

brake rotor has previously been used on a Lotus-Elise car, but production was found to be too expensive and was considered not viable for mass produced vehicles [52]. A Swedish company, called Floby, has investigated an aluminium MMC with silicon carbide reinforcement, under the trade name SiCAlight. This new rotor was found to reduce mass by 30-50% compared to an equivalent sized uncoated GCI [79]. However, the main limit for commercial implementation remains the high cost of production. A secondary drawback is a phenomenon that occurs at high operating temperatures. The aluminium matrix softens, exposing the silicon carbide fibres, thus increasing surface roughness and therefore pad wear. This process can also typically result in grooves forming on the surface of the rotor that lead to instability in the tribolayer [80, 37, 81].

2.4.2.4 Surface Coatings and Treatment for Lightweight Metal Alloys

The restricting factor in the adoption of composites in passenger vehicles is the high cost associated. Within a brake system, extreme temperatures and frictional conditions are experienced only at the surface of the rotor. Therefore, to reduce costs, instead of reinforcing the material throughout, the reinforcement could be concentrated at the frictional interface on the alloy surface. This reinforcement would be done through the application of a temperature resistant coating or surface treatment. When considering which alloy material to coat, aluminium would be the most suitable. Aluminium has the lowest density, and therefore the greatest weight reduction potential when compared to titanium and magnesium. In addition, titanium is significantly more expensive, whilst magnesium is flammable at normal brake operating temperatures.

Thermal spray processes can be applied to a wide range of materials, such as metals, cermets, ceramics, and composites. Atmospheric Plasma Spray (APS) involves injecting fine particles through a plasma stream. This technique can increase the frictional performance and hardness of the aluminium rotor, while also reducing brake fade [21]. However, Aranke et al. [21] found that such coating techniques were susceptible to cracks and high porosity. Suspension plasma spray (SPS) differs from APS as the particles prior to injection are suspended in liquid rather than gas. This offers an advantage in that it allows submicrometer and nanosized particles to be used during spraying, therefore facilitating a smaller porosity than APS, with denser coatings and superior intermellar bonding [82].

An alternative coating technique is cold gas dynamic spray (CGDS). This method is difficult to apply to GCI rotors, being limited to applications on materials with low

temperature ductility, such as aluminium alloys [83]. The materials capable of being deposited on the surface of the metal are also restricted to ductile metals. Poierer et al. [84] investigated the wear and corrosion of stainless steel deposited on the surface of an aluminium 356-T6 brake rotor. The coating was found to show good adhesion but with a poor wear rate. Therefore, for this process to be viable, it would need to be accompanied by an arc sprayed top coat using the PTA technique mentioned previously (Section 2.4.1) [83]. As explained above, PTA involves metallurgical bonding with copper and nickel, which are both toxic metals. This toxicity means that the CGDS is not suitable for brake rotor applications with and without the topcoat, with a poor wear rate or high levels of toxicity.

Finally, and perhaps the most promising technique, is plasma electrolytic oxidation (PEO) surface treatment. This method is currently being marketed for a range of products by Curtiss-Wright (Keronite). PEO involves the submersion of the metal in an electrolyte bath while high current and voltage are passed through. The resulting discharges produce a plasma on the surface of the metals, inducing the formation of a ceramic oxide film with dielectric breakdown [10]. PEO surface treatments can be applied to aluminium alloys and aluminium matrix composites alike, providing increased surface hardness and a more stable coefficient of friction than the traditional uncoated GCI. An oxide layer is formed on the aluminium alloy that is denser and more consistent than that of the MMC, thus resulting in a more consistent braking performance. The PEO process is limited to applications on metals such as aluminium, titanium, and magnesium due to the requirement for a protective oxide conversion layer to form on the surface of the rotor [21]. Shrestha et al. [65] conducted dynamometer tests on a PEO-treated AA6082 alloy rotor under AK master test conditions. When the rotor was paired with an LM friction material, a CoF value of 0.34-0.38 with good stability was found. Once the braking temperature reached above 300 °C, the vented rotor displayed increased performance due to superior cooling capabilities compared to the unvented counterpart. However, even at temperatures of 400 °C, both rotor designs showed significant reductions in pad wear, being half that of the uncoated GCI. Ghouri et al. [45] tested the corrosion resistance, with corrosive environments replicated by 96 hours of exposure to a 5 wt% salt fog. The PEO rotor was found to offer significant reductions in wear and PM emissions after exposure to the corrosive environment compared to the corroded uncoated GCI rotor, mainly due to its higher corrosion resistance.

2.4.3 Adhering to Euro 7 Legislation

The introduction of Euro 7 restricts the brake emissions of passenger ICEVs to 7 mg per kilometre travelled per vehicle [85]. The defined testing method for such vehicles is the worldwide harmonised light vehicle testing procedure (WLTP), performed on an enclosed brake dynamometer.

2.4.3.1 WLTP Cycle

The WLTP cycle was introduced in 2017, typically used to measure fuel consumption and CO_2 emissions. The WLTP cycle models real world driving conditions through 303 unique deceleration events, replicating a combination of low-speed urban, suburban, non-urban and high-speed motorway driving. Table 2.2 outlines the boundary conditions for the cycle, with a full list of all the pre-defined stops provided in Appendix A.

Table 2.2: Boundary conditions for WLTP cycle.

Boundary Condition	Value
Number of deceleration events	303
Driving distance	192 km
Average speed	43.7 km/h
Maximum speed	132.5 km/h
Average deceleration	0.97 m/s2
Maximum deceleration	2.18 m/s2

2.4.3.2 Small-Scale Testing

Traditionally the dynamometer tests that run the WLTP cycle use a full-scale set-up. The drawback of full-scale testing is the timely nature and high cost. Limmer [86] has developed a small-scale testing rig to reduce the cost, energy, and time consumption of such full-scale dynamometer testing. Often, the restriction with being able to conduct small-scale testing is due to lack of scalability of the results. However, as part of Limmer's research, he developed a scalable methodology in which operating conditions and rotor temperature were accurately replicated. A method previously used by Preston et al. [38] applied a constant energy density for accurate scalable results. In the case of brake rotors, to ensure that the same operating conditions are replicated as closely as possible, an identical frictional phenomenon must occur between the pad and the rotor. This relies on the sliding conditions, which are affected by the three geometric features shown in Equations 2.1-2.3:

1. The ratio of the friction surface area of the rotor to the pad:

$$R_A = \frac{A_{rotor}}{A_{pad}} \tag{2.1}$$

2. Sliding velocity gradient along the friction radius:

$$R_v = \frac{outer\ rubbing\ radius}{inner\ rubbing\ radius} \tag{2.2}$$

3. Pad aspect ratio, defined as the ratio of width to length:

$$R_{pad} = \frac{pad\ width}{pad\ length} \tag{2.3}$$

With the consideration of keeping these three ratios constant, the scaling factor, f, can be derived using Equation 2.4.

$$f = \frac{Area\ of\ pad\ \ (mm^2)}{Area\ of\ scaled\ pad\ \ (mm^2)} \tag{2.4}$$

Utilising a constant energy density, Limmer found the scaling factor for a standard brake system to lie between 11.72 and 17.22 [1]. Equation 2.4 indicates that the exact value depends on the cross-sectional surface area of the full-scale brake pad.

2.5 LCA Resources for the Brake Industry

2.5.1 Introduction to LCA

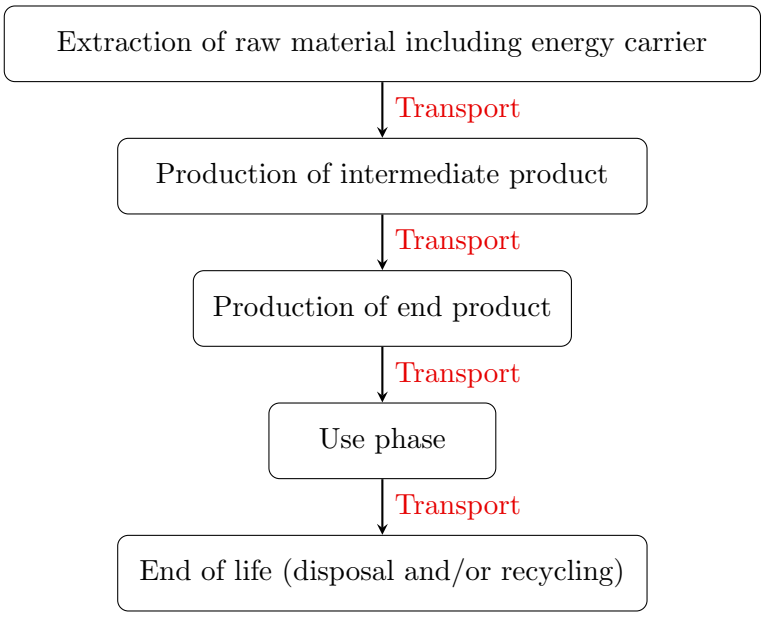

Figure 2.4: Overview of the life cycle of a product system.

Life cycle assessment (LCA) is a relatively new technique, developed in the 1970s, with internal standards (ISO14040 series) introduced in 1977. The US Society of Environmental Toxicology and Chemistry (SETAC) is responsible for the coordination of LCA development across the US and Europe [87]. LCA is a technique used to analyse and quantify the environmental aspects and potential impacts of a product life cycle, as shown in Figure 2.4. This cradle-to-grave approach helps to inform stakeholders of any problem shifting or trade-offs. Problem shifting can occur when the environmental impact of a material is reduced in one section of the life cycle, but inadvertently increases elsewhere [14]. ISO14044 and ISO14040 define the standardisation of LCA to have four distinct stages [40]:

1. Goal and Scope – defines the system boundary, time frame, and detail of the study.
2. Life Cycle Inventory Analysis – data is collected from primary and secondary sources on the inputs and outputs within the predefined system boundary.
3. Life Cycle Impact Assessment – The data collected in the previous stage is evaluated, being converted using characterisation factors (CFs) into impacts associated with predefined impact categories. The LCA impact analysis has several mandatory and optional elements:
    a. Selection of the impact categories, category indicators, and models for characterisation (Mandatory).
    b. Classification — Assignment of results (Mandatory).
    c. Characterisation — Calculation of category indicator results (Mandatory).
    d. Normalisation —- Calculation of the magnitude of the impact category indicator results relative to reference information (Optional).
    e. Grouping (Optional).
    f. Weighting (Optional).
    g. Additional analysis of data quality (Optional).
4. Interpretation - The final phase compiles the results, evaluating their relative importance to draw conclusions and recommendations.

These phases formulate an iterative approach with constant interpretation to inform any required alterations to the methodology, ensuring a robust study, as shown in Figure 1.2. A big topic of discussion in LCA is whether valuation can be classified as a separate additional phase. Valuation in the context of LCA is the potential weighting of one

factor over another should it be considered more important. ISO do not consider this to be part of the standardised structure. However, when comparative LCA results are not straightforward, it is sometimes necessary. The inclusion of a valuation stage within an LCA can sometimes be important to assist in understanding which factors are more important or harmful when considering trade-offs [14].

According to ISO legislation, the goal and scope should be clearly defined and consistent with the intended application. Within this phase of an LCA study, the methodology is defined. The scope should be specified at the start of the study, but due to the iterative nature of LCA, alterations may be required throughout the study. The goal is used to specify an explanation for [39, 41, 42, 88]:

- The range of application, which defines the objective of the study.
- Reasoning for the LCA study being conducted, giving the interest of realisation.
- The target group for the study
- Comparative assertions planned for the study, and what will the accessibility of results to the public be.

Defining the technical system boundary is one of the most important and extensive steps of LCA, usually done visually with the use of flow diagrams. A cut-off criteria for allocation can typically be used on the basis of mass, energy, and environmental relevance. If something makes up a proportion of less than 1% of the overall system, it can be excluded from the boundary [40]. In addition to this technical system boundary, geographical and temporal boundaries need to be considered. A functional unit (FU) can then be defined, quantifying a description of the output of the product system that is constant for all products in a comparative study. Again, because of the iterative approach of LCA, this can be altered later, if required. When conducting a comparative study, the length of time must also be included in the FU, thus defining the temporal boundary. Finally, when considering the level of detail that a study can be conducted to, the method for data acquisition is required. Primary data is preferred; however, where this is not possible, secondary sources and estimates are typically used [14].

During the inventory analysis phase, data is collected on the interactions between unit processes, the technosphere, and the environment. Infrastructure such as the construction of buildings and factories generally contribute less than 1% of the total energy per product and can therefore be excluded from the system boundary of an LCA study [89].

The allocation of environmental burdens should be assigned during this phase. Currently, there is no standard for this, so typically if system expansion or reduction is not possible, then the following allocation methods can be applied [14]:

- Mass-proportional allocation
- 50:50 rule, substitution, or cut-off rule with open loop recycling
- Other allocations with open loop recycling following goal definition.
- Credits in case of consideration of waste management
- Basket of benefit method with comparison of waste management technologies.

It is likely that these allocation methods may only be applied once preliminary results are achieved due to their complexity.

The LCA impact phase derives the potential environmental and health impacts resulting from the inputs and outputs per FU collected during inventory analysis. LCA impact analysis does not indicate actual impacts observed in the environment, only the potential association between the life cycle of the product or process and these impacts [90].

The final phase of LCA is the interpretation of the results, including the reporting and critical review of the analysis. This phase interprets the results from the inventory and impact assessment, providing recommendations aligned with the objective of the LCA study. The interpretation should thoroughly examine the consistency between the results and the original defined goal. There are strong regulations when considering a comparative LCA that will be made publicly available [14]. ISO 14044 defines the interpretation as having three stages [91, 40]:

1. Based on the results of the LCA study, the significant issue should be identified.
2. The completeness of the study is evaluated, with the inclusion of sensitivity analysis.
3. The limitations of the study are discussed, conclusions are drawn, and recommendations are made.

The reporting of results should be based on a scientific publication and the hypothesis, and theories formulated in a way that is eligible for falsification (thus refuted) [92]. The critical review section should ensure the following:

1. The methods used to carry out the LCA are consistent with the ISO standard.

2. The methods are scientifically and technically valid.
3. The data used are appropriate and reasonable in relation to the aim of the study.
4. The interpretations reflect the limitations identified and align with the objective of the study.
5. The study report is transparent and consistent.

During interpretation, sustainability and economic factors must be considered. An environmentally friendly option can never be commercially viable if it is too expensive. Consideration of how legislation might change and what will be required of the product in the future must also be included. LCA capability can be preserved and supplemented by economic (LCC) and social (social LCA) aspects where necessary [14].

2.5.2 LCA Models and Methodological Choices

A crucial part of any LCA is the methodological choices. These must be carefully considered, with any changes in the applied methodology having the potential to influence the results of the study. To date, LCA has been used for many different applications, although there is currently a lack of studies conducted on brake rotors. Therefore, part of the aim of the present research project is to assess and develop the suitability of LCA for this purpose.

Regarding the automotive sector, Del Pero et al. [13] conducted a comparative study on an ICEV and a BEV. This study provides a good overview of the methodology choices within an automotive application of LCA techniques. The chosen FU was 150,000 km driven by the car. The FU is useful to ensure a fair comparison between the two propulsion technologies with different range capabilities. Transportation during production, vehicle maintenance during use, and associated manufacturing processes were all excluded from the system boundary. These areas were to be excluded because of their negligible effect on the total impact of the life cycle and the lack of available information. The data collected for the sections within the system boundary was a combination of primary and secondary data. Primary data was collected using specific questionnaires regarding all parts and materials for the production stage. However, for the use phase, secondary data were mainly used from the GaBi 6.3 database. This data collection is required for all specific components, and so determining of typology and material volume is necessary, as well as researching the individual manufacturing processes.

The ability of LCA to assess eco-design in the automotive sector was investigated by Munoz et al. [93], who conducted a case study on polyolefinic door panels. Munoz et al. investigated the replacement of plastic door panels with prototype panels designed for recycling based on compatible polyefins. The method used to define the FU for the study of eco-design door panels started with describing the general function of the door panel. This is a common convention used throughout the literature. In this case, the function of the door panel was to provide ergonomic comfort to the passenger in the form of armrests, convenient storage, and well-placed window and wing mirror controls. From this function a physical model for the FU was defined, as these function requirements were equivalent for both the current and the prototype panel.

A clear method for defining a system boundary was detailed within the study of prototype door panels, defining three types of boundary. One between the product system and the environment, a second between the included and disregarded processes (cut-off), and the third between product systems (allocation). Within any LCA study, it is critical to clearly define the boundary between the system and the environment. The cut-off criteria were applied to avoid disproportionate effort within data collection. In the case of this door panel study, weight was used as a cut-off point, excluding the production phase of elements below 10 g. Various environmental impacts related to processes such as washing and maintenance checks were not allocated to the panel, as there was no direct relationship between them, and these processes are generic for the whole car. Weight has a direct impact on fuel consumption; therefore, allocation for this had to be considered, investigating the added fuel consumption per km due to weight increase. In terms of disposal, system expansion and subtraction were applied when considering the effects of different fuel sources to power cement kilns. This study provides a good example of how the change in fuel expenditure can be investigated when considering a lighter weight solution.

Lightweight brake rotor alternatives have the potential to reduce road impact through a reduction in the unsprung mass of the vehicle. However, this reduction in impact is likely to only alter the condition of the surface and is not significant to the structure of the road due to the fourth power law in the design [94]. A relevant application of LCA is a study on asphalt pavement completed by Huang et al. [87]. The asphalt study investigated the use of recycled and secondary materials in asphalt pavements. The applied FU was defined as 30,000 m^2 of the asphalt surface. When considering the system boundary of the asphalt surface system, some transport must be excluded due to lack of data. The

process of paving was also excluded, as it was the same in both comparison processes. To consider where the limit is established, it had to be assumed that there were no measurable effects on the lifetime of the asphalt layers during recycling. The upstream boundary was determined as the collection point for these recycled materials, due to the focus on the investigation of the use of recycled materials.

Ulf Olofsson et al. [95] conducted a streamlined LCA study to compare the environmental impact of a virgin uncoated GCI rotor and one refurbished using a laser cladding process. This is relevant to evaluate the viability of reinspecting brake rotors by applying a new coating over completely remelting or disposing of the raw materials in landfill. The recoated rotor was found to reduce CO_2 and energy consumption compared to the uncoated GCI rotor by 90% and 80% respectively. This clearly demonstrates the benefits coated rotors can offer in reducing environmental impact. This study focused on the impacts of energy consumption and CO_2. The rotor use stage was excluded from the system boundary, focussing on the recyclability of the coated rotor.

The most relevant study was completed by Gradin and Åström in 2020 [16], comparing two brake rotor materials, which can provide beneficial methodological choices to guide this piece of research. An additional focus of this study was to test the validity of simplifying the LCA by omitting identical parts within comparative case studies. It was found that simplifying the model in this way produced identical impact differences, which proved to be a reasonable approach. This study only compared a GCI rotor coated using a carbide-based thermal spray powder with an uncoated GCI counterpart. The advantages were found to be limited, with an increased resource requirement due to an added manufacturing stage. However, this was offset by the extended lifespan of the coated rotor. Therefore, there was a reduction in the requirement for spare parts and maintenance requirements. In this study, novel lightweight solutions were not considered, allowing room for further development. The functional unit was defined as the deceleration of a car during its lifetime (defined as 240,000 km). When determining the timescale for the functional unit during a comparative study, it is crucial to be as precise as possible. Overestimating the lifetime of the use phase can diminish the environmental impacts of the other phases. The system boundary for the brake rotor comparison omitted the assembly of the brake system due to the identical nature between the materials. The focus of determining the system boundary was placed on the brake rotor itself, from cradle-to-grave. A mass proportion allocation method was applied, calculating fuel production and consumption based on the brake rotor masses.

There are important findings from the limited LCA studies conducted within the brake or even automotive industry. These can all supply assistance in selecting the key methodological choices (made in Chapter 3), including:

- The FU is defined through the function of the product, followed by a specified lifetime for a comparative study. This can be done utilising a physical model (dimensions of a brake rotor).
- Cut-off criteria are applied to avoid disproportionate efforts in data collection.
- Mass proportion allocation is suitable for LCA applications on the braking system.
- The inclusion of fuel production and consumption accounts for the weight reductions. In some cases the emissions must be based on the total car mass to avoid mass non-scalability of the particulate emissions. However, this is unlikely to be needed due to the comparative nature of the present study.

2.5.3 Software Packages

The data manipulation and application of these methodological choices is usually performed using an LCA modelling software package. Currently, several software tools exist, such as GaBi, openLCA, SimaPro, and Umberto. A significant amount of care must be taken when selecting which software will be used, with each producing slightly different results [96]. These differences are due to the varying methodological choices and secondary data used in the impact assessment stage of the LCA. Each software has its advantages and disadvantages outlined in Table 2.3 [96].

However, the major drawback with any of these software packages is the lack of transparency. It is difficult to tell what methods and characterisation factors are being applied. Some also come with high costs attached. Therefore, there is an argument for the need for a purpose built LCA model, allowing for full customisation of the methodological choices specific to the braking industry.

Table 2.3: Positive and Negative Modelling Aspects of LCA Software Packages.

Software package	Positive modelling aspects	Negative modelling aspects
GaBi	- Good documentation of datasets. - Costs and social aspects can be modelled too. - It is possible to import/export datasets easily. - Professional database with hundreds of datasets. - Possibility to generate [a]EPDs.	- High cost of investment. - Most of datasets are aggregated.
openLCA	- Costs and social aspects can be modelled too. - Free for users. - Open source. - It is possible to import/export datasets easily. - Possibility to share datasets online. - Possibility to generate [a]EPDs.	- Lack of datasets freely available. - Many datasets are poorly documented. - Normalisation and weighting factors are not available for [a]ILCD/PEF method.
SimaPro	- Good documentation of datasets. - Social aspects can be modelled too. - Integrated with ecoinvent database. - Most of datasets are unit processes.	- High cost of investment. - Limited number of dataset formats.
Umberto NXT	- Cost aspects can be modelled too. - Integrated with ecoinvent/GaBi databases. - Good integration with Excel features.	- High cost of investment. - Cannot import/export datasets to traditional LCA formats (e.g. [a]ILCD). - Normalisation and weighting factors are not available.

[a] EPD refers to environmental product declaration, ILCD refers to international life cycle data system, and PEF refers to product environmental footprint.

2.6 Structured Analysis and Design Technique (SADT)

A major component of the LCA goal and scope phase is defining the system boundary. This process typically involves drawing flow diagrams that describe the life cycle of the product system. For a product such as brake rotors, there are many different processes involved within the life cycle that make such diagrams complex and difficult to follow. The Structured Analysis and Design Technique (SADT) is a methodology that can be used to analyse and design products through a hierarchical approach. The highest point of the hierarchy is referred to as a context diagram, represented by a singular activity box. The next level will break down the activity into 3-6 smaller activity boxes, a process to be repeated until the desired level of detail is achieved. Figure 2.5 outlines this hierarchical process. The levels of the hierarchy are assigned specific labels, with the highest level (context diagram) adopting the label A-0. Following this, the overall system breakdown would be assigned A0, and its breakdown A1, A2, A3 etc.

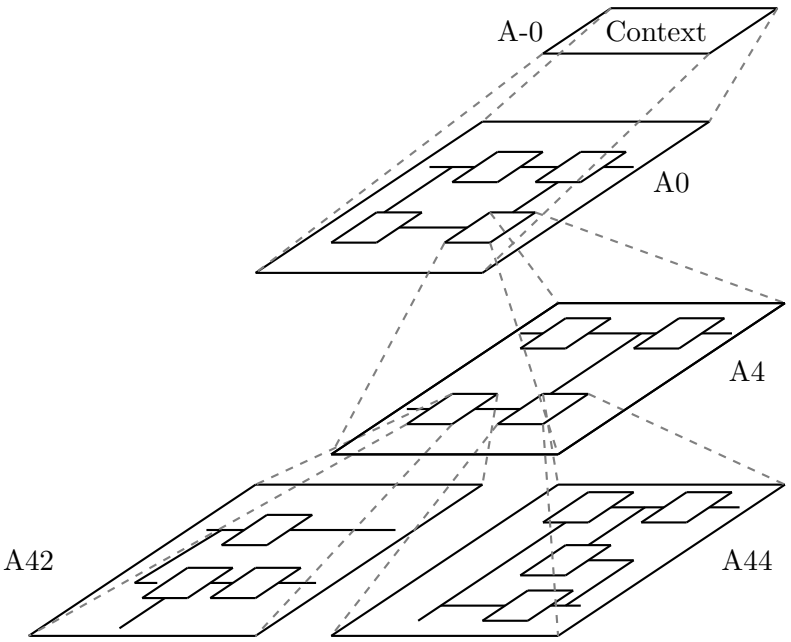

Figure 2.5: Hierarchical breakdown of SADT methodology [97].

There are several noticeable similarities to the process for defining LCA system boundaries, where unit processes are represented with boxes, and their interactions by arrows. It is therefore a viable assumption for the SADT to be adaptable for LCA applications. The history of the SADT process dates to the 1970s, originally developed by Ross [98] as an integrated definition of function modelling (IDEF0). The main application of this process to date is for use in computer-aided design (CAD) and industrial applications. The hierarchical approach is an attractive methodology for making complex systems more adaptable and easier to interpret.

Some activities within the diagrams can be bypassed, with their inputs remaining unchanged, an idea that could be carried forward to LCA, where some unit processes can be bypassed if data collection is not required. Unlike many flow diagrams, the SADT diagrams do not follow a sequence of time, rather the interactions between activities. A key benefit of the IDEFO method is that it opens itself up to an iterative approach, adding more detailed diagrams if needed later in a study. Finite element analysis (FEA) is a typical application of this methodology, with activity inputs including engineering drawings and non-geometric design data, and outputs including the analysis model, results, and final report. The mechanisms typically applied to each activity include the analyst and tools utilised (such as FEA software), with the control being the design requirements to ensure the end design is fit for purpose. Figure 2.6 outlines the interactions that take place with each activity.

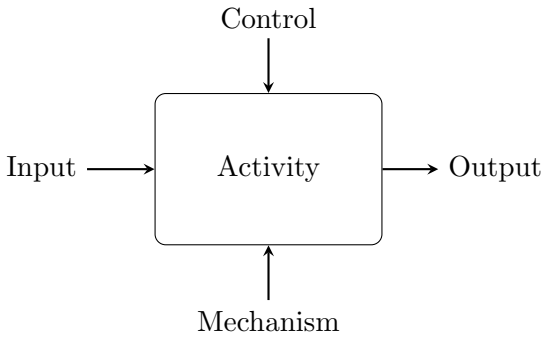

Figure 2.6: Standard SADT activity labelling notation [97].

2.7 Summary of Literature Review

It is apparent from the reviewed literature that non-exhaust emissions (NEE) have become a significant contributor to overall emissions in the transport industries, as a result of a reduction in exhaust emissions (EE) from an increase in battery electric vehicles (BEVs) and stricter legislation. Therefore, in recent years, there has been a shift in focus from reducing EE to reducing NEE. The available braking literature reveals that the current uncoated GCI brake system has poor wear and corrosion resistance, leading to harmful PM emissions being released during a braking event. Biologically related studies indicate that such emissions can have detrimental impacts on human health and the environment, being linked to increased cancer risk, increased heart rate variability, and damage to the cardiovascular system and lungs. Recent brake research on alternative brake materials focusses mainly on the use phase of the rotor, neglecting the potential for problem shifting between phases of the life cycle. There are very few studies utilising LCA applications within the brake industry. The studies that do exist exclude the economic aspects and

non-energy related emissions, such as PM emissions due to brake wear, and do not consider the potential environmental benefits of reducing the weight of the rotor. The present study aims to bridge some of these gaps in the literature. It can also be argued that current LCA software packages do not offer the flexibility of methodological choices specific to the brake industry within the UK, hence the requirement for the development of a brake specific LCA model as outlined in Chapter 3.

Chapter 3

LCA Methodology and Model Development

3.1 Introduction

In this chapter, the goal and scope of the life cycle assessment are defined for the present study of automotive friction brakes. Following the ISO 14040 standard, unit processes, system boundary, and model parameters are established. First, the model development allows key environmental impacts on the input-output inventory of each unit process to be assigned to preselected impact categories. Second, the modelling parameters provide an overview of material selection and the assumptions used in both case studies. Finally, a novel adaptation of an existing Structured Analysis and Design Technique (SADT) was undertaken to enable a clearer understanding and interpretation of the LCA models.

3.2 LCA Model Development for Automotive Friction Brake Applications

Section 3.2 outlines the development of the methodological choices and LCA model codebase specific to brake rotor applications. This development was designed for transparency and adaptability to be carried forward for future use on any chosen brake rotor material or brake component.

3.2.1 System Boundary

Depending on the performance requirements, the braking systems differ from one application to the next. The importance of material characteristics varies depending on the vehicle in question. When considering high-performance vehicles and race cars, cost becomes less of a concerning factor and the weight of components is more crucial. However, for passenger vehicles, low brake rotor wear, minimal maintenance requirements, and low costs are more important factors [99, 100]. In the present LCA study, the methodological choices have been selected based on the design requirements for such passenger vehicles.

Defining a system boundary within the LCA is an important step. If the boundary becomes too large, the study can become very time intensive, and sufficient data can become impossible to gather. However, if this boundary becomes too small, the results can become misleading. Identical stages within the life cycle can be omitted in a comparative study while still producing identical LCA impact results [16]. Brake components outside of the friction pair (rotor and pad), such as callipers or hydraulic cylinders, are independent of the chosen rotor material. Their manufacture and disposal processes can be considered identical across all brake rotors, allowing for omission from the system boundary without alteration to the final comparative results. However, the frictional interface, performance, and emissions released during a braking event are dependent on both the pad and the rotor materials. Therefore, the inclusion of both the static and the rotating parts of the friction pair was required within the present study. The chosen system boundary is shown in Figure 3.1. Note that closed-loop recycling (shown in green dashed lines) within the figure is only possible if the rotor material in question has a coating or surface treatment applied which can be removed for subsequent re-coating and re-use.

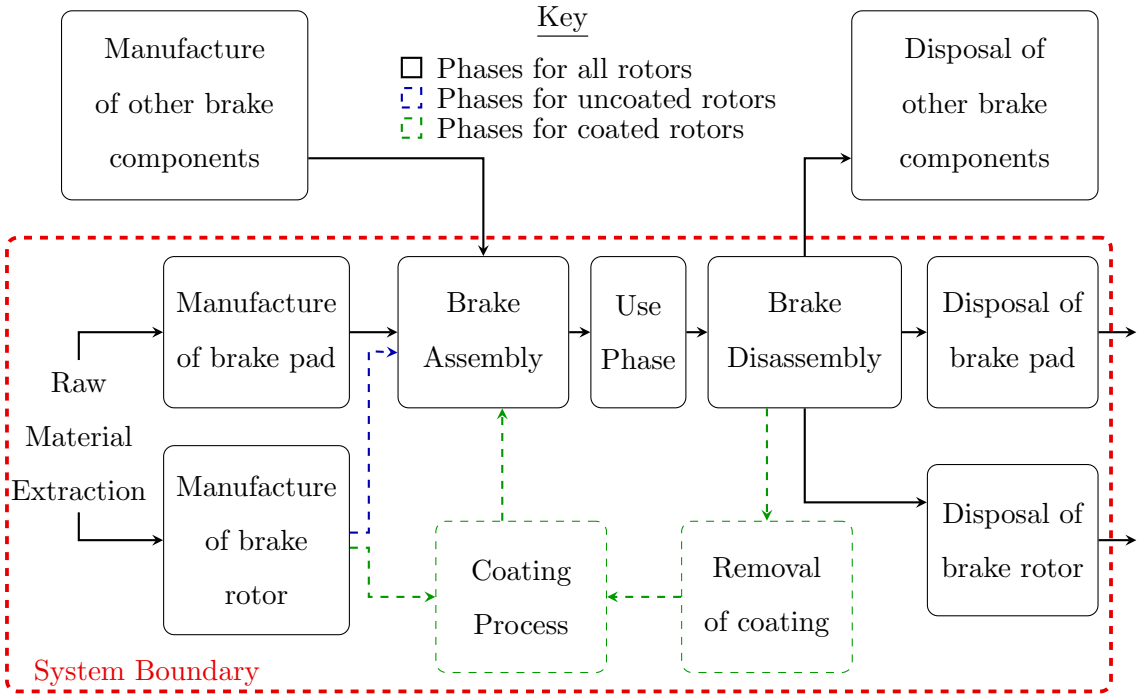

Figure 3.1: System boundary for automotive friction braking system.

3.2.2 Functional Unit (FU) Definition

The Functional Unit (FU) is used to provide a quantifiable description of the output of the product system that is constant for all products within a comparative study. The function of a frictional disc braking system is to decelerate the vehicle, or even bring it to a full stop, converting kinetic energy into heat via friction. For a comparative study,

the length of the use phase must be specified. The determination of this lifespan is a crucial decision. Increasing the length of the use phase could effectively amplify its significance, diminishing other phases. A study by Weymar and Finkbeiner [101] sampled more than 800,000 vehicles in Germany, performing a statistical analysis on the empirical lifetime of the vehicle for the purposes of an automotive LCA. Their conclusion was that a range of 170,000 km to 230,000 km was typical for passenger vehicles, depending on vehicle model and engine type, giving an average lifespan of 200,000 km for their LCA model in 2016. A separate report for the European Commission [102] suggests that the lifetime of road vehicles has increased linearly with the year of manufacture. Assuming that this linear trend continues beyond 2013 (limit of the European Commission data), the data can be extrapolated to provide a lifetime value for 2024, as shown in Figure 3.2. This extrapolation provides an average lifetime for petrol and diesel vehicles for 2016 of 200,159 km. This agrees well with the 200,000 km assumed by Weymar and Finkbeiner [101], providing validation for such an extrapolation. Further extrapolation, as shown in Figure 3.2, predicts a vehicle lifetime value of 242,268 km for 2024. This value will be rounded to 240,000 km for simplicity. The use of 240,000 km offers an additional benefit for model validation against the LCA study conducted by Gradin et al. [16], who applied the same distance. Therefore, the FU for the present study was defined as the deceleration of a vehicle over a lifetime of 240,000 km. This lifetime was modelled under the WLTP cycle to align with Euro 7 legislation. Therefore, FU could be alternatively defined as the deceleration of a vehicle over a lifetime of 1250 WLTP cycles (a WLTP models a driving distance of 192 km).

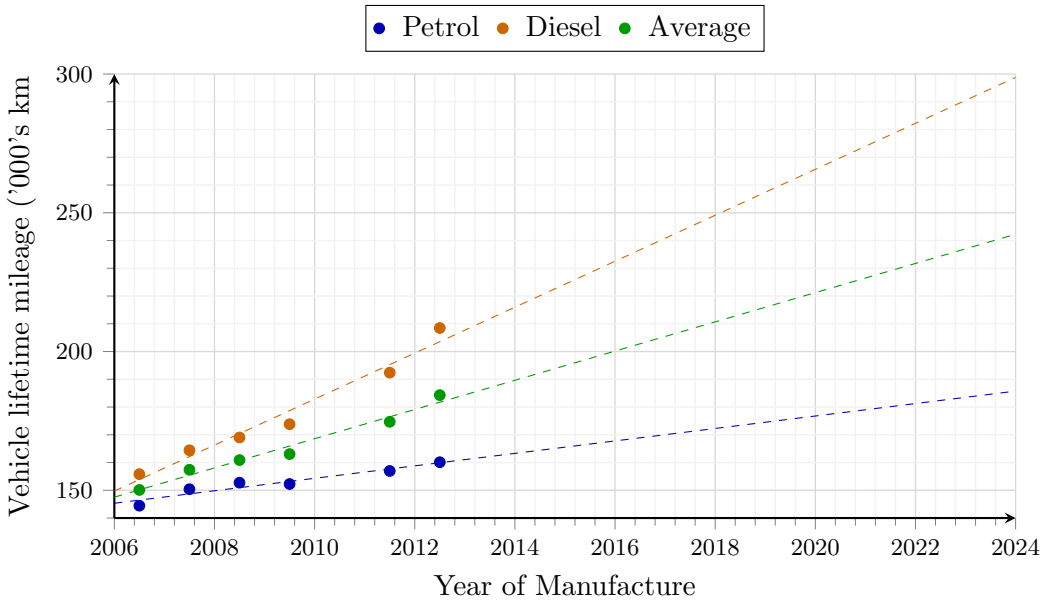

Figure 3.2: Data extrapolation based on a report for the European Commission to determine the average vehicle lifetime (km) for 2024.

3.2.3 Allocation Methods

The chosen allocation method has influence on the final results of an LCA study. Several allocation methods exist. These include economic allocation, mass allocation, system expansion, system reduction, and physical causation [40]. Physical causation would be the most suitable for coating processes involving chemical reactions, where scientific arguments and chemical equations can be utilised. However, the same allocation method must be used throughout the full life cycle for all brake rotors. This method therefore could not be applied because only some stages possess equations that are known. ISO 14044/14048 recommends avoiding system expansion as this can result in intractably large systems [14]. LCA studies are primarily based on mass flow analysis; therefore, mass allocation is the most commonly applied method. For this reason, this was the methodology selected for the present LCA study. An example of how this was applied was how the impacts of landfill or energy requirements were assigned to the rotor based on the weight of the brake rotor in question.

3.2.4 Life Cycle Impact Assessment

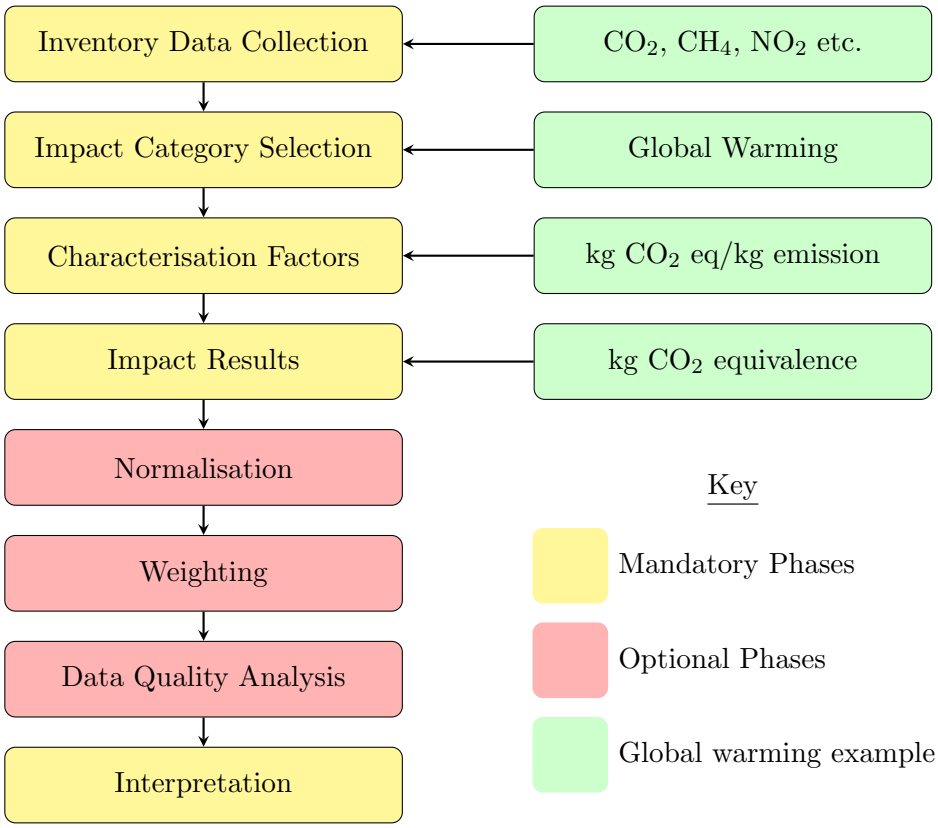

Figure 3.3: Procedure for LCA impact analysis (global warming example).

The energy and emissions inventory data provided in kilowatt hours, grams or tonnes are difficult to interpret and typically confidential. Additionally, they do not provide

information on how the environment or human health is impacted. Life cycle impact assessment is used to compile, interpret, and weight the results in a consistent and easily understandable method. According to ISO 14040 standard procedures, this impact assessment contains both mandatory and optional phases, as summarised in Figure 3.3, and detailed in Sections 3.2.4.1 and 3.2.4.2.

3.2.4.1 Mandatory Phases

The mandatory phases of any LCA study include the selection of impact categories, characterisation factors, and the generation of impact results. In previous LCA applications on braking systems, such as Olofsson's study on refinishing laser-clad rotors [95], only energy usage and CO_2 footprint were investigated. However, when considering human health, categories such as human toxicity and fine particulate matter formation are also important, especially the latter with the imminent introduction of Euro 7 legislation.

When considering which impact categories to investigate, they can be grouped into three sections [14]:

1. Output-based (global warming, stratospheric ozone depletion, photochemical ozone formation, acidification, eutrophication, and fine particulate matter formation).
2. Toxicity-related (human toxicity and ecotoxicity).
3. Resource-related (fossil and mineral resource scarcity).

Eutrophication is a fairly unknown impact category in which an environment can become enriched with nutrients, such as nitrogen and phosphorus from fertilisers, leading to excessive growth of plants and algae. Blooms of mucus-forming harmful algae were found in European waters as a direct result of an increase in the nitrate content. An increase in the number of plants has also been associated with oxygen depletion in certain areas [50, 51].

The ReCiPe 2016 methodology [49] was applied throughout the impact assessment phase of the present LCA study. This methodology was chosen because of its ability to map the standard impact categories (called midpoint impact categories within ReCiPe) used in previous LCA studies to fewer but broader endpoint categories. These endpoint categories include damage to human health, damage to ecosystems, and damage to resource availability. The process of mapping midpoint categories to endpoints is done through damage pathways. An example of this process is how particulate matter formation can

increase respiratory disease, therefore damaging human health. Each damage pathway is illustrated in Figure 3.4. The main benefit of including these endpoint categories is that they provide a more general overview to the user, directly comparing the impacts on the environment with those on human health. The inclusion of these endpoint categories provides added value to the present LCA study compared to past applications of the brake rotor technique.

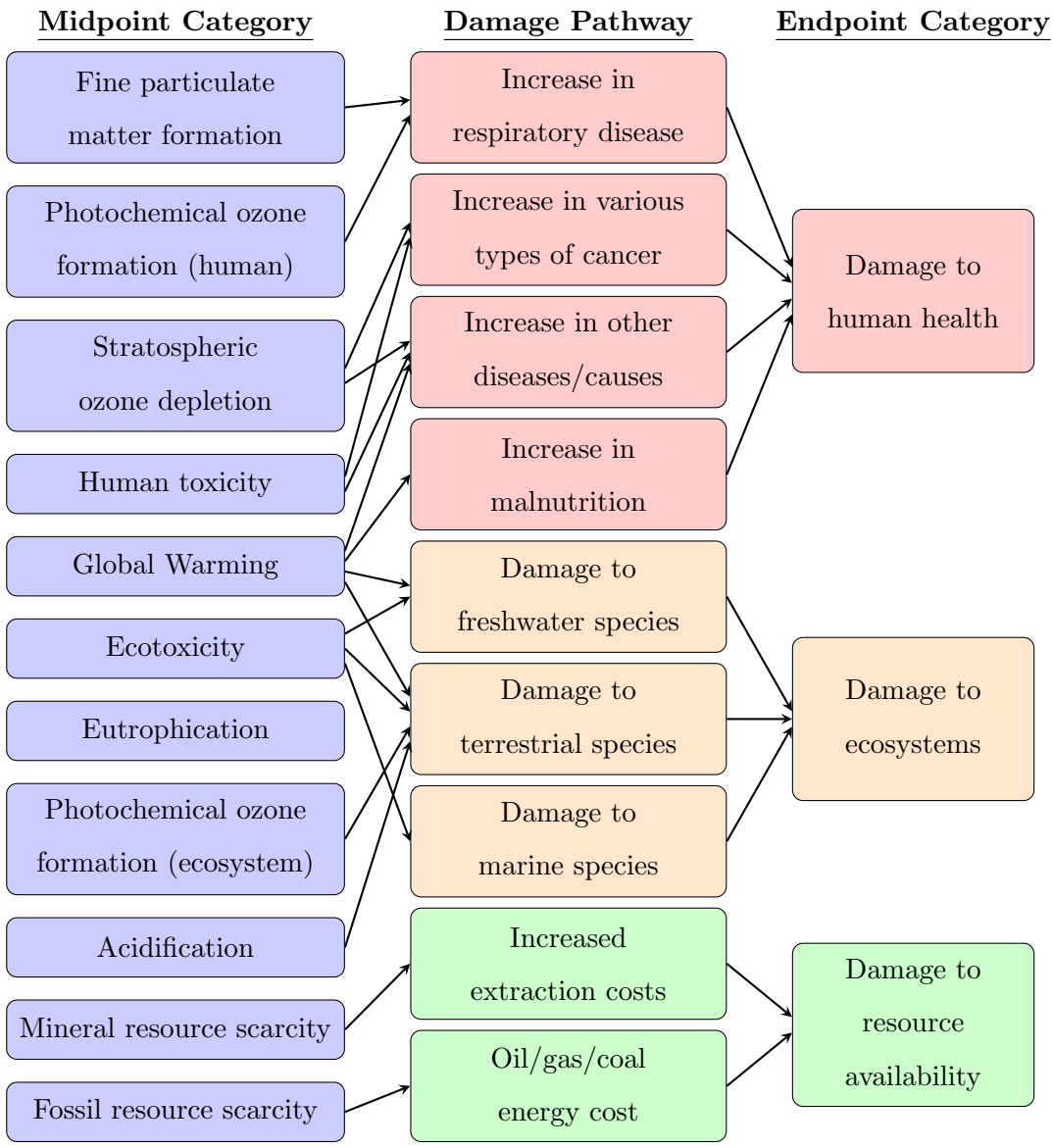

Figure 3.4: Damage pathways to map midpoint impact categories onto endpoint impact categories utilising the ReCiPe 2016 methodology [49].

Based on ISO standards guidelines and the LCA study conducted by Gradin and Åström [16, 103], a set of midpoint impact categories were selected for use in the present study. These midpoint and endpoint impact categories are presented in Tables 3.1 and 3.2, together with the selected unit and characterisation factors (CF). CFs are utilised to map the inventory data onto each impact category using Equations 3.1 and 3.2.

$$Midpoint\ Impact = Midpoint\ CF \times Inventory\ Data \tag{3.1}$$

$$Endpoint\ Impact = Endpoint\ CF \times Midpoint\ Impact \tag{3.2}$$

There are many sources that CFs can be selected from, all slightly altering the impact results. The ReCiPe methodology is the only one that includes endpoint impacts, and therefore the endpoint CF values had to be sourced from the ReCiPe databases. Impact categories and units can vary from source to source; therefore, to align with the endpoint category conversions, the ReCiPe databases were also the main source for midpoint CF values. However, for some inventory data, factors were not present within the ReCiPe database or, in cases such as eutrophication, were divided between freshwater and marine, each with different units. Therefore, where necessary, alternative sources were used [104]. How these alternative values were adapted to align with the ReCiPe methodology is explained in the footnotes of Tables 3.1 and 3.2. When selecting which CFs to apply, the time frame of the impacts should be considered. ReCiPe uses three different impact approaches: individualist (20 years), hierarchist (100 years), and egalitarian (1000 years). The IPCC (Intergovernmental Panel on Climate Change) advised against the use of more than 500 years, due to large uncertainties regarding background concentrations and their consistency. Meanwhile, a 20-year span is considered too short and does not provide adequate overview of long-term impacts [105, 106]. Therefore, for the present LCA study, the hierarchist (100-year timescale) was applied. This approach also allows comparability with other impact methods chosen because of its wide use.

Table 3.1: Midpoint impact categories and characterisation factors based on a hierarchist approach.

Impact Category	Inventory Loading	Characterisation Factor Value	Characterisation Factor Unit	Source
Global warming	CO_2	1	kg CO_2 eq.	ReCiPe 2016 [49]
	NO_2	298		
	CH_4	34		
Stratospheric ozone depletion	N_2O	0.011	kg CFC_{11} eq.	ReCiPe 2016 [49]
	CH_3Cl	0.022		
	CCl_4	0.895		
Fine particulate matter formation	$PM_{2.5}$	1	kg $PM_{2.5}$ eq.	ReCiPe 2016 [49]
[a]Acidification	SO_2	1	kg SO_2 eq.	ReCiPe 2016 [49]
	[b]NO_x	0.36		
	NH_3	1.96		

Continued on next page...

...Continued from previous page

Impact Category		Inventory Loading	Characterisation Factor Value	Characterisation Factor Unit	Source
[c]Photochemical ozone formation		[b]NO_x	1	kg NO_x eq.	ReCiPe 2016 [49]
		NMVOC	0.235		
[d]Photochemical ozone formation		CO	0.013	kg NO_x eq.	CML [107]
		CH_4	0.003		
		SO_2	0.023		
Human toxicity	[g]Emitted to air	SO_2	0.096	[e]kg 1,4-DCB eq.	CML [107]
		[b]NO_x	1.2		
		PM_{10}	0.82		
		NH_3	0.1		
[f]Human toxicity	[g]Emitted to air	HC	17.9	[e]kg 1,4-DCB eq.	ReCiPe 2016 [49]
		Heavy metals	1.11×10^{5}		
	Emitted to freshwater	HC	0.546		
		Heavy metals	3.66×10^{4}		
[h]Ecotoxicity	[g]Emitted to air	HC	19.8	[e]kg 1,4-DCB eq.	ReCiPe 2016 [49]
		Heavy metals	1.19×10^{6}		
	Emitted to freshwater	HC	58		
		Heavy metals	214		
Eutrophication		[b]NO_x	0.049	[i]kg P eq.	CML [107]
		NH_3	0.116		
		COD	7.26×10^{-3}		
		Phosphate	0.33		
		Nitrate	0.033		
Mineral resource scarcity		Iron ore	0.0175	kg Cu eq.	ReCiPe 2016 [49]
		Iron	0.0619		
		Aluminium	0.169		
		Bauxite	4.58×10^{-3}		
		Magnesium	0.79		
		Titanium	0.879		
		Chromium	0.0951		
Fossil resource scarcity		Crude oil	1	kg Oil eq.	ReCiPe 2016 [49]
		Natural gas	0.84		
		Hard coal	0.42		

Continued on next page...

...Continued from previous page

Impact Category	Inventory Loading	Characterisation Factor Value	Characterisation Factor Unit	Source
Fossil resource scarcity	Brown coal	0.22	kg Oil eq.	ReCiPe 2016 [49]
	Peat	0.22		

[a] Figures in acidification are for terrestrial acidification
[b] Figure for NO_2
[c] Values from ReCiPe are taken as a mean between human damage and ecosystem damage.
[d] Figures for Photochemical ozone formation from CML source are provided with the unit kg ethylene eq. These values require conversion into kg NOx equivalent, utilising the CF for ethylene in that category.
[e] 1,4-DCB eq. refers to 1,4-Dichlorobenzene equivalence.
[f] ReCiPe human toxicity figures are taken as a mean between carcinogenic and non-carcinogenic values.
[g] Figures from ReCiPe for emissions to air are taken as a mean value between urban and rural air. This calculation is not needed for CML as the CF provided are not divided between urban and rural air.
[h] Ecotoxicity figures are taken as a mean of terrestrial ecotoxicity, freshwater ecotoxicity and marine ecotoxicity.
[i] CML provides eutrophication values under the unit kg PO_4^{3-} equivalent. These values are converted into kg P equivalent utilising the characterisation factor within freshwater eutrophication from ReCiPe for PO_4^{3-} of 0.33 kg P eq.

Table 3.2: Endpoint impact categories and characterisation factors based on a hierarchist approach.

Impact Category	Inventory Loading	Characterisation Factor Value	Characterisation Factor Unit	Source
Damage to human health	Global warming	9.28×10^{-7}	DALY	ReCiPe 2016 [49]
	Stratospheric ozone depletion	5.31×10^{-4}		
	Fine particulate matter formation	6.29×10^{-4}		
	Photochemical ozone formation	9.10×10^{-7}		
	[a]Human toxicity	1.77×10^{-6}		
[b]Damage to ecosystems	Global warming	1.40×10^{-9}	Species.year	ReCiPe 2016 [49]
	Photochemical ozone formation	1.29×10^{-7}		
	Acidification	1.12×10^{-7}		
	Ecotoxicity	2.70×10^{-10}		
	Eutrophication	6.71×10^{-7}		
Damage to resource availability	Mineral resource scarcity	0.23	USD2013	ReCiPe 2016 [49]
	[c]Fossil resource scarcity	Crude oil - 0.46		
		Natural gas - 0.3		
		Hard coal - 0.34		

[a] Figures taken as mean between carcinogenic and non-carcinogenic human toxicity.
[b] Figures taken as mean between damage to terrestrial ecosystems, damage to freshwater ecosystems and damage to marine ecosystems where applicable. Eutrophication figure is only from damage to freshwater ecosystems due to marine ecosystems utilising the unit kg N eq. instead of kg P eq.
[c] There is no midpoint to endpoint characterisation factor for fossil resource scarcity. The endpoint impact is calculated directly from each fossil resource.

On occasion, there are some minor LCA impact loadings that are either not assigned to an impact category or for which a characterisation factor is not present. These are typically deemed to have a negligible effect, or the assessment of such loadings is involved in the ongoing development of techniques within the LCA impact method. Emissions typically released into water are found to be of this type due to dilution effects (except heavy metals and hydrocarbons) [108].

3.2.4.2 Optional Phases

Within the LCA, there are optional phases that are not required to complete an LCA study; however, they may improve the interpretation and clarity of the results. Firstly, normalisation can be performed. This is where the impact score is divided by a reference value to better understand the magnitude of each impact result [14]. For non-comparative studies the value used is typically the total output from the UK (or other relevant location) for each corresponding impact category. For products where different sections of the lifecycle take place in different countries, more generic total outputs would need to be used, for example, European or global totals could be implemented. Alternatively, a more simplistic approach for comparative studies is to divide each score by the maximum value for that impact category, normalising all results to an effective maximum score of 1. This method offers a higher level of interpretability to end users, who may not understand what the units for each impact category represent, or the significance of their magnitude. Therefore, this was the normalisation method selected in the present LCA study. Equations 3.3 and 3.4 were implemented to calculate such normalised values.

$$Midpoint\ Normalised\ Impact = \frac{Midpoint\ Impact\ Score}{Maximum\ Midpoint\ Impact\ Score} \tag{3.3}$$

$$Endpoint\ Normalised\ Impact = \frac{Endpoint\ Impact\ Score}{Maximum\ Endpoint\ Impact\ Score} \tag{3.4}$$

The second optional LCA phase is to weight the results based on their level of significance or desirability. As there is no scientific method for this weighting process during the presentation of LCA results, a consensus between stakeholders is usually needed. In the case of the braking industry, the three categories generally of greatest concern are PM emissions and the global warming effect at the midpoint level and the damage to human health at the endpoint. However, when conducting comparative studies, ISO [40] does not recommend the use of weightings, so this optional phase has not been officially

included in the present study for the presentation of results. Nonetheless, the increased importance of certain categories was considered when discussing impact scores within the LCA interpretation phase in Chapter 7.

The final optional phase of an LCA study is to test the validity of methodological decisions and environmental impacts. This process can also be used to refine the goal and scope based on the generated results. Typically, the parameter alterations that are required to be tested as optional sensitivity studies are determined after initial results have been generated.

3.2.5 Code Base Development

In the present study, the LCA model was built using Python and the accompanying Pandas library [109, 110]. The advantage this offers over other LCA software packages is full transparency and adaptability of the methodological choices, allowing for future optimisation specific for brake system applications. Both Python and the accompanying libraries offer maturity and stability for a broad audience, due to their open-source codebase. The Pandas library can offer automatic data alignment, indexing, and straightforward data manipulation [109]. These features make it an ideal tool for LCA, where a wide range of inventory can be implemented, whilst ensuring alignment of emissions data when calculating impacts. Python also offers excellent integration with General User Interface (GUI) development for a user-friendly experience. Using a GUI ensured that the modelling inputs were easily adaptable for future use on alternative materials by external users. GUI integration was achieved using the PyQt library, a commonly used tool for a variety of applications, from the development of accounting programmes to the visualisation of engineering problems [111]. The PyQt library allowed for full customisation of user inputs and display options for the generated results.

The specification of the GUI for the present study is described in Figure 3.5. It may not be possible to include all unit processes within the life cycle of the brake rotor due to data availability, leading to partial case studies being conducted. For example, a coating company may want to directly compare two coating processes but does not have the capability to gather data from the use phases. Therefore, it was important to incorporate the option to include any combination of the brake system life cycle phases in the GUI, as shown in the checklist tab in Figure 3.5. The user can first select the file path for where the inputted and outputted excel sheets will be stored, before selecting the relevant inventory document. The properties of the brake rotor are required to determine the

number of rotors required per FU duration, as well as the fuel consumption associated with the weight of the brake rotor. The inventory collected during testing was for a small scale set up, therefore it was important to include the relevant scaling parameters to allow for accurate extrapolation.

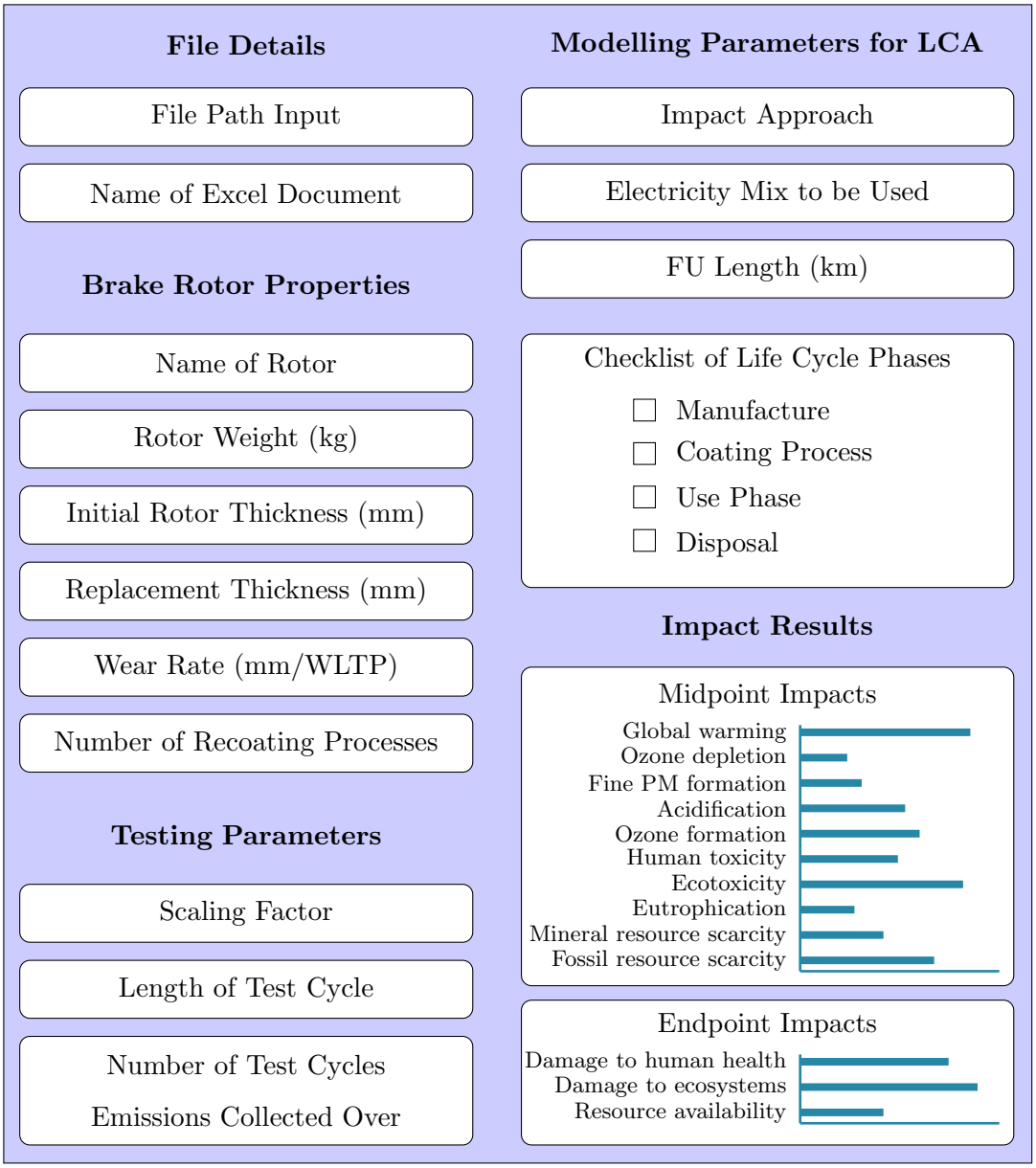

Figure 3.5: Design Specification for Python LCA model GUI.

The design of this Python model imported the inventory data from formatted Excel sheets. The final impact results were then exported back into an excel document within the predefined file path. Microsoft Excel is a flexible tool for structuring the collection of inventories, allowing widespread usage, and providing easy adoption of the model. Data sheets within Excel also allowed for good readability, facilitating easy collaboration with industrial partners on data collection [108]. To ensure compatibility between the Excel sheets and the Python model, there needed to be consistency with how the Excel inventory sheets are setup. The Python model required the Excel sheets to possess specific names

to ensure full readability of the ticked life-cycle phase data tables. If the life cycle phase was to be included in the study, then the appropriate sheet name from Table 3.3 was implemented. It was also crucial to remember that a Python script is case-sensitive.

Table 3.3: Required Excel sheet names for unit process inventory within excel document to be readable by Python model.

Life Cycle Phase		Sheet Name
Manufacturing process of the brake rotor	-	Manufacture of Rotor
Manufacturing process of the brake pad	-	Manufacture of Pad
Coating process for the rotor should a coating be added	-	Coating Process
Use phase (1250 WLTP cycles/240,000 km)	-	Use Phase
The removal process of the coating if there is one, either for reuse of the rotor material or for rotor disposal	-	Coating Removal
Disposal or recycling process of the brake rotor	-	Disposal of Rotor
Disposal or recycling process of the brake pad	-	Disposal of Pad

Once the excel sheets were read into the model, it was important that the table headings also remain consistent to ensure that the Python code knew where to find the correct data for manipulation. Figure 3.6 shows the correct table layout to use, with some examples of data input. Columns from E onwards vary depending on what unit process the inventory is for. These unit process titles were extracted to be applied as headings for the final impact results. However, the column titles for A-D had to remain unchanged, ensuring compatibility with the CF tables.

A	B	C	D	E	F	G
Flow Name	Flow Class	Emission Type	Unit	Iron Ore Mining	Iron Smelting	Casting
CO2	emissions	to air	kg	0.00	7.65	0.00
energy	rources	resources	kWh	0.02	0.31	4.05
heavy metals	emissions	to water	kg	0.00	0.00	0.00

Figure 3.6: Required column headings for the inventory tables within each excel sheet for correct data manipulation within Python environment (GCI manufacture example).

To ensure full transparency of the methodology applied within the Python model and to ensure easy adaptability and development of the codebase, appropriate documentation was required. Figure 3.7 outlines the flow diagram for each stage of data manipulation within the Python model. Customisability of the code was crucial to be able to test the sensitivity of the method choices and assumptions on the end impact results. Therefore, the electricity mix used, use phase duration, number of recoatings, and impact approach have all been coded as customisable inputs within the GUI.

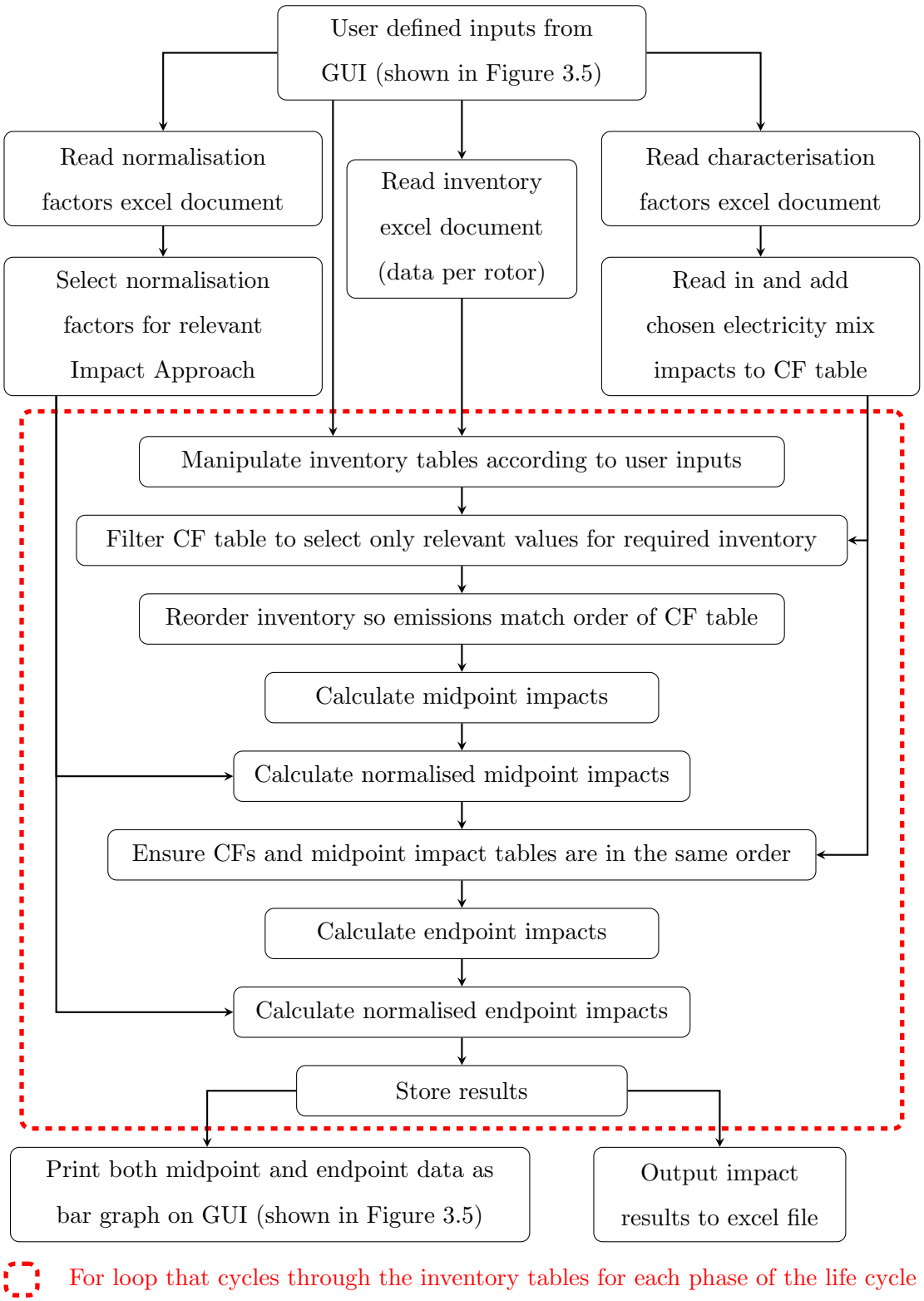

Figure 3.7: Flow diagram for the coding process to generate impact results and output them as an excel file.

The nature of the Python model is that each rotor had to be tested individually. Therefore, the comparative normalisation method used in the case studies to scale the impact scores between 0 and 1 could not be applied within the code. However, future users may require the use of the LCA model to investigate one material rather than conducting a comparative analysis, and so it was important to still include some form of normalisation of results

within the Python codebase. The normalisation method of dividing the impact score by the total output for that location was applied. The ReCiPe methodology [49] database provided such normalisation factors (NFs) to calculate normalised midpoint and endpoint impact values. The reason these were only used within the Python model and not for the present comparative study was that the values were slightly outdated, based on a world population from 2010. To calculate the normalised results within the codebase, Equations 3.5 and 3.6 were implemented. The normalisation factors that were applied within the Python code are outlined in Tables 3.4 and 3.5 [49]. These values normalise the impact scores per person, based on a 2010 world population of 6.9 billion.

$$Midpoint\ Normalised\ Impact = \frac{Midpoint\ Impact\ Score}{Midpoint\ NF} \tag{3.5}$$

$$Endpoint\ Normalised\ Impact = \sum_{\substack{\text{Endpoint}\\ \text{Category}}} \frac{Endpoint\ Impact\ per\ Midpoint\ Category}{Endpoint\ NF} \tag{3.6}$$

Table 3.4: Midpoint normalisation factors based on a hierarchist approach (per person in 2010).

Midpoint Category		Unit	Normalisation Factor
Global warming		kg CO_2 eq. per person	6.89×10^3
Stratospheric ozone depletion		kg CFC_{11} eq. per person	0.06
Fine PM formation		kg $PM_{2.5}$ eq. per person	25.6
Acidification		kg SO_2 eq. per person	41
Photochemical ozone formation		kg NO_x eq. per person	19.2
[a]Human toxicity		kg 1,4 – DCB eq. per person	1.56×10^4
[b]Ecotoxicity		kg 1,4 – DCB eq. per person	8.27×10^5
[c]Eutrophication		kg P eq. per person	0.65
Mineral resource scarcity		kg Cu eq. per person	1.20×10^5
[d]Fossil resource scarcity	Crude oil	kg Oil eq. per person	569.9
	Natural gas		0.4
	Hard coal		381.51
	Brown coal		31.46

[a] Figure is a mean value between carcinogenic and non-carcinogenic human toxicity.
[b] Figures taken as mean between terrestrial ecotoxicity, freshwater ecotoxicity marine ecotoxicity where applicable.
[c] Eutrophication figure is only from freshwater eutrophication due to marine eutrophication utilising the unit kg N eq. instead of kg P eq.
[d] Normalised fossil resource scarcity figure generated from fossil resources rather than fossil resource midpoint impact value.

Table 3.5: Endpoint normalisation factors based on a hierarchist approach (per person in 2010).

Endpoint Category	Midpoint Category		Normalisation	
	Category	Unit	Unit	Factor
Damage to human health	Global warming	kg CO_2 eq.	DALY per person	7.42×10^{-3}
	Stratospheric ozone depletion	kg CFC_{11} eq.		3.19×10^{-5}
	Fine PM formation	kg $PM_{2.5}$		1.61×10^{-2}
	Photochemical ozone formation	kg NO_x eq.		1.80×10^{-5}
	[a]Human toxicity	kg 1,4-DCB eq.		1.21×10^{-4}
[b] Damage to ecosystems	Global warming	kg CO_2 eq.	Species.year per person	1.12×10^{-5}
	Photochemcial ozone formation	kg NO_x eq.		2.24×10^{-6}
	Acidification	kg SO_2 eq.		8.42×10^{-6}
	Ecotoxicity	kg 1,4-DCB eq.		2.73×10^{-4}
	Eutrophication	kg P eq.		4.90×10^{-7}
Damage to resource availability	Mineral resource scarcity	kg Cu eq.	USD2013 per person	2.77×10^{4}
	Fossil resource scarcity	kg Oil eq.		2.91×10^{2}

[a] Figure is a mean value between carcinogenic and non-carcinogenic human toxicity.
[b] Figures taken as mean between damage to terrestrial ecosystems, damage to freshwater ecosystems and damage to marine ecosystems where applicable. Eutrophication figure is only from damage to freshwater ecosystems due to marine ecosystems utilising the unit kg N eq. instead of kg P eq.

3.3 Modelling Parameters for Case Studies

Within the present research, one of the objectives was to develop a methodology and an LCA model that will be used in future analysis of alternative brake rotor materials. To test the accuracy and robustness of the model, it was important to conduct case studies. Section 3.3 outlines the process used to collect inventory data and perform impact analysis on the selected rotor materials. The inventory per brake rotor was collected within Microsoft Excel sheets as detailed in Section 3.2.5. The Python model was used to generate impact results from the inventory data, which were then interpreted and analysed. The Python model GUI and full Python code are provided in Appendices B and C, respectively. When considering the case studies conducted for the present study, it was important to outline the more specific parameters that were used, such as the assumptions of the model. These assumptions have been applied to all four rotor materials reported in Chapters 5, 6 and 7 and can be extended to future brake rotor materials or adapted where required.

3.3.1 Selection of Case Study Materials and Coating Techniques

There are three potential overarching categories of brake rotors on which case studies could have been carried out. The first was the current uncoated GCI rotor, the second was a hard-coated GCI rotor, and the third was a lightweight alternative rotor. In the present LCA study, the standard uncoated GCI was used to provide a baseline for the comparison of the other two categories. One particular type of rotor was selected from each of these two categories based on what the literature indicated as the most suitable option, as well as on what data were available.

For the hard-coated GCI rotor, only a few coating methods were considered suitable for brake rotor applications. Traditional laser cladding (with standard feedstock powders) and PTA (plasma transferred arc) are typically nickel-based and copper-based processes, and so were ruled out of consideration because of environmental and cost concerns [21]. Hard chrome plating can produce carcinogenic toxic mist as a result of the inclusion of hexavalent chromium. Therefore, hard chrome was also not considered a suitable option within the braking industry [61, 62]. As discussed within the literature review (Chapter 2) HVOF (high velocity oxygen fuel), HVAF (high velocity air fuel), and EHLA (extreme high speed laser cladding) are all viable techniques that can be applied to a GCI brake rotor. The selection of EHLA for this study was primarily based on data availability but also on the speed of the application. Coordination with TWI (one of the leading developers of the technology) and Cummins-Meritor (who design and manufacture brakes for commercial vehicles) allowed small-scale samples to be produced. Such small-scale samples were cut from a full-size laser-clad GCI brake rotor and tested for PM emissions using the small-scale rig described in Chapter 4.

Coated metal alloys are the most advantageous solution for allowing a lightweight alternative rotor to be used in normal road vehicles. As discussed in the literature review, this was mainly due to carbon fibre composites being much more costly and metal matrix composites (MMCs) possessing lower maximum operating temperatures. MMCs are also typically more prone to corrosion effects than a coated Al rotor [44, 45]. The advantages and disadvantages of the various coating techniques are thoroughly discussed in the literature review. However, in summary, techniques such as APS (atmospheric plasma spray) were found to contain cracks, while CGDS (cold gas dynamic spray) was found to have poor wear resistance [21, 84]. PEO (plasma electrolytic oxidation) treated Al alloy rotors, on the other hand, offer an increased hardness and a more stable coefficient

of friction [45, 65]. Due to a close collaboration with Curtiss-Wright (Keronite), who specialise in PEO surface treatment, primary data for this coating technique were readily available. This surface treatment on both wrought and cast Al substrates was previously tested by Limmer [1] on the same small-scale test rig that was used in this present study for the laser-clad GCI rotor samples. This enabled a higher comparability of results between the two distinct categories of rotors.

3.3.2 Case Study Assumptions and Data Collection

The modelling assumptions can be divided into four main categories, surrounding the pad, the rotor, the required transport, conversion methods between fossil fuel units, energy supply, and data collection. Assumptions surrounding the conversion between fossil fuel units were required, as databases typically provide fuel consumption in litres or megajoules, whereas the LCA inventory requires the crude oil equivalence in kg. All of these assumptions are generic and were applied to all rotor materials. In some cases, some small specific assumptions, surrounding just one rotor material, were required. These are detailed as each rotor material is discussed in Chapters 5 and 6.

3.3.2.1 Brake Pad

The constituents that go into the manufacture of friction materials are highly complex and confidential. Detailed data on the constituent materials and their processing were not readily available. Gradin and Åström [16] investigated omitting identical stages within a similar comparative LCA study. They found that the results remained accurate and reliable compared to the results without omissions. This principle was applied to the present LCA study to overcome the restriction of missing data, provided that the manufacture and disposal phases of the pad were identical. Therefore, it was assumed that the same low metallic (LM) brake pad type would be used in all the brake rotor materials considered. For the laser-clad GCI rotor and the uncoated GCI rotor, the small-scale test sample pads were cut from the same full-sized friction material, making them perfectly identical. However, the PEO treated Al tests were conducted utilising a very similar LM friction material, but with slight changes in the constituents. Despite these slight changes, it was still reasonable to assume that the manufacture inventory was nearly identical, with the slight variations contributing to less than 1% and therefore being negligible. Ventilation and filtering are used in friction material manufacturing plants, causing slight differences in the emissions released to be extracted from the atmosphere. When brake pads are disposed of, the friction material is typically mostly worn away. The impacts from disposal are therefore mainly attributed to the back plate, which is constant across

all rotors within the case studies. Therefore, the associated impacts of both brake pad manufacturing and disposal were not included in the present comparative LCA study. The effect on the differences between pad wear rates (which are known from the comparative small-scale tests reported in Chapter 4) is discussed within the interpretation of the LCA results (Chapter 7).

3.3.2.2 Brake Rotor

As part of the FU, to ensure a fair comparison, the same rotor dimensions had to be used. The dimensions of the rotor used within the case studies were based on the ventilated rotor investigated by Shrestha et al. [65] as part of the RELIABLE project at Curtiss-Wright (Keronite). This study compared a PEO treated wrought Al alloy rotor with a standard uncoated GCI rotor of the same dimensions. The use of these dimensions for the present LCA study meant that there was already data available on the PEO surface treatment process, rather than requiring estimations. The outer diameter of the rotor was 350 mm with a total cheek thickness of 28 mm. The weight of each rotor varied, so it was important to include the fuel efficiency and energy savings during use that was associated with each rotor. A fuel consumption factor (FCF) was applied to determine the fuel usage correlated with the weight of the rotors, using the Equation 3.7. The typical FCF for a petrol passenger car is 0.2-0.5 l per 100 kg per 100 km driven [16, 112]. In the present study, an average value of 0.35 l was applied per 100 kg per 100 km.

$$Petrol\ Use\,(l) = FCF \times \frac{mass_{rotor}\,(kg)}{100} \times \frac{FU\ length\,(km)}{100} \tag{3.7}$$

$$Fuel + XO_2 \Rightarrow YCO_2 + ZH_2O \tag{3.8}$$

The amount of petrol used can be directly linked to CO_2 exhaust emissions. Equation 3.8 demonstrates the chemical interaction when combustion occurs. Petrol is known to have a density of 0.737 kg/l, with a specific carbon content of 0.9 kg_C/kg_{fuel} [16]. To convert the masses of carbon into CO_2 emissions, the atomic masses of carbon and oxygen were considered, as shown in Table 3.6 [113]. This calculation is based on the electronic supplementary material provided as part of Gradin and Åström's LCA study [16].

Table 3.6: Atomic masses of C, O and CO_2.

Element/Compound	Atomic Mass
C	12
O	16
CO_2	44

The atomic masses shown indicate that 1 kg of carbon converts into 3.67 kg of CO_2 that generates Equation 3.9. SO_2 and NO_x emissions were excluded from this study, as they were considered negligible compared to CO_2. The decision to include CO_2 while omitting other potential emissions aligns with common practices in similar studies. Furthermore, emissions such as NO_x and CO are regulated by legislation, which typically leads to low levels.

$$CO_2\,(kg) = petrol\ use\ \ (l) \times 0.737 \times 0.9 \times 3.67 \tag{3.9}$$

3.3.2.3 Transport

The case study rotor was based on a generic UK ICE passenger vehicle. When considering the impacts related to the transport between phases of the life cycle, there were four main stages: manufacture to assembly, assembly to use, use to disassembly, and disassembly to disposal. Figure 3.8 outlines the simplified life cycle diagram, detailing where transport was required.

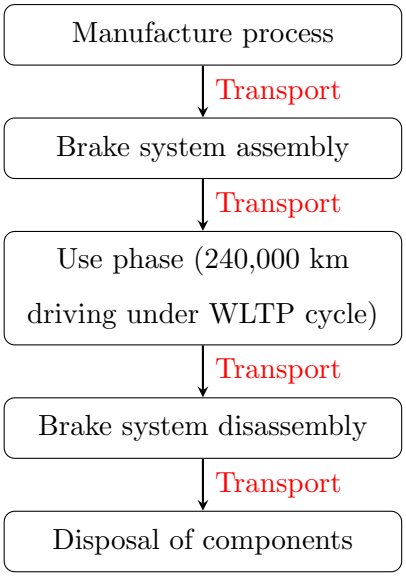

Figure 3.8: Life cycle transport requirements flow diagram.

It was assumed that for the use phase, each rotor material would be placed onto the same case study passenger vehicle. Therefore, any transport requirements from the assembly to use and from use to disassembly were considered identical between the rotors within the present LCA study and so were omitted. The transport required for disassembly to disposal was also assumed to be identical, assuming the same landfill location or recycling plant being used for all metals. Therefore, within the present comparative LCA study, the only transport impacts to be included were the manufacture to assembly (including the coating or surface treatment plant should such a process be required). The case study

vehicle was assumed to be from the Nissan factory in Sunderland, UK. Therefore, when calculating the required transport distances for manufacture to assembly, this was the location used.

The transport method used between each stage of the life cycle can influence the associated environmental impacts. If a material is flown halfway across the world for brake assembly, this could offset environmental benefits compared to a material sourced locally. All materials were assumed to be transported using commercial lorries with the exception of the use of cargo ships to cross the sea. When the vehicles transported the materials, it was assumed that they were fully loaded on delivery and empty on return. The mileage and transport used varied between different rotor materials as well as fuel efficiency. Fuel consumption (FC) was calculated using Equation 3.10.

$$FC\ \ (l/km) = \frac{FC_{fullload}\ \ (l/km) + FC_{empty}\ \ (l/km)}{2} \tag{3.10}$$

Similarly to the process outlined in Section 3.3.2.2, the associated CO_2 emissions were incorporated utilising Equation 3.9. FC values depend on the type of vehicle used. Table 3.7 [108] outlines the FC values for three types of vehicles. To reduce the carbon footprint, it was assumed that all materials were sourced within Europe.

Table 3.7: Transport fuel consumption data used within the present LCA study.

	Load limit (tonne)	FC (l/km, full loaded)	FC (l/km, empty)	FC (l/t*km)
Distribution truck	14	0.39	0.29	0.024
Long distance truck	32	0.47	0.29	0.012
Cargo Ship	n/a	n/a	n/a	0.003

3.3.2.4 Fossil Fuel Conversions

When considering the impacts of fossil fuels within LCA, the ReCiPe methodology requires the inventory to be categorised in its rawest form. This means that any inventory data collected surrounding diesel or petrol required conversion to a crude oil equivalence, or similarly coke was converted to a hard coal equivalence. Crude oil has an average percentage volume yield of 37.5% gasoline (petrol) and 33.5% diesel [114]. Hard coal has a much higher percentage yield, producing a 70% mass yield of solid coke [115]. Table 3.8 summarises the conversion factors used within the present LCA study.

Table 3.8: Conversion factors between fossil fuels and their sources.

Inventory	Value		Equivalence	Value	Source
Coke	1 kg	-	Hard Coal	1.43 kg	[115]
Diesel	1 kg	-	Crude Oil	2.99 kg	[116]
Petrol	1 kg	-	Crude Oil	3.13 kg	[116]
[a]Petrol	1 l	-	Petrol	0.73 kg	[116]
[b]Diesel	1 MJ	-	Diesel	0.02 kg	[116]

[a] Fuel consumption during use and transport is calculated in litres. Therefore, before this can be converted into crude oil equivalence, the mass of fuel must be calculated. In the case of the present study the fuel used is assumed to be petrol.
[b] Some inventory databases provide energy data in the form of MJ of diesel burned. This is therefore converted into mass of diesel prior to determining the crude oil equivalence.

3.3.2.5 Energy Supply

Most life cycle phases require energy generation. The proportion of non-renewable sources used can have a direct impact on the associated CO_2 emissions released and thus influence the effect on categories such as global warming. Stamford et al. [46] conducted a study investigating the impacts associated with energy generation based on different electricity scenarios. Five scenarios were researched; two based on a 65% reduction in greenhouse gas (GHG) emissions by 2050, one based on a 80% reduction in greenhouse gas (GHG) emissions by 2050 and two based on a 100% reduction in greenhouse gas (GHG) emissions by 2050. The scenarios 65% and 100% were subdivided according to the assumption if no new nuclear plants were built. Table 3.9 compares the UK electricity mix taken from the past year (July 2023 - July 2024) [117] with those predicted by each scenario for 2070. No scenario perfectly aligns with the UK mix, but since scenario 3 is the closest representation, this was the scenario applied to the initial results presented in Chapters 5 and 6. The effective characterisation factors were derived from the environmental and health impact results of the Stamford study, as these impacts were provided per kWh of energy, as shown in Table 3.10.

Table 3.9: Comparison of electricity scenarios to UK mix.

Scenario	Fossil Fuels	Nuclear	Renewables
1 (65%-a)	68%	0%	32%
2 (65%-b)	37%	30%	33%
3 (80%)	10%	29%	61%
4 (100%-a)	0%	0%	100%
5 (100%-b)	0%	50%	50%
UK mix	29%	14%	57%

Table 3.10: Midpoint characterisation factors for energy generation (scenario 3).

Midpoint Category	Characterisation Factor	
	Unit	Value
Global warming	kg CO_2 eq.	3.00×10^{-2}
Stratospheric ozone depletion	kg CFC_{11} eq.	2.80×10^{-9}
Photochemical ozone formation	[a]kg NO_x eq.	1.39×10^{-5}
Acidification	kg SO_2 eq.	2.40×10^{-4}
Eutrophication	kg P eq.	3.30×10^{-5}
Ecotoxicity	kg 1,4-DCB eq.	3.00×10^{1}

[a] Stamford [46] provides value for kg ethylene eq., which was converted into kg NO_x eq. using the ethylene CF value of 0.47 for that impact category.

There was a noticeable omission, from the midpoint impact categories investigated by Stamford, of the fossil resource scarcity from the coal and natural gas required to generate electricity. To overcome this problem, the required mass of coal and natural gas was determined using the percentage contributions per kWh of energy provided by Stamford. These masses were then added to the inventory and the standard ReCiPe 2016 CF values for hard coal and natural gas were applied. Table 3.11 outlines the data required for such a calculation using scenario 3.

Table 3.11: Energy density of coal and natural gas with scenario 3 contributions.

Description	Hard Coal	Natural Gas
% Contribution	9%	1%
kg/kWh [118]	0.124	0.094
kg/Nm^3	-	0.76 [119]

3.3.2.6 Data Collection

An important consideration for an LCA study is the availability of data and the sources used. Primary data were used where possible. Coordination with Curtiss-Wright (Keronite) and TWI was utilised for any required data surrounding the PEO surface treatment and the laser-clad coating process, respectively. Emissions during the use phase of each rotor were collected using a small-scale test rig based on the WLTP cycle. Most of these tests were conducted as part of previous PhD research [1], except for the laser-clad GCI rotor, the methodology and results of which are presented in Chapter 4. To fill in the data gaps surrounding material manufacture and disposal, secondary sources, such as the EcoInvent database [120, 121] were required. The inventory gathered could only be used for generic materials, without specifying the alloying type considered because these were secondary sources.

3.4 Adaptation of SADT Notation

System boundaries and life cycle diagrams can quickly become complex within LCA studies if every unit process phase at which data was gathered were included. A diagram such as the system boundary shown in Figure 3.1 can become difficult to follow once each process is broken down into the desired level of detail at which inventory data is gathered, as shown in Figure 3.9. Once all activity interactions are added to this diagram, the readability becomes very poor.

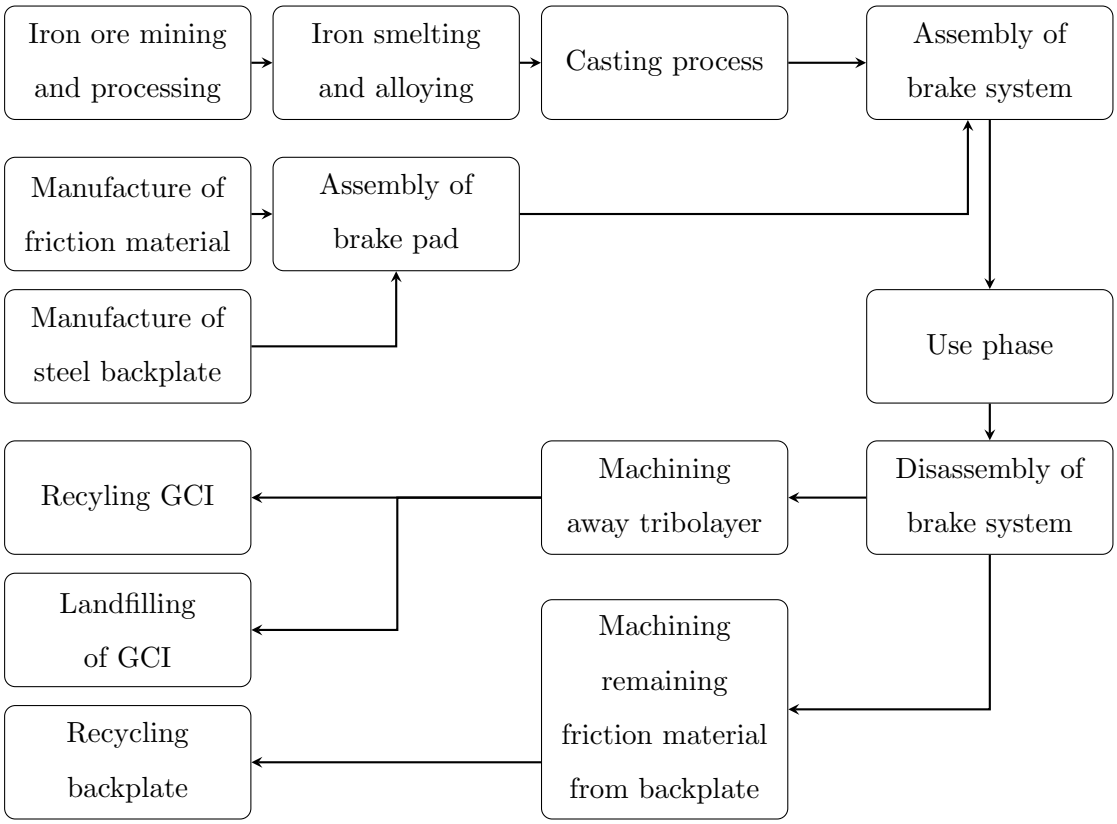

Figure 3.9: Unit process diagram for uncoated GCI braking system showing the high complexity and the requirement for simplification.

To deal with the complexity that can be associated with such LCA diagrams, in the present study a hierarchical systems analysis (SADT) process was adapted and used. SADT can be a useful tool for breaking down expansive diagrams into a more straightforward hierarchical approach. This process allows for easy adaptation and understanding when a small section is altered. An example of this would be for the uncoated GCI and laser-clad GCI rotors. The same diagram system could be used, with one small diagram added to describe the coating process. A high level of detail can be provided over several diagrams, each containing at most 3-6 life cycle processes as recommended for SADT. The SADT notation is initially designed for its applications in CAD and industrial projects.

Therefore, some adaptation was required to use in LCA studies. Typically, activities are represented as boxes, and the corresponding arrows represent activity interactions. These interactions are grouped into four categories (input, output, control, and mechanism), with each category assigned a different edge of the box as shown for traditional SADT in Figure 2.6.

For the adaptation of this notation for LCA applications, a greater focus was placed on inventory data collection. To replace traditional arrow labelling, the input and output arrows were redefined into two new categories and the control and mechanism arrows were removed. Inputs were now categorised between those from the technosphere (anything man-made) and those from the natural environment. The outputs were then classified into useful products and services and waste, by-products, and emissions. Figure 3.10 outlines the adapted diagram notation, with a definition for each process detailed in Table 3.12.

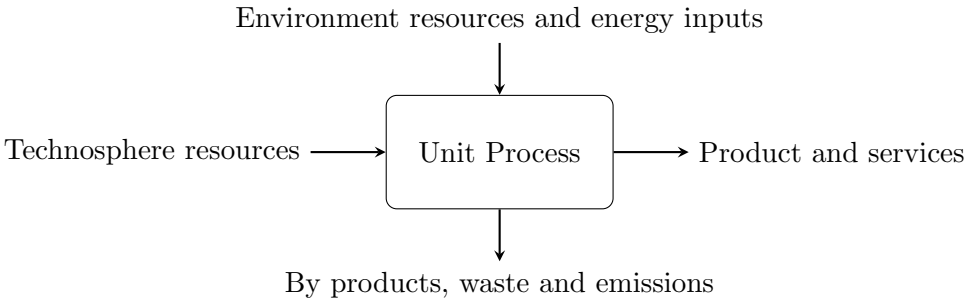

Figure 3.10: Adapted SADT diagram notation for LCA applications.

Table 3.12: Table of definitions for LCA unit process diagram notations.

Label		Definition
Unit process	-	Smallest element/activity analysed within the LCA inventory process where input and output data are quantified.
Technosphere resources	-	Inputs that are human made, including pre-products and materials.
Environmental resources and energy inputs	-	Input to the unit process that comes from the environment, including any energy inputs.
By-products, waste and emissions	-	Any output that is a by-product of the process (not the desired outcome), including the emissions released or any waste produced.
Product and services	-	The desired product from the process. Typically, this would be defined within the LCA functional unit.

Figure 3.11 demonstrates how this new notation and hierarchical approach can be applied to an LCA to simplify the diagrams used, thus improving readability and interpretability.

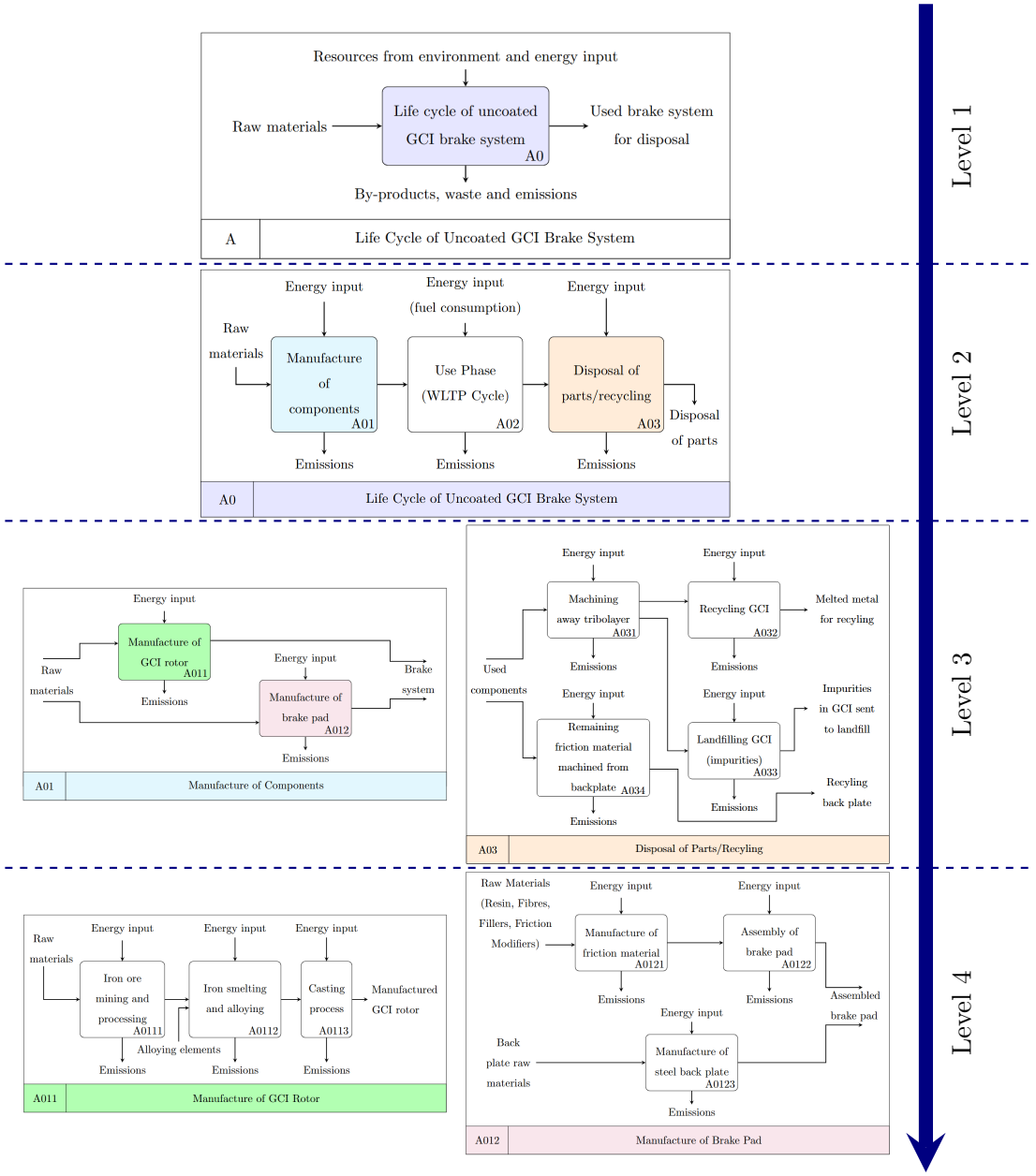

Figure 3.11: Hierarchical diagrams showing the life cycle of an uncoated GCI brake rotor utilising the SADT adapted for LCA (colour coded to relate to the parent diagram of the above level in the hierarchy.

The initial diagram in Figure 3.9, which contains 14 different activities, is reduced to a series of diagrams, each containing 3-6 activities. The top-level diagram (level 1) simply shows the overall activity being considered. For the braking system, this parent diagram outlines the overall inputs and outputs from the full life cycle of the brakes. Subsequent levels (2-5) break this activity down into more and more detail. Thus, the reader only needs to go down to the required level of detail for their needs. An added benefit of this method is that more detail can easily be added to any area of the life cycle by simply adding an extra hierarchical level. Colour codes were used to indicate which section of the

parent diagram each child diagram elaborated on. When emissions are mentioned, this refers collectively to all three emission pathways of air, water, and soil. The purpose of Figure 3.9 is to illustrate the hierarchical approach as opposed to providing details of the phases of the life cycle themselves. Clearer diagrams of each life cycle phase can be found in Section 5.2.1.

3.5 Summary of the Development of LCA Methodology and Modelling Approach

The system boundary of the present LCA model was defined to include both components of the friction pair (rotor and pad), but to exclude other components of the brake system, such as callipers. FU was defined as the deceleration of a vehicle for a lifetime of 240,000 km. It was assumed that since the same low metallic (LM) pad material was utilised on all four rotor materials (uncoated GCI, laser-clad GCI and PEO treated wrought and cast Al alloys), the manufacture and disposal phases of the pad material would be identical across the comparison, and so was omitted from the present study. However, PM emissions during the use phase differed as these depended on the wear rate of the pad material against different rotor surfaces. The transport between factories at different stages of the life cycle was assumed to be carried out purely by trucks and cargo ships, with the fuel economy calculations shown in Section 3.3.2.3. A Python model was built to manipulate the collected inventory data into useful impact categories at both the midpoint and the endpoint levels. This provided a good level of readability and transparency of the methodology applied, specific to automotive brake rotor applications. The adaptation of the SADT showed good promise in improving upon the complexity of LCA life cycle diagrams. This simplified approach offers improved readability and adaptability for future LCA studies.

Chapter 4

Laser-Clad GCI Emissions Testing

4.1 Introduction

As part of the present LCA study, particulate emissions during the use phase were collected from small-scale testing at the University of Leeds. The PEO treated wrought and cast Al and the uncoated GCI rotors underwent tests conducted by Limmer [1] as part of a previous doctoral research project. The same rig setup was used to collect particulate emissions data under the same methodology for the laser-clad GCI. Chapter 4 outlines the test setup that was utilised, presenting results on the CoF, wear rate, and PM emissions of the laser-clad rotor compared with the results obtained by Limmer for the uncoated GCI. In addition to this comparison, a summary of the PEO treated wrought and cast aluminium results from Limmer's study are provided.

4.2 Small-Scale Testing Procedure

It was important to replicate the same rig setup and methodology for conducting the laser-clad GCI tests as used previously to provide comparable results. The thesis written by Limmer [1] contains an in-depth discussion on the design and methodological choices for the small-scale testing setup. Section 4.2 provides an outline of the setup used and any information that is specific to the present LCA study.

4.2.1 Experimental Setup

Due to current coating abilities at TWI, a laser-clad coating was not able to be applied directly to the sample rotor used for the small-scale testing, with a 95.25 mm diameter. Therefore, two small samples were cut from the cheek of a full-sized commercial vehicle vented rotor that had previously been laser-clad by TWI for testing at Cummins-Meritor. This large rotor had already undergone full-scale dynamometer testing procedures, resulting in some small radial cracks apparent on the surface of the coating. The effect of these cracks on the particulate emissions released during small-scale testing was assumed to be negligible since the coating remained intact and the performance of the rotor during the Cummins-Meritor dynamometer testing was not affected by the cracking. For the present LCA study it was important to replicate the conditions used by Limmer [1] on

the other rotor materials exactly to ensure a fair comparison between the results gathered within the present research and those by Limmer. The outer diameters of the laser-clad samples were cut at 97 mm, which was slightly larger than the 95.25 mm used in Limmer's study. However, this did not affect the test results as the mean rubbing radius and pad dimensions remained the same. Figure 4.1 shows how the samples were cut from the cheek of the full-scale commercial rotor.

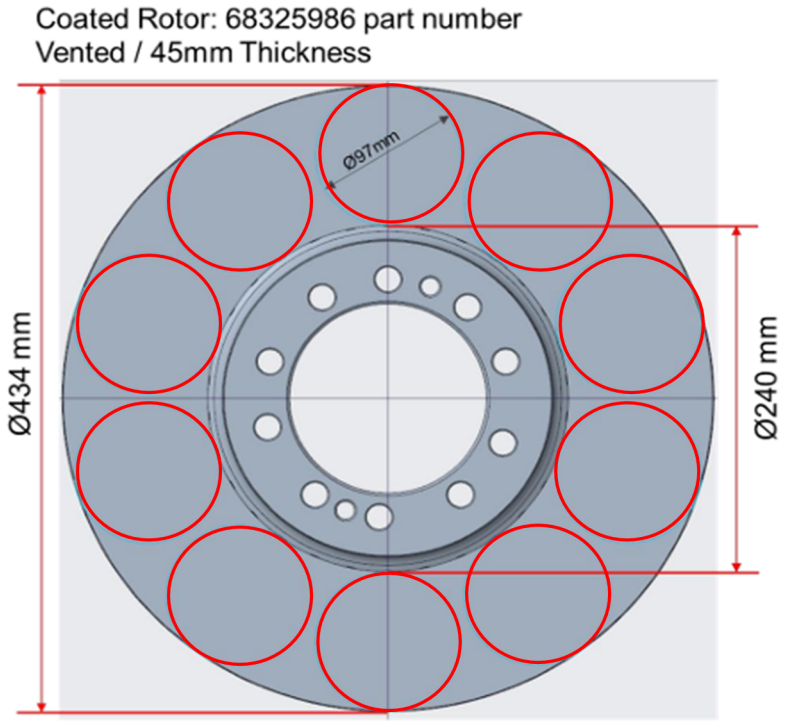

Figure 4.1: Drawing of small-scale brake rotor samples to be cut from full-scale commercial laser-clad GCI rotor.

The Bruker Universal Mechanical Tester (UMT) adapted for these small-scale tests utilises a pin-on-disc setup with a rotating lower drive and upper bidirectional load cell. The rotating drive has speed capabilities of up to 5000 rpm, with a maximum torque capacity of 5 Nm at a speed of 100 rpm. The load cell measures both vertical (axial) and transverse (circumferential) forces, and hence CoF can be calculated directly from the load cell results. The UMT allows vertical forces of up to 500 N to be applied during testing [1].

Figure 4.2a shows the small-scale friction material in the inverted position within the load cell, while Figure 4.2b illustrates the small-scale rotor loaded onto the rotating drive. A thermocouple was placed on the rotor surface during the testing to compare with the temperature profiles of the full-scale dynamometer testing.

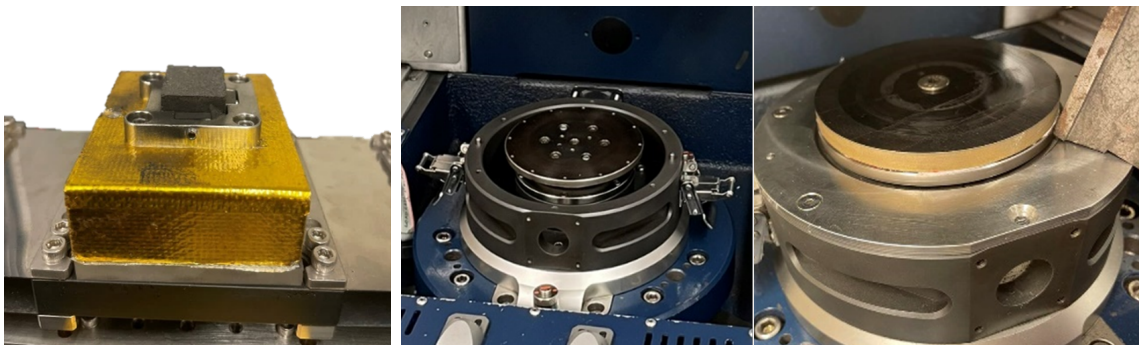

(a) Biderectional 500 N load cell (b) Bruker UMT rotational drive

Figure 4.2: Friction material loaded into the inverted upper biirectional 500 N load cell (4.2a) and small-scale rotor loaded into the Bruker UMT rotational drive (4.2b).

Limmer [1] designed a duct system to fully surround the small-scale brake rotor during the tests to ensure that only clean air entered the system through a HEPA filter (high-efficiency particulate air filter). This was crucial to ensure that all PM emissions collected were from the braking event. The ducting and enclosure around the sample are shown in Figure 4.3. The setup works by a vacuum pump, connected to the Dekati ELPI+, drawing air through the ducting and over the brake disc. The air passes through a HEPA filter to ensure that all particles collected originate from the brake rotor. The air flow is set to isokinetic conditions, based on the sampling flow rate of the dekati ELPI+ particle collector.

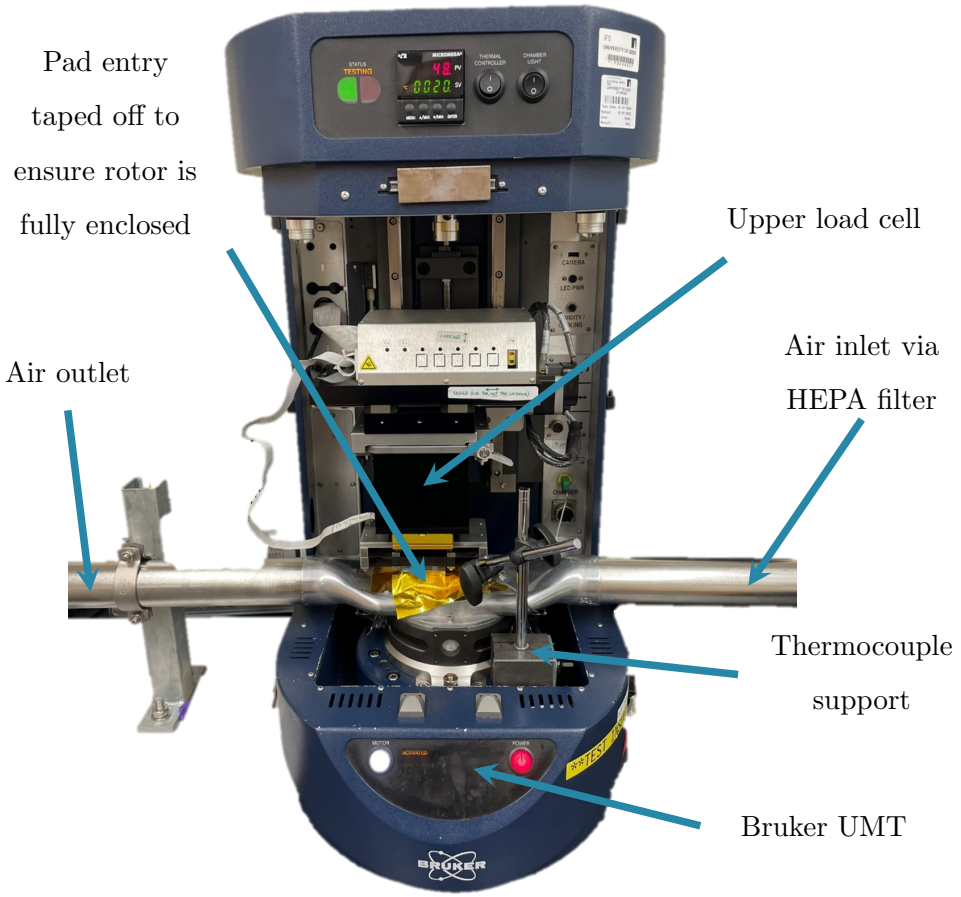

Figure 4.3: Labelled photo of Bruker UMT ducting setup for emissions collection.

To run the WLTP cycle within the tribometer, Limmer wrote a 303-sequence script within the Bruker software for emissions testing on small-scale rotors. Each brake sequence replicates a unique brake application defined by the WLTP cycle and consists of the following five stages:

1. Check the initial brake temperature (IBT).
2. Speed the brake rotor rpm up to the required value (only initiates once temperature reaches the IBT check value).
3. Apply the required braking force via the upper bidirectional load cell.
4. Reduce the rpm of the brake rotor to the required sliding speed to replicate the particular WLTP braking application.
5. Remove the vertical load by resetting the load cell to zero position and move onto the next brake application.

4.2.2 Test Procedure

The testing procedure was conducted using 8 sequential WLTP cycles. The first 5 cycles were used to bed the rotor in, ensuring a stable CoF was reached and that the friction pair behaved as they would in a normal driving cycle, with a sufficient tribolayer formed. The emission data was then collected over cycles 6-8 to provide three repeat readings. This 8 cycle process was applied to replicate the procedure conducted by Limmer [1], ensuring comparable results.

A Dekati ELPI+ was used to collect the emissions released during cycles 6-8. This uses a cascade impactor consisting of 15 stages. Each stage collects particles of their nominal cut-off size up to the cut-off size of the stage above. For example, for stage 11, the PM collected is 1.6 µm $\leq$ PM $<$ 2.5 µm. Table 4.1 [122] outlines the nominal cut-off and mean diameter sizes of the particles collected at each stage.

The particle masses at each stage were measured by weighing the impactor foils before and after each of the 6^{th}, 7^{th} and 8^{th} WLTP cycles. LCA standard procedure, using the ReCiPe methodology [49] and the Euro 7 legislation [85], requires that particle sizes be grouped into $PM_{2.5}$ and PM_{10} categories, which also aligns with the impending Euro 7 threshold values [18]. Stage 1 of the impactor does not contain a foil, so this stage cannot be weighed. Therefore, Equations 4.1 and 4.2 can be used to calculate the masses of $PM_{2.5}$ and PM_{10} emissions.

$$PM_{2.5}\ mass = \sum_{stage_i=2}^{stage_i=11} Particle\ mass\ collected\ at\ stage\ i \tag{4.1}$$

$$PM_{10}\ mass = \sum_{stage_i=2}^{stage_i=14} Particle\ mass\ collected\ at\ stage\ i \tag{4.2}$$

Table 4.1: Dekati ELPI + Impactor stage specifications [122].

Dekati ELPI+ Impactor Stage	Nominal cut-off size (µm)	Mean Diameter (µm)
15	10	-
14	5.3	7.3
13	3.6	4.4
12	2.5	3
11	1.6	2
10	0.94	1.2
9	0.6	0.75
8	0.38	0.48
7	0.25	0.31
6	0.15	0.19
5	0.094	0.12
4	0.054	0.071
3	0.03	0.04
2	0.016	0.022
1	0.006	0.01

4.3 WLTP Test Cycle Results

This section outlines the results generated from the laser-clad GCI samples. The results were then compared with those of Limmer [1]. First, the laser-clad GCI is compared with the uncoated GCI rotor - feeding directly into case study I. Second, both the PEO treated Al rotors are compared with the uncoated GCI, feeding into Case Study II.

4.3.1 Coefficient of Friction

The laser-clad GCI rotor sample was paired with a copper-free LM friction material. This was chosen to match the same friction material used in the study conducted by Limmer [1], as well as being a material commonly used in passenger vehicles in Europe. Figure 4.4 shows how the CoF stabilised as the rotor was bed in. The variation of CoF during Cycles 6-8 (emission gathering cycles) is outlined in Figure 4.5.

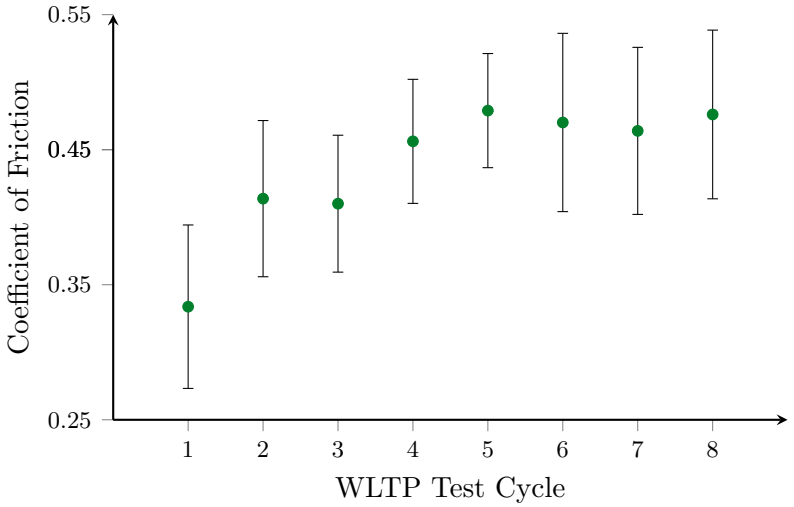

Figure 4.4: Coefficient of friction stabilising as laser-clad GCI rotor was bedded in.

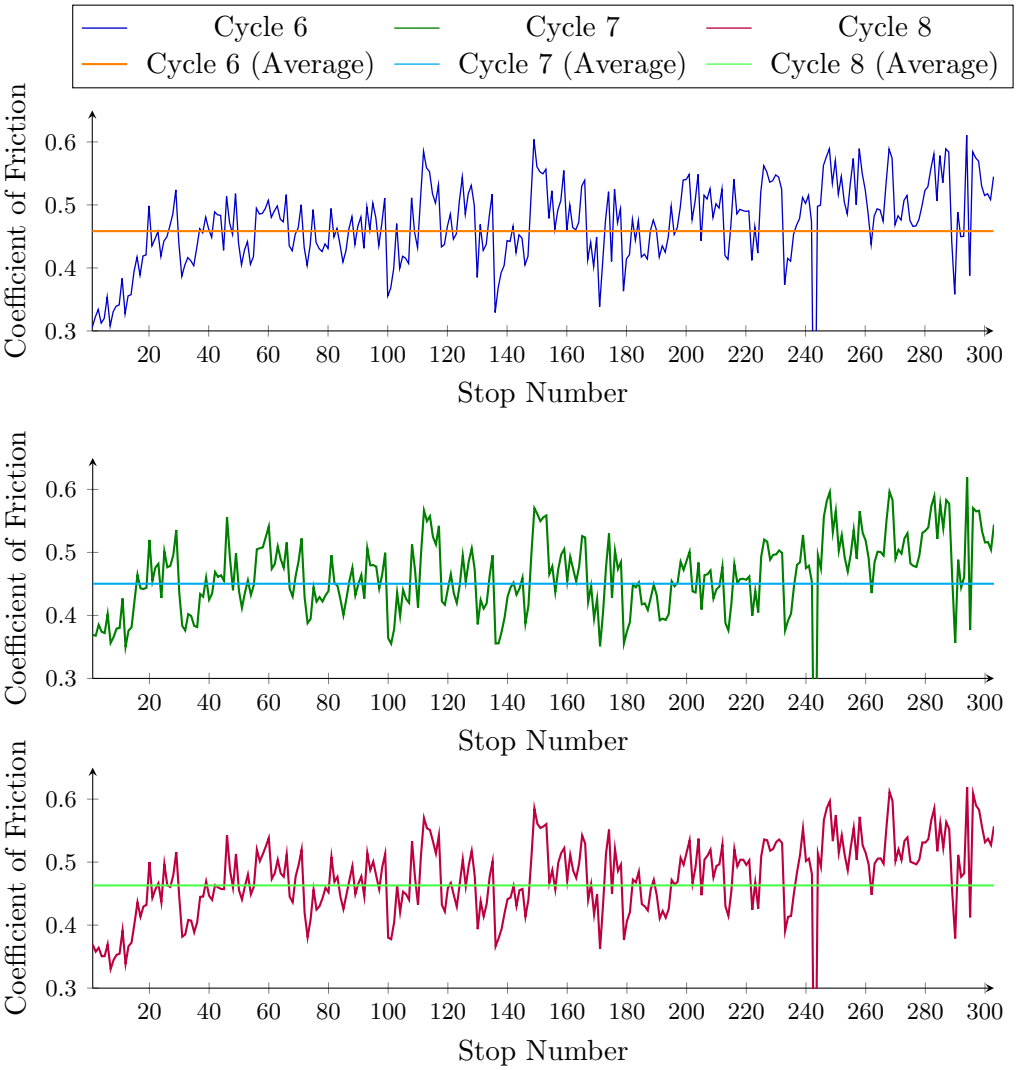

Figure 4.5: Laser-clad GCI CoF stability across 303 unique stops of the WLTP for each emissions gathering cycle (cycles 6-8).

It can be seen that a stable CoF of about 0.47 was reached from cycle 5 onwards. Throughout the 303 unique stops of each WLTP cycle, fluctuations in CoF were observed, which were characterised as standard deviation and shown as error bars in Figure 4.4. This

fluctuation remained relatively constant throughout all 8 cycles (0.032 to 0.056). Figure 4.5 plots how the CoF fluctuated between the 303 stops for the 3 emissions gathering cycles. A high level of stability was found, indicating that the selected LM friction material was a suitable friction partner for the laser clad rotor surface.

4.3.2 Wear Rate

The masses of the rotor and pad were measured before and after the 8 WLTP cycles at a precision of 2 and 4 decimal places, respectively. Figure 4.6 outlines the mass losses measured over these 8 cycles. The vast majority of the mass loss originated from the brake pad as a result of the very high wear resistance of the hard laser-clad coating on the rotor surface.

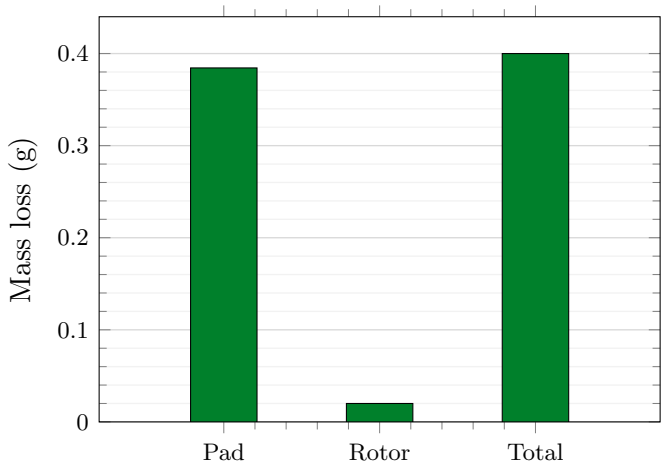

Figure 4.6: Mass loss of friction material and rotor over 8 WLTP cycles.

4.3.3 Particulate Matter Emissions

After the 5 bedding in cycles, PM emissions were collected for each of the remaining 3 cycles. The impactor foils from the Dekati ELPI+ were weighed before and after each of the WLTP cycles 6-8. The mass increases due to accumulated PM were then calculated for each stage of the impactor and averaged across these 3 cycles. The particles collected in stages 2-7 have such a small aerodynamic diameter (<0.6 µm), their masses were below that of the precision of the scales. The foil reading after the cycle would either be the same as before or occasionally a lower (negative) value would be recorded within this range. A negative reading would be due to the air flow removing some of the grease from the foil and an insignificant PM mass landing on it. Therefore, only the mass increases of Dekati ELPI+ stages 8-15 were investigated, as shown in Figure 4.7. The aerodynamic diameter labelled on the x-axis refers to the nominal cut-off particle diameter for that stage. For example, the result indicated at 0.38 µm aerodynamic diameter is the mass of particles found on stage 8 (0.38 µm $\leq$ PM $<$ 0.6 µm).

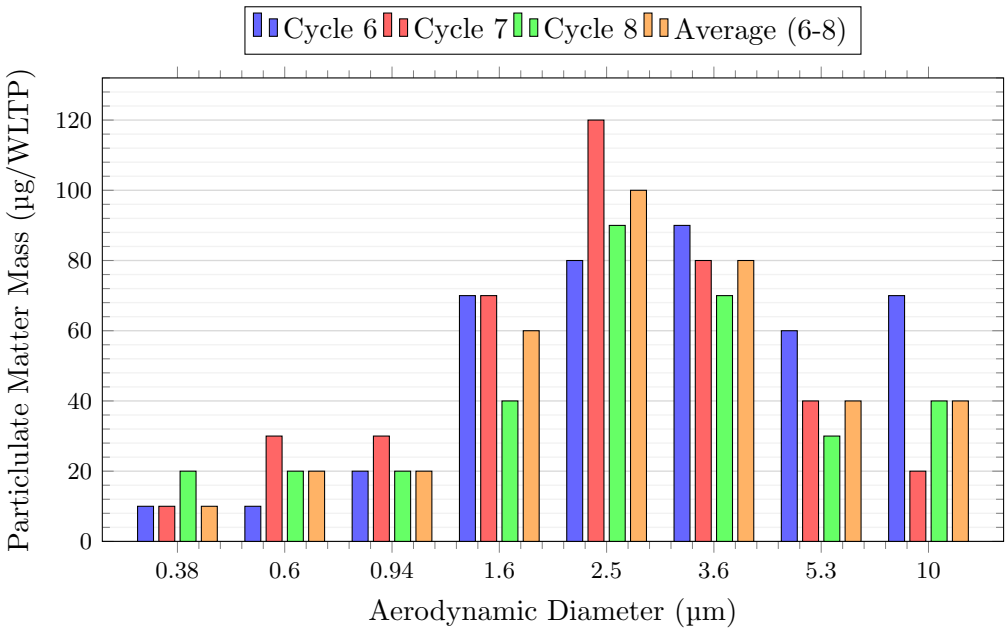

Figure 4.7: Particle mass collected at each stage of the Dekati ELPI+ from stages 8-15 across WLTP cycles 6-8.

The small variations in PM across the 3 cycles could have been due to slight fluctuations in the air speed across the brake rotor, affecting the pick-up of particles from the rotor surface. It was impossible to have air flow at a perfectly constant speed throughout the experiment due to variations in the laboratory pressure at the exit of the ducting system. LCA studies require that the PM inventory be grouped into $PM_{2.5}$ and PM_{10}. Figure 4.8 outlines the results of such a calculation using Equations 4.1 and 4.2.

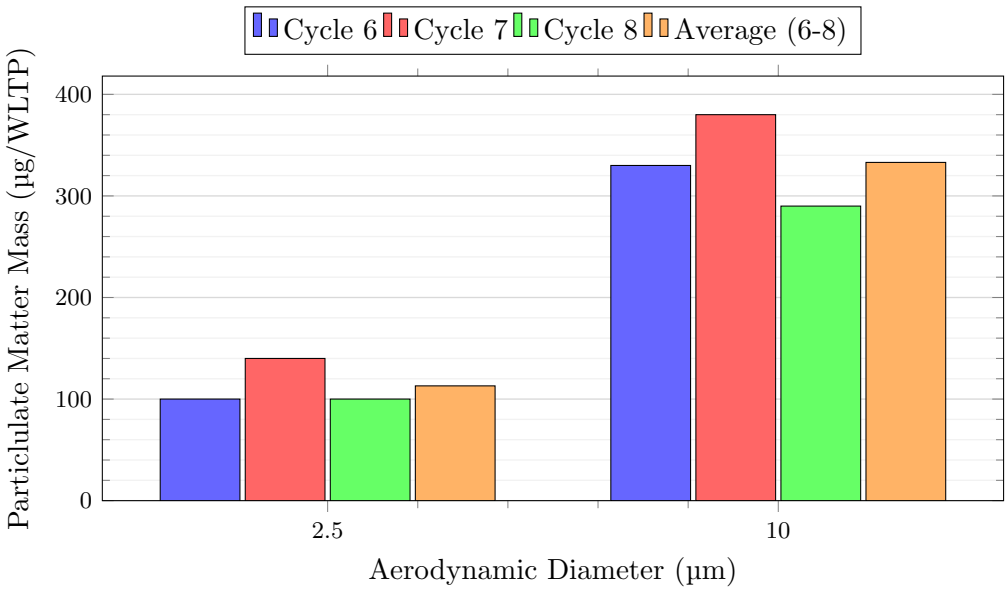

Figure 4.8: Particle matter mass of $PM_{2.5}$ and PM_10 across WLTP cycles 6-8.

4.3.4 Case Study I: Small-Scale Test Results

Case study I, presented in Chapter 5, compares the laser-clad GCI rotor with the uncoated GCI rotor. It was found that both rotors reached a stable CoF after the 5 bedding cycles

(as indicated by Figure 4.9). Figure 4.10 outlines the stability of both rotors across the 303 stops for cycles 6-8. It was found that the fluctuations in CoF across the 303 unique brake events of the WLTP cycle were very similar for the laser-clad GCI compared to its uncoated counterpart. This indicated that the inclusion of a hard laser-clad coating did not detrimentally impact the stability of the CoF during a braking event. Data from Figures 4.9 and 4.10 can be simplified to a box plot. This clearly outlines the CoF value and stability of each rotor. Figure 4.11 shows that the CoF was slightly lowered when testing the same friction material on the laser-clad GCI rotor (0.47 compared to 0.49), with slightly higher variability. However, Ghouri et al. [11] recommended a CoF value of 0.3-0.4, which is closer to the value demonstrated by the laser-clad rotor.

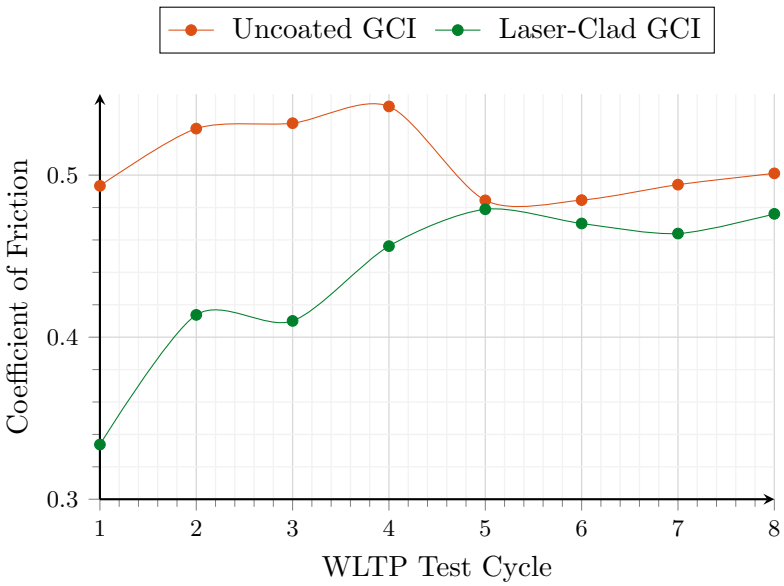

Figure 4.9: Comparison of bedding in processes across 8 WLTP cycles (case study I).

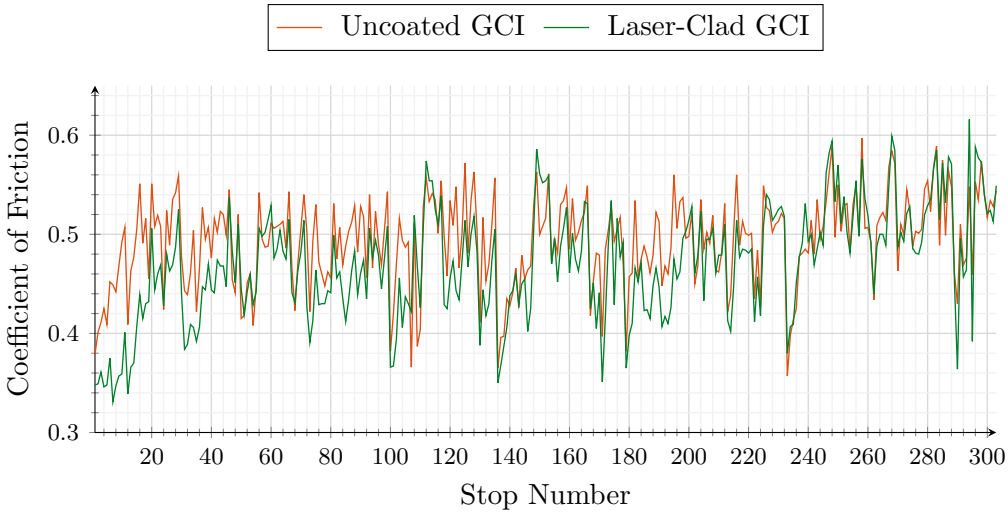

Figure 4.10: Material comparison of frictional stability across all 303 unique WLTP braking events (case study I).

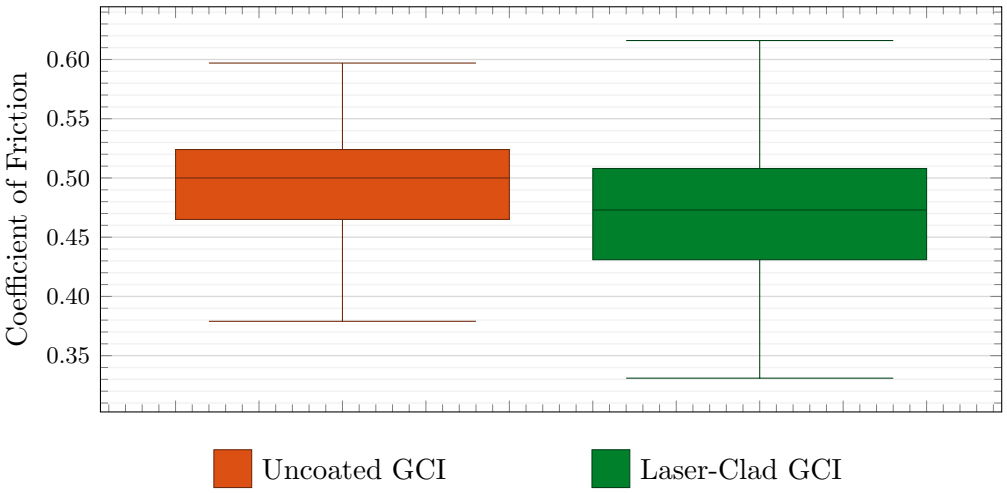

Figure 4.11: Box plot for the comparison of CoF values for each rotor across WLTP cycles 6-8 (case study I).

When investigating rotor and pad mass loss, the laser-clad rotor suffered significantly lower mass loss compared to uncoated GCI (78% reduction), indicating the benefits of adding a hard coating to the rotor surface. This large decrease will lead to significant reductions in maintenance requirements, allowing one rotor to potentially last the full lifetime of a vehicle without replacement. As previously explained, most of the overall wear for the laser clad rotor friction pair came from the pad. These results are shown in Figure 4.12.

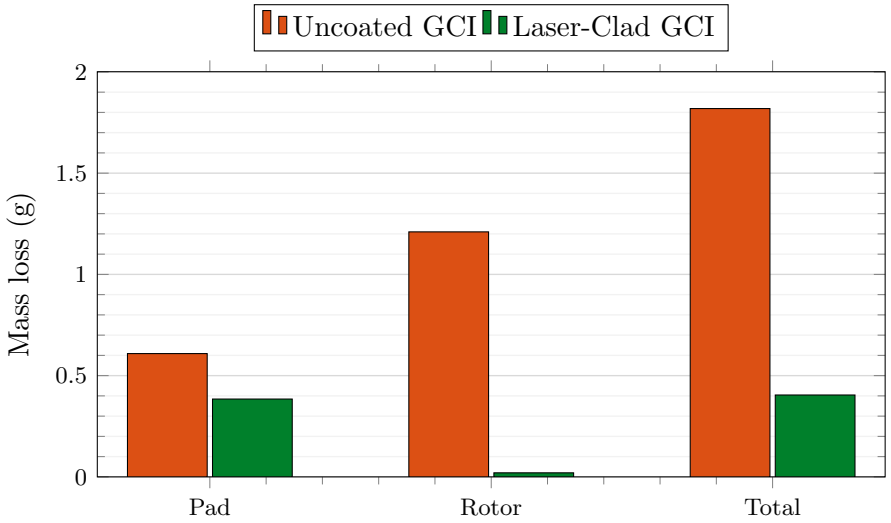

Figure 4.12: Comparison in mass loss of both the frictional material and the brake rotor across all 8 WLTP cycles (case study I).

Figure 4.13 outlines the significant reductions in particle mass found at each stage of the Dekati ELPI+ for the laser-clad GCI compared to the uncoated rotor. These results can then be combined into $PM_{2.5}$ and PM_{10} values for use within the present LCA, as shown in Figure 4.14. A correlation can be seen between the amount of wear on the rotor and pad and the resulting emissions released. The results provided in Figures 4.13 and 4.14 are for the PM masses collected within the Dekati ELPI + over the entire WLTP cycle averaged between cycles 6-8. The uncoated GCI rotor was found to suffer the same phenomenon

for stages 2-8 as the laser-clad GCI rotor did for stages 2-7. This was where insignificant mass was deposited on the foils as a result of the particle size being too small. Stage 8 ($0.38 \leq PM < 0.6$) was therefore also omitted from the graphs within case study I, along with stages 2-7 that were previously omitted.

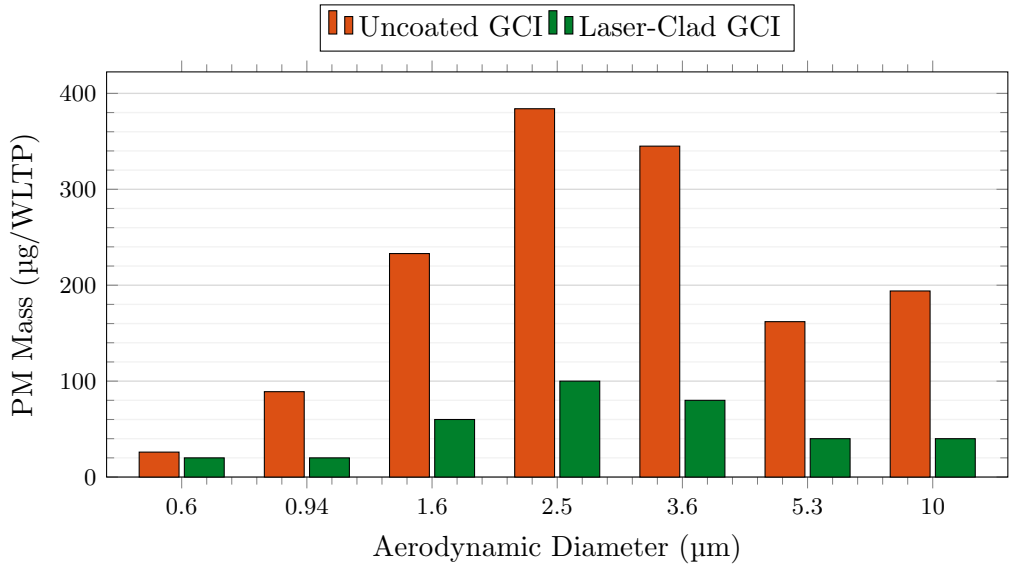

Figure 4.13: Particle mass collected at each stage of the Dekati ELPI+ from stages 8-15 across WLTP cycles 6-8.(case study I).

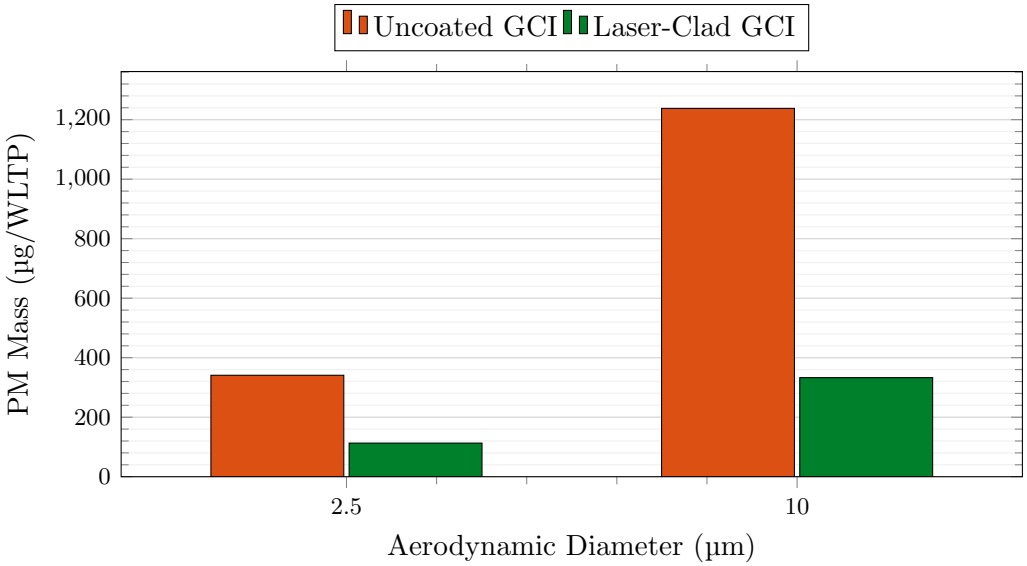

Figure 4.14: $PM_{2.5}$ and PM_{10} emissions as measured from the Dekati ELPI+ (case study I).

4.3.5 Case Study II: Small-Scale Test Results

This section does not contain any results generated as part of the current research, merely providing a summary of the results gathered by Limmer [1] for use within the present LCA study. Two PEO treated Al rotors underwent the tests, utilising the same low metallic (LM) friction material. The exact composition of this material varied slightly compared to the friction material used for both the laser-clad GCI and the uncoated GCI. However,

it is assumed that these differences had minimal effect on the overall present LCA study. The difference between the two Al rotors prior to the PEO treatment is that one was cast, while the other was machined from a wrought Al billet. Lost wax investment casting using wax models constructed with fused filament fabrication was used to produce the cast rotor [1]. The wrought Al rotor was a 6082 alloy, while the cast Al had a higher silicon content to improve fluidity for the casting process. It was found that the wrought Al possessed 22% higher ultimate and yield strength [1]. Before PEO treatment, both rotor surfaces were ground with 600-grit paper to ensure a smooth and even surface treatment.

Figure 4.15 shows that similarly to the two GCI rotors, the PEO treated Al rotors reached a stable CoF within the first 5 bedding cycles. The PEO treated cast rotor took a little longer to bed in than the wrought Al6082, however, both showed similar stability across the 303 stops of the WLTP cycle as indicated in Figure 4.16. The fluctuations in CoF value throughout the 303 brake events follow very similar patterns for both the PEO treated Al rotors as for the uncoated GCI, indicating similar stability. The main noticeable difference in Figure 4.16 is the change in average CoF, translating the graph vertically. The cast Al was found to have a slightly lower CoF (0.45) than the uncoated GCI (0.49), while the wrought Al possesses a much higher value (0.67). This could be due to a varying surface roughness and the pad composition not being fully optimised for either PEO treated Al rotor. Figure 4.17 simplifies the variation of CoF between the 303 unique brake events as a box plot, averaged over cycles 6-8.

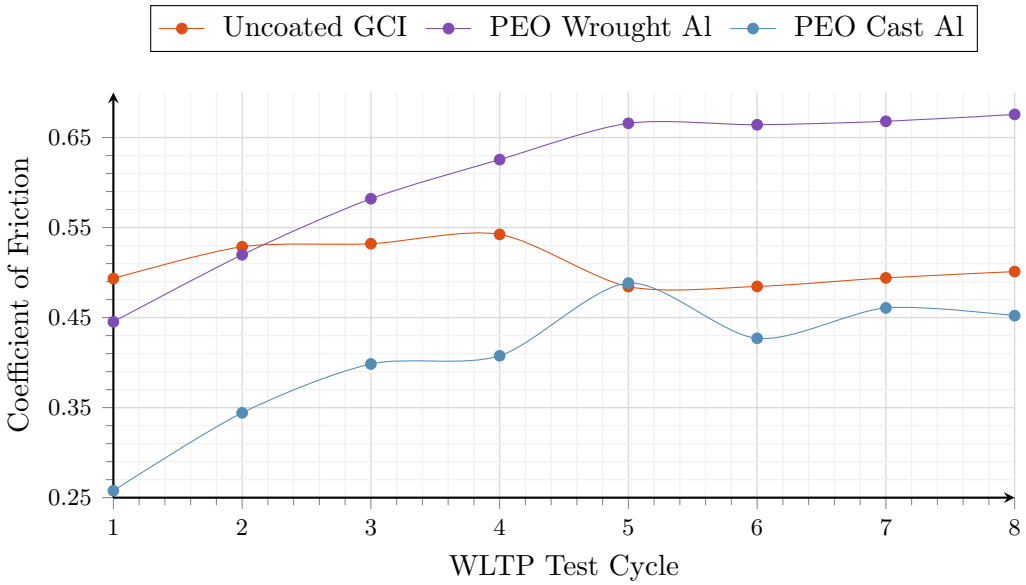

Figure 4.15: Comparison of bedding in processes across 8 WLTP cycles (case study II).

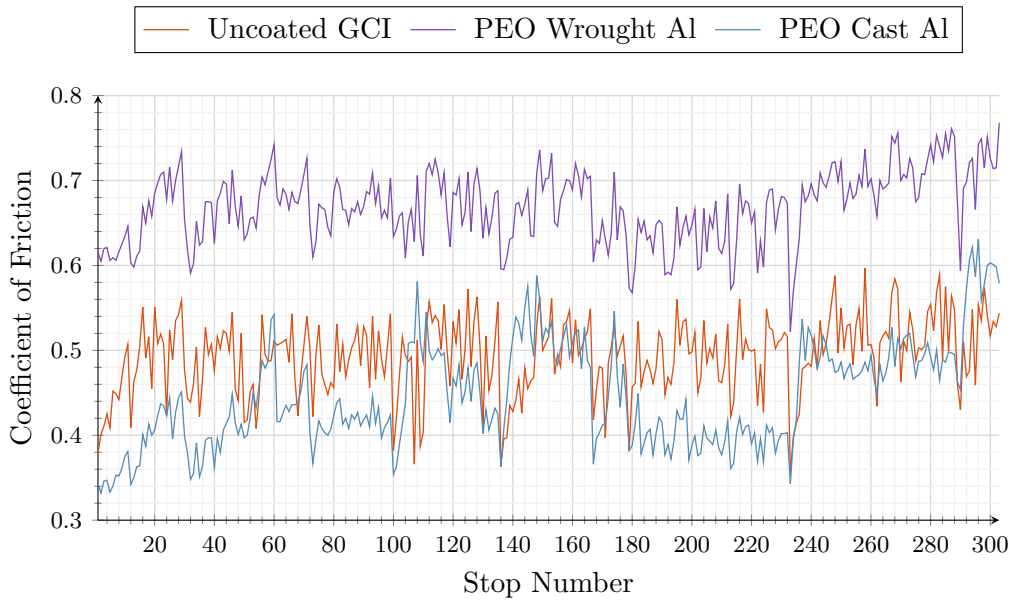

Figure 4.16: Material comparison of frictional stability across all 303 unique WLTP braking events (case study II).

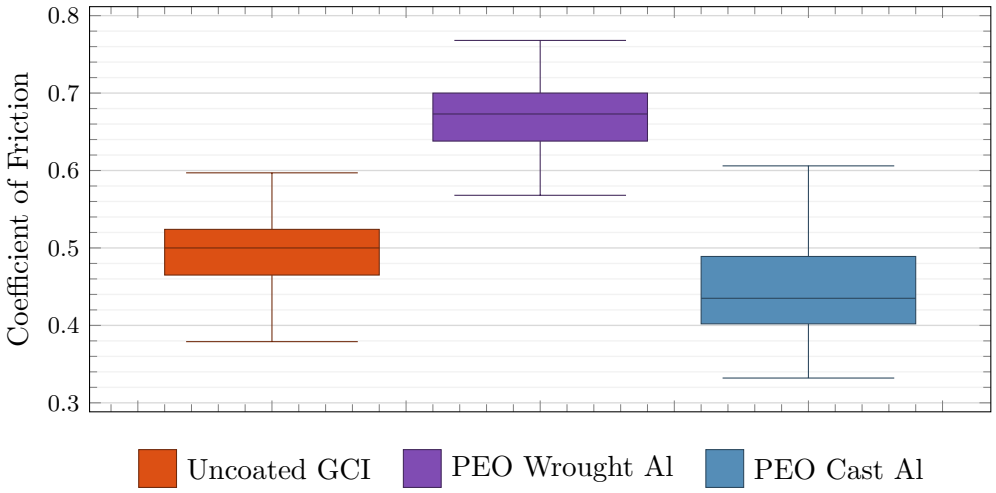

Figure 4.17: Box plot for the comparison of CoF values for each rotor across WLTP cycles 6-8 (case study II).

The PEO treated wrought Al shows a higher CoF in comparison to the PEO treated cast Al. However, this higher CoF could be reduced in the future with a more optimised friction material composition. For the present LCA study, this higher CoF is not a cause for concern, as the same frictional stability was found for the other materials. The force threshold used for each brake stop within the Bruker software was also based on the friction force and not the brake pressure force. Therefore, the PM collected for the comparison would not be affected, as with a higher CoF, the load cell would simply apply less pressure, so the same amount of braking work was performed for each WLTP cycle. As with the laser-clad GCI rotor, both PEO treated Al rotors suffered significantly lower mass loss compared to the uncoated GCI, outlined in Figure 4.18. Reductions of 82% and 59% were found for wrought and cast PEO-Al, respectively.

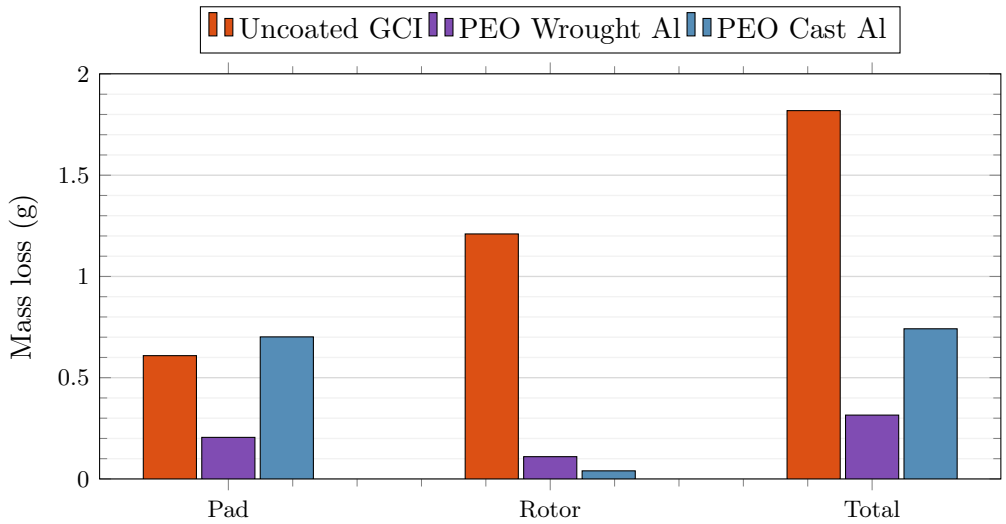

Figure 4.18: Comparison in mass loss of both the frictional material and the brake rotor across all 8 WLTP cycles (case study II).

The cast PEO-Al showed greater pad wear than the wrought PEO-Al rotor. This increased pad wear can most likely be attributed to the rougher surface of the cast Al alloy as a result of a more porous nature with more pronounced asperities [1]. The wear rate of both PEO treated rotors could likely be lowered further once the friction material for each is optimised. The same correlation can be said for case study II as for case study I, where the significant reduction in rotor wear has influenced a similarly large reduction in PM emissions. Figure 4.19 shows that the PM emissions for both PEO treated rotors were significantly lower compared to the uncoated GCI. The increased wear rate of the cast PEO-Al rotor is likely what leads to the slightly higher emissions found compared to the wrought PEO-Al. The results provided in Figures 4.19 and 4.20 are for the PM masses collected within the Dekati ELPI + over the entire WLTP cycle, averaged over cycles 6-8.

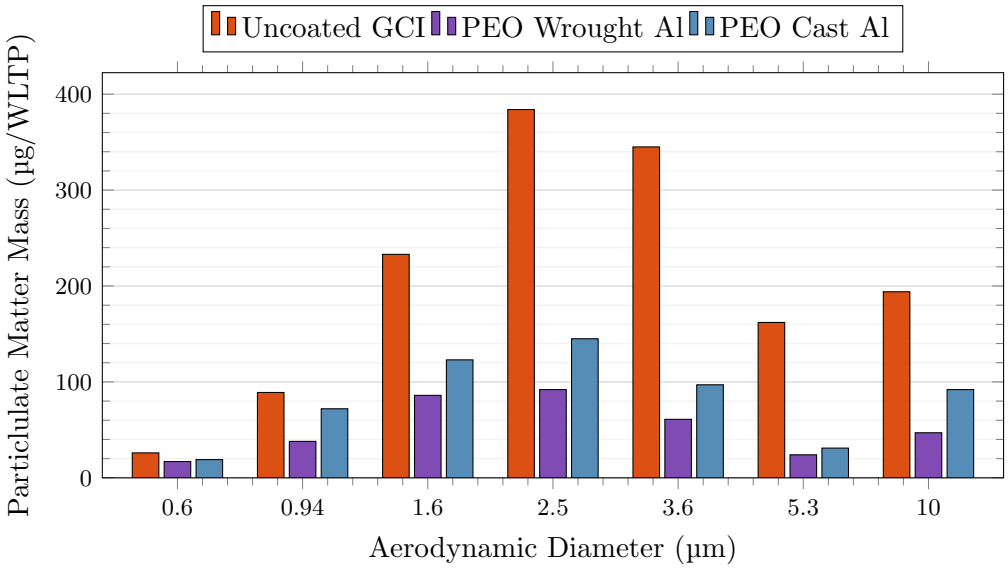

Figure 4.19: Particle mass collected at each stage of the Dekati ELPI+ from stages 8-15 averaged across WLTP cycles 6-8. (case study II).

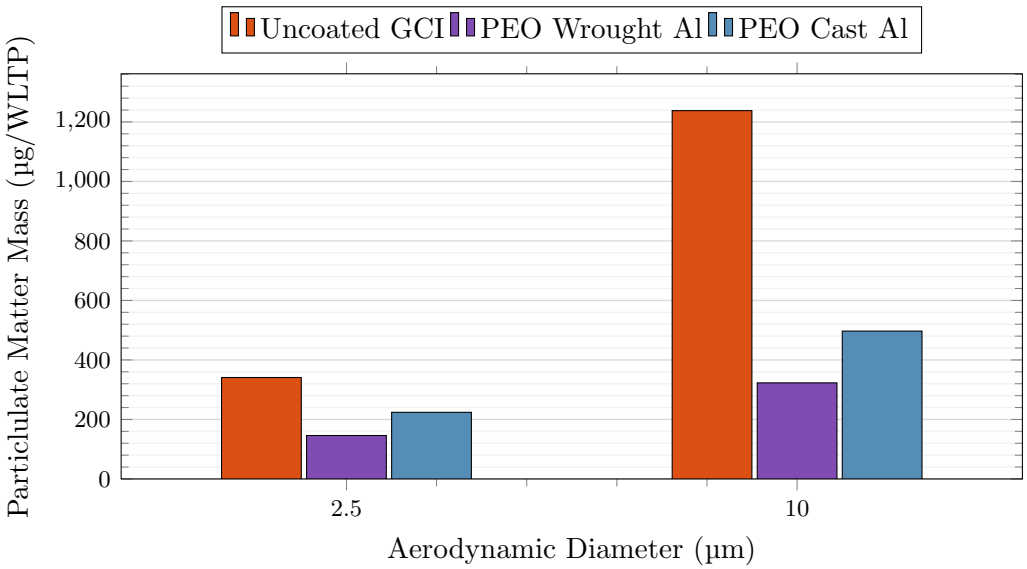

Figure 4.20: $PM_{2.5}$ and PM_{10} emissions as measured from the Dekati ELPI+ averaged across WLTP cycles 6-8 (case study II).

4.4 Number of Rotors Required per Use Cycle

A crucial calculation for any LCA study is to determine the number of components required per FU duration, that is, the full 240,000 km FU duration, which was assumed to consist of 1250 WLTP cycles. This is necessary to determine the true impacts of the manufacturing and disposal phases in order to provide a fair comparison between two different rotor materials with different lifespans. The mass losses of the small-scale rotor samples were measured before and after the 8 WLTP cycles, and the average mass loss per WLTP cycle was calculated. Using the density of the surface material of the rotor and the rubbing area of the small-scale samples, Equations 4.3 and 4.4 were applied to estimate the dimensional wear rate per WLTP cycle and hence the number of rotors required per FU duration. The data used and the results of these calculations are summarised in Table 4.2.

$$Wear\ rate\ (mm/WLTP) = \frac{mass\ loss\ (g/WLTP)}{(Density\ (g/mm^3))\,(Rubbing\ area\ (mm^2))} \tag{4.3}$$

$$No.\ rotors\ per\ FU = \frac{Wear\ rate\ (mm/WLTP) \times (1250)}{Allowable\ rotor\ wear\ before\ replacement\ (mm)} \tag{4.4}$$

Table 4.2: Number of rotors per FU duration.

Variable	Unit	Value	
		Uncoated GCI	Laser-clad GCI
Mass loss	g/8WLTP	1.21	0.02
Mass loss	g/WLTP	0.1513	0.0025
Density	g/mm^3	7.5×10^{-3} [1]	[a]7.186×10^{-3}
Rubbing radius	mm	29	29
Pad width	mm	16	16
Wear rate	mm/WLTP	6.92×10^{-3}	1.19×10^{-4}
Initial rotor thickness	mm	28	28.4
Replacement rotor thickness	mm	[b]26	[c]28.25
No. rotors per FU	-	4.3	1.0

[a] Density of laser-clad layer was determined based on a 80/20 wt% 430L steel to TiC mix, with densities of 7750 and 4930 respectively [123].
[b] Value based on internal discussions with industry experts, estimating 2 mm allowable wear.
[c] Value based on 25% of hard top layer of the laser-clad coating remaining

The same method to calculate the wear rate could not be applied to the two PEO-Al rotors. The PEO alumina layer was found to have an initially more brittle outer layer that crumbles away easily during the bedding in process because of the somewhat porous and rough surface of the as-produced PEO layer being exposed. Therefore, it was postulated that the mass loss during the bedding in process (WLTP cycles 1-5) would be much higher than during the emissions testing (WLTP cycles 6-8). As the rotor mass was not measured after the 5^{th} WLTP cycle due to the time constraints of reacclimatising the samples to the measurement laboratory between weight measurements, the mass loss from cycles 6-8 was unknown. It was assumed that during these later cycles, after full bedding in, a similar wear rate would have been found as for the laser-clad rotor because of similar PM emissions being released during use. Therefore, it was assumed that only one PEO coated rotor would be required for the functional unit distance of 240000 km, as for the laser-clad GCI rotor.

4.5 Scaling Emissions and Comparing to Euro 7 Limits

To directly compare the PM emission results with those set out in the Euro 7 legislation, the data needs to be scaled from the Dekati ELPI+ values to a PM_{10} value for the whole vehicle. The Dekati ELPI+ only samples a small portion of the air that exits through the exhaust pipe of the system. To calculate the volumetric flow of the exhaust air, the cross-sectional area of the exhaust pipe and the air speed were measured. The air speed

can be adjusted by varying the inlet blower power. However, there is some natural suction (negative ambient pressure) from the laboratory ventilation system. The ventilation system is connected as one unit to the rest of the equipment in the laboratory space and so if another experiment is being run, the level of negative pressure can vary. The exhaust ducting from the Bruker UMT is connected directly to the laboratory ventilation system, which therefore can cause slight fluctuations in the exhaust air speed. To account for this, regular air speed measurements were taken within the ducting throughout the WLTP cycles.

The vacuum pump drawing air through the Dekati ELPI+ was programmed to sample air at 10 l/min $\left(Q_{Dekati} = 0.6\ m^3/h\right)$, generating a sampling air speed of 3.77 m/s (based on an internal sampling probe diameter of 7.5 mm). The power of the HEPA filter blower was adjusted so that the exhaust air speed matched this 3.77 m/s to provide sampling under isokinetic conditions. Given that the internal diameter of the exhaust duct was 50 mm, the average exhaust flow rate was calculated to be $Q_{Exhaust} = 26.6\ m^3/h$. Table 4.3 summarises these values for use within Equation 4.5 to calculate the total PM mass of the small-scale setup, based on the Dekati ELPI+ sampling.

$$PM_{small\text{-}scale\ test}\ (mg/WLTP) = PM_{dekati}\ (mg/WLTP) \times \frac{Q_{exhaust}\ \left(m^3/h\right)}{Q_{dekati}\ (m^3/h)} \quad (4.5)$$

Table 4.3: Experimental setup values required for scaling results under isokinetic conditions.

Description	Value	Unit
Diameter of exhaust pipe	50	mm
Dekati sampling diameter	7.5	mm
Air speed	3.77	m/s
Scaling Factor	13.57	-
WLTP driving distance	192	km

To scale these small-scale test values to a full-scale rotor, Limmer [1] determined an energy-based scaling factor that lies between 11.72-17.22. The exact value is dependent on the ratio between the area of the full-scale pad and the small scale pad (as outlined in Section 2.4.3.2, Equation 2.4). In the present study the area of the full-scale pad was unknown. However, an estimation for the scaling factor can be made utilising the ratio between the small-scale and full-scale rotor areas, thus generating Equation 4.6.

$$f = \frac{Area\ of\ full\text{-}scale\ rotor\ \left(mm^2\right)}{Area\ of\ small\text{-}scale\ rotor\ (mm^2)} \quad (4.6)$$

The full-scale rotor had a diameter of 350 mm, compared to the 95 mm diameter of the small-scale setup, providing an estimated scaling factor of 13.57. This estimated value lies within the range provided by Limmer [1], and was therefore applied for the present LCA study. It must also be considered that the test rig only applies a brake pad to one side of the rotor in the pin-on-disc setup. Therefore, to replicate the double-sided calliper design of a full-scale automotive disc brake, the results from the small-scale test were also doubled, thus deriving Equation 4.7.

$$PM_{full\text{-}scale\ rotor}\ (mg/WLTP) = PM_{small\text{-}scale\ test}\ (mg/WLTP) \times 13.57 \times 2 \quad (4.7)$$

The above result was divided by 192 km (the equivalent driving distance of the WLTP cycle), deriving Equation 4.8, which converts mg/WLTP cycle into mg/km

$$PM_{full\text{-}scale\ rotor}\ (mg/km) = \frac{PM_{full\text{-}scale\ rotor}\ (mg/WLTP)}{192} \quad (4.8)$$

The limits provided by Euro 7 are per vehicle and therefore the PM_{10} value for each rotor, calculated according to Equation 4.8, was multiplied by 4 to provide a value for the whole vehicle, as shown in Equation 4.9. This calculation assumes that all four rotors are the same size, producing the same number of emissions each. However, due to load transfer during a braking event, the front brakes generate more braking power than the rear. As a result, the front brakes are typically larger and will release more emissions than the rear. Despite this difference, it was assumed that the results generated by the Bruker UMT and Dekati ELPI+ setup were an average between both front and rear rotors. Therefore, simply multiplying by 4 to give values for the full vehicle could be taken as an accurate estimate.

$$PM_{full\ vehicle}\ (mg/km) = PM_{full\text{-}scale\ rotor}\ (mg/km) \times 4 \quad (4.9)$$

Figure 4.21 shows the whole vehicle emissions calculated as above, compared to the maximum allowable values for each vehicle classification under Euro 7 up to December 2029. Euro 7 limits PM_{10} for battery electric passenger vehicles to 3 mg/km, while alternative powertrain vehicles have a less stringent limit of 7 mg/km [85]. The 3 mg/km line has been included in Figure 4.21, but as the present study focussed on diesel/petrol powered vehicles, the 7 mg/km threshold is more relevant. It must also be noted that the WLTP cycle, utilised during the small-scale testing, was designed for conventional ICEVs rather than for the reduced use of friction brakes on EVs. It was found that the uncoated GCI exceeded the Euro 7 limit for alternative powertrain passenger vehicles by a factor of 4.5. Both the wrought PEO-Al and laser-clad GCI rotors were found to slightly exceed the limit. However, it should be noted that neither the coating nor, in particular,

the friction material have been optimised at this stage of their development. The cast PEO-Al was found to release higher amounts of PM_{10} than the other two coated rotors, due to the increased surface roughness. Although still a significant reduction of 60% was found compared to uncoated GCI.

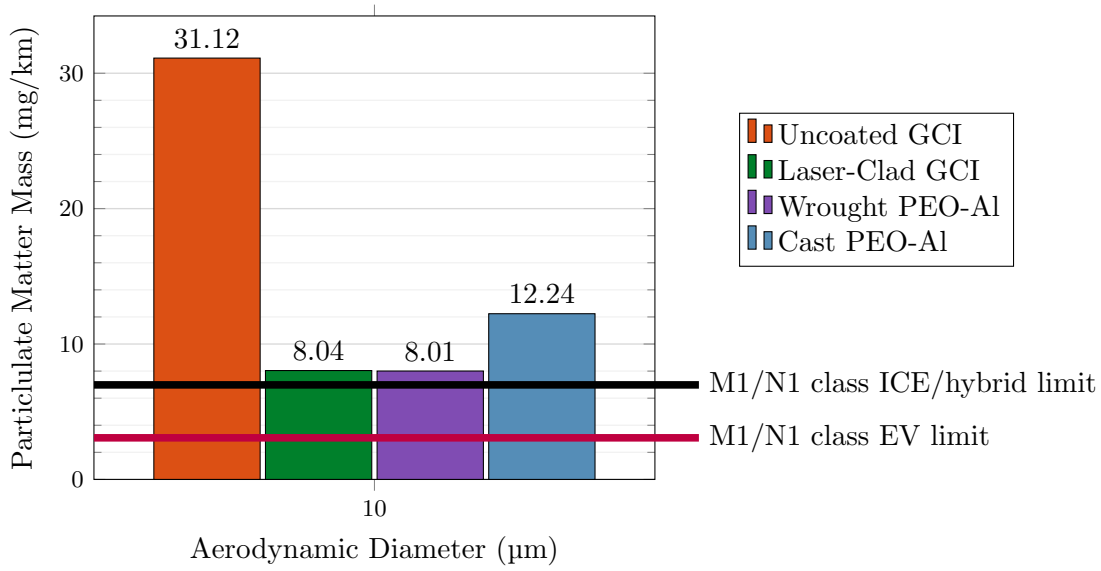

Figure 4.21: PM_{10} emissions released from each rotor material compared against Euro 7 thresholds.

4.6 Summary of Laser-Clad GCI Testing

To summarise, the emission results presented in this chapter have demonstrated that there is a clear requirement to replace the current uncoated GCI rotor, due to the PM_{10} released predicted to exceed the Euro 7 ICEV limits by a factor of 4.5. The laser-clad GCI and both the PEO treated rotors offer significant reductions in both the gravimetric wear rates and the related PM emissions released over the WLTP cycle. Stable CoF values were achieved within all these alternative rotor materials; however, further optimisation of the friction material would still be required before such rotors could enter series production. Both the PEO treated Al rotors and the laser-clad GCI offer attractive alternatives to the uncoated GCI, offering similar levels of reduction in wear and PM emissions. However, the PEO-Al rotor also offers a significant weight reduction compared to the standard GCI, which will also reduce energy consumption and GHG emissions. These impacts of the use phase as well as those that arise during the manufacture and end-of-life disposal phases were taken into account in the case studies presented in Chapters 5 and 6.

Chapter 5

Case Study I: GCI Rotors

5.1 Introduction

Chapter 5 presents the LCA results for both the uncoated GCI and the laser-clad GCI rotors. The adapted SADT notation was utilised for both rotors, demonstrating a good example of the benefits of the technique. The diagrams were generated first for the uncoated GCI rotor, with only three diagrams requiring adaptation for the laser-clad GCI. The specific assumptions used for each rotor material are listed, followed by details of the inventory data collection and impact analysis.

5.2 Life Cycle Diagrams

The SADT diagrams are laid out first for the uncoated GCI rotor, and second, the relevant diagrams are adapted to show how the life cycle is altered with the inclusion of a laser-clad coating. Uncoated GCI is currently the most widely used material within the brake industry [124], and therefore the associated impact results provide a good baseline for comparison within the present case study.

5.2.1 Uncoated GCI

Figures 5.1 - 5.6 display the diagrams included within the hierarchical illustration shown in Figure 3.11. The inputs and outputs for the entire rotor life cycle were summarised by the parent diagram shown in Figure 5.1. This diagram illustrates the first level of the hierarchy within the adapted SADT system. The diagram notation used was A, A0, A01 etc, due to the uncoated GCI being the first rotor that was investigated.

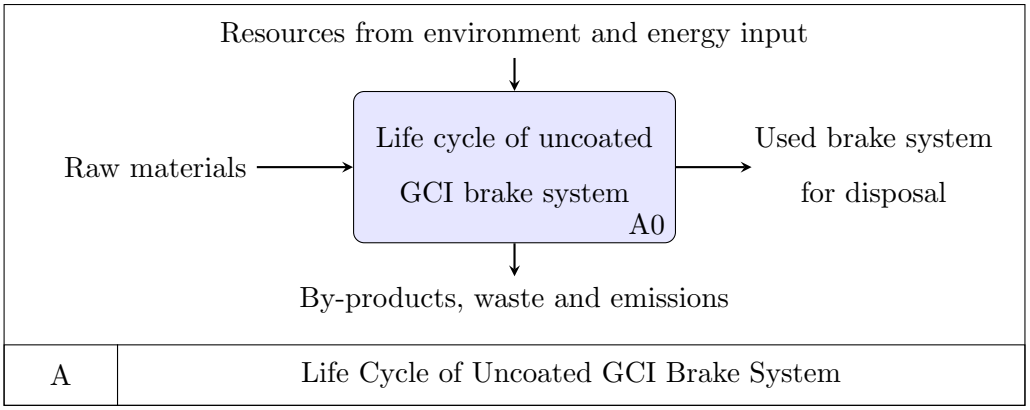

Figure 5.1: Uncoated GCI parent diagram.

In addition to the diagram code, a colour code was included to indicate which unit process of one level of the hierarchy is linked to which diagram of the following hierarchical level. The three main components that contribute to the full life cycle of a brake system are the phases of manufacture (A01), use (A02), and disposal (A03) of all related components within the system boundary. Therefore, the second level of the hierarchy (first child diagram) illustrates the interactions of these three phases, as shown in Figure 5.2.

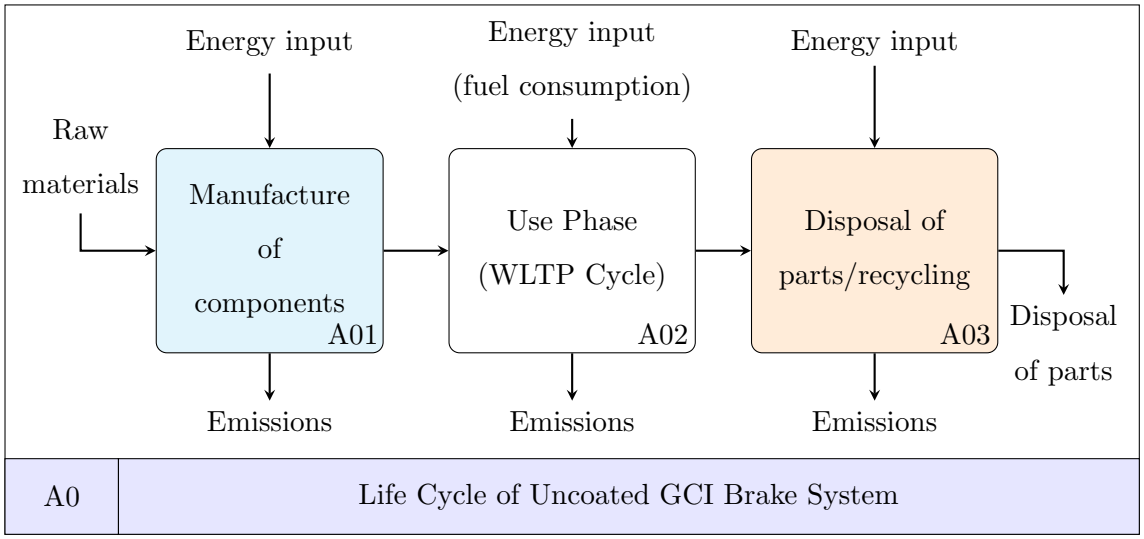

Figure 5.2: Level 2 hierarchical child diagram for uncoated GCI rotor (full life cycle).

The use phase of the rotor (A02) is a simple process to define, applying the FU of 1250 WLTP cycles (240,000 km). A02 is the stage at which data is collected for the use phase of the rotor; therefore, this activity cannot be broken down any further. The interactions within the use phase are inputs of the manufactured braking system and fuel consumption and outputs of a used braking system and the emissions released during the WLTP cycles. Level 3 of the hierarchical system has two diagrams, one describing the component manufacturing process (A01) and one describing the disposal process (A03). The manufacturing process can be divided between the pad and the rotor (A011 / A012), as illustrated in Figure 5.3. Figure 5.4 details the disposal of components, including machining of any remaining tribolayer or particles fused to the brake pad rotor (A031), prior to disposal through recycling (A032) and landfilling (A033). Similarly for the brake pad, any remaining friction material is machined off prior to recycling the steel backplate (A034). To improve the sustainability of the brake industry, companies such as Green Friction [125] are currently researching ways to recycle and reuse the remaining friction material.

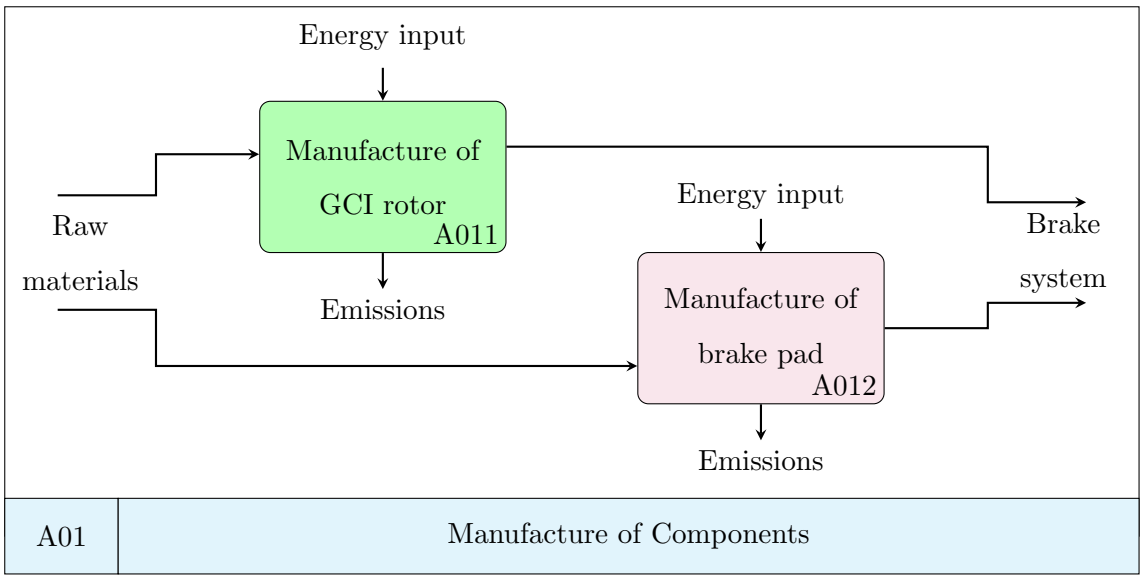

Figure 5.3: Level 3 hierarchical child diagram for uncoated GCI (manufacture of components).

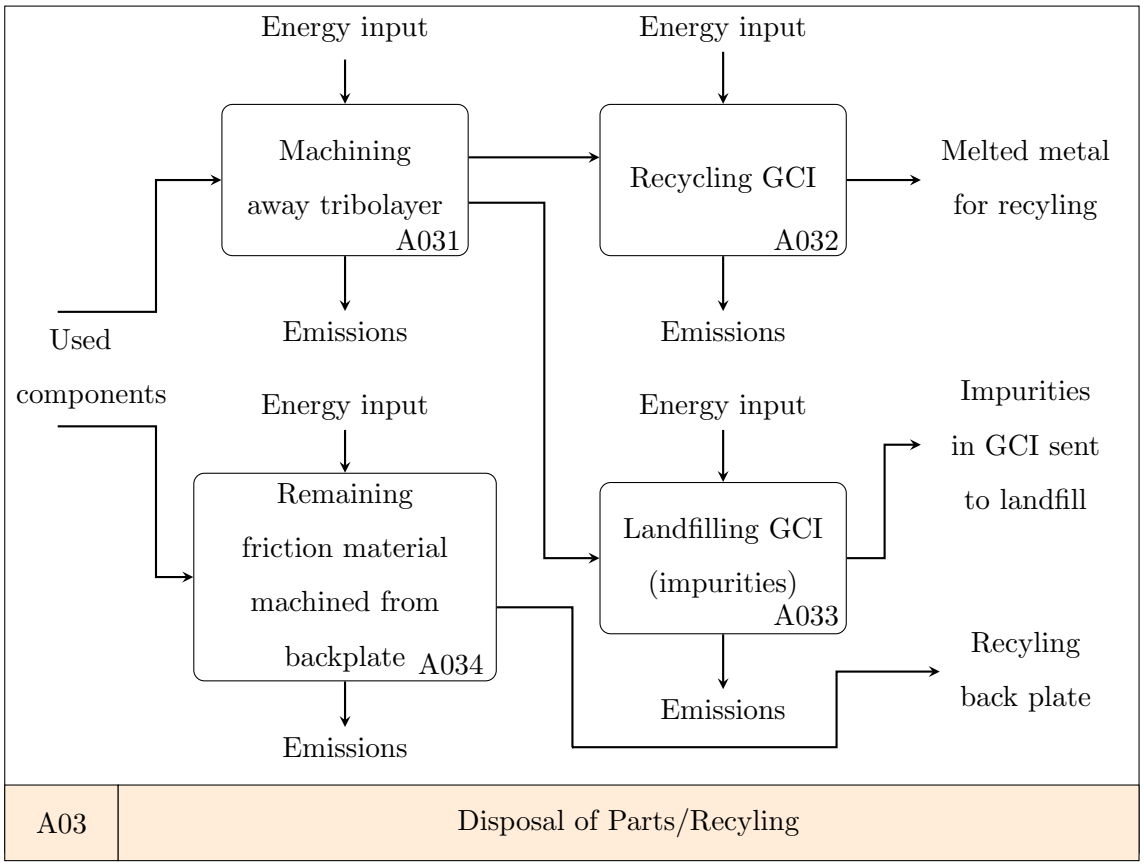

Figure 5.4: Level 3 hierarchical child diagram for uncoated GCI (disposal of components).

Diagram A03 displays the disposal stages at which the inventory data was collected. Therefore, this is the most detailed diagram required for this phase, meaning that level 4 of the hierarchy is only required to show increased detail of the manufacturing process. This level is the final level of the present hierarchical system. The manufacturing processes are broken down into individual unit processes, for which data was then gathered. As shown in Figure 5.5, the first stage of the rotor manufacturing process involves the mining and

processing of raw materials (A0111). The resulting iron ore is smelted to form ingots ready for casting (A0112). The ingots are then melted, combined with any alloying constituents, and poured into the sand moulds as part of the casting process (A0113). Figure 5.6 indicates how the pad is manufactured by assembling the friction material and the back plate into one component (A0123). The manufacture of the friction material (A0121) could have been further broken down, as this is a complex process involving a number of different operations and materials. However, this was considered unnecessary for the present comparative study, in which the pad material was assumed to be the same for all rotors considered, so pad manufacturing was omitted from data collection.

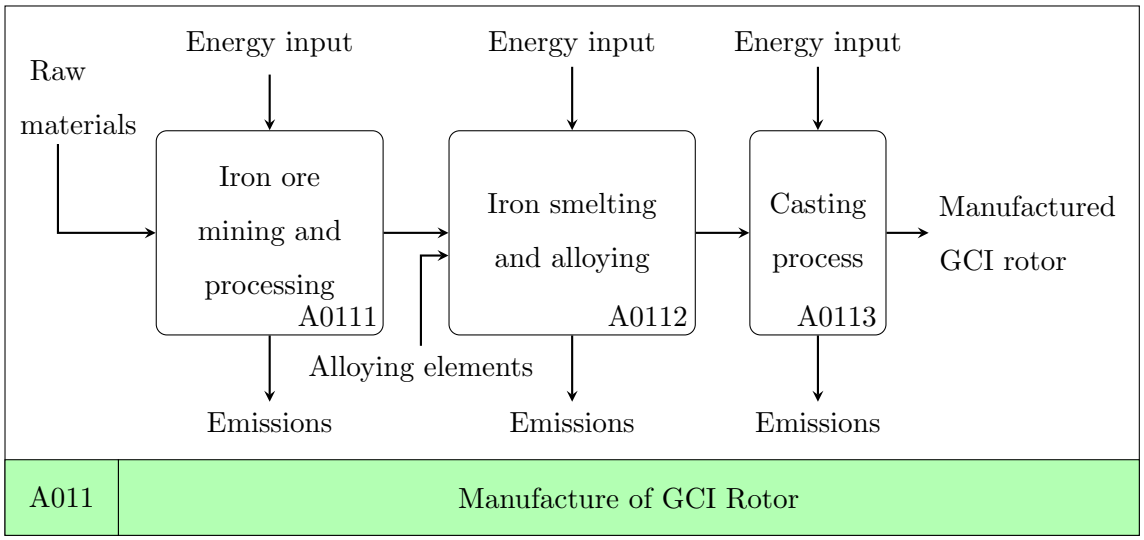

Figure 5.5: Level 4 hierarchical child diagram for uncoated GCI (manufacture of GCI rotor).

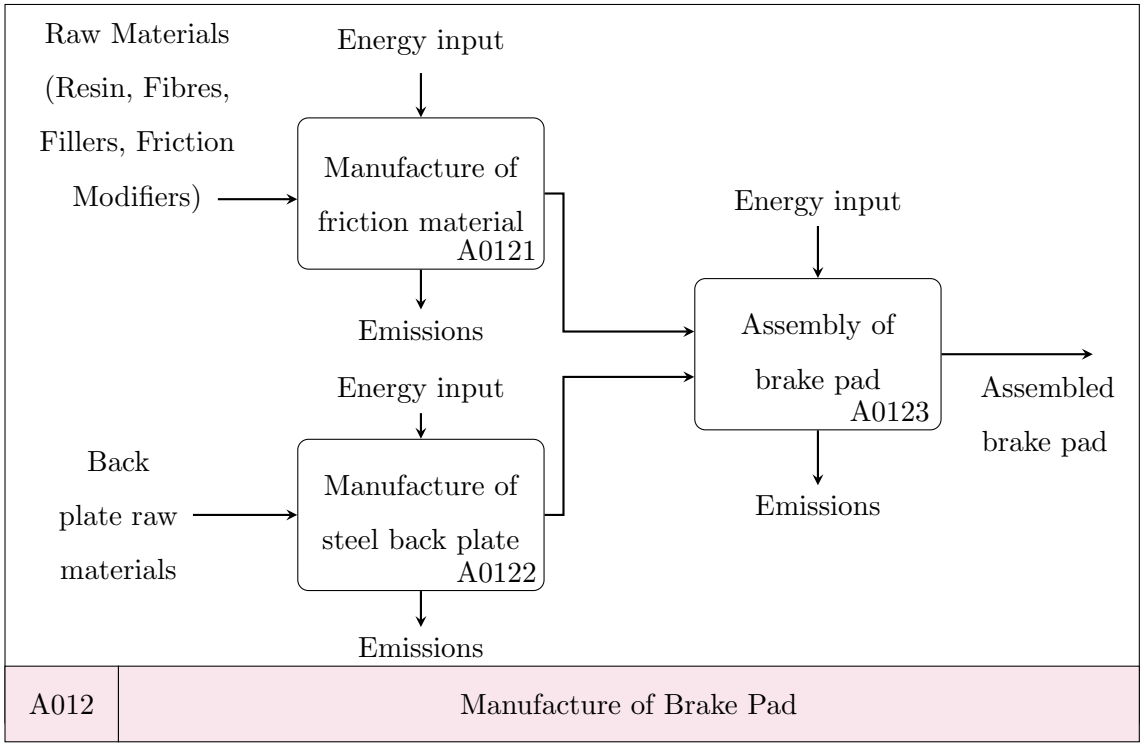

Figure 5.6: Level 4 hierarchical child diagram for uncoated GCI (manufacture of brake pad).

5.2.2 Diagram Amendments for Laser-Clad GCI

The laser-clad GCI rotor offers key advantages over other alternatives, such as the utilisation of infrastructure already in place for manufacturing uncoated GCI rotors. The only phase requiring alteration is the manufacture of the rotor, with the added inclusion of the laser-clad coating process. The diagram notation used is B, B0, B01 etc, due to the laser-clad rotor being the second that was investigated. Diagrams A, A011 and A012 did not require alterations and so did not need to be redrawn. These diagrams were simply relabelled B, B011, and B012 (but not reshown) when referring to the laser-clad rotor. Figure 5.7 (B0) outlines the inclusion of the recoating ability of the laser-clad GCI rotor, generating closed-loop recycling. Figure 5.8 illustrates the alteration to diagram A01, with the addition of the coating process and the ability to repurpose the rotor after use by recoating. At the end of life, the remaining coating is machined off (B031) and the laser cladding process is repeated to repurpose the rotor and reduce the demand on raw materials. The second level 3 diagram, showing the disposal of components, therefore, also required a minor alteration to include an output arrow, demonstrating this closed-loop recycling. This amended diagram is shown in Figure 5.9 to form B03.

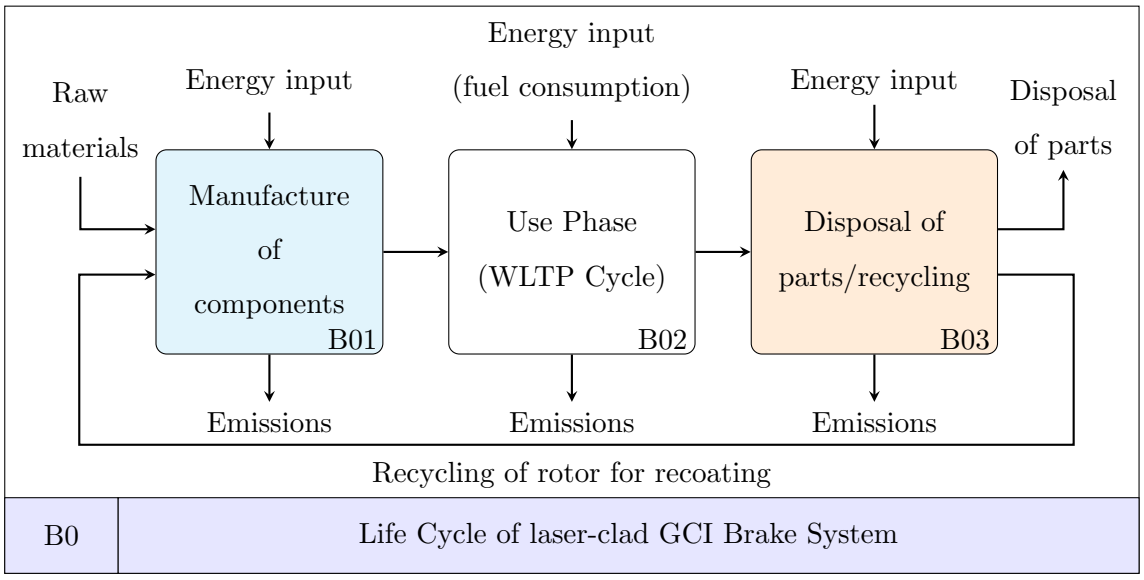

Figure 5.7: Level 2 hierarchical child diagram for laser-clad GCI rotor (full life cycle).

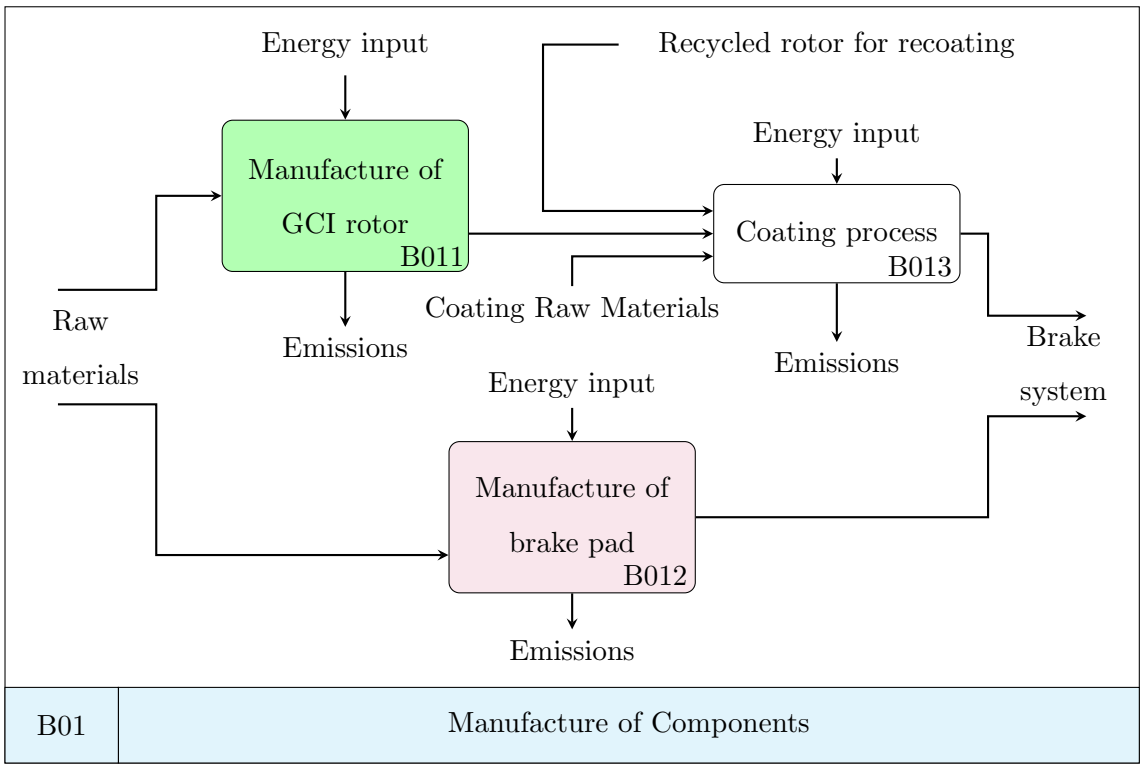

Figure 5.8: Level 3 hierarchical child diagram for laser-clad GCI (manufacture of components).

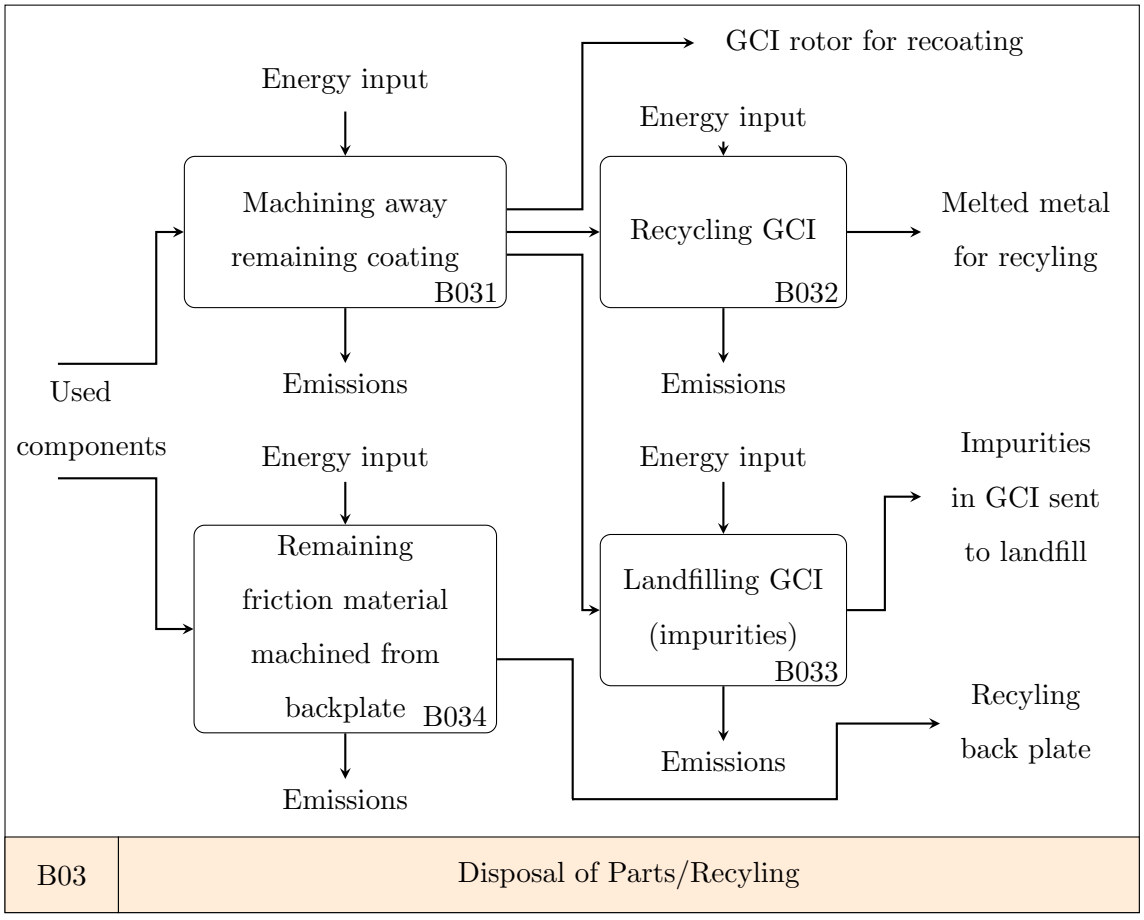

Figure 5.9: Level 3 hierarchical child diagram for laser-clad GCI (disposal of components).

5.3 Inventory Analysis

This section outlines the assumptions, data collection, and calculations made as part of the inventory analysis phase of the present LCA case study (case study I).

5.3.1 Case Study Assumptions and Data Collection

Assumptions are required prior to data collection, which assists in the definition of what data are required and what form such data should take within the present case study. The generic assumptions that were discussed in Section 3.3.2 for use within both case studies are summarised below.

- Low metallic (LM) brake pads were assumed to be used for all rotor materials; therefore, the manufacture (A012/B012) and the disposal (A034/B034) of the brake pads were classified as identical phases and therefore were omitted from the comparative study.

- The energy input (petrol consumption) and accompanying CO_2 emissions associated with the weight of the brake rotor were calculated and included in the use phase of the product system (Equations 3.7 and 3.9). The weight of the pads and other components, such as the calliper, were omitted from this calculation because they were assumed to be identical for all rotors considered.

The GCI manufacturing process involves the addition of alloying elements to achieve the desired properties of the material. These alloying components typically vary from manufacturer to manufacturer. Therefore, within the present case study, generic data was used for a standard GCI material, obtained from the EcoInvent database [120, 121], which is summarised in Table 5.1. It is important that no impurities are present within the brake rotor due to the high performance demands and safety requirements of the braking system. To ensure that this was the case, within the present LCA study it was assumed that 100% of the GCI rotor was manufactured from raw materials and not recycled scrap.

Table 5.1: Inventory data for the manufacture of 1 kg of GCI (A011/B011) - EcoInvent [120, 121].

Flow Name	Emission Type	Unit	Iron Ore Mining and Processing (A0111/B0111)	Iron Smelting and Alloying (A0112/B0112)	Casting Process (A0113/B0113)
energy	resources	kWh	2.53×10^{-3}	3.26×10^{-2}	4.24×10^{-1}
diesel	resources	MJ	4.54×10^{-2}	0	0
iron	resources	kg	8.22×10^{-1}	0	0
hard coal	resources	kg	0	1.11×10^{-1}	0
natural gas	resources	Nm^3	0	1.23×10^{-3}	2.50×10^{-2}
bentonite	resources	kg	0	2.33×10^{-5}	0
chromium	resources	kg	0	9.61×10^{-7}	0
dolomite	resources	kg	0	1.98×10^{-4}	0
steel	resources	kg	0	5.44×10^{-6}	0
$PM_{2.5}$	to air	kg	2.56×10^{-4}	1.12×10^{-4}	1.66×10^{-4}
PM_{10}	to air	kg	2.56×10^{-3}	1.27×10^{-4}	3.32×10^{-4}
heavy metals	to air	kg	5.03×10^{-7}	3.95×10^{-7}	4.31×10^{-6}
CH_4	to air	kg	0	9.13×10^{-5}	0
CO	to air	kg	0	1.46×10^{-2}	2.32×10^{-3}
CO_2	to air	kg	0	8.01×10^{-1}	0
N_2O	to air	kg	0	2.41×10^{-10}	0
NMVOC	to air	kg	0	1.49×10^{-5}	0
NO_x	to air	kg	0	5.69×10^{-4}	1.80×10^{-4}
HC	to air	kg	0	6.47×10^{-6}	7.70×10^{-5}
SO_2	to air	kg	0	4.83×10^{-4}	7.70×10^{-5}
HCl	to air	kg	3.32×10^{-5}	5.20×10^{-6}	
HF	to air	kg	0	7.16×10^{-6}	2.35×10^{-6}
H_2S	to air	kg	0	7.72×10^{-6}	0
COD	to water	kg	9.32×10^{-5}	0	0
heavy metals	to water	kg	0	2.63×10^{-12}	0
nitrate	to water	kg	0	1.84×10^{-9}	0
phosphorus	to water	kg	0	1.20×10^{-10}	0

The disposal process (A03/B03) contains three main sections: machining away any remaining tribolayer/coating (A031/B031), recycling and landfilling the GCI (A032/B032 and A033/B033) and the disposal of the brake pad (A034/B034). As mentioned previously,

the disposal of the brake pad was assumed identical between rotors and so was omitted from the case study comparison. It would require more energy to machine the hard coating than the tribolayer, although this would still only take several minutes. Therefore, the difference in energy requirement between these machining processes was considered negligible in comparison to the energy requirement for other phases of the life cycle and was omitted.

At the end of the life of the brake rotor, a large portion of the GCI can be recycled (A032/B032). This is done in open-loop mode as it is assumed that the manufacture of the brake rotor uses 100% raw (unrecycled) materials. The emissions from the melting of the GCI were assumed to be extracted and treated prior to release into the environment, and therefore only the energy required to melt the metal was considered. It was assumed that 90% of the remaining GCI after use goes through this recycling process, while the remaining 10% must be landfilled due to impurities, unsuitable material contamination or residual matter after processing [126]. The thermophysical properties of GCI were used to calculate the energy required to melt 1 kg of material. Table 5.2 [127] outlines the values for the required calculation, carried out using Equations 5.1 and 5.2.

$$Energy\ to\ melt\ \ (J/kg) = \Delta H_f + C_{p_s}\left(T_s - T_0\right) + C_{p_l}\left(T_l - T_s\right) \tag{5.1}$$

$$Energy\ to\ melt\ \ (kWh/kg) = \frac{Energy\ to\ melt\ \ (J/kg)}{[a]3.6 \times 10^6} \tag{5.2}$$

[a] 3.6×10^6 Joules is equal to 1 kWh [128]

Table 5.2: Thermophysical properties of GCI.

Thermophysical Property	Symbol	Value	Unit
Specific heat, solid	C_{p_s}	660	J/kg.K
Specific heat, liquid	C_{p_l}	950	J/kg.K
Initial temperature	T_0	298.15	K
Solidus temperature	T_s	1356	K
liquidus temperature	T_l	1463	K
Latent heat of fusion	ΔH_f	240×10^3	J/kg

Table 5.3 outlines the inventory data associated with the landfill of 1 kg of GCI [129]. The allocation by mass was used to determine the resources and emissions from the landfill associated with disposing of 1 kg of material.

Table 5.3: Resources required for landfill operation per kg disposed (A033/B033).

Flow Name	Emission Type	Unit	Landfilling GCI
energy	resources	kWh	9.63×10^{-4}
diesel	resources	kg	6.24×10^{-1}
clay, unspecified	resources	kg	4.47×10^{1}
CO_2	to air	kg	2.16×10^{-1}
CO	to air	kg	1.10×10^{-4}
NO_x	to air	kg	1.68×10^{-5}
PM_{10}	to air	kg	7.74×10^{-8}
SO_2	to air	kg	7.74×10^{-5}
CH_4	to air	kg	5.17×10^{-2}
HCl	to air	kg	3.29×10^{-5}
HF	to air	kg	3.14×10^{-6}
H_2S	to air	kg	1.10×10^{-4}
heavy metals	to air	kg	1.26×10^{-9}
HC	to air	kg	6.92×10^{-11}

5.3.1.1 Uncoated GCI

The inventory data specific to the uncoated GCI rotor was only in the use phase. Limmer [1] conducted small-scale testing on an uncoated GCI rotor as part of previous Ph.D. research conducted at the University. Table 5.4 outlines the particulate masses collected from the brake rotor during a single WLTP testing cycle, averaged over test cycles 6-8. The methodology for this process was described in Chapter 4

Table 5.4: Inventory data for the WLTP small-scale testing – Uncoated GCI (as collected on Dekati foils)(A02).

Flow Name	Emission Type	Unit	WLTP Cycle
$PM_{2.5}$	to air	kg	3.48×10^{-7}
PM_{10}	to air	kg	1.24×10^{-6}

5.3.1.2 Laser-Clad GCI

The laser-clad GCI rotor uses the same inventory data for manufacturing and disposing of GCI as the uncoated GCI rotor. The additional inventory of manufacture required for the laser-cladding process. Data were collected from TWI, as a primary data source, surrounding such a process. The laser cladding process is conducted in two layers. Table 5.5 outlines the data for the laser-clad coating inventory. Based on internal discussions

with TWI, it was assumed that this coating process could be repeated up to 4 times (5 coatings total), allowing for 5 cycles of use for each manufactured GCI rotor.

Table 5.5: Primary data information for the laser-clad coating process (B013).

Data Description	Data Value
Laser power	16 kW
Plug efficiency	40%
layer cycle time	30 seconds
layer 1	430L steel
layer 2	80:20 wt% split 430L steel:TiC
layer 1 thickness	100 µm
layer 2 thickness	150 µm
layer 2 thickness loss on postprocess grinding	50 µm
% waste during coating	20%

The use phase testing under WLTP cycle conditions also differed. The same small-scale testing protocol was conducted for the laser-clad GCI rotor, replicating the methods used by Limmer [1] for the uncoated GCI as described in Chapter 4. Table 5.6 summarises the inventory data collected on each foil of the Dekati, averaged over WLTP cycles 6-8.

Table 5.6: Inventory data for the WLTP small-scale testing – Laser-clad GCI (as collected on Dekati foils)(B02).

Flow Name	Emission Type	Unit	WLTP Cycle
$PM_{2.5}$	to air	kg	1.00×10^{-7}
PM_{10}	to air	kg	3.20×10^{-7}

5.3.1.3 Transport

An important part of any LCA study is the inclusion of impacts associated with the transport of materials between phases. The transport demands after the rotors were fitted to the vehicles were considered to be constant for both the uncoated and coated rotors. Therefore, only fuel consumption and associated CO_2 emissions for transporting manufactured material from the assumed German GCI foundry to the location of the Nissan assembly factory in Sunderland were included. Tables 5.7 and 5.8 outline the transport distances assumed for the uncoated and laser-clad GCI rotors, respectively, in the present study. It was recognised that this is only an example of the potential transport scenario and the nature of the model means that it is adaptable to consider other transport logistics that may apply, should initial results illustrate the transport as being a significant contributing factor to the environmental impact of the whole life cycle.

Table 5.7: Transport distances for uncoated GCI.

Starting Location	Destination	Distance (km)	Transport method
Germany	Calais port	744	Long distance truck
Calais port	Dover port	50	Cargo ship
Dover port	Nissan factory	562	Long distance truck

Table 5.8: Transport distances for Laser-clad GCI.

Starting Location	Destination	Distance (km)	Transport method
Germany	Calais port	744	Long distance truck
Calais port	Dover port	50	Cargo ship
Dover port	TWI, Rotherham	401	Long distance truck
TWI, Rotherham	Nissan Factory	206	Long distance truck

5.3.2 Life Cycle Inventory Calculations

The life cycle inventory calculations were necessary to ensure that the inventory data collected was correctly scaled based on the rotor specifications of the case study and the definition of FU.

5.3.2.1 Rotor Manufacture

The manufacturing inventory was scaled in the same way for both rotors. To scale these data, the inventory values per kg of GCI were multiplied by the total weight required, followed by the number of rotors required per FU duration. In casting procedures, some waste is generated because the metal solidifies in the gating system. This system is a series of channels that allow the molten metal to flow into the mould cavity. However, when this excess is machined off, it can be remelted and fed back into the raw material pipeline for the next rotor, so in terms of inventory scaling, only the rotor mass was used. Based on the case study rotor dimensions of a 350 mm diameter and a cheek thickness of 28 mm, the uncoated GCI rotor was estimated to be 9.55 kg. In Section 4.4, it was determined that 4.3 uncoated GCI rotors were required per FU duration, while only 1 laser-clad GCI was needed. Equation 5.3 was used to calculate the manufacture inventory for the full rotor.

$$Manufacture\ inventory = Rotor\ weight \times inventory\ per\ kg \times No.\ rotors\ per\ FU \quad (5.3)$$

5.3.2.2 Coating Process

The inventory for the laser-clad coating process was based on estimates and internal discussions with TWI. To calculate the masses of the raw materials required, the relative densities and required volumes were used. The density for 430L steel was taken as 7750 kg/m^3 and for TiC as 4930 kg/m^3 [123]. Equations 5.4 - 5.7 outline the process to determine the required mass of materials required for the coating, as well as the total rotor mass used for fuel consumption calculations during use.

$$Surface\ area\ to\ coat = \left((External radius)^2 - (Internal radius)^2\right)\pi \tag{5.4}$$

$$Material\ mass = Density \times Surface\ area \times Layer\ thickness \tag{5.5}$$

$$Total\ material\ required = \%\ waste \times (layer\ 1\ mass + layer\ 2\ mass) \tag{5.6}$$

$$Energy\ requirement = \frac{Laser\ power \times Duration}{Efficiency} \tag{5.7}$$

5.3.2.3 Use Phase

The use phase emissions data were calculated from the mass measurements on the Dekati foils at an air sampling rate of 10 l/min. The Dekati extracts a small sample of air that passes over the small-scale rotor and out through the exhaust duct. Therefore, the foil masses of this small air sample were scaled to provide estimate values for the entire exhaust duct using Equation 5.8.

$$PM_{small\text{-}scale\ test}\ (mg/WLTP) = PM_{dekati}\ (mg/WLTP) \times \frac{Q_{exhaust}\ \left(m^3/h\right)}{Q_{dekati}\ (m^3/h)} \tag{5.8}$$

An energy-based scaling factor of 13.57 was utilised to scale such small-scale test data up to a full-sized rotor. This value was estimated using the ratio between the surface area of the full-scale rotor and the surface area of the small-scale counterpart. The small-scale test rig applied a pin-on-disc approach and so only generated wear from one rotor surface. Therefore, the results also needed to be doubled. The complete methodology of this scaling approach is outlined in Chapter 4 (Equations 4.5-4.8). Fuel consumption and associated CO_2 emissions were also determined. Such calculations were based on the total rotor weight and are described in Chapter 3 through Equations 3.7 and 3.9.

The uncoated GCI rotor had an estimated weight of 9.55 kg based on the case study dimensions of a 350 mm diameter and 28 mm cheek thickness. To calculate the total mass for the laser-clad GCI rotor, the mass of the coating constituents was added. These values

have already been determined as part of the coating inventory calculations; however, post-process grinding results in the final thickness of layer 2 being 0.1 mm rather than the initial 0.15 mm, so 66% of the previous material mass was used. Equation 5.9 was applied here.

$$Laser\text{-}clad\ GCI\ mass = \sum_{masses} (UncoatedGCI,\ Mass_{layer1},\ Mass_{layer2}) \tag{5.9}$$

$$Laser\text{-}clad\ GCI\ mass = 9.55 + 0.122 + 0.113 = 9.78\ kg$$

5.3.2.4 Disposal of Rotor

Similarly to the manufacture of the rotor, the disposal inventory was scaled by multiplying the inventory per kg by the mass of GCI followed by the number of rotors required per FU (4.3 for uncoated GCI and 1 for laser-clad GCI). The assumption was that 10% of the rotor was landfilled while the remaining material was recycled [126]. The inventory was therefore scaled using Equations 5.10-5.12.

$$Landfill\ inventory = 0.1 \times Mass\ of\ GCI \times Landfill\ inventory\ per\ kg \tag{5.10}$$

$$Recycling\ inventory = 0.9 \times Mass\ of\ GCI \times Energy\ to\ melt\ \ (kWh/kg) \tag{5.11}$$

$$Disposal\ Inventory = No.\ rotors\ per\ FU \times \sum_{Inventory} (Landfill,\ Recycling) \tag{5.12}$$

5.3.2.5 Transport

The distances shown in Tables 5.7 and 5.8 were used to calculate the fuel consumption from the transport of materials between the life cycle phases, as described in Equation 5.13. Equation 3.9 was then applied to determine the mass of associated CO_2 emissions.

$$Petrol\ use\ \ (l/tonne) = \sum_{Methods\ of\ transport} (FC \times distance) \tag{5.13}$$

5.4 Life Cycle Impact Assessment

The results of the present case study are presented in the following life cycle impact assessment. Due to the large magnitude differences of the results between the impact categories, these impact scores are shown in tabular form. The impact scores were then

normalised between 0 and 1, with respect to the highest value, for each impact category, to be plotted graphically. For each individual rotor material, the percentage representation of each life cycle phase is illustrated, prior to an overall comparison between the two rotors.

5.4.1 Uncoated GCI

5.4.1.1 Midpoint Impact Results

Tables 5.9 - 5.11 display the impact results generated from the Python LCA model for the midpoint impacts of the uncoated GCI rotor. The percentage contributions of each phase of the life cycle (i.e. manufacture, transport, use, and disposal) were plotted to help assess the biggest phase contributors to the overall impact during the complete life cycle of the rotor. Figure 5.10 indicates this phase contribution breakdown of the uncoated GCI rotor.

Table 5.9: Midpoint impact results from the manufacture of an uncoated GCI rotor (A011).

Midpoint Impact Category	Iron Ore Mining and Processing (A0111)	Iron Smelting and Alloying (A0112)	Casting Process (A0113)	Transport
Global Warming (kg CO_2 eq.)	3.14×10^{-3}	3.32×10^{1}	5.25×10^{-1}	1.57
Stratospheric Ozone Depletion (kg CFC_{11} eq.)	2.93×10^{-10}	3.87×10^{-9}	4.90×10^{-8}	0
Fine Particulate Matter Formation (kg $PM_{2.5}$ eq.)	1.06×10^{-2}	4.60×10^{-3}	6.85×10^{-3}	0
Acidification (kg SO_2 eq.)	2.51×10^{-5}	3.10×10^{-2}	1.04×10^{-2}	0
Photochemical Ozone Formation (kg NO_x eq.)	1.45×10^{-6}	3.18×10^{-2}	8.96×10^{-3}	0
Human Toxicity (kg 1,4-DCB eq.)	2.38	1.87	1.98×10^{1}	0
Ecotoxicity (kg 1,4-DCB eq.)	2.79×10^{1}	5.98×10^{1}	7.37×10^{2}	0
Eutrophication (kg P eq.)	3.14×10^{-5}	1.05×10^{-3}	8.96×10^{-4}	0
Mineral Resource Scarcity (kg Cu eq.)	2.10	3.77×10^{-6}	0	0
Fossil Resource Scarcity (kg oil eq.)	1.13×10^{-1}	9.02	1.21	1.48

Table 5.10: Midpoint impact results for the use phase of an uncoated GCI rotor (A02).

Midpoint Impact Category	Use Phase
Global Warming (kg CO_2 eq.)	1.95×10^{2}
Stratospheric Ozone Depletion (kg CFC_{11} eq.)	0
Fine Particulate Matter Formation (kg $PM_{2.5}$ eq.)	5.24×10^{-1}
Acidification (kg SO_2 eq.)	0
Photochemical Ozone Formation (kg NO_x eq.)	0
Human Toxicity (kg 1,4-DCB eq.)	1.53
Ecotoxicity (kg 1,4-DCB eq.)	0
Eutrophication (kg P eq.)	0
Mineral Resource Scarcity (kg Cu eq.)	0
Fossil Resource Scarcity (kg oil eq.)	1.83×10^{2}

Table 5.11: Midpoint impact results for the disposal of an uncoated GCI rotor (A032/A033).

Midpoint Impact Category	Landfilling GCI	Recycling GCI
Global Warming (kg CO_2 eq.)	8.15	3.22×10^{-1}
Stratospheric Ozone Depletion (kg CFC_{11} eq.)	1.11×10^{-11}	3.01×10^{-8}
Fine Particulate Matter Formation (kg $PM_{2.5}$ eq.)	0	0
Acidification (kg SO_2 eq.)	1.34×10^{-3}	2.58×10^{-3}
Photochemical Ozone Formation (kg NO_x eq.)	6.86×10^{-4}	1.49×10^{-4}
Human Toxicity (kg 1,4-DCB eq.)	2.07×10^{-3}	0
Ecotoxicity (kg 1,4-DCB eq.)	1.26×10^{-1}	3.22×10^{2}
Eutrophication (kg P eq.)	3.10×10^{-6}	3.54×10^{-4}
Mineral Resource Scarcity (kg Cu eq.)	1.93	0
Fossil Resource Scarcity (kg oil eq.)	7.70	6.15×10^{-2}

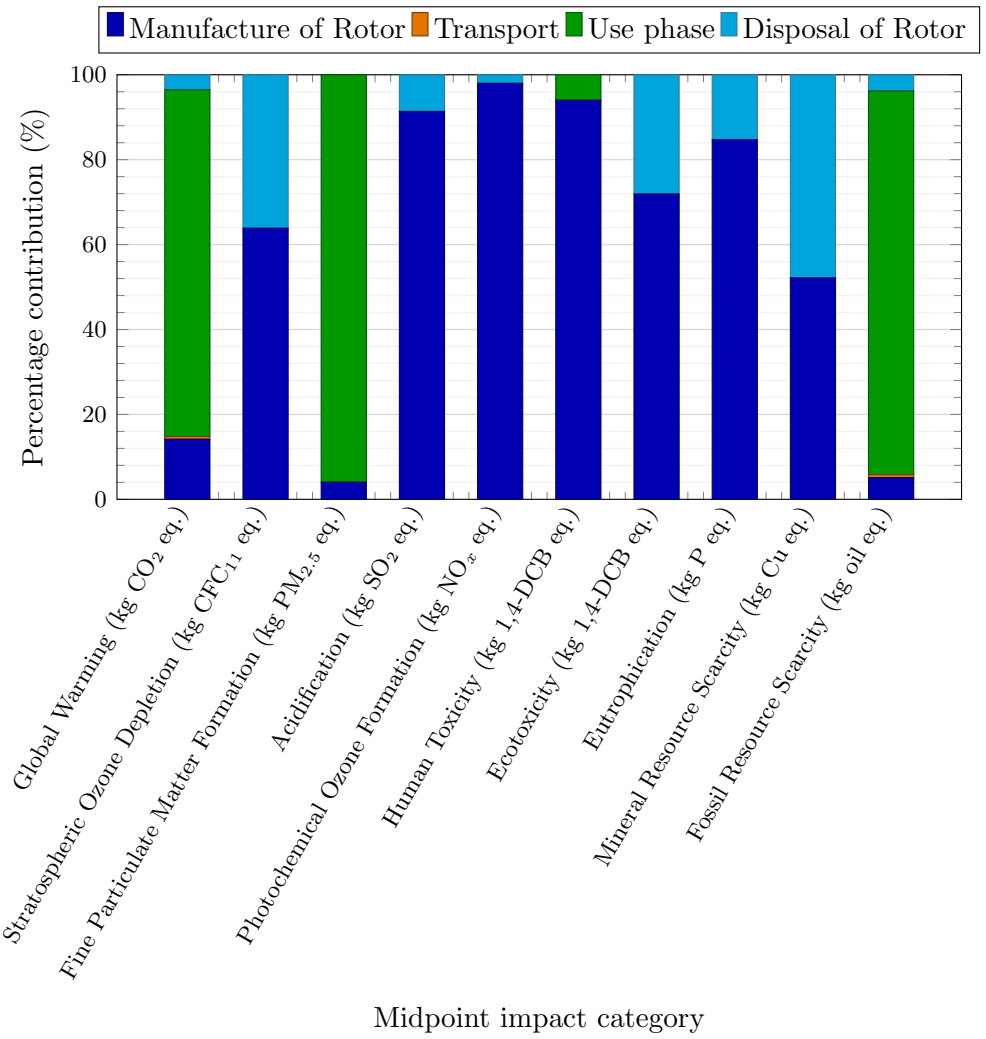

Figure 5.10: Life cycle midpoint impact results for uncoated GCI (unit process percentage contribution).

It can be seen in Figure 5.10 that impact categories such as global warming (81%), fossil resource scarcity (90%), and fine particulate matter formation (96%) are all heavily influenced by the use phase of the rotor. Global warming impact is related to the CO_2 emissions associated with fuel consumption, and therefore is dependent on the mass of the rotor. Fuel consumption is also the cause for the fossil resource scarcity impact due to the required crude oil extraction to produce petrol. The use phase is the largest emitter of PM throughout the rotor life cycle, which leads to its large contribution to the impact of fine particulate matter formation.

The manufacturing phase was found to have the largest influence on acidification (91%), photochemical ozone formation (98%) and human toxicity (94%). All three categories are heavily influenced by the emission of NO_x and SO_2, with the addition of CO for photochemical ozone formation. The disposal phase was found to have contributed a magnitude 2-4 times smaller to these emissions compared to the large amounts of CO and NO_x released during the iron smelting and casting processes.

Impact categories such as stratospheric ozone depletion, ecotoxicity, eutrophication, and mineral resource scarcity were found to depend both on the manufacture and disposal phases of the GCI. This was likely due to the fact that these impact categories are the most heavily associated with energy requirements, with the exception of mineral resource scarcity. Similar magnitudes of energy input were required during both the casting and the recycling of the GCI. The manufacturing phase was found to contribute to a higher proportion of stratospheric ozone depletion, ecotoxicity, and eutrophication (64%, 72% and 85%) than the disposal phase (36%, 28% and 15%). The additional emission of hydrocarbons and heavy metals during manufacture compared to disposal was linked to the increase seen in ecotoxicity, while the release of NO_x and N_2O from smelting can be attributed to increases in eutrophication and stratospheric ozone depletion, respectively. Mineral resource scarcity was found to have an equal split between the clay required for the landfill site and the raw minerals required during manufacture. It was apparent from Figure 5.10 that the transport of rotors during the manufacturing phase had negligible contribution (<1%) to these midpoint impacts and so could potentially be removed from the LCA without affecting overall results.

5.4.1.2 Endpoint Impact Results

Tables 5.12 - 5.14 display the impact results generated from the Python LCA model for the endpoint impacts of the uncoated GCI rotor. The percentage contribution of each phase to the unit process endpoint impact was plotted to help assess the main impact contributors from the life cycle of the rotor. Figure 5.11 indicates this phase breakdown.

Table 5.12: Endpoint impact results from the manufacture of an uncoated GCI rotor (A011).

Endpoint Impact Category	Iron Ore Mining and Processing (A0111)	Iron Smelting and Alloying (A0112)	Casting Process (A0113)	Transport
Damage to Human Health (DALY)	1.09×10^{-5}	3.71×10^{-5}	3.99×10^{-5}	1.46×10^{-6}
Damage to Ecosystems (Species.year)	7.58×10^{-9}	7.41×10^{-8}	2.04×10^{-7}	2.20×10^{-9}
Damage to Resource Availability (USD2013)	5.37×10^{-1}	7.45×10^{-1}	3.44×10^{-1}	6.74×10^{-1}

Table 5.13: Endpoint impact results for the use phase of an uncoated GCI rotor (A02).

Endpoint Impact Category	Use Phase
Damage to Human Health (DALY)	5.13×10^{-4}
Damage to Ecosystems (Species.year)	2.73×10^{-7}
Damage to Resource Availability (USD2013)	8.37×10^{1}

Table 5.14: Endpoint impact results for the disposal of an uncoated GCI rotor (A032/A033).

Endpoint Impact Category	Landfilling GCI	Recycling GCI
Damage to Human Health (DALY)	7.57×10^{-6}	2.99×10^{-7}
Damage to Ecosystems (Species.year)	1.18×10^{-8}	8.84×10^{-8}
Damage to Resource Availability (USD2013)	3.96	8.09×10^{-3}

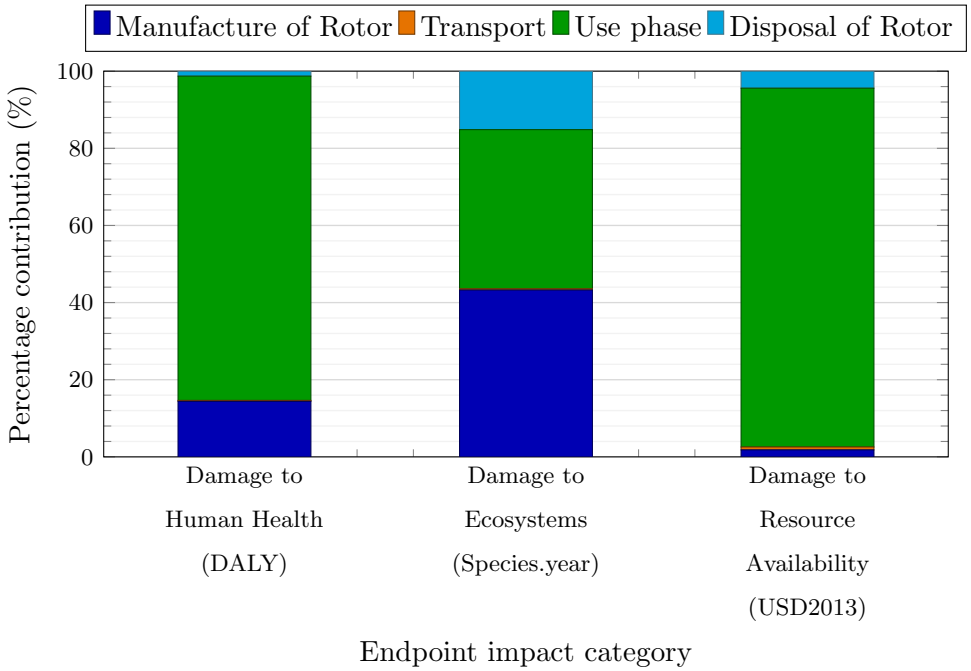

Figure 5.11: Life cycle endpoint impact results for uncoated GCI (unit process percentage contribution).

The use phase was found to be a significant contributor to human health damage (84%), along with a contribution from GCI manufacture (14%). The lack of contribution from GCI disposal can be attributed to the five associated midpoint impact categories (global warming, fine particulate matter formation, stratospheric ozone depletion, photochemical ozone formation, and human toxicity) which are almost solely dependent on manufacture and use (92%).

PM emissions and CO_2 exhaust emissions during use were found to have equal contributions to ecosystem damage as energy demand, NO_x and SO_2 during manufacture (both ~42%). The disposal contributed the remaining ~15% as a result of the associated

energy demand. Similarly to damage to human health, damage to resource availability was mainly attributed to the use phase of the rotor (93%). The impact of fossil resource availability is related to the scarcity of mineral resources and the depletion of fossil fuels. The amount of crude oil required for fuel consumption during use significantly outweighed the mineral resource scarcity impact, causing the use phase to be the dominant contributor to damage to resource availability. Again, the contribution of rotor transport to these end-point impact categories was found to be negligible (<1%).

5.4.2 Laser-Clad GCI

5.4.2.1 Midpoint Impact Results

Tables 5.15 - 5.18 display the impact results generated from the Python LCA model for the midpoint impacts of the coated GCI rotor. The percentage contribution of each phase was plotted to help assess the biggest impact contributors throughout the life cycle of the rotor. Figure 5.12 indicates this phase breakdown.

Table 5.15: Midpoint impact results from the manufacture of a laser-clad GCI rotor (B011).

Midpoint Impact Category	Iron Ore Mining and Processing (B0111)	Iron Smelting and Alloying (B0112)	Casting Process (B0113)	Transport
Global Warming (kg CO_2 eq.)	1.44×10^{-4}	1.52	2.41×10^{-2}	6.33×10^{-2}
Stratospheric Ozone Depletion (kg CFC_{11} eq.)	1.34×10^{-11}	1.78×10^{-10}	2.25×10^{-9}	0
Fine Particulate Matter Formation (kg $PM_{2.5}$ eq.)	4.86×10^{-4}	2.11×10^{-4}	3.14×10^{-4}	0
Acidification (kg SO_2 eq.)	1.15×10^{-6}	1.42×10^{-3}	4.77×10^{-4}	0
Photochemical Ozone Formation (kg NO_x eq.)	6.65×10^{-8}	1.46×10^{-3}	4.11×10^{-4}	0
Human Toxicity (kg 1,4-DCB eq.)	1.09×10^{-1}	8.57×10^{-2}	9.07×10^{-1}	0
Ecotoxicity (kg 1,4-DCB eq.)	1.28	2.74	3.38×10^{1}	0
Eutrophication (kg P eq.)	1.44×10^{-6}	4.83×10^{-5}	4.11×10^{-5}	0
Mineral Resource Scarcity (kg Cu eq.)	9.64×10^{-2}	1.73×10^{-7}	0	0
Fossil Resource Scarcity (kg oil eq.)	5.17×10^{-3}	1.25×10^{-1}	5.55×10^{-2}	5.95×10^{-2}

Table 5.16: Midpoint impact results for the coating process of a laser-clad GCI rotor (B013).

Midpoint Impact Category	Coating	Transport
Global Warming (kg CO_2 eq.)	3.97×10^{-2}	5.77×10^{-2}
Stratospheric Ozone Depletion (kg CFC_{11} eq.)	3.70×10^{-9}	0
Fine Particulate Matter Formation (kg $PM_{2.5}$ eq.)	0	0
Acidification (kg SO_2 eq.)	3.17×10^{-4}	0
Photochemical Ozone Formation (kg NO_x eq.)	1.83×10^{-5}	0
Human Toxicity (kg 1,4-DCB eq.)	0	0
Ecotoxicity (kg 1,4-DCB eq.)	3.97×10^{1}	0
Eutrophication (kg P eq.)	4.36×10^{-5}	0
Mineral Resource Scarcity (kg Cu eq.)	2.19×10^{-2}	0
Fossil Resource Scarcity (kg oil eq.)	7.57×10^{-3}	5.42×10^{-2}

Table 5.17: Midpoint impact results for the use phase of a laser-clad GCI rotor (B02).

Midpoint Impact Category	Use Phase
Global Warming (kg CO_2 eq.)	1.99×10^{2}
Stratospheric Ozone Depletion (kg CFC_{11} eq.)	0
Fine Particulate Matter Formation (kg $PM_{2.5}$ eq.)	1.51×10^{-1}
Acidification (kg SO_2 eq.)	0
Photochemical Ozone Formation (kg NO_x eq.)	0
Human Toxicity (kg 1,4-DCB eq.)	3.96×10^{-1}
Ecotoxicity (kg 1,4-DCB eq.)	0
Eutrophication (kg P eq.)	0
Mineral Resource Scarcity (kg Cu eq.)	0
Fossil Resource Scarcity (kg oil eq.)	1.88×10^{2}

Table 5.18: Midpoint impact results for the disposal of a laser-clad GCI rotor (B032/B033).

Midpoint Impact Category	Landfilling GCI	Recycling GCI
Global Warming (kg CO_2 eq.)	3.74×10^{-1}	1.48×10^{-2}
Stratospheric Ozone Depletion (kg CFC_{11} eq.)	5.11×10^{-13}	1.38×10^{-9}
Fine Particulate Matter Formation (kg $PM_{2.5}$ eq.)	0	0
Acidification (kg SO_2 eq.)	6.13×10^{-5}	1.18×10^{-4}
Photochemical Ozone Formation (kg NO_x eq.)	3.15×10^{-5}	6.83×10^{-6}
Human Toxicity (kg 1,4-DCB eq.)	9.52×10^{-5}	0
Ecotoxicity (kg 1,4-DCB eq.)	5.77×10^{-3}	1.48×10^{1}
Eutrophication (kg P eq.)	1.42×10^{-7}	1.62×10^{-5}
Mineral Resource Scarcity (kg Cu eq.)	8.84×10^{-2}	0
Fossil Resource Scarcity (kg oil eq.)	3.53×10^{-1}	2.82×10^{-3}

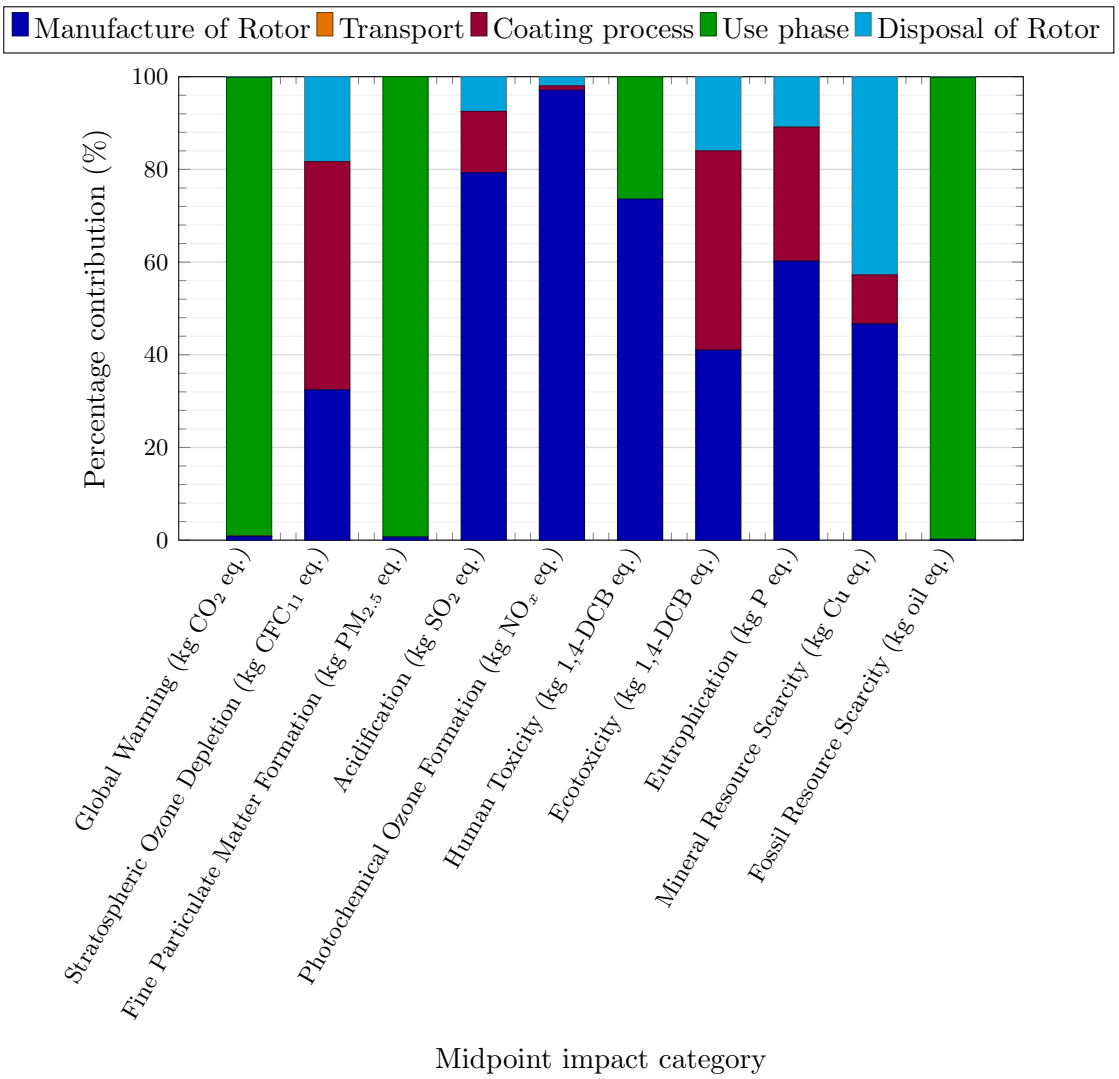

Figure 5.12: Life cycle midpoint impact results for laser-clad GCI rotor (unit process percentage breakdown).

The contribution of the use phase to the overall impacts at the midpoint was increased from that of the uncoated GCI. This is because the manufacture and disposal processes of the laser-clad rotor are now shared over 5 use phases, due to the recoating potential. Furthermore, the reduced wear rate meant that each rotor lasted 4.3 times longer before replacement was required. Impact categories such as global warming were found to now be almost exclusively caused by CO_2 exhaust emissions associated with fuel consumption (99% compared to 81% for uncoated GCI). Impact categories such as eutrophication, ecotoxicity, and stratospheric ozone depletion that were found to be related to the energy consumption during the manufacture and disposal of the unclad rotor were now found to be relatively evenly split between the manufacture, the laser-cladding process, and disposal phases.

5.4.2.2 Endpoint Impact Results

Tables 5.19 - 5.22 display the impact results generated from the Python LCA model for the endpoint impacts of the uncoated GCI rotor. The percentage contribution of each phase to the endpoint impacts was then plotted to help assess the relative impact contributors during the life cycle of the rotor. Figure 5.13 indicates this phase breakdown.

Table 5.19: Endpoint impact results from the manufacture of a laser-clad GCI rotor (B011).

Endpoint Impact Category	Iron Ore Mining and Processing (B0111)	Iron Smelting and Alloying (B0112)	Casting Process (B0113)	Transport
Damage to Human Health (DALY)	5.00×10^{-7}	1.70×10^{-6}	1.83×10^{-6}	5.87×10^{-8}
Damage to Ecosystems (Species.year)	3.48×10^{-10}	3.40×10^{-9}	9.36×10^{-9}	8.86×10^{-11}
Damage to Resource Availability (USD2013)	2.46×10^{-2}	1.07×10^{-2}	1.58×10^{-2}	2.72×10^{-2}

Table 5.20: Endpoint impact results from the coating process of a laser-clad GCI rotor (B013).

Endpoint Impact Category	Coating	Transport
Damage to Human Health (DALY)	3.68×10^{-8}	5.36×10^{-8}
Damage to Ecosystems (Species.year)	1.09×10^{-8}	8.08×10^{-11}
Damage to Resource Availability (USD2013)	6.05×10^{-3}	2.48×10^{-2}

Table 5.21: Endpoint impact results for the use phase of a laser-clad GCI rotor (B02).

Endpoint Impact Category	Use Phase
Damage to Human Health (DALY)	2.81×10^{-4}
Damage to Ecosystems (Species.year)	2.79×10^{-7}
Damage to Resource Availability (USD2013)	$8.57\times10^{+1}$

Table 5.22: Endpoint impact results for the disposal of a laser-clad GCI rotor (B032/B033).

Endpoint Impact Category	Landfilling GCI	Recycling GCI
Damage to Human Health (DALY)	3.47×10^{-7}	1.37×10^{-8}
Damage to Ecosystems (Species.year)	5.42×10^{-10}	4.05×10^{-9}
Damage to Resource Availability (USD2013)	1.82×10^{-1}	3.71×10^{-4}

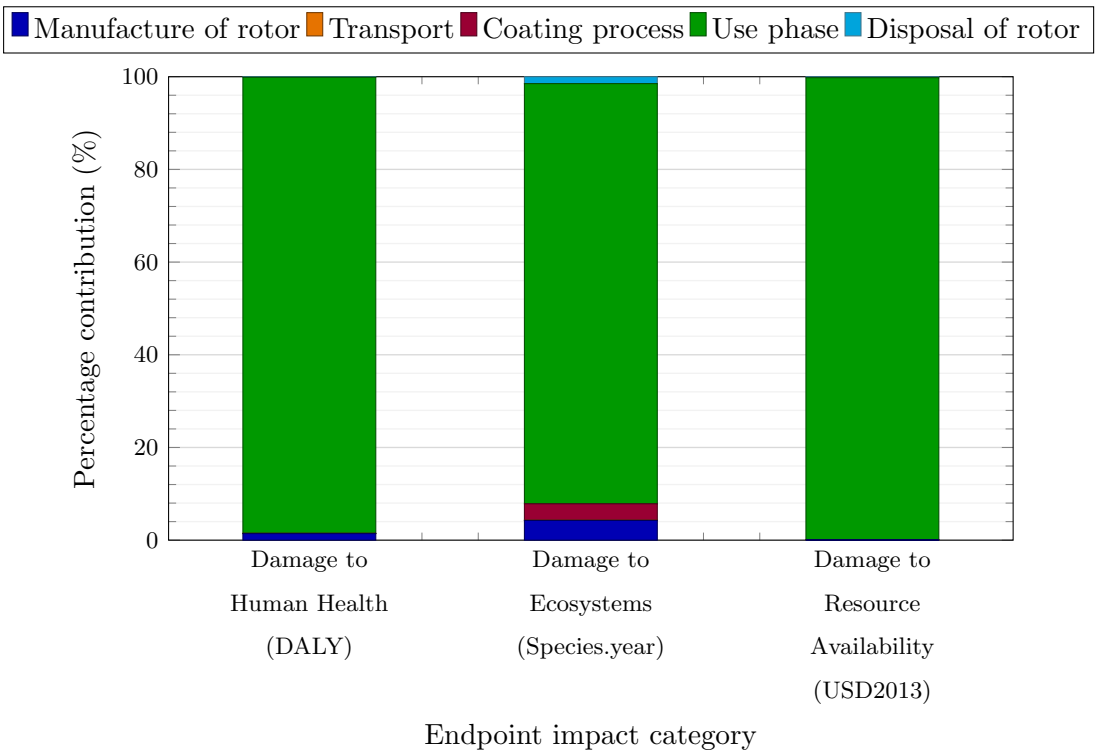

Figure 5.13: Life cycle endpoint impact results for laser-clad GCI (unit process percentage breakdown).

Similarly to the midpoint impacts, the endpoint impacts were found to be primarily driven by the use phase of the rotor. Likewise, the reduction in the contribution of manufacturing and disposal to endpoint impacts, compared to the uncoated GCI, was attributed to the potential for recoating and the lower wear rate. This meant that each manufactured GCI rotor effectively lasted 21.5 times longer than the uncoated counterpart, as each rotor will last 4.3 times longer and can be recoated 4 times.

5.4.3 Comparison of Uncoated GCI and Laser-Clad GCI Rotors

5.4.3.1 Midpoint Impact Results

The impact results were normalised by dividing by the maximum value for each impact category from the uncoated and laser clad GCI rotor LCA results. This comparison scales each impact value between a score of 0 and 1 as shown in Figure 5.14.

Figure 5.14 shows that the laser-clad GCI rotor reduced the impact of the uncoated GCI in every midpoint category. Impact categories that were solely related to the manufacture and disposal of GCI were reduced by 90-95% for the laser-clad GCI rotor (the fluctuation in reduction being due to the contribution of the added coating process to each impact category). This was due to the significantly reduced wear rate as well as the recoating ability at the end of use. The higher wear rate of the uncoated GCI required 4.3 rotors

per FU duration (240,000 km) compared to only 1 laser-clad GCI rotor. Additionally, it was assumed that each laser-clad GCI rotor could be refurbished 4 times, therefore, allowing the manufacture and disposal impacts for a single-use rotor to be divided by a factor of 5.

The reductions in global warming and fossil resource scarcity impact were found to be much lower. This was due to the fact that these two categories are heavily associated with fuel consumption and accompanying CO_2 emissions during the use phase of each rotor. Despite the increase in weight of the laser-clad rotor (9.78 kg compared to 9.55 kg), only a 2.4% increase in fuel consumption was observed. Therefore, an overall decrease in impact scores was still found in these two categories due to the large reductions in impact from the manufacturing and disposal phases outweighing the effects of increased fuel consumption.

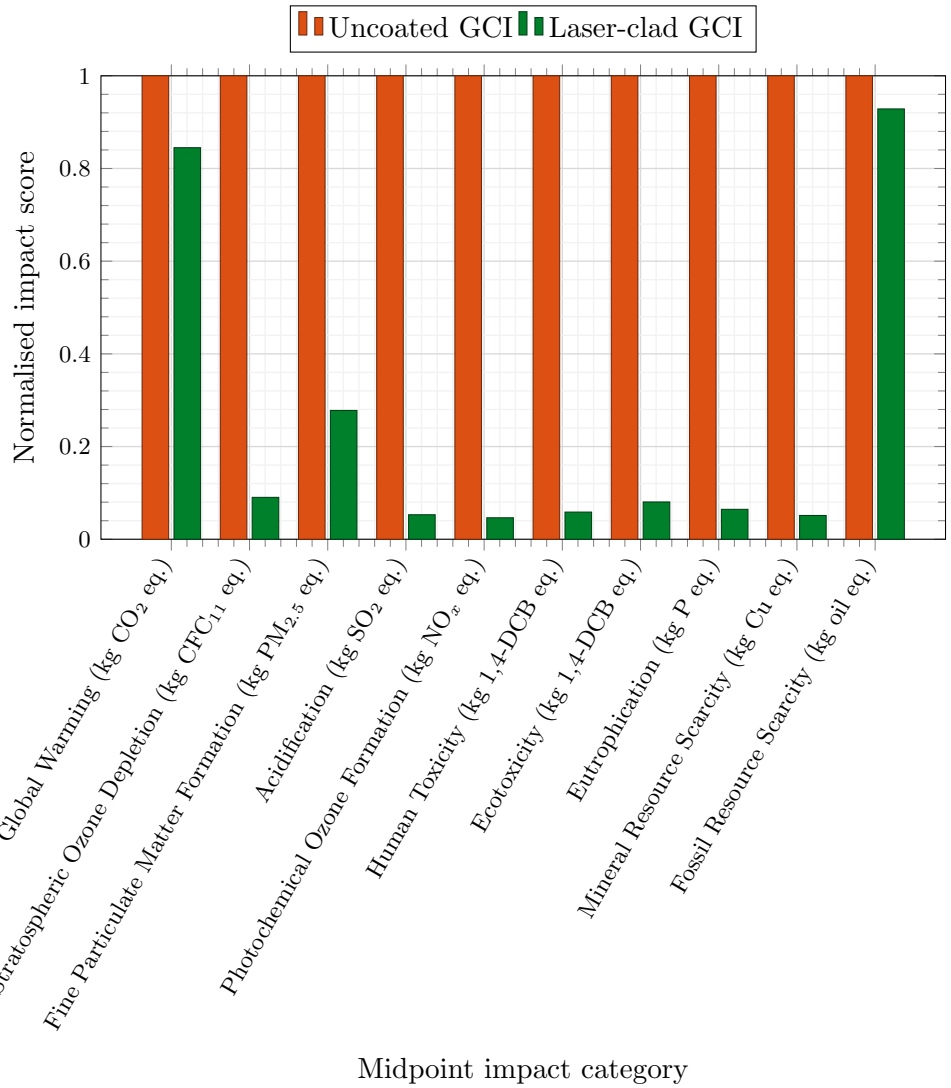

Figure 5.14: Comparison of midpoint impact results for case study I (uncoated GCI and laser-clad GCI rotors).

5.4.3.2 Endpoint Impact Results

The endpoint impacts were normalised using the same process as for the midpoint impacts, as shown in Figure 5.15. Both impacts on human health and ecosystems for the laser-clad rotor were found to be approximately half those of the uncoated GCI. This was due to the recoating potential of the laser-clad rotor, allowing the manufacturing impacts to be shared across five rotor life cycles as well as significant reductions in wear rate and PM emissions. However, the same decrease was not found for the damage to resource availability. This endpoint impact category was mainly influenced by fossil resource scarcity. The laser-clad rotor increased the total rotor mass, thus increasing fuel consumption during use. Despite this increase in fuel consumption, there was a 4% decrease in damage to resource availability, as seen in Figure 5.15. This decrease was as a result of the small contribution of around 3% that the manufacturing and disposal phases were found to have on this endpoint impact category.

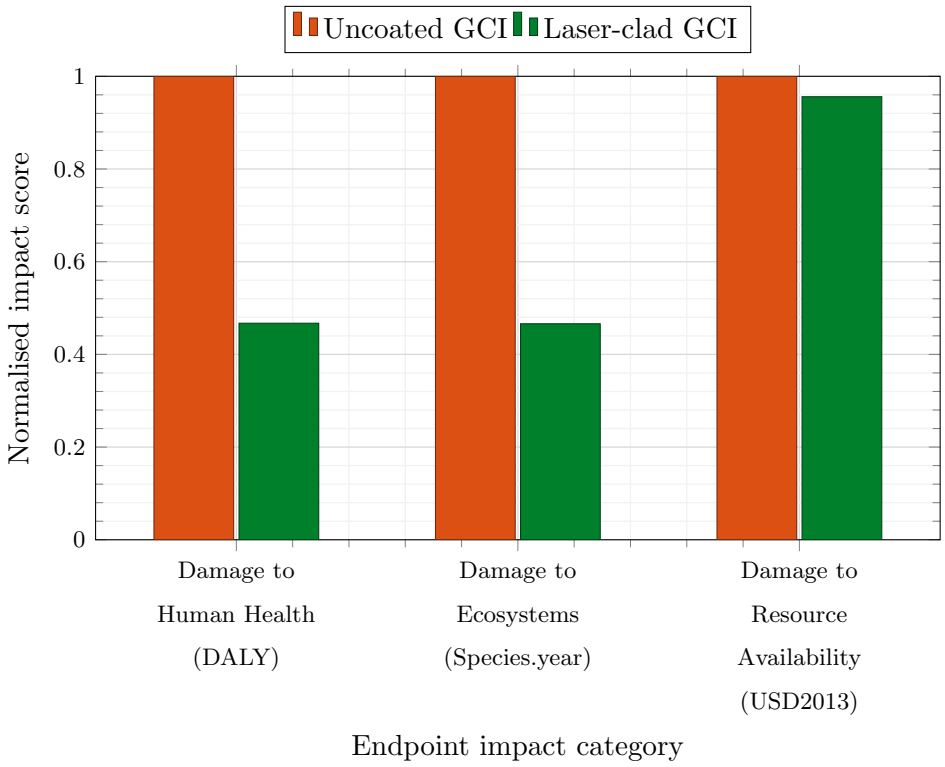

Figure 5.15: Comparison of endpoint impact results for case study I (uncoated GCI and laser-clad GCI rotors).

5.5 Summary of Case Study I

The detailed LCA results presented in this chapter allowed for a realistic and robust comparison to be made between the environmental impacts of a laser-clad GCI brake rotor with that of the standard uncoated GCI. The largest life cycle phase contributors to the impact results found for both types of rotor were the use phase, together with the

energy demands during the manufacturing and disposal phases. The reduced wear rate of the laser-clad rotor reported in Chapter 4 allowed the assumption that one of such rotor would last the full 240,000 km without replacement compared to the 4.3 uncoated GCI rotors that would otherwise be required. This assumption resulted in significant reductions in impacts associated with the manufacture and disposal of the brake system. Additionally, the impacts from manufacture and disposal were further reduced (up to 95% in some categories) for the laser-clad GCI rotor, which was assumed to be recoated up to 4 times before the GCI substrate required final disposal. This assumption effectively meant that one laser-clad rotor could withstand 5 FU durations compared to the uncoated GCI rotor, which, based on its measured wear rate, would only last 23% of one FU duration before replacement was necessary.

Chapter 6

Case Study II: Lightweight Alternatives

6.1 Introduction

Chapter 6 outlines the LCA results from wrought and cast PEO-Al rotors after both grades have undergone PEO surface treatment to improve surface hardness and reduce wear. Similarly to case study I, the adapted SADT diagram notation was applied, first for the wrought PEO-Al rotor, before being adapted where necessary for the cast PEO-Al rotor. The specific assumptions for Case Study II are defined in Section 6.3.1, followed by the details of the inventory analysis and impact assessment.

6.2 Life Cycle Diagrams

Both the wrought and cast Al rotors undergo very similar manufacturing methods; the first variation is machined directly from a wrought billet material (e.g. Al6082) while the second is cast directly from an Al billet (with increased silicon content).

6.2.1 PEO Treated Wrought Aluminium Alloy

The wrought PEO-Al rotor was the third rotor to be investigated, and so the adapted SADT diagram notation C, C0, C01 etc. was used. The overall inputs and outputs for the entire life cycle were summarised by the parent diagram shown in Figure 6.1, indicating the first level of the hierarchy.

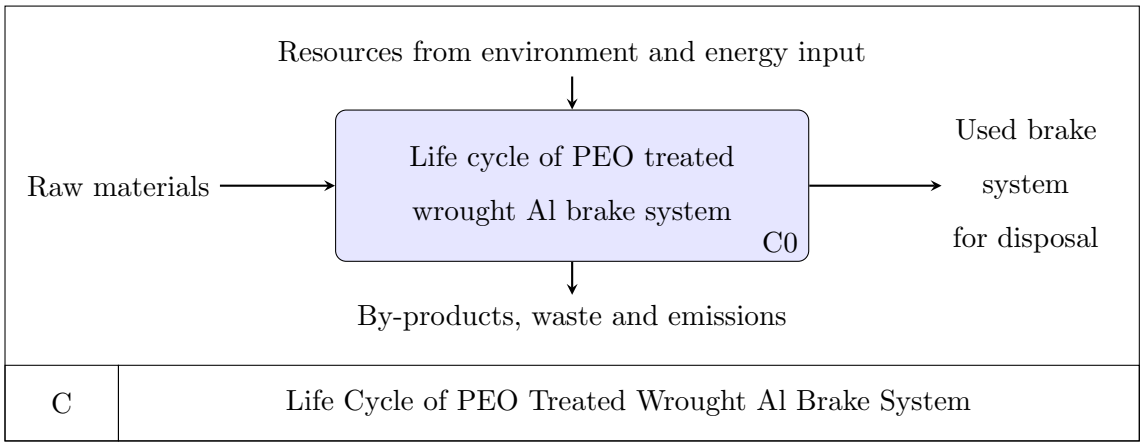

Figure 6.1: PEO treated wrought aluminium parent diagram.

Figure 6.2 displays level 2 of the hierarchy, breaking down the full life cycle of the brake system into its three main components: manufacture (C01), use (C02), and disposal (C03). Similarly to case study I, a colour code was included to indicate which unit process of one level of the hierarchy is linked to which diagram of the following hierarchical level. The PEO surface treatment process can be repeated several times on a previously used rotor, allowing for closed-loop recycling, as indicated in the diagram.

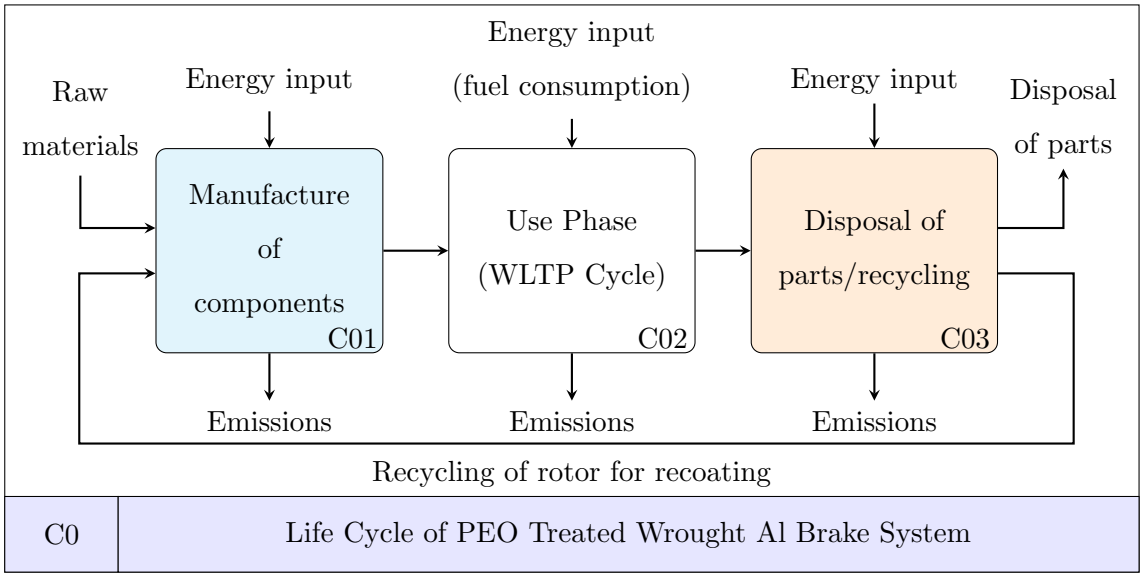

Figure 6.2: Level 2 hierarchical child diagram for PEO treated wrought aluminium rotor (full life cycle).

The manufacturing and disposal phases were divided between the pad and the rotor, providing more detail to each process. Figure 6.3 outlines the first diagram of level 3 of the hierarchy, providing details on the manufacture of the rotor and pad (C011 and C012), as well as the PEO surface treatment process (C013).

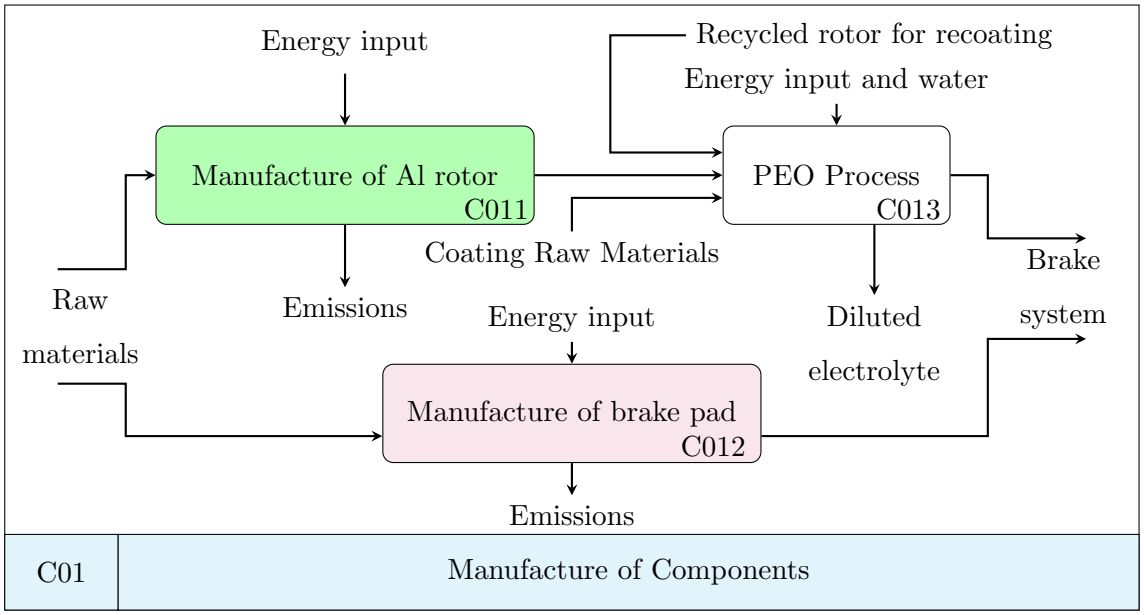

Figure 6.3: Level 3 hierarchical child diagram for PEO treated wrought aluminium rotor (manufacture of components).

The second diagram from level 3 of the hierarchy is shown in Figure 6.4, which shows the disposal phase, where closed-loop recycling was used, reducing the demand for raw materials. Instead of machining off the remaining alumina layer at end-of-life, alkali etching (C031) and acid desmutting (C032) can be utilised. This process involves placing the rotor in a bath of alkali followed by a bath of acid to chemically remove the alumina layer.

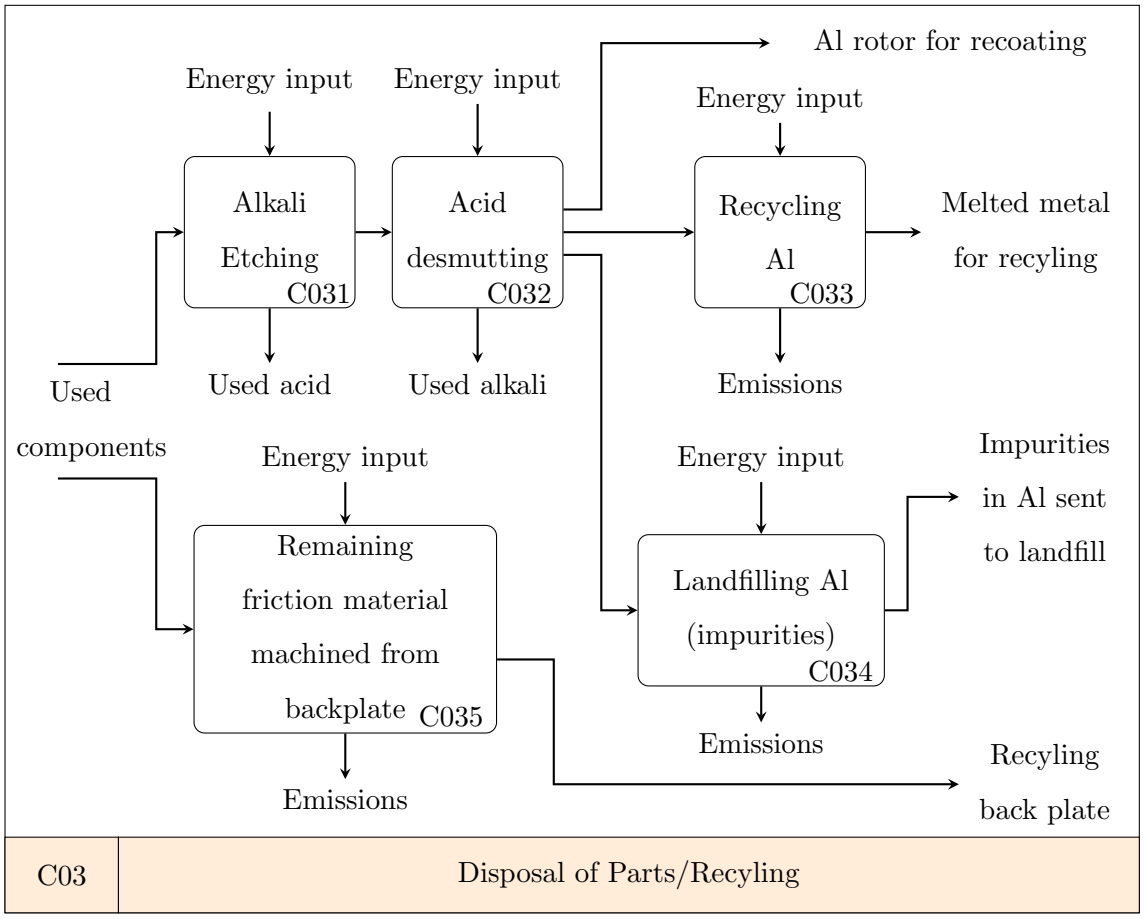

Figure 6.4: Level 3 hierarchical child diagram for PEO treated wrought aluminium rotor (disposal of components).

The final stage of the hierarchical diagram system indicates the manufacturing process of the Al rotor (C011), shown in Figure 6.5, as well as the assembly process to combine the friction material with the backplate to form the brake pad (C012) shown in Figure 6.6.

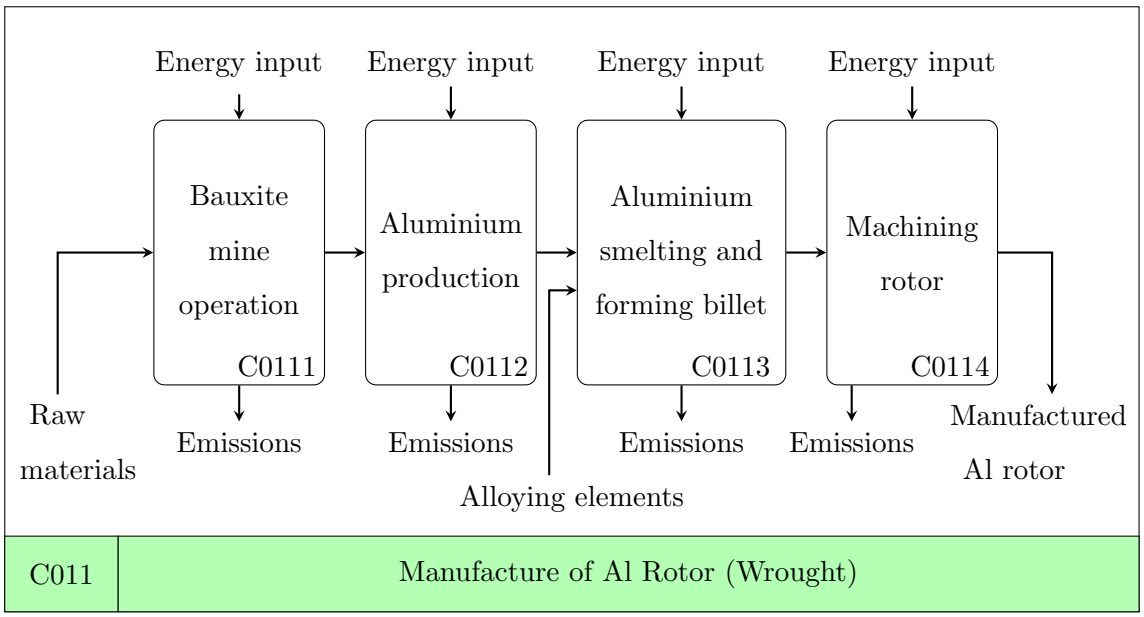

Figure 6.5: Level 4 hierarchical child diagram for PEO treated wrought aluminium rotor (manufacture of Al rotor).

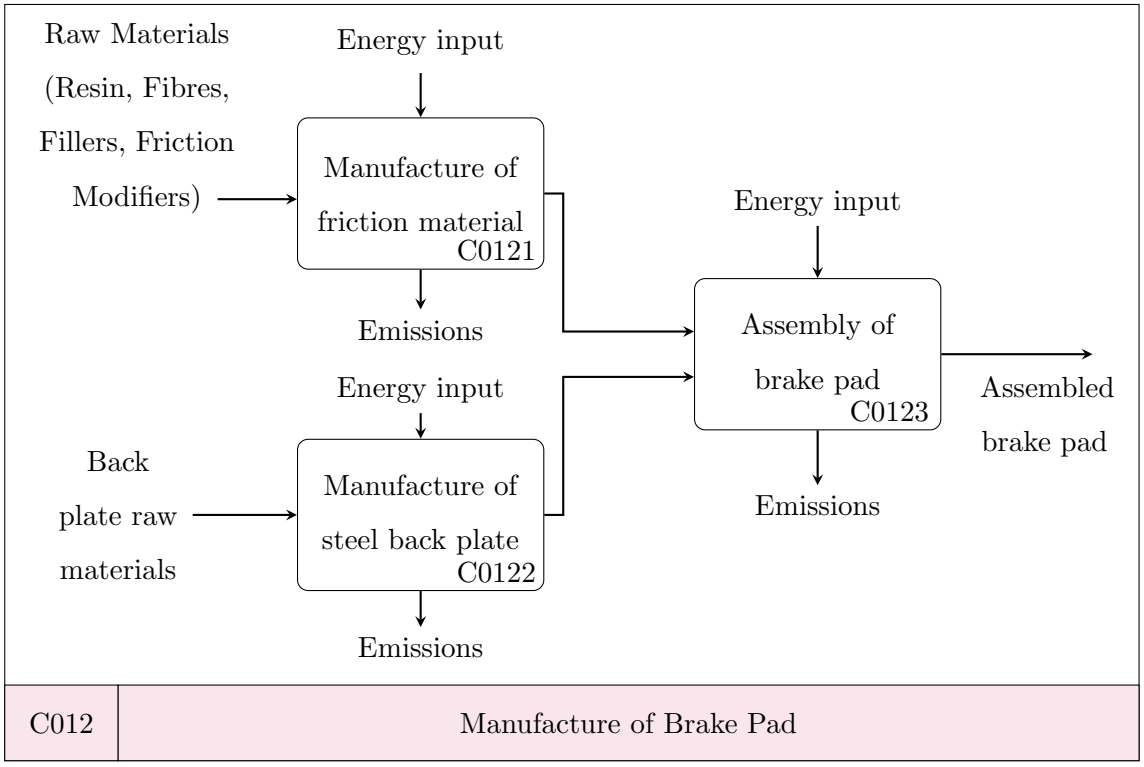

Figure 6.6: Level 4 hierarchical child diagram for PEO treated wrought aluminium rotor (manufacture of brake pad).

6.2.2 Diagram Amendments for PEO Treated Cast Aluminium Alloy

The cast Al rotor has the potential to offer benefits over wrought Al, such as the requirement of fewer raw materials. 60% of the mass of the wrought Al is typically lost during the machining process of the rotor from a solid billet, which means 2.5 times the amount of raw Al is required compared to that of the cast rotor. The diagram notation

applied for the cast PEO-Al is D, D0, D01 etc., as this was the fourth and final rotor that was investigated within the present LCA study. Diagrams C, C0, C01, C03 and C012 remain unchanged compared to the wrought PEO-Al and so were simply relabelled D, D0, D01, D03, D012 (but not reshown) when referring to the cast rotor. Figure 6.7 illustrates the alterations in diagram C011, with the change in manufacture technique becoming diagram D011.

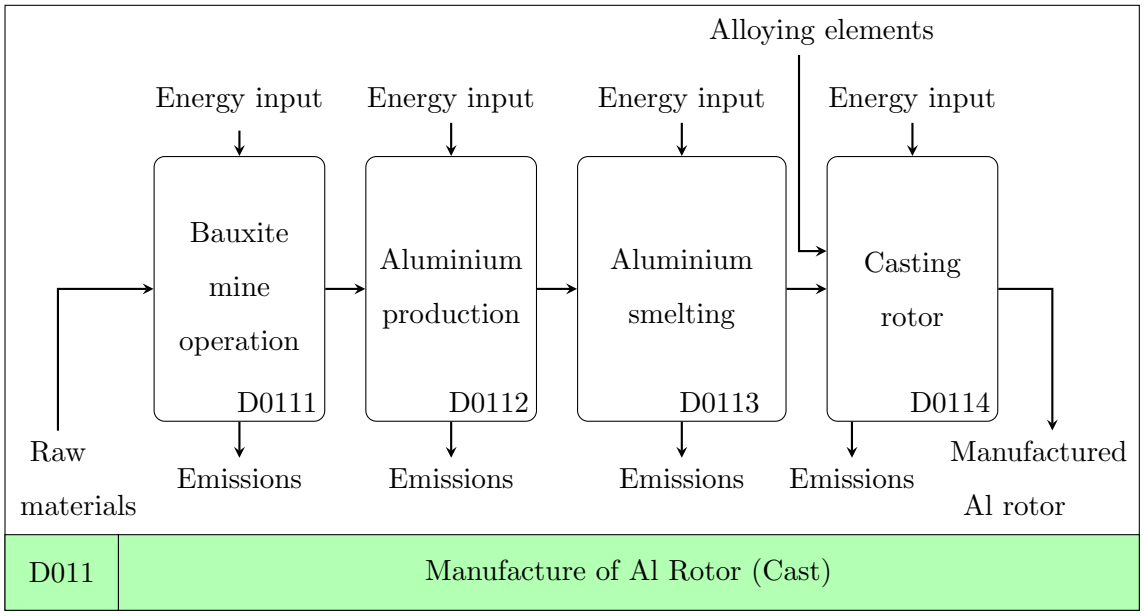

Figure 6.7: Level 4 hierarchical child diagram for PEO treated cast aluminium rotor (manufacture of Al rotor).

6.3 Inventory Analysis

This section outlines the assumptions and calculations made as part of the inventory analysis phase of the present LCA case study (case study II).

6.3.1 Case Study Assumptions and Data Collection

The assumptions were made to help define what data was required and in what form it should take. These assumptions required a detailed description to ensure the repeatability of a study. The following summarises the generic assumptions applied for the present LCA study, previously explained in Section 3.3.2.

- Low metallic (LM) brake pads were assumed to be used for all rotor materials; therefore, the manufacture (C012/D012) and disposal (C035/D035) of the brake pad were classified as identical phases and thus excluded from the comparative study.

- The energy input (petrol consumption) and CO_2 exhaust emissions associated

with the weight of the brake rotor were calculated and included in the use phase of the product system (Equations 3.7 and 3.9). The weight of the pads and other components, such as the caliper, were omitted from this calculation because they were assumed to be identical for all rotors considered.

Similarly to case study I, the inventory data for the manufacture of Al was based on a standard unspecified alloy type, obtained from the EcoInvent database [120, 121]. The inventory data collected are summarised in Table 6.1. It was assumed that 100% of the Al came from raw materials to avoid impurities present in a recycled Al that compromise the high safety requirements of the braking system.

The inventory provided in Table 6.1 refers to both cast and wrought Al rotors. The wrought rotor inventory assumed that the smelted Al was formed into a wrought billet before machining the rotor, whereas for the cast rotor the Al alloy was assumed to be directly cast into the rotor shape, including features such as the ventilation vanes. The inventory per 1 kg for the smelting and billet casting process is the same for both rotors. The difference is the amount of material required, with the required wrought billet mass being 2.5 times that of the wrought rotor itself. To machine the rotor, the solid billet would need to be milled, drilled, and surface finished into the final shape. Typically, a medium-sized milling machine has a power requirement of 5.6 kW [130], but the duration of the required milling process is unknown. However, even if such a process required several hours, the energy requirement would be less than 5% of the combined energy demand of the smelting and PEO processes and therefore it was a reasonable assumption to omit the machining of the billet from the present LCA case study.

There are three main processes to dispose of the brake system at end of life: alkali etching and acid desmutting (C031/D031 and C032/D03) prior to recoating the rotor, recycling and landfilling the Al rotor (C033/D033 and C034/D034), and steel pad backplate and disposal of the remaining friction material (C035/D035), as shown in Figure 6.6. These latter two processes were assumed identical between all rotors, and so they were assumed to have negligible affect on the comparative results and were omitted from this study. As the alkali etching and acid desmutting process is currently only theorised prior to recoating the Al rotors, it was assumed that for the purpose of the present LCA study, the energy demand would not be greater than that for machining off the coating of the laser-clad GCI rotor (which has already been assumed to be negligible). Any emissions from the chemical processing of the PEO coating to allow recycling were assumed to be extracted and treated prior to release into the environment.

Table 6.1: Inventory data for the manufacture of 1kg of Al (C011/D011) - EcoInvent [120, 121].

Flow Name	Emission Type	Unit	Bauxite Mine Operation (C0111/D0111)	Alumina Production (C0112/D0112)	Alumina Smelting and [a]Casting (C0113/D0113)
aluminium	resources	kg	1.17	0	0
gallium	resources	kg	3.64×10^{-4}	0	0
energy	resources	kWh	8.28×10^{-3}	5.70×10^{-1}	1.64×10^{1}
diesel	resources	MJ	1.40×10^{-1}	0	0
bauxite	resources	kg	0	5.52	0
Al hydroxide	resources	kg	0	2.97	0
coke	resources	kg	0	0	5.55×10^{-1}
iron	resources	kg	0	0	3.40×10^{-3}
Al fluoride	resources	kg	0	0	1.65×10^{-2}
Al oxide	resources	kg	0	0	1.92
steel	resources	kg	0	0	7.10×10^{-3}
$PM_{2.5}$	to air	kg	2.71×10^{-5}	1.13×10^{-4}	9.50×10^{-4}
PM_{10}	to air	kg	2.71×10^{-4}	2.40×10^{-4}	1.48×10^{-3}
mercury II	to air	kg	0	2.28×10^{-7}	0
NO_x	to air	kg	0	1.19×10^{-3}	8.25×10^{-4}
SO_2	to air	kg	0	2.19×10^{-3}	1.37×10^{-32}
HF	to air	kg	0	0	5.00×10^{-4}
PAH	to air	kg	0	0	2.86×10^{-5}
CO_2	to air	kg	0	0	9.17×10^{-2}
CO	to air	kg	0	0	9.17×10^{-2}
COD	to water	kg	0	1.36×10^{-4}	0
mercury II	to water	kg	0	8.90×10^{-10}	0
sodium II	to water	kg	0	3.80×10^{-3}	0
PAH	to water	kg	0	0	2.92×10^{-8}

[a] Casting process for the wrought Al is forming the wrought billet ready to machine. However, for the cast Al this process refers to the direct casting of the rotor. The energy requirement for machining the wrought rotor from the billet is unknown but can be assumed to be negligible in comparison to the high energy demand of Al smelting process.

Similarly to case study I, a significant proportion of Al can be recycled at the end of life through an open-loop process, which means it is not of sufficient quality for remanufacturing. The emissions from melting Al for general recycling were assumed to be extracted and treated prior to release into the environment, and therefore only the energy

required to melt the metal was considered. This energy requirement was determined using the thermophysical properties of Al, described in Table 6.2, with the required calculation defined by Equations 6.1 and 6.2.

$$Energy\ to\ melt\ \ (J/kg) = \Delta H_f + C_{p_s}\left(T_s - T_0\right) + C_{p_l}\left(T_l - T_s\right) \tag{6.1}$$

$$Energy\ to\ melt\ \ (kWh/kg) = \frac{Energy\ to\ melt\ \ (J/kg)}{^{[a]}3.6 \times 10^6} \tag{6.2}$$

[a] $3.6{\times}10^6$ Joules is equal to 1 kWh [128]

Table 6.2: Thermophysical properties of Al.

Thermophysical Property	Symbol	Value	Unit	Source
Specific heat, solid	C_{p_s}	917	J/kg.K	[131]
Specific heat, liquid	C_{p_l}	1080	J/kg.K	[131]
Initial temperature	T_0	298.15	K	
Solidus temperature	T_s	[a]880.65/825.65	K	[132]
liquidus temperature	T_l	[a]880.65/825.65	K	[132]
Latent heat of fusion	ΔH_f	$396{\times}10^3$	J/kg	[133]

[a] The values are provided for wrought/cast aluminium (wrought on left and cast on right). The wrought aluminium is a 6082 alloy (taken as AlSiMgMn from data source), while the cast aluminium had a slightly higher silicon content (taken as AlSi7Mg from data source)

It was assumed that 90% of the Al was recycled, while the remaining 10% had to be landfilled due to impurities, unsuitable material contamination and residual matter after processing [126]. Table 6.3 outlines the inventory associated with the landfilling of 1 kg of material [129]. Allocation by mass was used to determine the resources and emissions from landfill associated with disposing of 1 kg of material.

The coating process data was provided by Keronite Ltd. The process is currently not being undertaken for a mass market within the brake industry. Therefore, the data are based on estimates if the PEO treatment process was scaled up, based on values used as part of the RELIABLE study reported by Shrestha et al. [65]. The raw data are confidential and protected by a non-disclosure agreement and so cannot be disclosed.

Table 6.3: Resources required for landfill operation per kg disposed (C034/D034).

Flow Name	Emission Type	Unit	Landfilling Al
energy	resources	kWh	9.63×10^{-4}
diesel	resources	kg	6.24×10^{-1}
clay, unspecified	resources	kg	4.47×10^{1}
CO_2	to air	kg	2.16×10^{-1}
CO	to air	kg	1.10×10^{-4}
NO_x	to air	kg	1.68×10^{-5}
PM_{10}	to air	kg	7.74×10^{-8}
SO_2	to air	kg	7.74×10^{-5}
CH_4	to air	kg	5.17×10^{-2}
HCl	to air	kg	3.29×10^{-5}
HF	to air	kg	3.14×10^{-6}
H_2S	to air	kg	1.10×10^{-4}
heavy metals	to air	kg	1.26×10^{-9}
HC	to air	kg	6.92×10^{-11}

6.3.1.1 PEO Treated Wrought Aluminium Alloy

The main difference between the two rotors is the mass loss during the manufacturing process and the PM emissions released during the use phase. For the latter, the tests were conducted on the wrought PEO-Al rotor by Limmer [1] using the same small-scale test rig setup as outlined in Chapter 4. Table 6.4 outlines the PM emissions collected on the Dekati foils from the wrought brake rotor under the WLTP cycle, averaged across the WLTP test cycles 6-8.

Table 6.4: Inventory data for the WLTP small-scale testing – wrought PEO-Al (as collected on Dekati foils)(C02).

Flow Name	Emission Type	Unit	WLTP Cycle
$PM_{2.5}$	to air	kg	1.41×10^{-7}
PM_{10}	to air	kg	3.19×10^{-7}

6.3.1.2 PEO Treated Cast Aluminium Alloy

Limmer [1] also conducted small-scale tests on the cast PEO-Al material. Table 6.5 outlines the PM masses per WLTP cycle collected on the Dekati, averaged between cycles 6-8, from the cast Al samples undergoing the WLTP cycle.

Table 6.5: Inventory data for the WLTP small-scale testing – cast PEO-Al (as collected on Dekati foils)(D02).

Flow Name	Emission Type	Unit	WLTP Cycle
$PM_{2.5}$	to air	kg	2.14×10^{-7}
PM_{10}	to air	kg	4.87×10^{-7}

6.3.1.3 Transport

As was assumed within case study I, the transport demands once the rotors were assembled onto the vehicles were assumed constant between rotors and so omitted from the study. The transport requirements for the manufactured Al rotor before and after the PEO treatment process would be the same for bot the wrought and cast rotors; however, to make this study comparable with case study I, these requirements were included. Table 6.6 outlines the distances and transport methods assumed for both Al rotors within case study II.

Table 6.6: Transport distances for wrought and cast PEO-Al rotors.

Starting Location	Destination	Distance (km)	Transport method
Germany	Calais port	744	Long distance truck
Calais port	Dover port	50	Cargo ship
Dover port	Keronite, Haverhill	201	Long distance truck
Keronite, Haverhill	Nissan Factory	402	Long distance truck

6.3.2 Life Cycle Inventory Calculations

The life cycle inventory calculations were necessary to ensure that the inventory data collected was correctly scaled based on the rotor specifications of the case study and the definition of FU.

6.3.2.1 Rotor Manufacture

The method for scaling the manufacturing inventory data collected from secondary sources per kg was the same for both rotors. However, the mass of Al required varied. The same rotor geometry was assumed as in case study I, with a diameter of 350 mm and a cheek thickness of 28 mm. Based on these dimensions, the PEO treated Al rotor had a mass of 3.85 kg. When machining the wrought Al rotor from the billet, 60% of the mass of the initial billet is lost. Therefore, the effective mass of Al required for the wrought alloy rotor was calculated using Equation 6.3.

$$Wrought\ billet\ mass = \frac{Rotor\ weight}{0.4} = 9.625\ kg \tag{6.3}$$

Equation 6.4 was then utilised to scale the gathered inventory shown in Table 6.1 (per kg) to provide the total manufacture inventory for the full rotor. The number of rotors required per FU was assumed to be 1, therefore, there is no requirement to multiply this by the number of rotors, as was for the uncoated GCI.

$$Rotor\ manufacture\ inventory = material\ mass \times inventory\ per\ kg \tag{6.4}$$

6.3.2.2 Use Phase

The coating process inventory is confidential and did not require calculations for this comparative case study as the final estimates are based on full-scale wrought and cast rotors. The next phase for discussion was the use phase. As discussed in Section 4.4, the same method used to calculate the wear rate for the uncoated GCI and laser-clad GCI rotors could not be used for either of the PEO treated Al rotors. This process used the total mass loss, surface area, and density to calculate the wear rate throughout the WLTP cycle. However, the PEO alumina layer can sometimes have a more brittle outer layer that crumbles away easily prior to the durable and wear-resistant surface. Therefore, the mass loss during the bedding in process (WLTP cycles 1-5) would be a lot higher than what would follow during the emissions testing (WLTP cycles 6-8). As the mass of the rotor was not measured after cycle 5 due to time constraints of reacclimatisation to the measurements lab between WLTP cycles, the mass loss from only cycles 6-8 was unknown. It was assumed that during these cycles, a similar wear rate would have been portrayed as for the laser-clad GCI rotor due to similar PM emissions being released during use. Therefore, it was assumed that only one coated rotor was required for the FU distance of 240,000 km, based on the performance of the laser-clad GCI rotor.

The small-scale tests collected PM masses at a sampling rate of 10 l/min on Dekati foils. This was scaled up using the same method specified in Chapter 4, to produce values for the full-scale rotor (Equations 4.5 - 4.8). Similarly to case study I, this required an energy based scale factor of 13.57 to be applied to the small scale results. Rotor mass has a direct impact on fuel consumption during use and associated CO_2 exhaust emissions. Equations 3.7 and 3.9, shown in Chapter 3, were used to perform the calculations of these two elements of the inventory (i.e. fuel consumption and CO_2 exhaust emissions).

6.3.2.3 Disposal of Rotor

The disposal of the rotor comes in two parts. 10% of the Al is sent to landfill due to impurities, while 90% can be recycled. The values shown in Table 6.3 were utilised in Equation 6.5 to determine the inventory data for landfilling 10% of the Al rotor at the end of life.

$$Landfill\ inventory = 0.1 \times Mass\ of\ Al \times Inventory\ per\ kg \tag{6.5}$$

For the remaining 90% of Al that can be recycled, Equations 6.1, 6.2 and 6.6 were developed based on the thermophysical data provided in Table 6.2. The description of what each variable represents within Equation 6.1 is shown in Table 6.2. To calculate the overall disposal inventory, Equation 5.12 was applied.

$$Recycling\ inventory = 0.9 \times Mass\ of\ Al \times Energy\ to\ melt\ \ (kWh/kg) \tag{6.6}$$

6.3.2.4 Transport

The distances shown in Table 6.6 were used to calculate fuel consumption and associated CO_2 emissions from material transport during the manufacturing phases. The same equations outlined in case study I were applied for this process (Section 5.3.2.5, Equations 3.9 and 5.13).

6.4 Life Cycle Impact Assessment

The results of the impact assessment are first shown in tabular form. The percentage of contribution to the overall impact from each life cycle phase is then presented for each rotor prior to an overall comparison. Within the comparison, the uncoated GCI results were included to provide a baseline. Due to the varying magnitudes of each impact category, the results were normalised between 0 and 1 by dividing each impact value by the maximum for that category.

6.4.1 PEO Treated Wrought Aluminium Alloy

6.4.1.1 Midpoint Impact Results

Tables 6.7 – 6.10 display the impact results generated from the Python LCA model for the midpoint impacts of the wrought PEO-Al rotor. From these impact values, the percentage representation of each life cycle phase was plotted to help assess which processes from the life cycle make the most contribution. Figure 6.8 indicates this phase breakdown.

Table 6.7: Midpoint impact results from the manufacture of a wrought Al rotor (C011).

Midpoint Impact Category	Bauxite Mine Operation (C0111)	Alumina Production (C0112)	Al Smelting and [a]Casting (C0113)	Transport
Global Warming (kg CO2 eq.)	4.78×10^{-4}	3.29×10^{-2}	3.83	2.13×10^{-2}
Stratospheric Ozone Depletion (kg CFC11 eq.)	4.46×10^{-11}	3.07×10^{-9}	8.85×10^{-8}	0
Fine Particulate Matter Formation (kg PM2.5 eq.)	5.22×10^{-5}	2.17×10^{-4}	1.83×10^{-3}	0
Acidification (kg SO2 eq.)	3.83×10^{-6}	5.31×10^{-3}	3.60×10^{-2}	0
Photochemical Ozone Formation (kg NO_x eq.)	2.21×10^{-7}	2.39×10^{-3}	4.87×10^{-3}	0
Human Toxicity (kg 1,4-DCB eq.)	4.28×10^{-4}	3.53×10^{-3}	9.83×10^{-2}	0
Ecotoxicity (kg 1,4-DCB eq.)	4.78×10^{-1}	3.29×10^{1}	9.49×10^{2}	0
Eutrophication (kg P eq.)	5.26×10^{-7}	1.36×10^{-4}	1.11×10^{-3}	0
Mineral Resource Scarcity (kg Cu eq.)	0	4.86×10^{-2}	4.06×10^{-4}	0
Fossil Resource Scarcity (kg oil eq.)	1.62×10^{-2}	6.28×10^{-3}	8.22×10^{-1}	2.00×10^{-2}

[a] Refers to forming the wrought billet ready for machining.

Table 6.8: Midpoint impact results for the PEO treatment process of a wrought Al rotor (C013).

Midpoint Impact Category	PEO Process	Transport
Global Warming (kg CO2 eq.)	1.50	4.47×10^{-2}
Stratospheric Ozone Depletion (kg CFC11 eq.)	1.40×10^{-7}	0
Fine Particulate Matter Formation (kg PM2.5 eq.)	0	0
Acidification (kg SO2 eq.)	1.20×10^{-2}	0
Photochemical Ozone Formation (kg NO_x eq.)	6.93×10^{-4}	0
Human Toxicity (kg 1,4-DCB eq.)	0	0
Ecotoxicity (kg 1,4-DCB eq.)	1.50×10^{3}	0
Eutrophication (kg P eq.)	1.65×10^{-3}	0
Mineral Resource Scarcity (kg Cu eq.)	0	0
Fossil Resource Scarcity (kg oil eq.)	2.86×10^{-1}	4.20×10^{-2}

Table 6.9: Midpoint impact results for the use phase of a wrought PEO-Al rotor (C02).

Midpoint Impact Category	Use Phase
Global Warming (kg CO2 eq.)	7.85×10^{1}
Stratospheric Ozone Depletion (kg CFC11 eq.)	0
Fine Particulate Matter Formation (kg PM2.5 eq.)	2.13×10^{-1}
Acidification (kg SO2 eq.)	0
Photochemical Ozone Formation (kg NO_x eq.)	0
Human Toxicity (kg 1,4-DCB eq.)	3.94×10^{-1}
Ecotoxicity (kg 1,4-DCB eq.)	0
Eutrophication (kg P eq.)	0
Mineral Resource Scarcity (kg Cu eq.)	0
Fossil Resource Scarcity (kg oil eq.)	7.39×10^{1}

Table 6.10: Midpoint impact results for the disposal of a wrought PEO-Al rotor (C033/C034).

Midpoint Impact Category	Landfilling Al	Recycling Al
Global Warming (kg CO2 eq.)	3.80×10^{-1}	1.42×10^{-2}
Stratospheric Ozone Depletion (kg CFC11 eq.)	5.19×10^{-13}	1.32×10^{-9}
Fine Particulate Matter Formation (kg PM2.5 eq.)	0	0
Acidification (kg SO2 eq.)	6.23×10^{-5}	1.13×10^{-4}
Photochemical Ozone Formation (kg NO_x eq.)	3.20×10^{-5}	6.56×10^{-6}
Human Toxicity (kg 1,4-DCB eq.)	9.67×10^{-5}	0
Ecotoxicity (kg 1,4-DCB eq.)	5.86×10^{-3}	1.42×10^{1}
Eutrophication (kg P eq.)	1.45×10^{-7}	1.56×10^{-5}
Mineral Resource Scarcity (kg Cu eq.)	8.98×10^{-2}	0
Fossil Resource Scarcity (kg oil eq.)	3.59×10^{-1}	2.71×10^{-3}

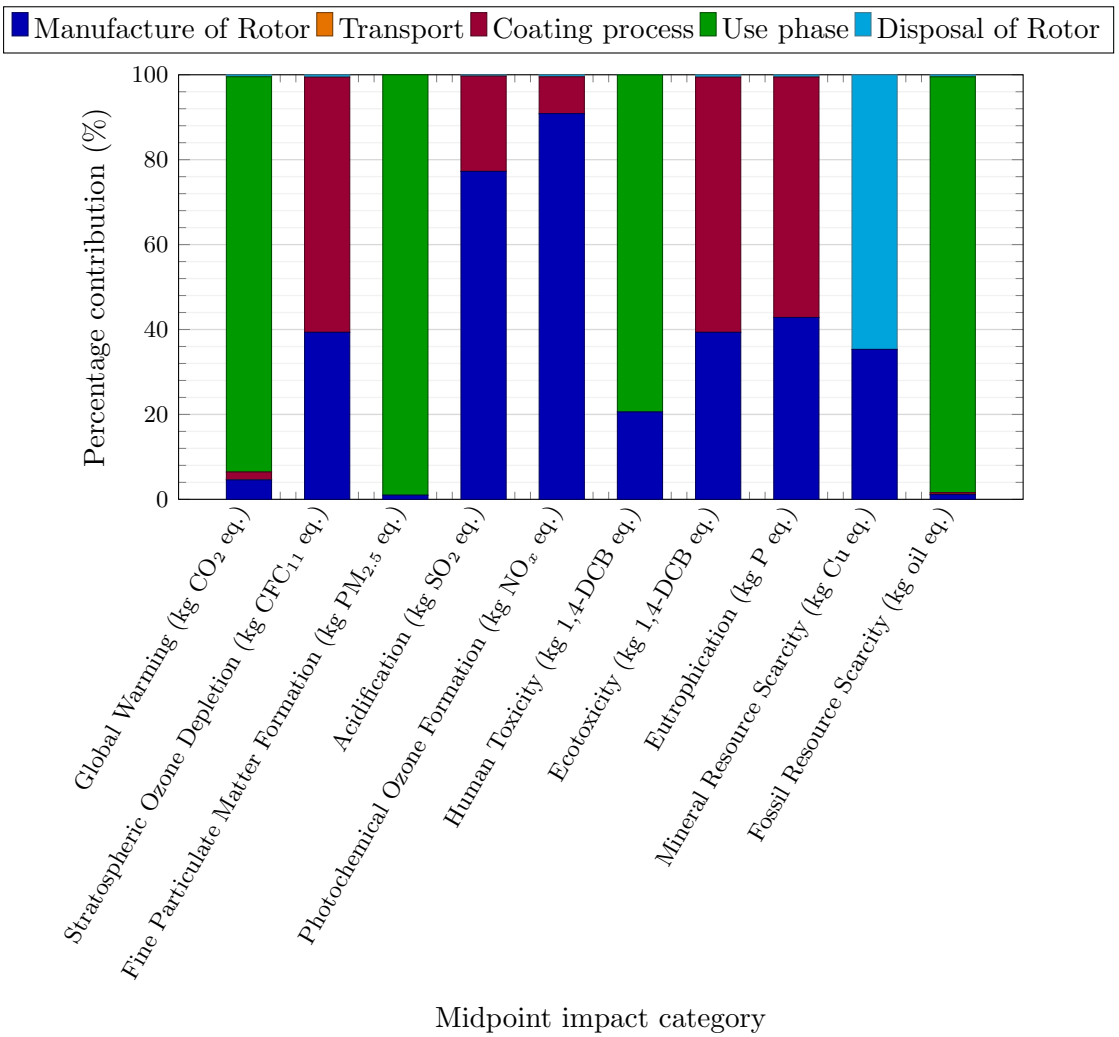

Figure 6.8: Life cycle midpoint impact results for wrought PEO-Al showing unit process percentage contribution.

The major contributor to the impacts associated with the PEO coating process was the energy demand. Therefore, Figure 6.8 provides a clear visualisation of which impact categories are highly affected by energy generation. Stratospheric ozone depletion, ecotoxicity, and eutrophication are all directly related to the production of fossil fuels. Therefore, the impact of the coating and manufacturing processes in these areas was influenced by the energy sources used for the generation of electricity. The impacts of the disposal were significantly lower compared to those in other stages of the life cycle because of the efficiency in the recycling of Al. The exception to this is mineral resource scarcity as a result of the clay walls required for landfill sites that led to a 65% contribution from the disposal phase.

Figure 6.8 shows that the human toxicity impact, which would typically be dependent on the NO_x and CO emissions from manufacture, was found to have a greater than expected contribution from the use phase. This was due to the manufacturing impacts being shared out across five use phases as a result of the closed-loop recycling of the PEO-Al rotor.

Global warming was found to mainly be caused by the CO_2 emissions associated with fuel consumption during the use phase (93%), with a minor contribution from energy demands for the manufacture of Al (5%) and the PEO surface treatment process (2%). Fossil resource scarcity was almost solely affected by the use phase (98%) as a result of the fuel consumption. Similarly, the fine particulate matter formation was also almost solely associated with the use phase (99%), due to the wear particles released during the many braking events in the WLTP cycle. Again, the contribution of the transport of the rotors was negligible compared to the other impact sources and so could be neglected in this and future similar LCA studies.

6.4.1.2 Endpoint Impact Results

Table 6.11: Endpoint impact results from the manufacture of a wrought Al rotor (C011).

Endpoint Impact Category	Bauxite Mine Operation (C0111)	Alumina Production (C0112)	Al Smelting and [a]Casting (C0113)	Transport
Damage to Human Health (DALY)	3.41×10^{-8}	1.75×10^{-7}	4.88×10^{-6}	1.98×10^{-8}
Damage to Ecosystems (Species.year)	1.31×10^{-10}	1.05×10^{-8}	2.71×10^{-7}	2.98×10^{-11}
Damage to Resource Availability (USD2013)	7.35×10^{-3}	1.21×10^{-2}	7.60×10^{-2}	9.14×10^{-3}

[a] Refers to casting the wrought billet ready for machining.

Table 6.12: Endpoint impact results for the PEO treatment process of a wrought Al rotor (C013).

Endpoint Impact Category	PEO Process	Transport
Damage to Human Health (DALY)	1.39×10^{-6}	4.15×10^{-8}
Damage to Ecosystems (Species.year)	4.12×10^{-7}	6.26×10^{-11}
Damage to Resource Availability (USD2013)	3.77×10^{-2}	1.92×10^{-2}

Table 6.13: Endpoint impact results for the use phase of a wrought PEO-Al rotor (C02).

Endpoint Impact Category	Use Phase
Damage to Human Health (DALY)	2.07×10^{-4}
Damage to Ecosystems (Species.year)	1.10×10^{-7}
Damage to Resource Availability (USD2013)	3.37×10^{1}

Table 6.14: Endpoint impact results for the disposal of a wrought PEO-Al rotor (C033/C034).

Endpoint Impact Category	Landfilling Al	Recycling Al
Damage to Human Health (DALY)	3.53×10^{-7}	1.32×10^{-8}
Damage to Ecosystems (Species.year)	5.51×10^{-10}	3.89×10^{-9}
Damage to Resource Availability (USD2013)	1.85×10^{-1}	3.56×10^{-4}

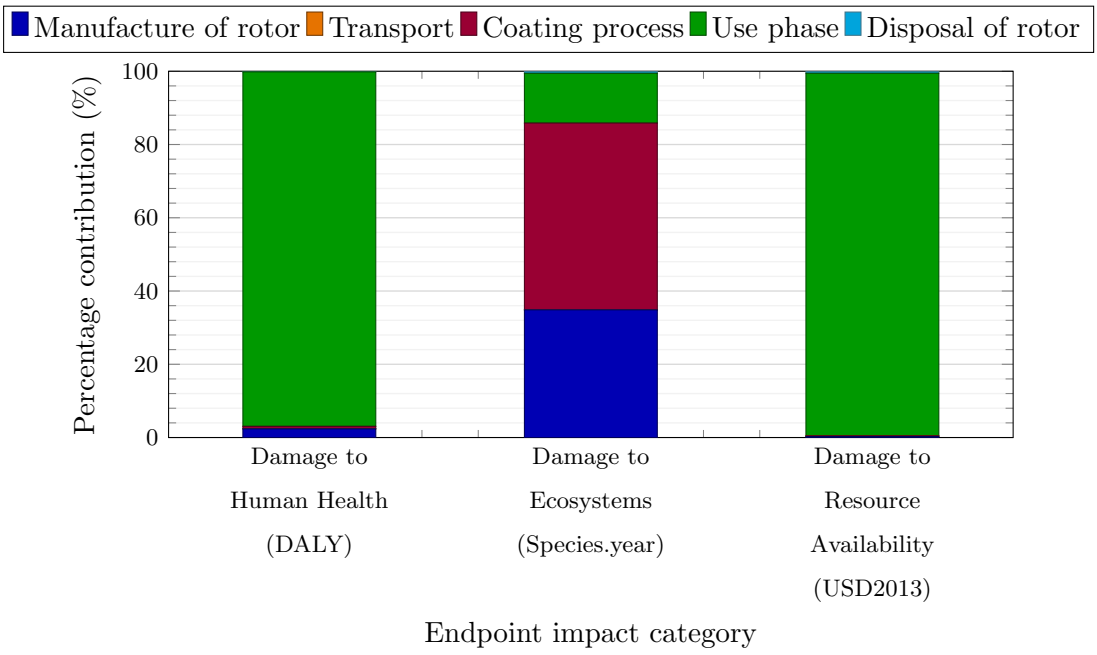

Figure 6.9: Life cycle endpoint impact results for wrought PEO-Al showing unit process percentage contribution.

Tables 6.11 – 6.14 display the wrought PEO-Al endpoint impact results generated from the Python LCA model. Figure 6.9 displays the percentage representation of each unit process towards the endpoint impacts to identify the biggest contributors to the impact. The damage to human health and resource availability was mainly caused by the use phase of the wrought PEO-Al rotor (97%). The minimal impact from disposal was due to the high recyclability of Al and the recoating potential. The energy required to melt Al was significantly less than that for Al smelting and the PEO process. CO_2 associated with fuel consumption and PM emissions released from brake wear greatly influenced human health damage due to adverse effects such as affected cardiovascular function.

The damage to the ecosystem was heavily associated with midpoint impact categories, such as ecotoxicity and eutrophication. Therefore, as expected from the midpoint results shown in Figure 6.8, most of this ecosystem damage was associated with the manufacture and the PEO process itself (35% and 51%. The degree of this impact can be heavily affected by the electricity mix used, for instance, by what proportion of that mix comes from renewable and non-hydrocarbon sources.

The damage to resource availability was caused by the use of fossil fuels such as hydrocarbons to provide energy input to the system. It was found that the fuel consumption during use completely outweighed the fossil fuels required for energy generation during manufacture or the PEO process. Therefore, the damage to resource availability had had a 99% contribution from the use phase of the wrought PEO-Al rotor.

6.4.2 PEO Treated Cast Aluminium Alloy

6.4.2.1 Midpoint Impact Results

Tables 6.15 – 6.18 display the cast PEO-Al midpoint impact results generated from the Python LCA model. Figure 6.10 highlights the percentage contribution of each phase to help assess which processes in the life cycle would benefit the most improvement.

Table 6.15: Midpoint impact results from the manufacture of a cast Al rotor (D011).

Midpoint Impact Category	Bauxite Mine Operation (C0111)	Alumina Production (C0112)	Al Smelting and [a]Casting (C0113)	Transport
Global Warming (kg CO2 eq.)	1.91×10^{-4}	1.32×10^{-2}	1.53	2.13×10^{-2}
Stratospheric Ozone Depletion (kg CFC11 eq.)	1.79×10^{-11}	1.23×10^{-9}	3.54×10^{-8}	0
Fine Particulate Matter Formation (kg PM2.5 eq.)	2.09×10^{-5}	8.68×10^{-5}	7.31×10^{-4}	0
Acidification (kg SO2 eq.)	1.53×10^{-6}	2.12×10^{-3}	1.44×10^{-2}	0
Photochemical Ozone Formation (kg NO_x eq.)	8.84×10^{-8}	9.58×10^{-4}	1.95×10^{-3}	0
Human Toxicity (kg 1,4-DCB eq.)	1.71×10^{-4}	1.41×10^{-3}	3.93×10^{-2}	0
Ecotoxicity (kg 1,4-DCB eq.)	1.91×10^{-1}	1.32×10^{1}	3.79×10^{2}	0
Eutrophication (kg P eq.)	2.10×10^{-7}	5.44×10^{-5}	4.44×10^{-4}	0
Mineral Resource Scarcity (kg Cu eq.)	0	1.95×10^{-2}	1.62×10^{-4}	0
Fossil Resource Scarcity (kg oil eq.)	6.46×10^{-3}	2.51×10^{-3}	3.29×10^{-1}	2.00×10^{-2}

[a] Refers to casting the rotor directly.

Table 6.16: Midpoint impact results for the PEO treatment process of a cast Al rotor (D013).

Midpoint Impact Category	PEO Process	Transport
Global Warming (kg CO2 eq.)	1.50	4.47×10^{-2}
Stratospheric Ozone Depletion (kg CFC11 eq.)	1.40×10^{-7}	0
Fine Particulate Matter Formation (kg PM2.5 eq.)	0	0
Acidification (kg SO2 eq.)	1.20×10^{-2}	0
Photochemical Ozone Formation (kg NO_x eq.)	6.93×10^{-4}	0
Human Toxicity (kg 1,4-DCB eq.)	0	0
Ecotoxicity (kg 1,4-DCB eq.)	1.50×10^{3}	0
Eutrophication (kg P eq.)	1.65×10^{-3}	0
Mineral Resource Scarcity (kg Cu eq.)	0	0
Fossil Resource Scarcity (kg oil eq.)	2.86×10^{-1}	4.20×10^{-2}

Table 6.17: Midpoint impact results for the use phase of a cast PEO-Al rotor (D02).

Midpoint Impact Category	Use Phase
Global Warming (kg CO2 eq.)	7.85×10^{1}
Stratospheric Ozone Depletion (kg CFC11 eq.)	0
Fine Particulate Matter Formation (kg PM2.5 eq.)	3.23×10^{-1}
Acidification (kg SO2 eq.)	0
Photochemical Ozone Formation (kg NO_x eq.)	0
Human Toxicity (kg 1,4-DCB eq.)	6.02×10^{-1}
Ecotoxicity (kg 1,4-DCB eq.)	0
Eutrophication (kg P eq.)	0
Mineral Resource Scarcity (kg Cu eq.)	0
Fossil Resource Scarcity (kg oil eq.)	7.39×10^{1}

Table 6.18: Midpoint impact results for the disposal of a cast PEO-Al rotor (D033/D034).

Midpoint Impact Category	Landfilling Al	Recycling Al
Global Warming (kg CO2 eq.)	1.52×10^{-1}	5.52×10^{-3}
Stratospheric Ozone Depletion (kg CFC11 eq.)	2.08×10^{-13}	5.15×10^{-10}
Fine Particulate Matter Formation (kg PM2.5 eq.)	0	0
Acidification (kg SO2 eq.)	2.49×10^{-5}	4.41×10^{-5}
Photochemical Ozone Formation (kg NO_x eq.)	1.28×10^{-5}	2.55×10^{-6}
Human Toxicity (kg 1,4-DCB eq.)	3.87×10^{-5}	0
Ecotoxicity (kg 1,4-DCB eq.)	2.35×10^{-3}	5.52
Eutrophication (kg P eq.)	5.79×10^{-8}	6.07×10^{-6}
Mineral Resource Scarcity (kg Cu eq.)	3.59×10^{-2}	0
Fossil Resource Scarcity (kg oil eq.)	1.44×10^{-1}	1.05×10^{-3}

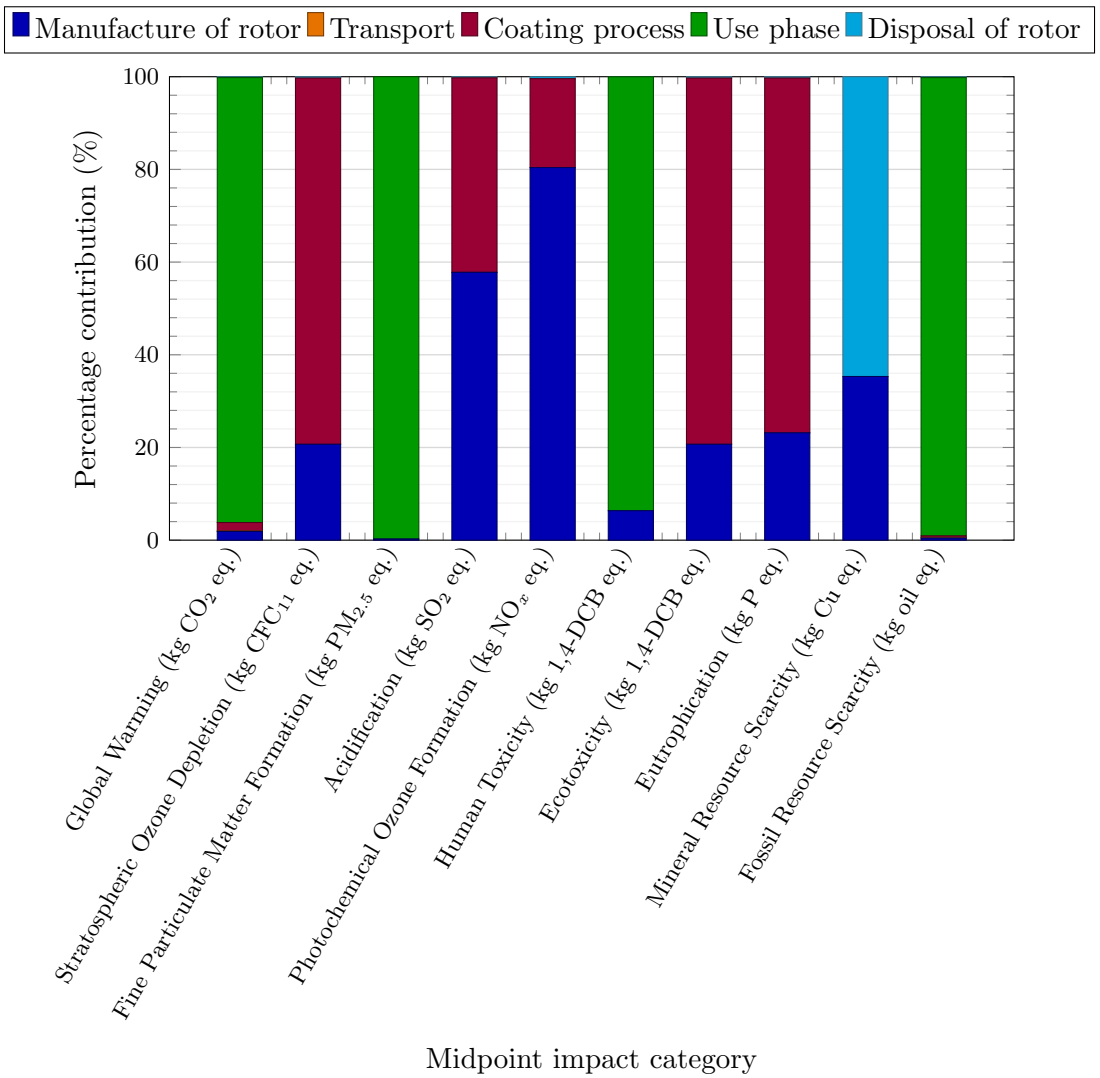

Figure 6.10: Life cycle midpoint impact results for cast PEO-Al showing unit process percentage contribution.

When considering the percentage contributions from the cast Al rotor, a very similar breakdown of the contributions was seen as for the wrought Al. The main difference was a decrease in the manufacturing contribution. This was due to 60% less raw material required when the rotor was directly cast compared to machining the rotor with a wrought Al billet. Although it cannot be seen from Figure 6.10, the main drawback of a cast PEO-Al rotor compared to wrought PEO-Al is the use phase. The overall impact scores of categories such as fine particulate matter formation were predicted to increase on the basis of the small-scale test results. These showed that the increased surface roughness of the cast PEO-Al (91% increase in arithmetical mean roughness height compared to the wrought Al) led to an increased pad wear of approximately 242 wt% (0.7 g versus 0.2 g over the 8 WLTP cycles) [1]. Therefore, higher masses of PM emissions were recorded during the WLTP braking cycle. This variation in wear and emissions rates between cast and wrought PEO-Al materials is discussed in Chapter 4.

6.4.2.2 Endpoint Impact Results

Tables 6.19 – 6.22 display the endpoint impact results generated from the Python LCA model for the cast PEO-Al rotor. Figure 6.11 displays the percentage contribution of each life cycle phase towards each endpoint impact, in order to identify the biggest impact contributors.

Table 6.19: Endpoint impact results from the manufacture of a cast Al rotor (D011).

Endpoint Impact Category	Bauxite Mine Operation (D0111)	Alumina Production (D0112)	Al Smelting and [a]Casting (D0113)	Transport
Damage to Human Health (DALY)	1.36×10^{-8}	7.02×10^{-8}	1.95×10^{-6}	1.98×10^{-8}
Damage to Ecosystems (Species.year)	5.25×10^{-11}	4.19×10^{-9}	1.08×10^{-7}	2.98×10^{-11}
Damage to Resource Availability (USD2013)	2.94×10^{-3}	4.83×10^{-3}	3.04×10^{-2}	9.14×10^{-3}

[a] Refers to casting the rotor directly.

Table 6.20: Endpoint impact results for the PEO treatment process of a cast Al rotor (D013).

Endpoint Impact Category	PEO Process	Transport
Damage to Human Health (DALY)	1.39×10^{-6}	4.15×10^{-8}
Damage to Ecosystems (Species.year)	4.12×10^{-7}	6.26×10^{-11}
Damage to Resource Availability (USD2013)	3.77×10^{-2}	1.92×10^{-2}

Table 6.21: Endpoint impact results for the use phase of a cast PEO-Al rotor (D02).

Endpoint Impact Category	Use Phase
Damage to Human Health (DALY)	2.77×10^{-4}
Damage to Ecosystems (Species.year)	1.10×10^{-7}
Damage to Resource Availability (USD2013)	3.37×10^{1}

Table 6.22: Endpoint impact results for the disposal of a cast PEO-Al rotor (D033/D034).

Endpoint Impact Category	Landfilling Al	Recycling Al
Damage to Human Health (DALY)	1.41×10^{-7}	5.12×10^{-9}
Damage to Ecosystems (Species.year)	2.20×10^{-10}	1.51×10^{-9}
Damage to Resource Availability (USD2013)	7.39×10^{-2}	1.39×10^{-4}

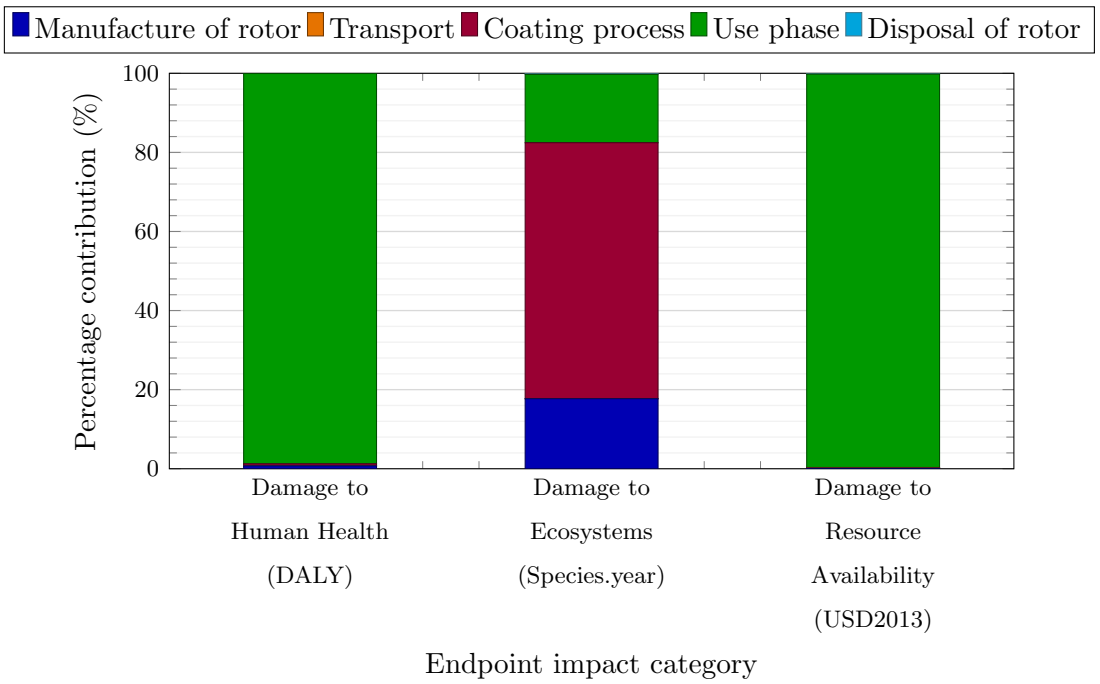

Figure 6.11: Life cycle endpoint impact results for cast PEO-Al showing unit process percentage contribution.

Very similar trends were seen for the cast PEO-Al rotor as for the wrought rotor in terms of life cycle phase contributions to the endpoint impacts. Damage to ecosystems is heavily associated with midpoint impact categories such as ecotoxicity and eutrophication, which are influenced by energy demand. Therefore, this endpoint impact was largely due to the coating and manufacture phases (65% and 18%). Damage to resource availability is caused by the use of fossil fuels, such as hydrocarbons. Therefore, being almost solely associated with fuel consumption due to the weight of the rotor (99%). The damage to human health was found to have a small contribution from the manufacture and the coating process (<1%), due to the energy demand. However, the greatest influencer was the CO_2 emissions associated with fuel consumption and the PM emissions from brake wear during the use phase. A noticeable difference between cast and wrought PEO-Al rotors was a diminished contribution from the manufacture and disposal phases as a result of the requirement for 60% less raw materials for the cast rotor compared to the machined-from-solid wrought rotor.

6.4.3 Comparison of PEO treated Wrought and Cast Aluminium Rotors

6.4.3.1 Midpoint Impact Results

The impact results for both wrought and cast PEO-Al rotors, as well as uncoated GCI (as a baseline), were normalised by dividing by the maximum value for each impact category from the LCA of all 3 rotors. This process scales each impact value between 0 and 1, with the comparison shown in Figure 6.12.

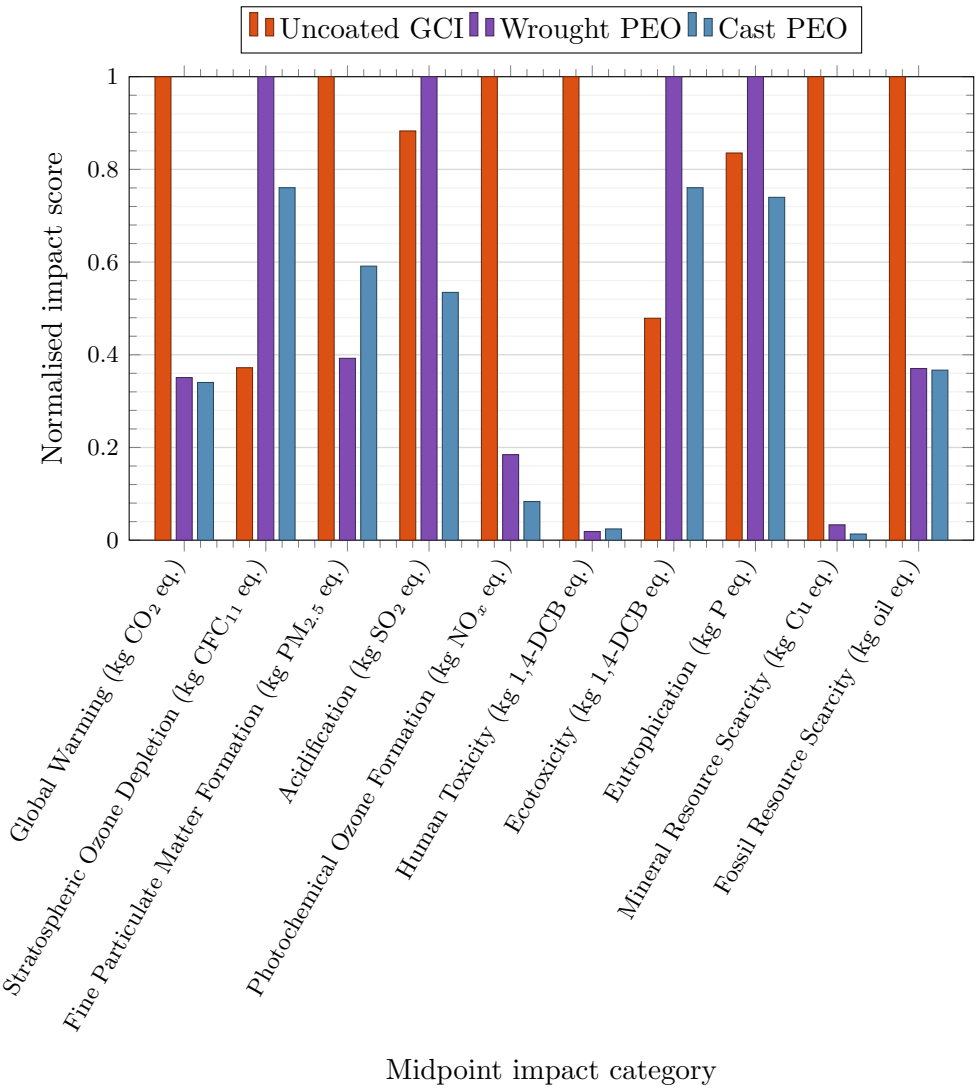

Figure 6.12: Comparison of midpoint impact results for case study II (uncoated GCI and wrought/cast PEO-Al).

For most of the midpoint impact categories, PEO treated Al rotors improved upon the current uncoated GCI. Significant reductions in fuel consumption and associated CO_2 emissions found for both PEO-Al rotors as a result of the light weight effect led to large decreases in the impacts of global warming (65%) and fossil resource scarcity (63%). The wear rate during the braking event was also reduced based on the small-scale test results, more so for the wrought PEO-Al rotor than for the cast PEO-Al, leading to significant reductions in fine particulate matter formation compared to the uncoated GCI (61% and 41% for wrought and cast, respectively). Furthermore, the manufacturing process was found to contribute less to SO_2 and NO_x emissions, especially with the recoating potential, allowing for reductions in photochemical ozone formation (81-91%) and human toxicity (98%). Such large reductions in human toxicity were also attributed to the PM_{10} reductions from reduced brake wear. Similarly to case study I, the recoating potential meant that considerably fewer minerals were required per FU, leading to a reduction in mineral resource scarcity of ~98%.

However, it is apparent from Figure 6.12 that the main drawback of PEO-Al rotors is the high energy demand due to the smelting process, as well as the energy demand for the PEO treatment process. These higher energy requirements compared to uncoated GCI caused an increase in the impacts on stratospheric ozone depletion, acidification, ecotoxicity, and eutrophication. The cast PEO-Al rotor performed better in these categories due to the requirement for 60% less raw Al, with acidification and eutrophication impacts reduced to below that for uncoated GCI. Impacts on all four categories could be reduced through improvements in the efficiency of the PEO process, as well as an increase in use of renewable or non-hydrocarbon energy sources for both the Al smelting and PEO treatment phases.

6.4.3.2 Endpoint Impact Results

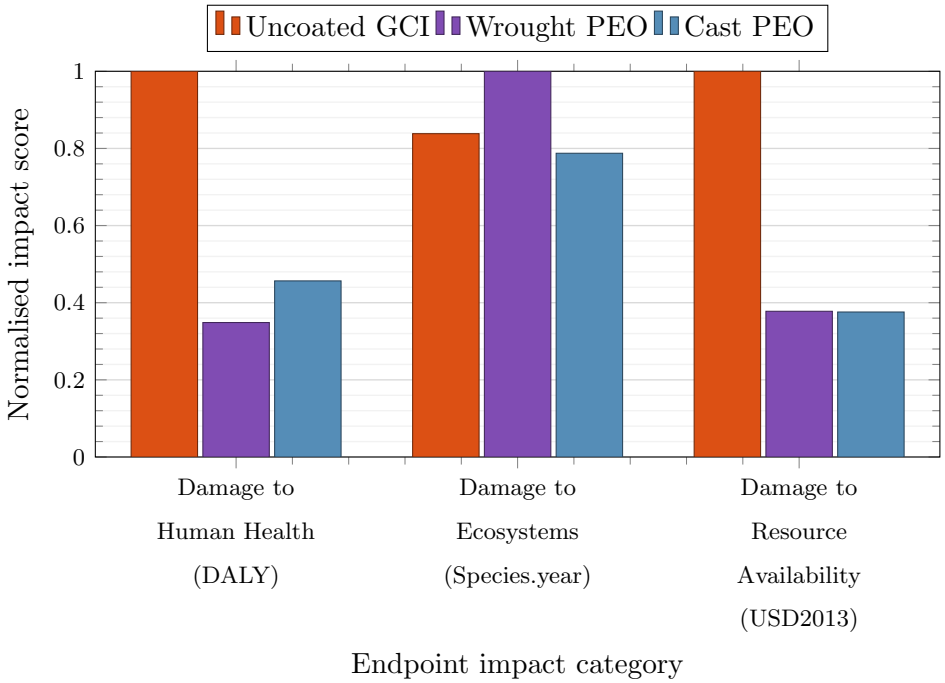

Figure 6.13: Comparison of endpoint impact results for case study II (uncoated GCI and wrought/cast PEO-Al).

In a process similar to the midpoint impacts, the endpoint scores were normalised based on the LCA for the 3 rotors, as shown in Figure 6.13. The reduced fuel consumption and associated CO_2 exhaust emissions as a result of the light weighting effects of the PEO-Al rotors was found to carry over into significant reductions in damage to human health. Furthermore, improved wear resistance, leading to reductions in PM emissions, also contributed to reduced human health damage compared to uncoated GCI. A smaller reduction was found for the cast PEO-Al than for the wrought PEO-Al because of the increased surface roughness and wear rate. However, both rotors were still found to reduce this impact by at least 50%.

An increase in ecosystem damage was found for the wrought PEO-Al rotor (22%). This was related to the increases observed in stratospheric ozone depletion, ecotoxicity, and eutrophication, which can be attributed to the higher energy demand from the Al smelting and PEO surface treatment process. As a result of the cast PEO-Al requiring 60% less raw materials, the damage to ecosystems was lowered to 4% below that of the uncoated GCI. As the PEO treated rotors are currently not in production, the assumed energy demand for the process per rotor is likely to be significantly higher than it would be if the rotors were mass manufactured. Therefore, with this potential for mass production realised, it is likely that the impact scores for damage to ecosystems will be lowered in comparison with the current uncoated GCI rotors. The damage to resource availability was directly related to fuel consumption; therefore, the same 62% decrease was found for both PEO-Al rotors as a result of the weight reduction.

6.5 Summary of Case Study II

The LCA presented above has considered environmental impacts from two alternative types of PEO treated Al alloy rotors, one based on machining the rotor from a wrought billet and the other by directly casting the near net shape of the rotor. The PM emissions from the use phase and the energy demand from Al smelting and the PEO surface treatment process were found to be the largest contributors to the overall impact results for both these PEO-Al rotors. The reduction in wear rate and fuel consumption during use caused significant reductions in CO_2, SO_2 and PM emissions and their associated impact categories. The light-weighting effect of Al offered up to 60% fuel consumption savings due to the reduced weight of the braking system during the vehicle use phase. However, it was found that the combined energy demand for the Al smelting and PEO processes was much greater than that of the process of manufacturing the uncoated GCI rotor. Therefore, the overall impact on the ecosystem was found to increase for the PEO-Al rotors. However, this disadvantage would likely be marginalised once the Al rotors were mass manufactured, and this is also achieved by improving the efficiency of the PEO surface treatment process. When comparing the wrought and cast rotors to one another, it was found shown that the cast rotor had a lower impact during manufacture and disposal due to less Al being required, whereas the wrought rotor had a lower use phase impact due to a reduction in wear and PM emissions. Improving the quality of the as-processed PEO surface (e.g. by post-process machining) would likely reduce the impact on human health even further (especially for the cast material).

Chapter 7

Discussion

7.1 Introduction

One of the key purposes of Chapter 7 is to discuss the improvements in methodological choices and novel nature of the adapted SADT notation, followed by discussions of emissions testing accompanied by comparisons with recent legislation. Furthermore, the interpretation phase of the present LCA study was undertaken, based on previous discussions made during Chapters 5 and 6. The interpretation of any LCA study aims to discuss the results, with the consideration of the stake holders, making certain recommendations. In this chapter, the LCA results are compared between case studies I and II, with weighting methods considered. The robustness of the methodological choices is tested through sensitivity studies, as well as a discussion of the validity of assumptions. Finally, as with considering the results of any LCA study, the potential limitations of this study are outlined.

7.2 Requirement for the Research and Gaps in Existing Knowledge

From the review of the literature, shown in Chapter 2, it became clear that to improve the effects on human health, reduce the emissions released, and reduce the impact on the environment, an alternative solution was required to the current uncoated GCI rotor. Two major drawbacks were found surrounding the uncoated GCI rotor. Firstly, low wear resistance was found to cause high levels of PM emissions compared to alternatives [1], leading to damaging effects on human health, such as cardiovascular problems [54]. Secondly, the low corrosion resistance of GCI, investigated by Ghouri [11], leads to increases in both the number and mass of PM emissions released after corrosion, while reducing the coefficient of friction during braking. With the introduction of electric vehicles, this effect was likely to be more detrimental due to the reduced frequency in the use of friction brakes. Extensive research has already been conducted within the braking industry for the purpose of reducing such emissions and corrosion problems, with the current front running solution being a coated GCI rotor.

Life cycle assessment techniques are useful for assessing novel brake rotor alternatives. Superficially attractive brake rotor materials have the potential for hidden environmental impacts during manufacture or disposal that could outweigh the benefits from the use phase. Therefore, it is crucial to investigate the full life cycle of each material, from cradle-to-grave, especially with most solutions involving an additional manufacturing process, such as laser-cladding or electrochemical treatment. This problem shifting can be a concern, with certain trade-offs that need to be considered. A coated rotor may reduce wear, emissions, and maintenance requirements, but will add an additional manufacturing process that may come with its own environmental impacts.

Most previous research has concentrated on the use phase of the life cycle, since current and planned legislation has focussed on the PM and carbon emissions during vehicle use. With the recent introduction of emission gathering methods within the brake industry, a significant proportion of recent research has focussed specifically on wear resistance and braking performance, due to the pending introduction of Euro 7 legislation significantly limiting PM emissions from friction brakes. Several potential coating techniques to reduce emissions were quickly ruled out, such as plasma transferred arc (PTA) treatment due to the use of heavy metals (nickel/copper) [21] or hard chrome plating as a result of the toxic carcinogenic hexavalent chromium fumes [61, 62].

To date, there have only been two major studies that have used LCA techniques applied to brake rotor materials. Both compare a hard-coated GCI rotor with an uncoated GCI counterpart. Olofsson [95] investigated the refurbishment potential of recoating a rotor at the end-of-life, focussing solely on the carbon footprint and energy consumption of each rotor. Gradin and Åström [16], on the other hand, conducted a more extensive LCA study with the inclusion of 17 different impact categories. They compared a carbide-based thermal spray-coated GCI rotor against an uncoated counterpart, with an additional investigation of the validity of omitting identical parts within a comparative LCA study. The present research aimed to fill some of the gaps left by both of these studies, developing on their individual methodological choices, whilst including alternative lightweight solutions. The ReCiPe methodology used by Gradin and Åström [16] has the option to include endpoint impact categories, which were omitted from their study. In contrast, these endpoint impact categories were included in the present study to provide stakeholders with a broader and more general overview of the results. Moreover, the present study included consideration of a lightweight rotor, namely a wrought or cast Al alloy with a PEO alumina coating applied to its rubbing surfaces.

7.3 Research Methodology

Key methodological considerations within an LCA study are the system boundary and the FU definition, as outlined in Chapter 3. The chosen system boundary for the present study included the brake pad, but excluded other components of the vehicle and brakes such as the caliper, thereby aligning with similar boundaries implemented in previous friction brake studies [16, 95].

Omitting such parts can sometimes make it difficult to interpret the significance of the impact magnitude compared to the entire vehicle. However, the inclusion of these subsidiary components would cause the study to expand significantly, becoming too time intensive and with the data much more difficult to collect. The omission of parts within any LCA system boundary requires careful consideration as this can lead to misleading results [16]. Omitting parts that would be identical for different rotor materials allows for significant reductions in the required resources, and the impact reductions of alternative materials can still be accurately identified through the comparison. Although omitting certain parts can result in the neglect of key impacts, the ILCD handbook [134] indicates that provided that the cut-off criteria for additional parts are in line with the goal and scope of the study, then omission is acceptable without serious consequences for the validity of the LCA results. This hypothesis was validated by Gradin and Åström [16], who produced results that show repeatable reductions between materials despite omitting certain parts. As the aim of the present LCA study was to assess alternative novel brake rotor materials in comparison to the current GCI brake rotor, the omission of certain identical parts for the different materials was deemed justifiable. However, emissions and brake performance are highly dependent on the friction pair, so the brake pad was included within the system boundary in case the pad material needed to be changed to match the particular rotor surface in some future iteration of the study.

The robustness of the chosen functional unit was analysed through a sensitivity analysis discussed in Section 7.6.1. Currently, there are minimal LCA studies within the brake industry to compare the results to. Both Gradin and Åström's study [16] and Olofsson's study [95] only investigated a coated GCI brake rotor, omitting lightweight alternatives. The original use of a functional unit distance of 240,000 km aligns with the choice made by Gradin and Åström [16]. The end impact results cannot be directly compared with either study due to the fact that the brake pad material used in both previous studies is not disclosed, as well as differences in the methodologies applied in the different studies.

Ulofsson [95] only investigated the energy usage and CO_2 footprint of an uncoated GCI and a laser-clad GCI, while Gradin and Åström [16] divided certain categories between the impacts of freshwater, marine and terrestrial, while also including the SO_2 emissions associated with fuel consumption.

The main areas of improvement within the methodology of the present study were the inclusion of endpoint impact categories, the adaptation of SADT notation for use in defining unit process diagrams, and the development of a purpose built, Python based, LCA model for wider use within the brake industry. Another important contribution of the present LCA study was the collection of primary data from suppliers and experimental work. Using the ReCiPe 2016 impact method allowed for the inclusion of important endpoint impact categories. Although Gradin and Åström [16] applied the same ReCiPe methodology, their study omitted such endpoint analysis. These were a valuable addition to provide a more general overview to the relevant stakeholders of the performance of each rotor material. For example, such endpoint categories allow for the direct comparison of the impact on the environment with the damage to human health.

The adapted SADT notation was used throughout both case studies reported in this thesis to provide detail on the life cycle phases of each automotive brake rotor. This technique was found to offer superior adaptability over traditional LCA flow diagrams, allowing for extra detail to be easily added, or certain life cycle phases adapted without the requirement for a full new diagram. Providing only 3-6 unit processes per diagram allows the reader to digest the information provided more easily, avoiding complex and confusing diagrams that can easily become too expansive when considering realistic LCA studies. The adaptation of this technique proved particularly useful for brake rotor applications, where multiple components and processes require consideration.

When investigating software packages that could be used for LCA techniques within the brake industry, a lack of transparency was found. These packages are typically built for generic applications, and it is often difficult to determine the exact methodologies being applied. When applying LCA techniques to braking systems, a level of customisation is required. Much of the data required can be considered confidential, such as friction material compositions, so it was important to develop a tool that allows different components and processes within the life cycle to be investigated separately, whilst also having good adaptability to keep up with the ever changing legislation. The Python model developed for the present study was found to offer superior customisability, allowing for

easy consideration of 'what if' scenarios as technology changes and methodological choices need to be adapted. Python and the accompanying libraries were found to offer maturity and stability, giving advantages over other commercial LCA software. They offer a robust and transparent data handling capability and streamlined integration with other analysis pipelines, while having the added benefit of being open source. The customisability was found to allow for easy improvement of the model as well as refinement of the methodology adopted, whilst always aligning with the needs of the end user.

7.4 Emissions Testing and Comparison with Legislation

Emissions data is a crucial part of the present LCA study to assess the impact of PM emissions released from the brake system during use. However, full-scale brake emissions testing can be very time intensive and expensive. The small-scale test rig discussed in Chapter 4 is able to overcome these cost and time restrictions. This equipment has already been used by Limmer [1] to obtain emissions data for uncoated GCI, cast PEO-Al and wrought PEO-Al samples. PM emissions data for a laser-clad GCI rotor are currently not available in the open literature, and so it was a requirement for the present study to undertake experimental emissions testing of such a rotor surface. To ensure a fair comparison between the rotors, the experimental setup and applied methodology used by Limmer [1] were replicated. Data collected both as part of the present investigation and by Limmer [1] were provided by analysing only a sample of the exhaust air of the small-scale setup. The present research builds upon these data, applying isokinetic condition calculations and an energy-based scaling factor. This allowed direct comparisons to be made against the impending Euro 7 emission legislation, as shown in Figure 4.21, indicating that only coated rotors are capable of meeting the stringent limitations placed on PM emissions.

7.5 Comparison of Case Study I and II

The impacts from each life cycle phase were quantified for the uncoated and laser-clad GCI-based rotors in Chapter 5 and for the wrought and cast PEO-Al rotors in Chapter 6. This section provides an overall comparison between the results from the 2 case studies to further scrutinise the problem shifting potential, especially regarding the effects of introducing a lightweight rotor in place of the current GCI. For the present study, the impact results were divided into the three main phases of the life cycle: manufacture, use, and disposal. Any impacts associated with the coating or surface treatment processes were grouped with the manufacture phase. As this is a comparison between rotors, the

actual magnitudes of the impact scores are less important than the comparative values. Therefore, the impact results were normalised using the same process as for the individual case studies (Equations 3.3 and 3.4), in each case dividing by the maximum value for that category for all four rotor types to scale all results between 0 and 1, with the latter indicating the maximum damage in each category. This normalisation process was conducted separately for each phase of the life cycle. Direct comparisons with the uncoated GCI rotor have already been made throughout Chapters 5 and 6, and it is clear from Chapter 4 that only a coated rotor has the potential to meet the stringent Euro 7 legislation. Therefore, the focus has been placed on comparing the laser-clad GCI and the PEO treated Al rotors.

7.5.1 Manufacture Phase

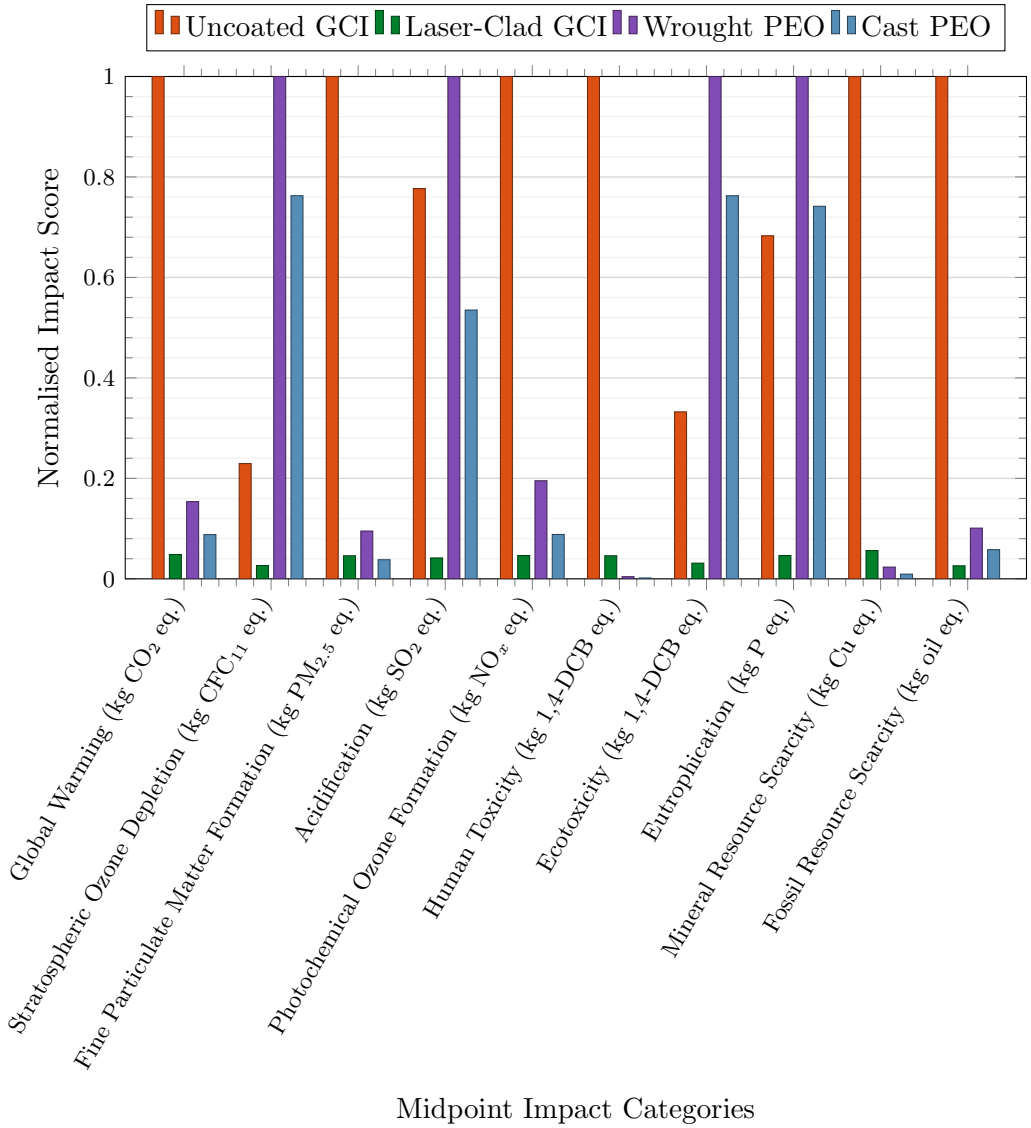

Figure 7.1: Normalised midpoint impact results from the manufacture phase of each rotor.

Figure 7.1 outlines the normalised midpoint impacts from the manufacturing phase of each rotor, including the coating or surface treatment. It was found that the laser-clad GCI rotor almost always offered the lowest impacts during manufacture, despite the fact that the PEO-Al rotors offered the same recoating potential. However, this comparison does not consider the fact that laser-cladding is an expensive process. The two exceptions to this generalisation were human toxicity (~99.7% compared to 95% for laser-clad GCI) and mineral resource scarcity (~98% compared to 94% for laser-clad GCI). The drawback of both PEO-Al rotors compared with the laser-clad GCI was the high energy demand during the smelting of Al ore and the energy requirements of the PEO surface treatment itself. The effects are lessened for the cast PEO-Al compared to the wrought PEO-Al due to the requirement for 60% less raw Al for the manufacture of the cast rotor. Even after the recoating potential was taken into account, it was found that wrought PEO-Al and cast PEO-Al required, respectively, 4 times and 3 times the amount of energy to manufacture, compared to the uncoated GCI, reflected in increases in stratospheric ozone depletion, ecotoxicity, and eutrophication impacts shown in Figure 7.1. However, the laser-clad rotor required a tenth of the energy required for the uncoated GCI due to its much longer surface life and the potential for recoating. Stratospheric ozone depletion was the most dependent on energy requirements, with an increase of 282% (averaged between wrought and cast Al) versus a decrease of 87% for the laser-clad GCI compared to the uncoated GCI rotor. Similar effects were found for acidification, ecotoxicity and eutrophication, where the recoating potential and reduced wear rate of the laser-clad GCI rotor led to significant impact reductions, while this benefit was outweighed by the high energy demand for the manufacture of both PEO-Al rotors.

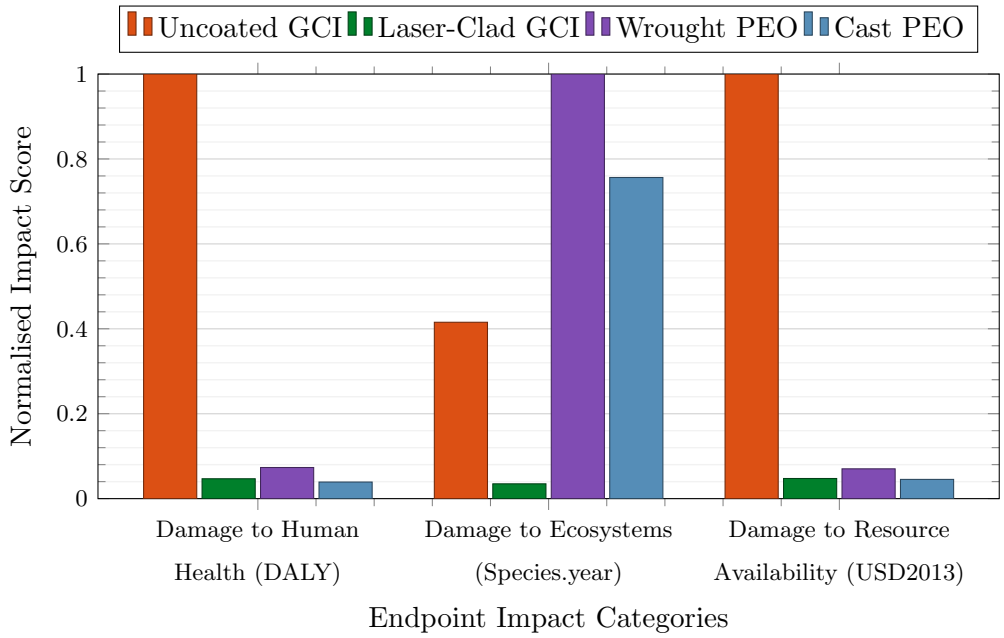

Figure 7.2: Normalised midpoint impact results from the manufacture phase of each rotor.

Figure 7.2 illustrates the endpoint impacts from the manufacture phase of each rotor, including any coating or surface treatment process. It can be seen that the damage to human health and resource availability was significantly reduced for all 3 coated rotors compared to the uncoated GCI. This was mainly due to the long service life and the ability to reuse these coated rotors, meaning that many more GCI rotors would be required for the same overall service life (assumed to be 5 FU's) as one coated rotor. The damage to ecosystems was found to be influenced by the energy demand during manufacture. Therefore, both PEO-Al rotors were found to have significantly higher impacts in this category compared to the laser-clad GCI. Such impacts could be reduced through improved energy efficiency and increased proportion of renewable energy sources used. The capability of casting Al over the machining of a wrought billet also allowed for damage reductions due to the reduced mass of Al required (average of 36% across all endpoint impacts). Energy demand had minimal influence on resource availability and human health in comparison to other factors, and so the same recoating potential benefits were found for the three coated rotors.

7.5.2 Use Phase

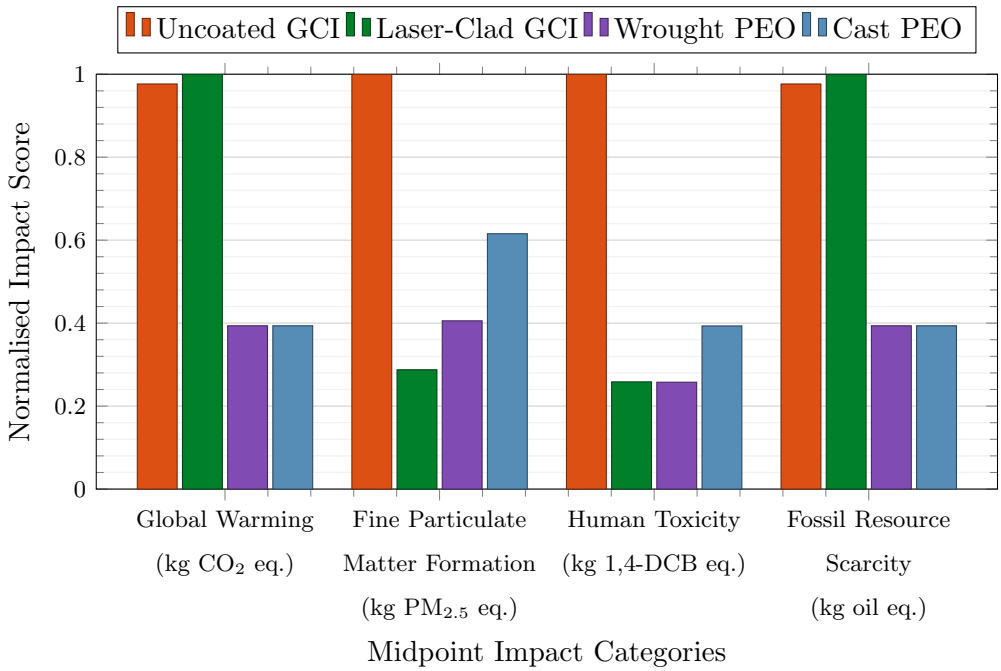

Figure 7.3: Normalised midpoint impact results from the use phase of each rotor.

Figure 7.3 outlines the midpoint impacts from the use phase of each rotor. Emissions and fuel consumption during use affected only certain categories. Therefore, those who were not affected by this phase of the life cycle were omitted from the figure. Based on the ReCiPe impact methodology, human toxicity and fine particulate matter formation were

found to be unsurprisingly dependent on PM emissions released during use. The three coated rotors released significantly fewer $PM_{2.5}$ and PM_{10} emissions than the uncoated GCI due to reduced wear rates. The cast PEO-Al impacted these two categories more than the wrought PEO-Al owing to the increased pad wear due to the higher surface roughness of the cast Al coating. Global warming and fossil resource scarcity were found to depend on fuel consumption and associated CO_2 exhaust emissions. Fuel consumption was dependent on the weight of the brake rotor. Therefore, slight increases were found for the laser-clad coating, while significant decreases were found for both the PEO-Al rotors because of their lightweight effects. Apart from PM emissions, both the cast and wrought PEO-Al rotors had the same midpoint impacts because they both weighed 3.85 kg.

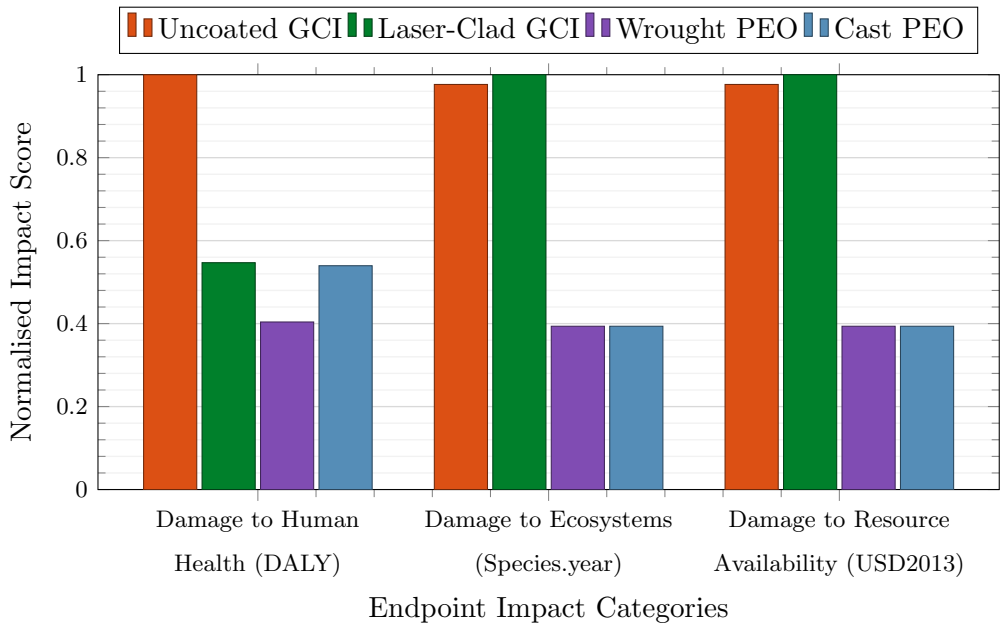

Figure 7.4: Normalised endpoint impact results from the use phase of each rotor.

Figure 7.4 outlines the endpoint impacts from the use phase. The damage to human health during the use phase was found to be largely influenced by PM released as a result of brake wear, with a minor contribution from CO_2 emissions associated with fuel consumption. The cast PEO-Al and laser-clad rotors were found to offer the same 45% reduction in human health damage compared to the uncoated GCI, with the increased wear of the cast PEO-Al counterbalancing the increased CO_2 emissions of the laser-clad GCI as a result of the increased weight. The wrought PEO-Al rotor offered an additional reduction of 15% due to a wear rate and PM emissions similar to those of the laser-clad rotor, but with only 40% of the rotor weight. Damage to ecosystems and resource availability during use were solely dependent on the fuel consumption and CO_2 emissions. Due to the 60% weight savings of both PEO treated Al rotors, these were found to offer a similar 60% reduction compared to the laser-clad GCI.

7.5.3 Disposal Phase

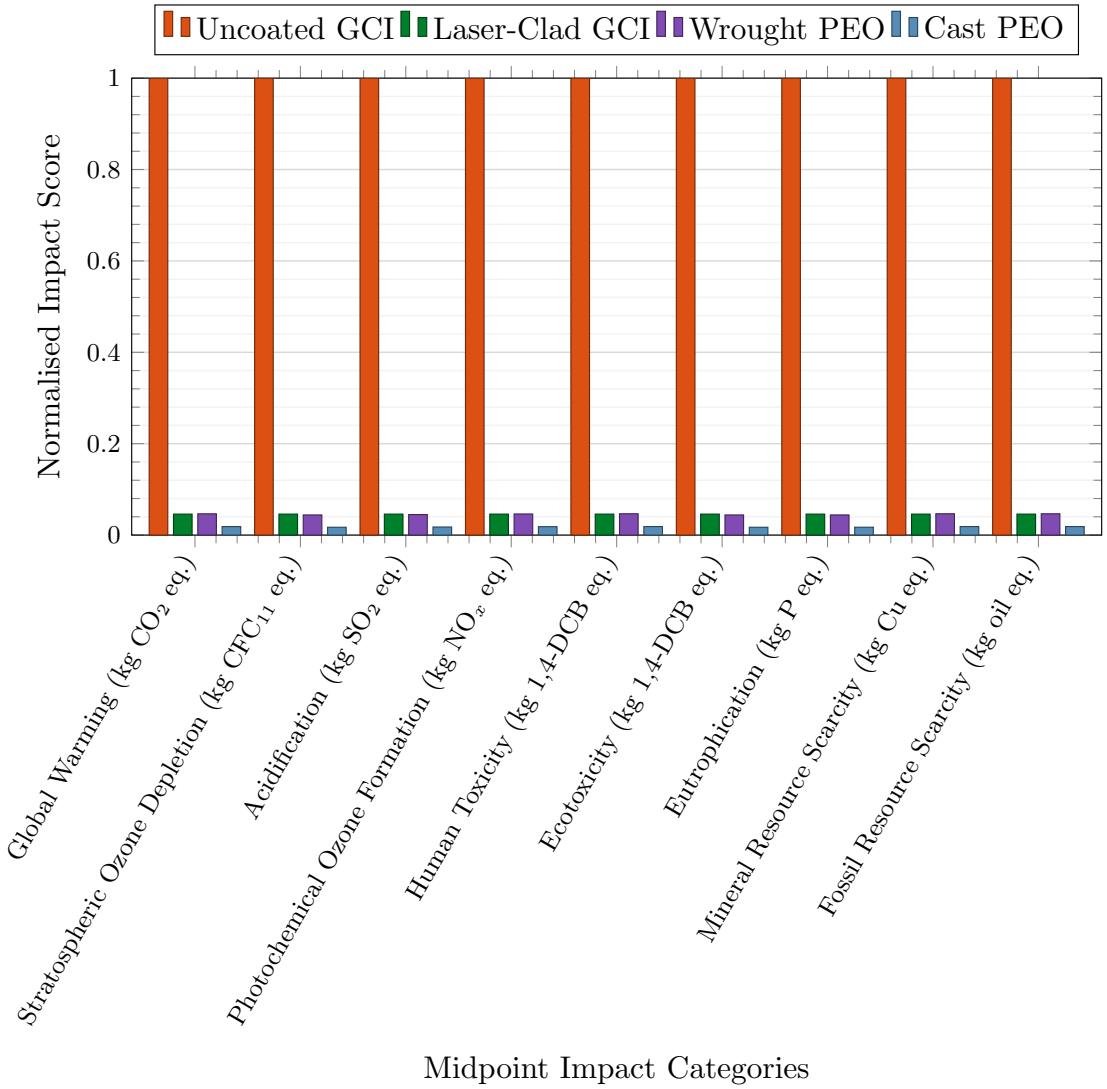

Figure 7.5: Normalised midpoint impact results from the disposal phase of each rotor.

Figure 7.5 outlines the midpoint impacts from the disposal of each brake rotor at end of life. The disposal phase was found to have no impact on fine particulate matter formation, so this was removed for the figure. The impacts of disposal are assumed to be generated from recycling 90% of GCI or Al, the other 10% going to landfill due to impurities [126]. The energy required to melt 1 kg of Al for recycling was found to be 5% less than for the recycling of 1 kg of GCI. However, because the mass of Al required for the wrought billet was slightly higher than that of the GCI prior to the laser-cladding process, both rotors were found to offer the same 95% reduction in all midpoint impact categories compared to the uncoated GCI. Such significant impact decreases from the disposal process can be explained by considering the laser-clad GCI, where the same disposal process of recycling and landfilling the GCI at end of life was assumed as for the uncoated counterpart. However, for the uncoated GCI rotor, this disposal occurred 4.3 times in each FU duration.

In contrast, with the recoating potential of the laser-clad rotor, this disposal only occurred once every 5 FU cycles. A further 3% decrease was found for the cast PEO-Al due to 60% less Al that needed to be disposed of.

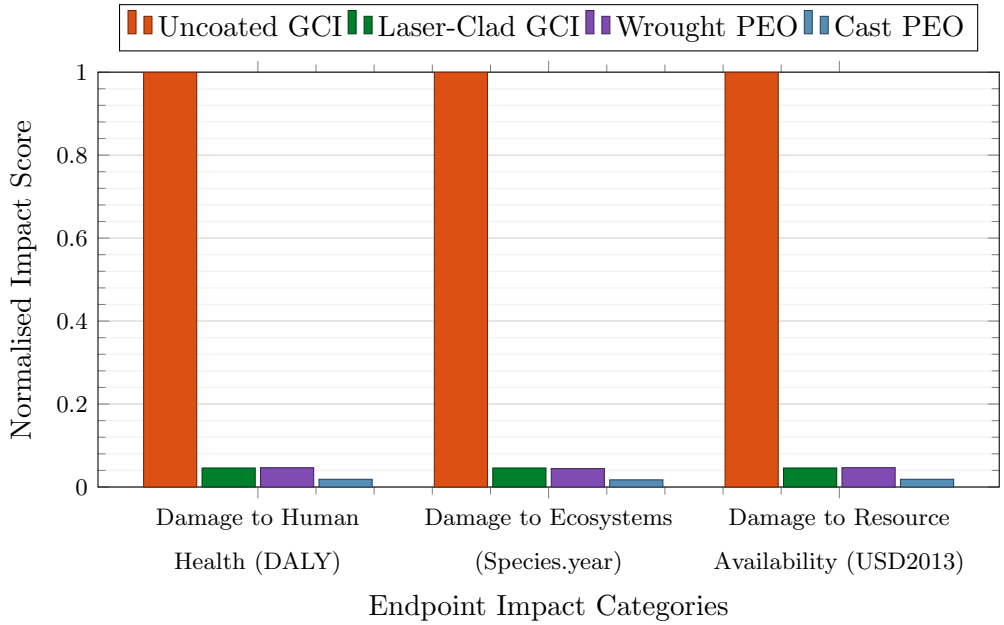

Figure 7.6: Normalised endpoint impact results from the disposal phase of each rotor.

Figure 7.6 illustrates the endpoint impacts from the disposal phase of each rotor. The endpoint impacts for the disposal of each rotor followed the same trend as the midpoint impacts. A 95% reduction was found in the three impact categories for the wrought PEO-Al and laser-clad GCI due to the refurbishment process and wear reduction allowing each coated rotor to be used for a much longer life before final disposal. The reduction in the required material mass to be disposed of for the cast PEO-Al rotor gave a further 3% reduction in endpoint impacts compared with the uncoated GCI.

7.5.4 Full Life Cycle

Figure 7.7 outlines the overall midpoint impacts for the whole life cycle of each rotor which illustrates the potential for problem shifting to occur. If the use and disposal phases of the brake rotors were viewed in isolation, the PEO treated Al rotors would be significantly more favourable. The improved wear resistance compared to the uncoated GCI and the additional benefit of lightweight effects compared to the laser-clad rotor meant that the PEO rotors not only offered reduced PM emissions, but also reduced fuel consumption and accompanying CO_2 exhaust emissions. Despite the same recoating potential, the drawback of both PEO-Al rotors was the high energy demand of the Al smelting and PEO processes in comparison with the laser-clad GCI. As a result of such an energy requirement, the problem becomes shifted onto the manufacture phase of the rotor

resulting in overall increases for impact categories such as stratospheric ozone formation, ecotoxicity and eutrophication when compared to uncoated or laser-clad GCI. For midpoint impact categories such as PM formation, photochemical ozone formation and human toxicity, all three coated rotors showed similar reductions in impact. These categories were heavily influenced by the recoating potential through manufacture and disposal as well as the improved wear resistance and reduced PM emissions during use. The laser-clad GCI rotor offered little reduction in global warming and fossil resource scarcity impacts (7-16%) compared with the uncoated GCI as these categories were heavily influenced by the fuel consumption and associated CO_2 exhaust emissions during use. However, due to the significant weight savings of the Al rotors, both the cast and wrought PEO-Al rotors were found to reduce impacts to both the categories of global warming and fossil resource scarcity by ~65%.

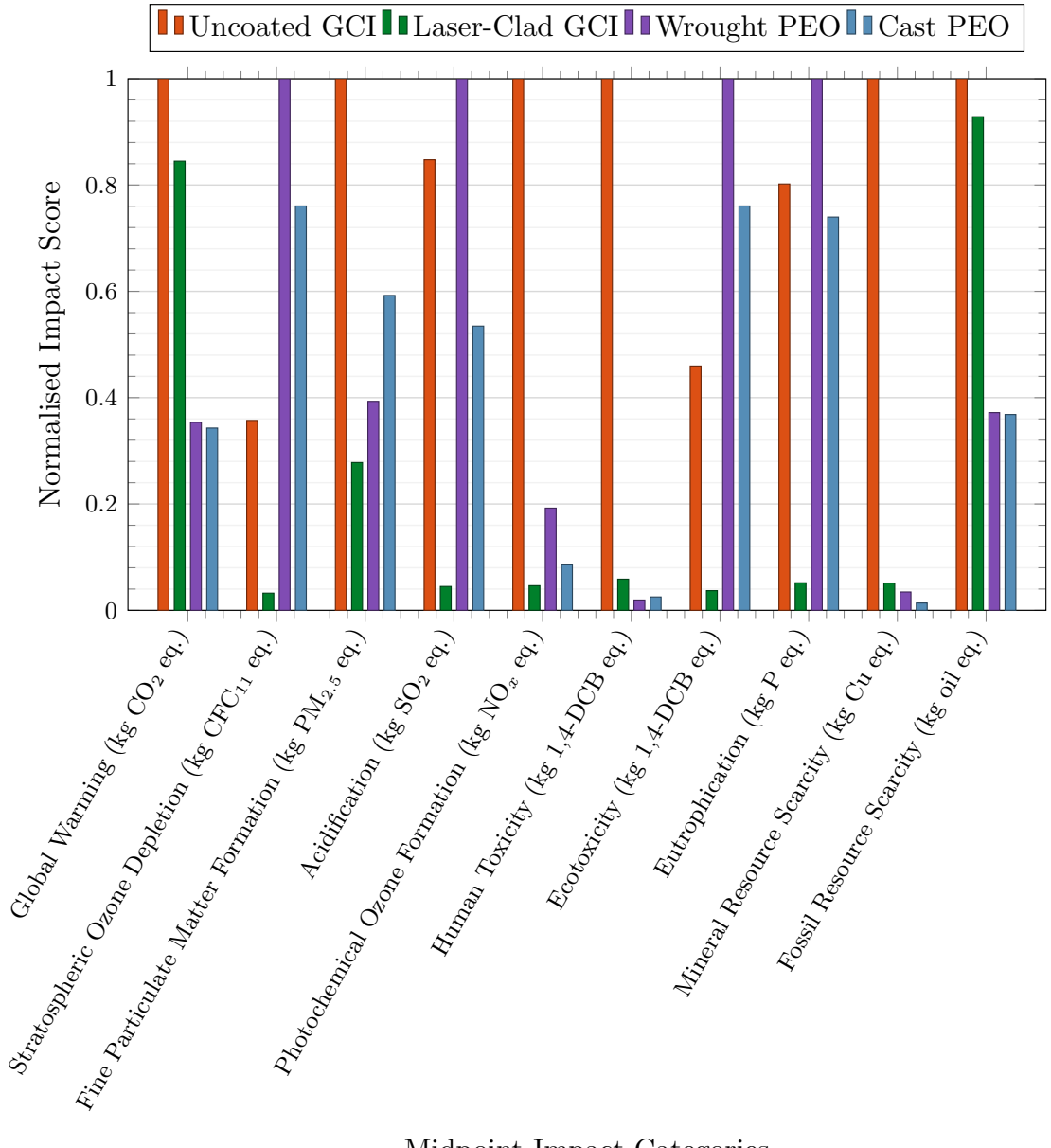

Figure 7.7: Normalised midpoint impact results of each brake rotor.

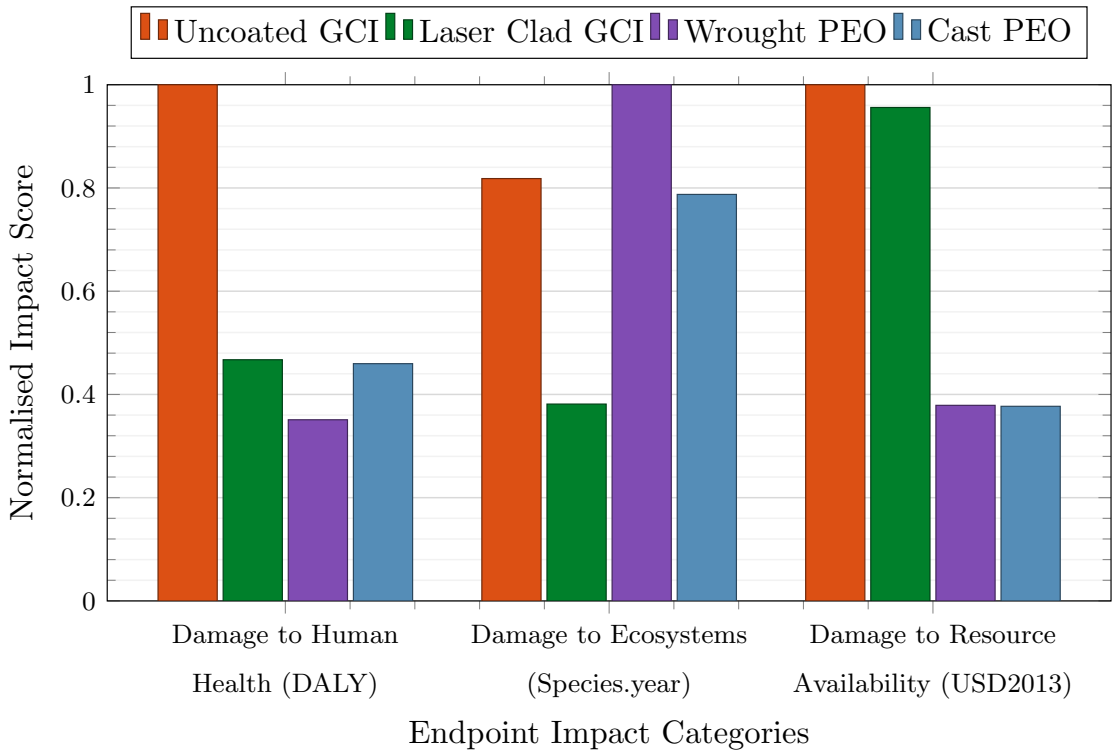

Figure 7.8: Normalised endpoint impact results of each brake rotor.

Figure 7.8 outlines the endpoint impacts from the overall rotor life cycles. The damage to human health was found to have the majority 85-95% contribution from the use phase of each rotor, largely influenced by the CO_2 exhaust emissions associated with fuel consumption and the PM emissions released from brake wear. The combined lightweight effect and low wear rate of the wrought PEO-Al rotor meant that a reduction of 65% was predicted compared to the uncoated GCI. As a result of the higher wear rate of the cast Al and the increased mass of the laser-clad GCI, both these two rotors were predicted to offer only a 54% reduction in comparison.

For ecosystem damage, it was found that the high energy requirement to manufacture Al outweighed the energy reduction and lower CO_2 emissions due to the lightweight effects during the use phase. This meant that while the laser-clad rotor had a 62% reduction as a result of the recoating potential, the wrought PEO-Al rotor was found to give a 22% increase in ecosystem damage. As a result of 60% less raw Al required to manufacture the cast PEO-Al, the ecosystem impact was reduced to 4% below that of the uncoated GCI, although this was still double the ecosystem damage from the laser-clad GCI rotor.

In Chapters 5 and 6, the damage to resource availability was found to be almost solely related to the use phase of the brake rotor. Therefore, this endpoint impact was highly dependent on the weight of the brake rotor. Both PEO-Al brake rotors were assumed to

have the same 60% weight reduction compared to the GCI rotors. Despite the increase in fuel consumption of the laser-clad GCI rotor, due to the added weight of the coating, a 4% decrease in damage to resource availability was still predicted compared to the uncoated GCI, as seen in Figure 7.8. This decrease was due to the small contribution from the manufacturing and disposal phases, where the impacts were significantly reduced compared to the uncoated GCI due to the recoating potential.

7.5.5 Weighting Results

Weighting the results of an LCA study is an optional phase. The results discussed so far within Section 7.5 effectively weight each impact category equally. However, certain categories may be of greater importance. Typically, the government-led incentive is to strive for a carbon-neutral industry, while the upcoming Euro 7 legislation aims to restrict PM emissions. Therefore, impacts of global warming and fine particulate matter formation could be considered to have a higher level of importance than other categories. Furthermore, an implicit motivation for the government-led incentive for a carbon-neutral industry is to reduce the environmental impacts that occur in partnership with global warming, such as ozone depletion and ecotoxicity. The drive to reduce PM emissions can be regarded as a desire to reduce the known damage to human health from such emissions.

ISO legislation [91] generally recommends avoiding the use of different impact weightings in a comparative study. Typically, such a process requires input from the stakeholders and there is no scientific method for this process. However, within the context of the present research, the various legislative committees and governmental bodies could be considered the stakeholders, and so, despite the fact that no relative weightings were applied, the midpoint impact categories associated with a carbon-neutral industry and lowered PM emissions were isolated for further discussion, as shown in the Kiviat (spider web) diagram of Figure 7.9.

If all six categories were evenly weighted, one could argue that the indication for the most suitable rotor is the one with the lowest shaded area on a Kiviat (spider) plot, as shown in Figure 7.9. Based on this premise, the laser-clad GCI, wrought PEO-Al, and cast PEO-Al were found to offer an average overall impact reduction of 55%, 35%, and 41%, respectively, at this midpoint level, compared to the uncoated GCI. However, this does not take into account the fact that the laser-cladding process is expensive or that the energy requirement for the PEO process is based on manufacturing a single rotor and therefore would likely be considerably lower if this process was to enter mass

manufacturing. Furthermore, it can be argued that not all six impact categories shown in Figure 7.9 should be equally weighted when considering an alternative solution to the current uncoated GCI rotor.

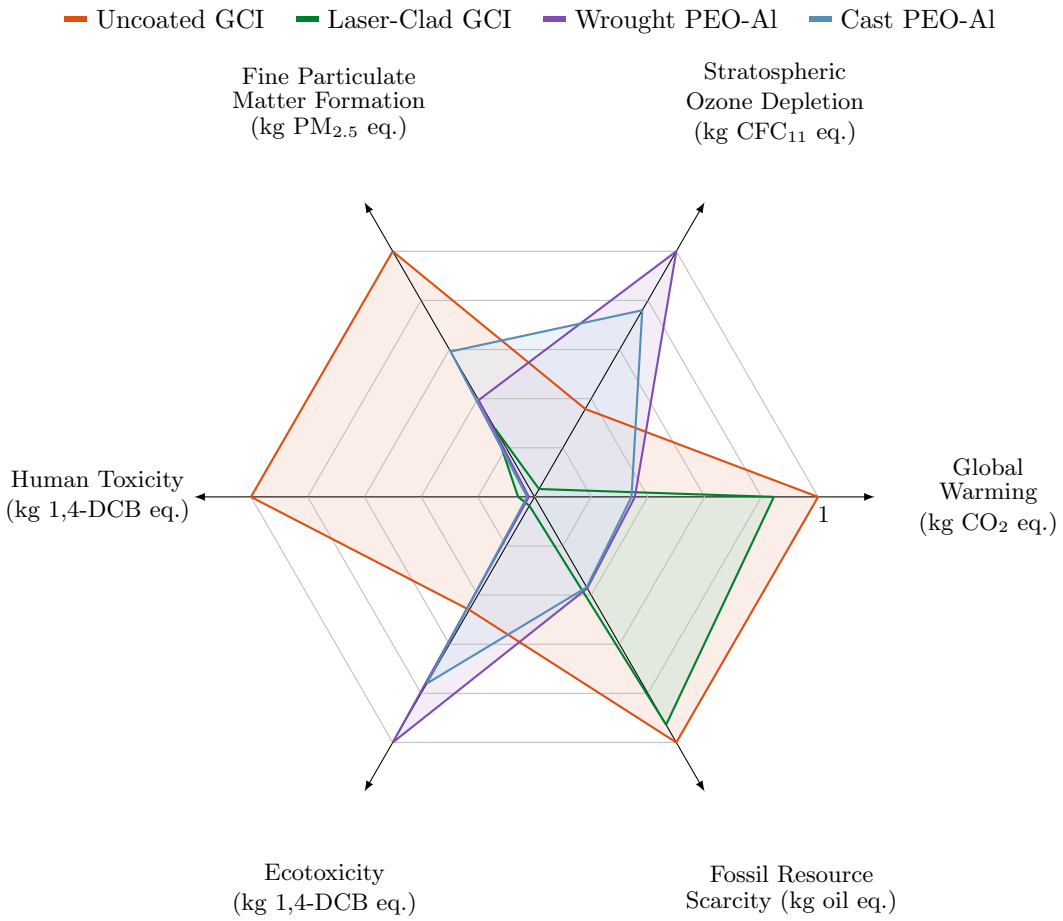

Figure 7.9: Kiviat diagram showing the normalised midpoint impact scores for the six main categories associated with the government's drive for a carbon neutral industry and Euro 7.

To consider a broader generalisation when comparing the damage to the environment directly with the damage to human health, the Kiviat plot shown in Figure 7.10 was constructed from the results for the 3 endpoint impact categories. Based again on the assumption that each endpoint impact is equally weighted, the most suitable rotor is the one with the lowest shaded area on the Kiviat (spider) plot. Figure 7.10 indicates that the laser-clad GCI, wrought PEO-Al and cast PEO-Al gave average enclosed area reductions of 36%, 39% and 42% respectively compared to the area for the uncoated GCI. The reduction in raw Al required for the cast rotor was found to outweigh the drawbacks of an increased wear rate during use and hence gave a somewhat larger reduction in the enclosed area (overall impact) than the other two coated alternatives.

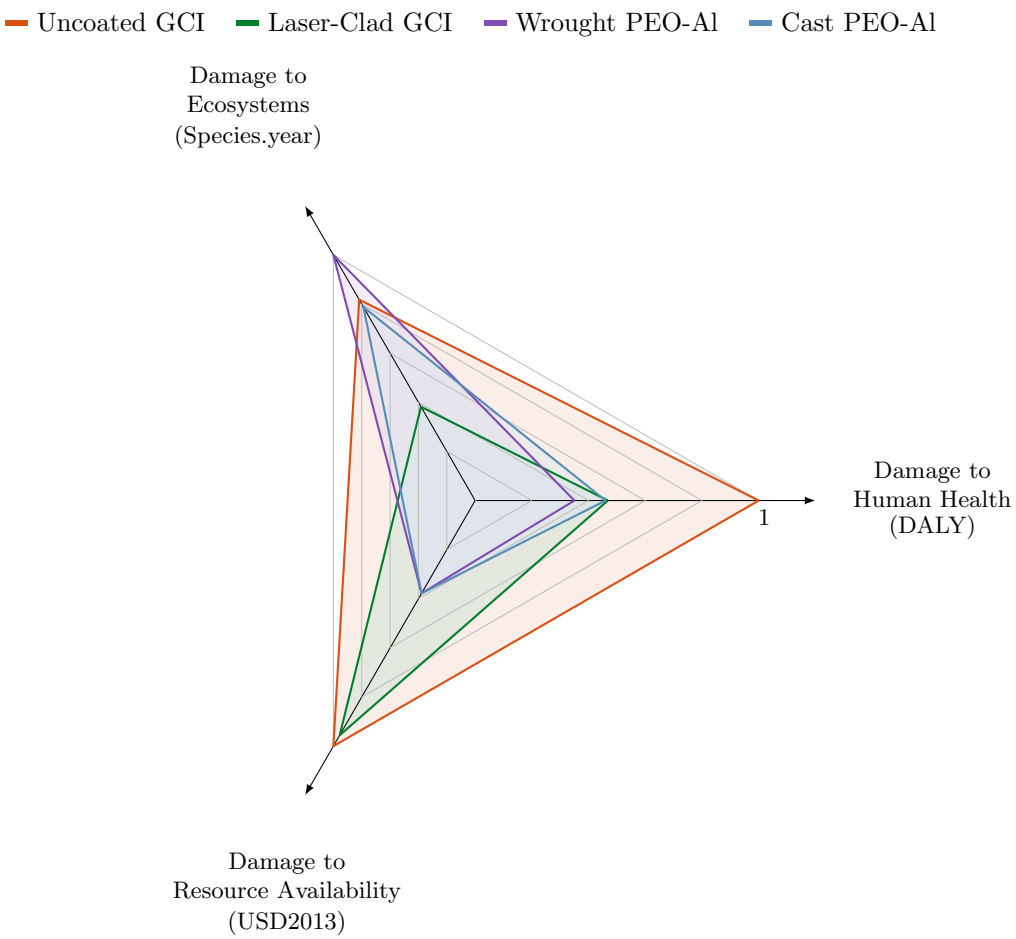

Figure 7.10: Kiviat diagram showing the normalised endpoint impact scores.

7.6 Review of Assumptions and Sensitivity Analysis

It is important to discuss the validity of the assumptions applied during any LCA study, as incorrect assumptions can lead to misleading results. Gradin and Åström [16] investigated the validity of omitting identical parts in a comparative LCA and found that the relative magnitude of impact reductions between the different materials remained unchanged. On this basis, it was considered valid to omit the manufacture and disposal of the brake pad during the present study because it was assumed that the same friction material was utilised for each rotor. However, since the pad wear rate during use can fluctuate between the different brake rotors, the number of pads required per FU can change. Therefore, despite the friction material being the same, the manufacturer and disposal impacts would increase in line with the number of pads required per FU. As friction material compositions are highly confidential, the collection of inventory on such phases was unachievable, so the focus of the present study was to develop the LCA model for general use within the brake industry but to focus solely on the impacts associated with the rotors themselves.

The transport data used within the present LCA could also have had an influence on the results. After assembly of the brake system, the transport was considered identical for all rotors and so could be justifiably omitted from the LCA. However, the distances from the manufacturing location to the assembly plant varied for the different rotors. The impacts of fuel consumption for the transport of the rotors were found to contribute on the order of 1% to the total impacts in all cases. Therefore, the impact associated with the transport of the rotor was deemed insignificant. Therefore, the fact that the transport data used were from 2007 [108] and could be considered outdated was not a concern. Likewise, assumptions about the precise transport arrangements should not affect the validity of the results.

Each phase of the life cycle (apart from transport) was found to have significant contributions to certain impact categories. Therefore, when investigating, through sensitivity studies or in-depth discussion, the significance of methodological choices and assumptions on the final results, it was important to consider choices that could influence all phases of the life cycle. The remaining assumptions during the definitions of the methodology outlined in Chapter 3 were the FU applied, the electricity mix used, the vehicle's powertrain, the number of recoatings possible before disposal of the coated rotors and the proportion of recycled materials used during the manufacture of new rotors.

7.6.1 Functional Unit Duration

When investigating the phase breakdown of the impacts for each rotor within the case studies, it was shown that the use phase made the largest contribution to many of these impact categories. Varying the assumed lifespan of the vehicle can amplify or reduce the significance of the use phase. Therefore, a sensitivity analysis was performed to examine the effect of varying the original assumption of 240,000 km within the case studies reported in Chapters 5 and 6. For this sensitivity study, the FU distance was varied between 160,000 km and 320,000 km.

Figure 7.11 outlines an example of changing the FU duration for the global warming impact, often considered the most important environmental damage indicator, from the full life cycle of the rotors. It can be seen that, as the FU duration increases, the global warming indicators (fuel consumption and accompanying CO_2 emissions) also increase in a linear fashion. Similarly, as the FU duration increases, the number of rotors required per FU increases linearly, thus causing the global warming impact associated with the manufacture and disposal phases of the rotors to also increase linearly. However, the

proportion in which the impacts changed for every 20,000 km increment in the FU was the same for all the rotors considered. This phenomenon was found to occur for every impact category for all 4 rotor materials. Thus, the comparison between the relative values for each rotor remains unchanged and is therefore considered valid.

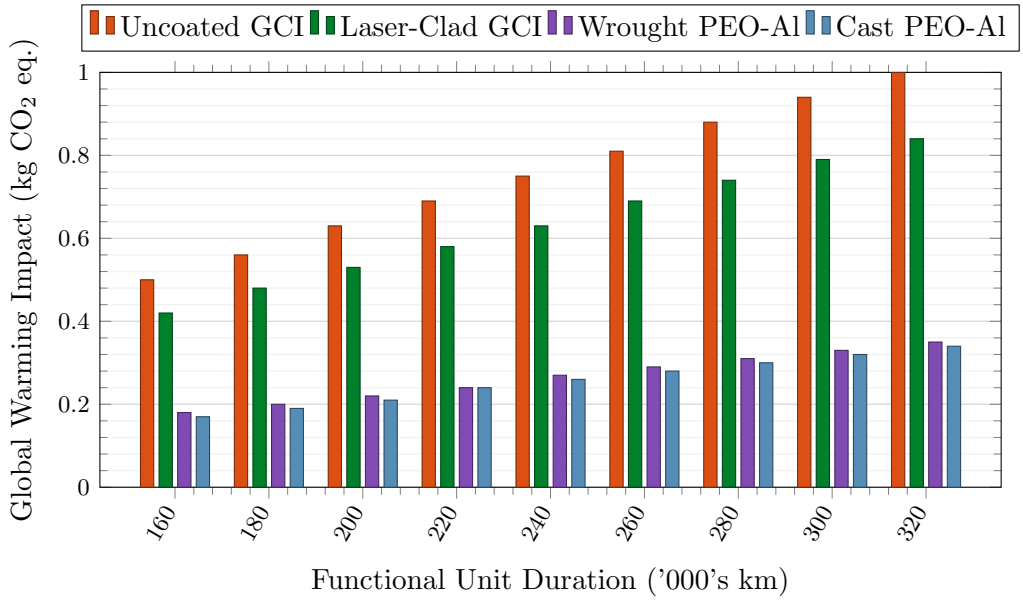

Figure 7.11: Midpoint impact results for sensitivity analysis of functional unit duration ('000's km) - Global warming example.

7.6.2 Electricity Mix

The proportion of fossil fuel energy sources used could have an influence on the impact results, typically for the manufacturing phase where it was found that a large proportion of the PEO-Al rotor impacts were associated with energy generation. For both case studies, the electricity mix was chosen based on the current UK mix [117], applying a 10% fossil fuel, 61% renewable, and 29% nuclear electricity generation split. However, this electricity mix will vary from country to country and with time as the proportion of fossil fuel energy generation is set to decrease. Therefore, it was considered important to test the sensitivity of the results to the assumed electricity generation mix. Stamford's [46] study included five different electricity generation scenarios, varying from 68% fossil fuel contribution down to 0%. In the present study, the generation of results for all five scenarios was not considered necessary, so only the two extremes were chosen alongside the previous assumption of 10% fossil fuels. Table 7.1 outlines the proportion within each investigated mix.

Based on the study conducted by Stamford [46] the electricity mix only impacted global warming, stratospheric ozone depletion, acidification, photochemical ozone formation, eutrophication, and ecotoxicity, with the added inclusion of fossil resource scarcity for

the present study. Therefore, only these seven impact categories were included in the sensitivity study. The impact results for each electricity mix were normalised between 0 and 1, similar to the case studies conducted.

Table 7.1: Description of electricity mixes used within sensitivity analysis.

Fossil Fuels	Nuclear	Renewables
68%	0%	32%
10%	29%	61%
0%	0%	100%

Figure 7.12 outlines the midpoint impact results for each rotor material. As expected, the energy mix used had a minimal effect on those impact categories heavily associated with the use phase of the rotor, such as global warming, and fossil resource scarcity. For all four rotors, only a small proportion of global warming and fossil resource scarcity were attributed to manufacture (including coating, where applicable) and disposal. Fossil resource scarcity was mainly due to the fuel consumption associated with the rotor, while CO_2 released as a result of this consumption greatly affected the level of observed global warming impacts. The decreases in the proportion of fossil fuels from 68% to 0% only offered an additional 1% decrease in global warming and fossil resource scarcity for the two PEO-Al rotors.

Comparatively the change in the electricity mix also had little effect on photochemical ozone depletion. This was likely due to the fact that Stamford's study found that the range in such an impact was only 1.32×10^{-5} kg NO_x eq. when varying the proportion of fossil fuels. In comparison, the range found for acidification and ecotoxicity was much larger. Despite the fact that the latter three impact categories were all maximum for the wrought PEO-Al rotor, the margin by which this was the case decreased by 10%, 40% for acidification and ecotoxicity respectively. No pattern was found between the degree to which the impact contribution was divided between manufacture, coating and disposal, and the decrease in impacts observed. The likely effect is due to the fact that energy demand is a larger contributing factor to ecotoxicity and eutrophication, compared to emissions. It could be considered an important part of future work to include the variation of electricity mix at different life cycle stages, to reflect the changes in the electricity mix used in the country of manufacture. Both PEO-Al rotors were found to be more sensitive to the proportion of fossil fuels used as a result of their higher energy demand for manufacture.

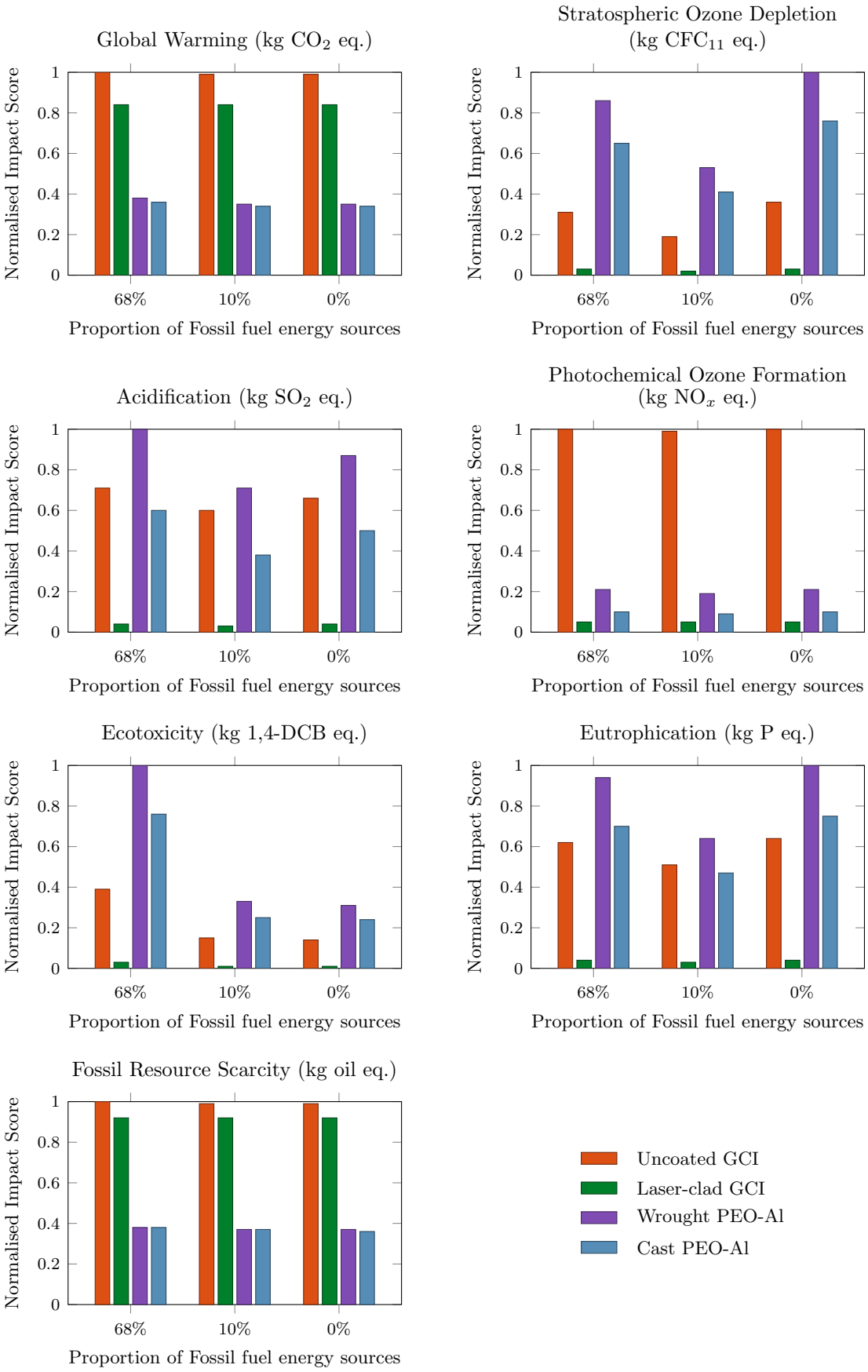

Figure 7.12: Midpoint impact results for sensitivity analysis of electricity mix used (varying the proportion of fossil fuel energy sources).

For midpoint impact categories, such as stratospheric ozone depletion or eutrophication, Figure 7.12 shows that impacts from the four rotors actually increased as the proportion of fossil fuel sources decreased from 10% to 0%. This was potentially a result of the proportion of nuclear and wind sources within the mix compared to solar and biomass energy sources, which typically have slightly higher impacts.

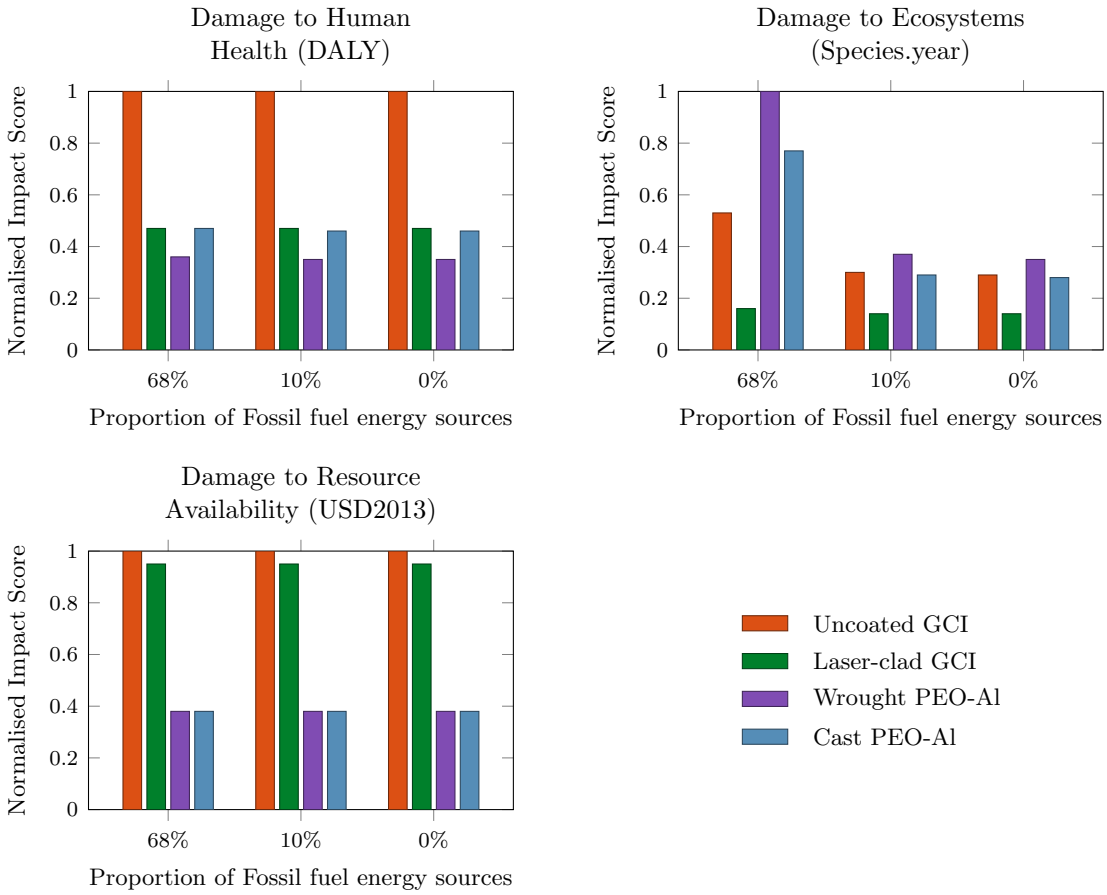

Figure 7.13: Endpoint impact results for sensitivity analysis of electricity mix used (varying proportion of non-hydrocarbon energy sources).

A similar sensitivity was conducted for the endpoint impact categories. Figure 7.13 illustrates the results for each rotor material. Damage to human health is related to midpoint impact categories such as human toxicity, global warming, and fine particulate matter formation. All of these categories are highly related to the use phase of the rotor, with minimal association with manufacture and disposal. This was especially the case with the coated rotors when the manufacture and disposal are distributed between 5 rotor lifespans for all three coated rotors. Therefore, no variation was found when the proportion of fossil fuels was altered.

It can be seen in Figure 7.13 that the wrought PEO-Al rotor had the maximum damage to the ecosystem impact for the three electricity mixes, although the comparative margin in which this occurred became smaller as less fossil fuels were used. The greatest difference

was when the proportion of fossil fuels decreased from 68% to 10%, while little to no difference was found between fossil fuels 10% and 0%. The uncoated GCI rotor went from being 47% lower than the wrought PEO-Al impact to 16% lower, while the laser-clad GCI went from 84% lower to 60% lower. Comparatively the difference between the wrought and cast PEO-Al rotors remained unchanged, as expected since the only difference between the two rotors during manufacture and disposal was that the cast rotor required 60% less raw Al.

Similarly to human health, Figure 7.13 shows that the variation of the proportion of fossil fuels was found to have virtually no impact on the damage to resource availability. This was due to the only influential midpoint impact category, namely fossil resource scarcity, having a minimal change (∼1%). This result was expected because the resource availability endpoint impact category was found to be solely dependent on the use phase (due to the fuel consumption requirement during use based on the ICEV assumption). As discussed in Section 7.6.3 below, if BEVs were the considered powertrain, then it would be likely for the resource availability endpoint impacts to decrease with a decrease in the proportion of fossil fuels used for recharging.

7.6.3 Electric Vehicles

For the case studies I and II reported in Chapters 5 and 6, it was assumed that the vehicles in question were petrol ICEVs. The inclusion of fuel consumption and accompanying CO_2 exhaust emissions was necessary to properly model the lightweight effect of the two PEO-Al rotors on ICEVs which still constitute the overwhelming majority of the passenger vehicle fleet in the UK and elsewhere. Other emissions such as SO_2 and NO_x were omitted from the present study because they were assumed to be negligible compared to CO_2. Emissions such as NO_x and CO are limited by legislation and therefore levels are generally very low [17, 18]. The petrol consumption and accompanying CO_2 emissions associated with the weight of the brake rotor were calculated and included within the use phase of the product system (Equations 3.7 and 3.9). The weight of the pads and other components, such as the calliper, were omitted from this calculation because they were assumed to be the same for all rotors considered. ICEVs were also initially assumed because the small-scale testing to gather emissions data used a WLTP cycle designed to simulate the braking duty cycle of a light ICEV. This cycle would be considered unrepresentative for the reduced frequency of use of friction brakes within a BEV fitted with regenerative braking.

However, with the increasing sales of electric vehicles, consideration should be given to the effects that such a change in power train would have on the LCA results. In particular, the proportion of renewables used for recharging the batteries would have a direct effect on the energy demand impacts associated with an BEV throughout its life.

For the rotor use phase, the consumption of hydrocarbon fuel and the associated CO_2 exhaust emissions of a petrol ICEV can be compared with the impacts of generating the electricity required to recharge a BEV throughout the 240,000 km FU duration. Table 7.2 shows the impacts of global warming and fossil resource scarcity for 1 kWh of generated power for each of the three electricity mixes discussed in Section 7.6.2.

Table 7.2: Impacts from generating 1 kWh of energy for 3 different electricity mixes.

Proportion of fossil fuel sources	Global warming impact (kg CO_2 eq./kWh)	Fossil resource scarcity (kg oil eq.)
68%	0.12	4.11×10^{-2}
10%	0.03	5.73×10^{-3}
0%	[a]0.04	0

[a] global warming impact increases even with a decrease in fossil fuel contribution as a result of the proportion of nuclear and wind sources decreasing. Stamford's study [46] found that nuclear and wind were found to have lower contributions to global warming impact than solar and biomass.

Petrol has an energy density of 46 MJ/kg [135] which equates to 12.78 kWh/kg (3.6×10^6 J is equal to 1 kWh [128]). Therefore, based on the hydrocarbon fuel consumption during use that is associated with the weight of each rotor, an equivalent energy generation requirement for a BEV was calculated. Figure 7.14 and Figure 7.15 outline the relative global warming and fossil resource scarcity impacts associated with each rotor caused by the need for this energy generation during the use phase and full life cycle respectively. The three electricity mixes that were investigated within Section 7.6.2, in comparison to the corresponding ICEV (using the case study energy mix of 10% fossil fuel energy sources for the manufacture and disposal phases) are shown.

Figure 7.14 shows that replacing the ICE with a battery powered system significantly reduced both the global warming and fossil resource scarcity impacts during the use phase of the rotors. When the proportion of fossil fuel energy sources decreased from 68% to 10%, the impacts of global warming during use were even further reduced. However, a slight increase in impact occurred unexpectedly in the 0% fossil fuel case. This was likely due to the greater reliance on solar and biomass for this 0% fossil fuel scenario, which have a global warming potential of 50 and 100 g CO_2 eq/kWh respectively, whereas the

use of nuclear and wind in the mix 10% only gives a global warming potential of 4.7 and 6.2 g CO_2 eq/kWh [46]. Figure 7.14 shows that the fossil resource scarcity associated with the use phase decreased dramatically with decreasing the proportion of fossil fuel energy sources with zero impact predicted at 0% fossil fuel sources. Despite these large decreases, it was found that comparatively the differences between the impacts for the different rotor materials remained the same for the use phase of the rotors.

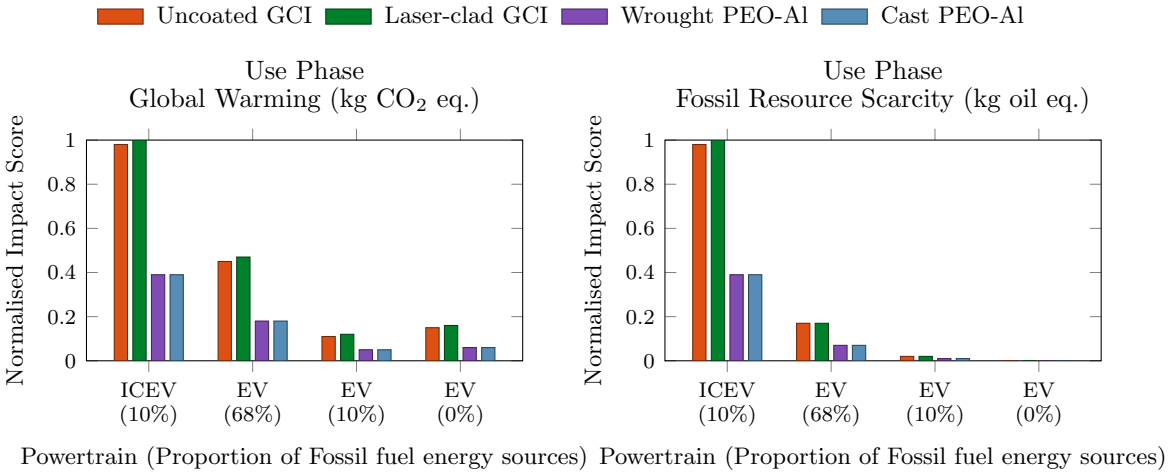

Figure 7.14: How varying the powertrain and proportion of fossil fuel energy sources affects global warming and fossil resource scarcity impacts associated with rotor weight (use phase).

In contrast, when looking at the full life cycle results shown in Figure 7.15, comparative changes were found for both global warming impact and fossil resource scarcity impacts. This is mainly due to the variations in the energy mix associated with the manufacture and disposal phases that alter the impacts in these phases, as seen in Section 7.6.2. This alteration can partly be attributed to the fact that, when a battery powered system replaces an ICE, the use phase of the rotor becomes a smaller contributing factor to the full life cycle impacts.

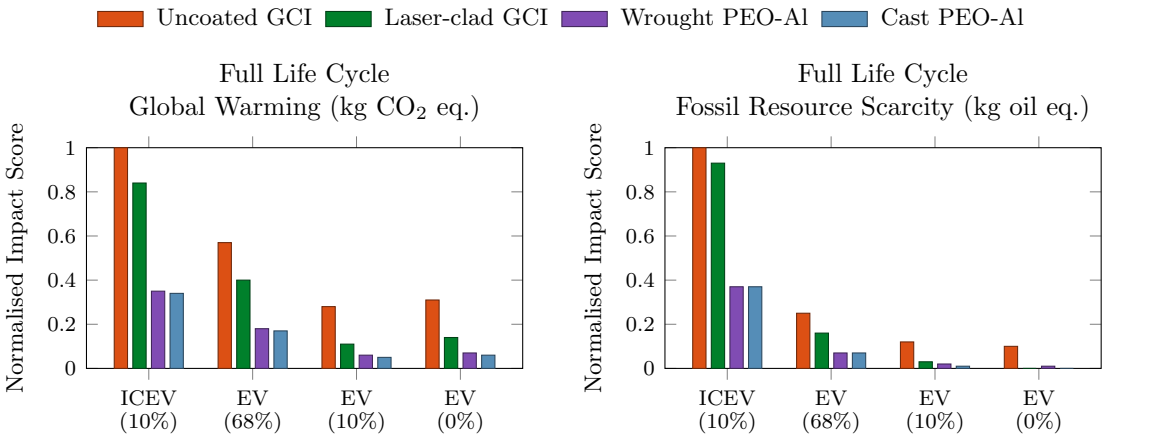

Figure 7.15: How varying the powertrain and proportion of fossil fuel energy sources affects global warming and fossil resource scarcity impacts associated with rotor weight (full life cycle).

It should be noted that these results do not take into account the average savings of 10-15% fuel consumption that can be achieved by regenerative braking in BEVs [136]. However, the inclusion of this would be complicated and the WLTP would not be an accurate representation of the braking cycle due to the reduced frequency of use of the friction brakes. The most important result shown in Figure 7.15 was that, comparatively, there was no change in relative global warming or fossil resource scarcity impact during the use phase between the four rotor types. They were all affected to the same degree when moving to an electric powertrain and changing the electricity mix to recharge the BEV batteries. The exception to this was for the impact of fossil resource scarcity when 0% fossil fuel energy sources were used, reducing the impact of the four rotors to zero. Global warming was not reduced to zero when 0% fossil fuel energy sources were used as a result of wind and solar energy generation that continues to maintain a small amount of global warming impact throughout their life cycle due to installation and disposal demands. The relative impact on global warming during use of the four rotors remained the same, with the PEO-Al rotors offering a significant reduction compared to the GCI alternatives, largely due to the reduction in rotor weight. What is also obvious from Figure 7.14 and 7.15 is the big reduction that can be achieved in global warming impacts for all rotor types by moving to BEVs with a high renewable electricity source for recharging which of course explains why so many governments are pushing BEVs as one of the main ways of reducing GHG emissions.

7.6.4 Recoating Potential

In principle the recoating potential of the three coated rotors can offer significant reductions in environmental and human health impacts, allowing the manufacturing and disposal burdens to be shared over several rotor lifetimes. However, the process of recoating a rotor is currently only theorised, and there is a possibility that as a result of the high safety requirements of a braking system, such a process would not be allowed even for re-engineered aftermarket components. Figure 7.16 outlines how the comparative midpoint impact results would differ should the recoating potential be removed from the LCA for the 3 coated rotors.

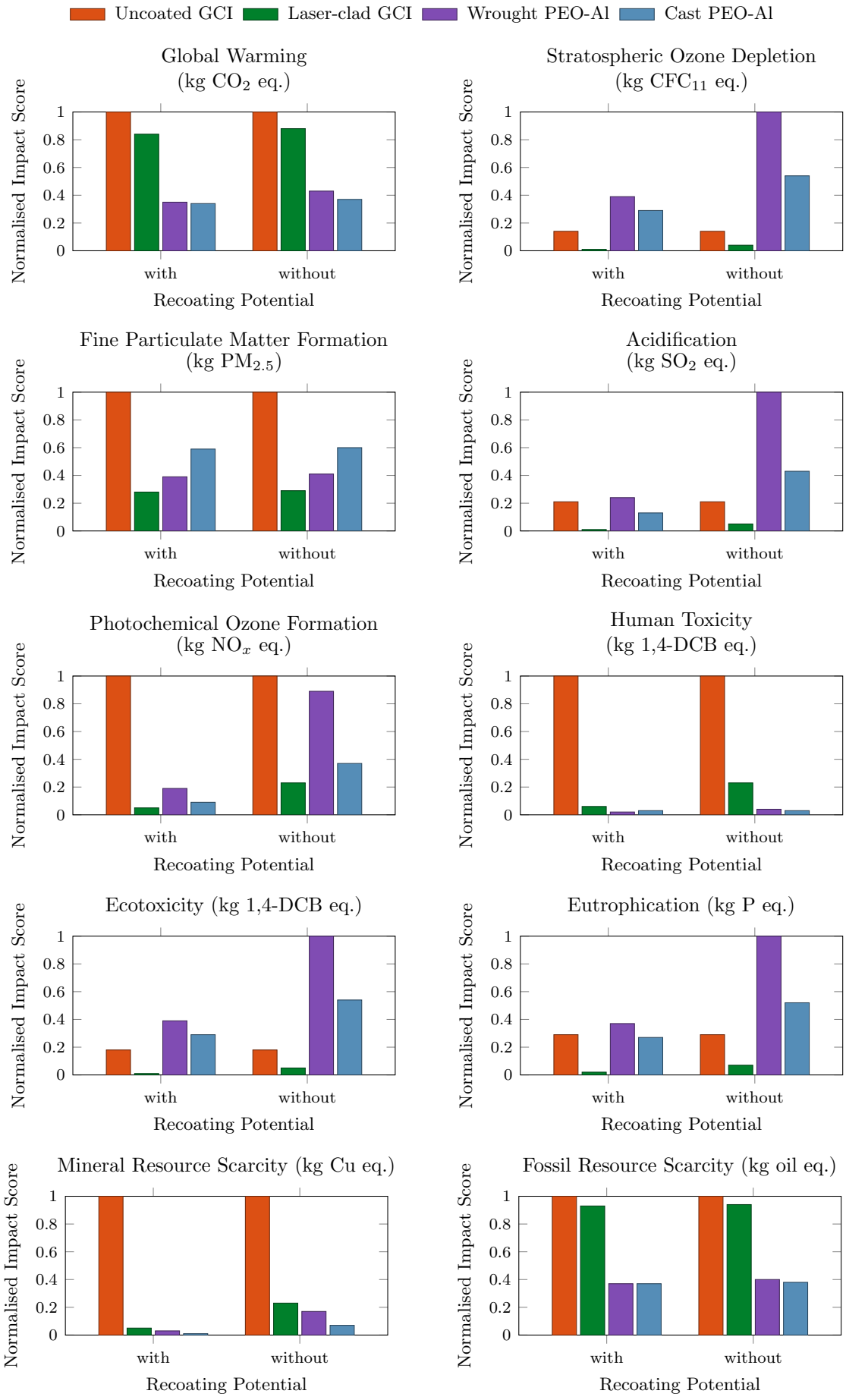

Figure 7.16: Normalised midpoint impacts from all four rotors with and without recoating potential.

Figure 7.16 shows that impact categories with a high influence from the use phase, such as global warming, fossil resource scarcity, and fine particulate matter formation, were largely unchanged when the recoating potential was removed from the analysis. The percentage change when removing the recoating potential appeared to be relatively similar for each of the three coated rotors, although the laser-clad GCI had a slightly smaller increase, while the wrought PEO-Al had a slightly higher one. This was likely due to the fact that the PEO-Al rotors had a larger contribution from the manufacture and disposal life cycle phases than the laser-clad. The midpoint impact categories that had the largest increase were photochemical ozone formation, acidification, and mineral resource scarcity. As found in the individual case studies, all 3 of these impacts did not receive a contribution from the use phase of the rotor. Despite these increases being up to 4 times the value for corresponding recoated rotor, significant improvements were still found compared to the uncoated GCI, as a result of the reduced wear rate allowing the coated rotors to each last the full 240,000 km FU before replacement. Figure 7.17 outlines how the comparative endpoint impact results would differ should the recoating potential be removed.

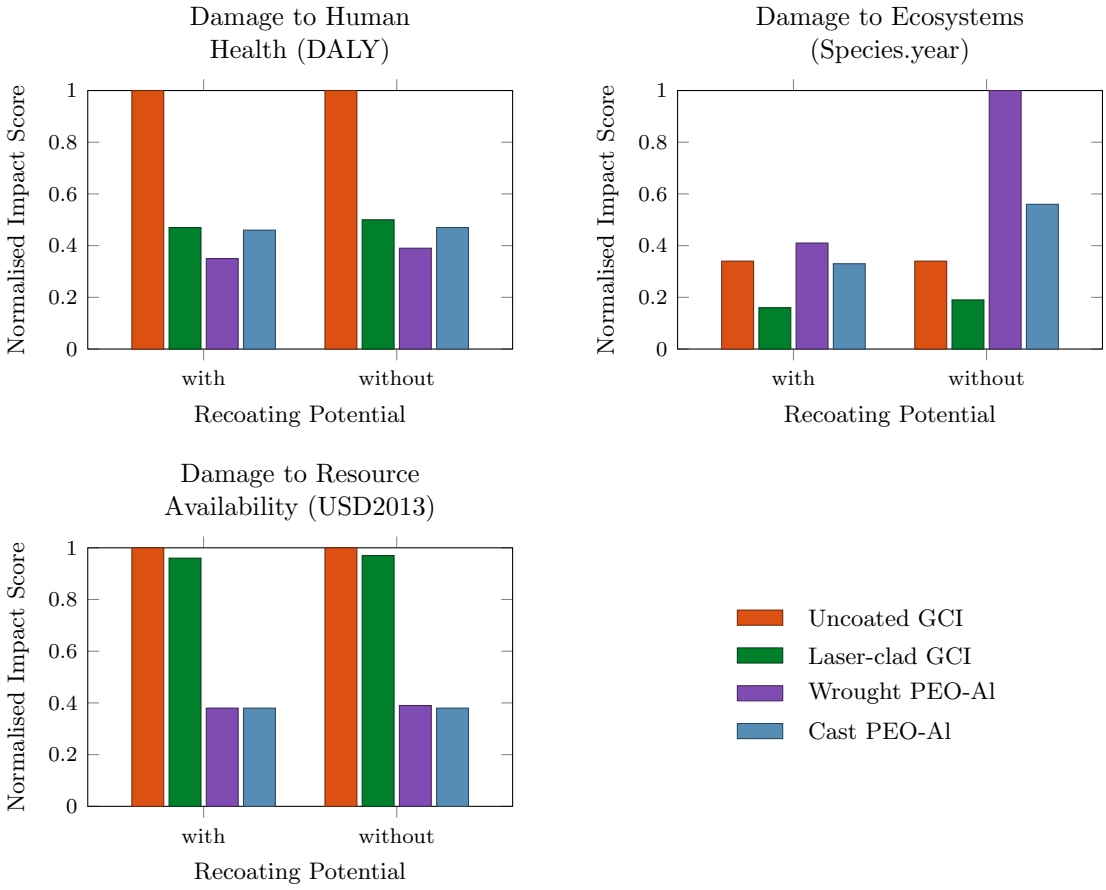

Figure 7.17: Normalised endpoint impacts from all four rotors with and without recoating potential.

The same trend was found with the endpoint impacts as with the midpoint categories, in that those categories heavily influenced by the manufacture and disposal phases such as

damage to ecosystems were found to have larger increases when the recoating potential was removed. The key benefits of using a coated rotor were still found as a result of the significantly reduced wear rate in the categories of damage to human health and resource availability. These benefits could be extended further should corrosion affects be included in future LCA work.

7.7 Summary

The present research filled several gaps in the current literature, including consideration for the first time of lightweight brake materials within an LCA study. Building on from the methodological choices made by Gradin and Astrom [16], the ReCiPe endpoint categories were added to provide a more generalised and broader overview of the environmental and human health impacts of each rotor. The novel investigation of lightweight rotors showed key benefits from the reduction in fuel consumption during use. The self-developed Python model was found to offer a fully transparent and adaptability modelling package for future use within the braking industry. The adapted SADT notation proved to be a useful tool for simplifying complex LCA systems. Small-scale testing allowed an accurate comparison of PM emissions during the use phase of the rotor, whilst improving upon the high cost and time intensive process of full-scale testing. For the first time emissions data was gathered for a laser-clad GCI rotor, and the results were all scaled to a full-sized vehicle, clearly showing only the coated or surface treated rotors were capable of meeting the impending Euro 7 legislation.

Applying a coating or surface treatment to a rotor has been shown to offer several benefits, such as reducing wear rate during use and allowing for manufacturing and disposal impacts to be shared across several life cycles through recoating the rotor. Lightweight alternatives, such as PEO treated Al, offer significant benefits during use, reducing the unsprung mass and fuel consumption of the vehicle. Theoretically, the resulting road abrasion would also reduce [137], however, this further reduction in non-exhaust emissions was not considered within the present study. Al rotors, however, do have a trade-off, increasing certain midpoint impacts as a result of the high energy demand of smelting bauxite. Being able to cast a rotor rather than machining from a wrought billet significantly reduces the amount of material required and thus also reduces the manufacturing and disposal impacts. However, in the case of the cast PEO-Al rotors, this came with the trade-off of increased surface roughness and pad wear during use, resulting in higher PM emissions.

The chosen functional unit duration has a linear effect on the result, amplifying or shrinking the significance of the use phase but not changing the relative ranking of the four rotor types. The assumed electricity generation mix, on the other hand, had little impact on most categories, only influencing stratospheric ozone depletion, ecotoxicity and eutrophication. The Al rotors were found to be more sensitive to the proportion of fossil fuels used because of their higher energy demand during manufacture. Comparatively, the results between different rotor types were found to be unchanged during the use phase when the ICEV was replaced by a battery BEV, and even with the recoating potential removed, the coated rotors still offered significant benefits as a result of their reduced wear rates.

Chapter 8

Conclusions and Future Work Recommendations

8.1 Introduction

Chapter 8 outlines key findings of the present study, highlighting the benefits of applied methodology and the contributions to knowledge and understanding. Recommendations are made for future research to be undertaken following on from the present study.

8.2 Conclusions

The unique LCA approach developed in the present research has proven its suitability to analyse and quantify the environmental and human health impacts of the braking system. The development of a fully adaptable LCA model specific to the automotive braking system allows future analysis of materials and components to be easily performed. This offers the benefit of being able to assess the environmental impact of friction materials as they are optimised for the new brake rotors or to investigate alternative rotor materials developed to align with potential future legislation that may be enforced.

The new methodology added the consideration of endpoint impacts, which were able to provide stakeholder with a more generalised overview of the LCA results. The development of the adapted SADT notation was found to be a useful tool to simplify complex LCA systems to more adaptable and easier to interpret diagrams. This adapted notation could be usefully applied in the more general LCA field, and it is likely that a further paper will be written to highlight this potential to the wider LCA community. In the present study, a brake specific LCA Python model was developed with full adaptability to be able to alter the input parameters to ensure that new materials aligned with any new legislation can be modelled. The brake components included within the model are adaptable to allow individual investigations depending on the requirements of the stake holders. For example, a friction material manufacturer could compare alternative compositions directly to ensure that no problem shifting occurs while optimising performance for use with new brake rotor materials.

It had been demonstrated that small-scale testing techniques can provide results in significantly less time and at much lower cost than conventional dynamometer testing, whilst still being valid for use within a comparative LCA environment. This has enabled a noticeable gap in the literature to be plugged in the sense that emissions results for a laser-clad GCI rotor are now openly available for the first time. By extrapolating the results from the small-scale tests, it was clearly demonstrated that to meet the stringent Euro 7 legislation on PM emissions, a rotor with some kind of hard coating or surface treatment will be required. In this context, both the laser-clad GCI and PEO treated Al rotors showed significant reductions in the wear rate of both the pad and the rotor, leading to significant reductions in both $PM_{2.5}$ and PM_{10} emissions.

The refurbishment potential of a coating or surface treatment of a GCI rotor was clearly demonstrated by consideration of the laser-clad GCI in case study I. The ability to recoat or retreat a used rotor to extend its life span allowed the manufacture and disposal impacts to be shared over a number of FU durations. This led to a predicted reduction of 95% in the manufacturing and disposal impacts compared to the uncoated GCI, despite the impacts of multiple coating processes required throughout the product life cycle. Distributing the manufacturing impacts across multiple FU durations was especially beneficial in reducing ecosystem damage, given that manufacturing accounted for 42% of the impact from the uncoated GCI rotor. The overall conclusion from this case study is that a coated GCI rotor has lower overall environmental impacts than the current uncoated GCI and can therefore be a viable means of meeting the impending PM emissions legislation with the danger of problem shifting understood and kept within a permissible limit. The impacts of global warming and fossil resource scarcity were found to be largely driven by the use phase of each rotor. Consequently, the benefits of recoating were significantly diminished due to the increased rotor weight during operation. Despite this, the laser-clad GCI rotor still demonstrated a small reduction in both impact categories compared to the uncoated GCI rotor. The fine particulate matter formation impact was primarily influenced by wear during use rather than recoating benefits, resulting in a 72% decrease. All other impact categories showed substantial reductions of 90–95%, directly attributed to the recoating potential and the extended lifespan achieved through reduced wear. At the endpoint level, the damage to human health and ecosystems was reduced by 53% compared to the uncoated GCI rotor. However, resource availability saw only a 4% reduction, primarily due to the increased rotor weight and the resulting higher fuel consumption during use.

The potential problem shifting was identified when alternative lightweight materials, such as a surface treated Al alloy, were investigated in case study II. The manufacture of Al rotors requires significantly higher energy demands because of the energy-extensive smelting process, thus potentially negating some of the refurbishment benefits from recoating a new rotor. Despite the higher environmental and health impacts found for categories such as ecotoxicity, stratospheric ozone depletion, and eutrophication during manufacturing, these negative impacts were balanced by the benefits of a significant reduction in wear and PM emissions during the use of the PEO-Al rotors. Furthermore, weight reduction with Al was found to offer several benefits. Although transport impacts were not found to make a significant overall contribution, environmental and health impacts during transport would be lessened due to reduced weight of the rotors. The significant rotor weight reduction of approximately 60% compared to GCI will lower fuel consumption, diminishing impacts on categories such as global warming and fossil resource scarcity. This then translates into benefits for the ecosystem and resource availability at the endpoint impact level.

Casting Al instead of machining from a solid wrought billet was estimated to reduce the amount of alloy required by ∼60%, reducing the energy demand associated with smelting. This in turn reduced the impacts on manufacture and disposal by an average of 52% at midpoint impact level and 48% at endpoint impact level. The current drawback of using cast Al was the rougher surface finish even after the PEO surface treatment was applied, resulting in increased wear and PM emissions during use compared to the smoother wrought surface. However, this LCA case study has shown that the PEO treatment of a cast or wrought Al alloy can reduce the rotor wear and associated emissions to a level that would meet the impending legislation without significant negative problem shifting effects.

When investigating the validity of the methodological choices, it was found that the duration of the chosen FU, despite amplifying or diminishing the significance of the use phase, had no effect on the overall comparison between the different rotors. Similarly, the powertrain used had minimal effect on this comparison, with a BEV simply reducing the global warming and fossil resource scarcity impact associated with the rotor during use compared to an ICEV, as expected. Removing the recoating potential was found to increase impact categories associated with the manufacture and disposal phases of coated rotors by up to a factor of four. However, the significantly reduced wear rates meant that the coated rotors still offered significant reductions in the overall environmental and human health impact. Increasing the proportion of renewables within the electricity

mix was found to influence the PEO-Al more, due to their high energy demand for Al smelting, although once the mix rose above about 60-70% renewable sources, the effect of this change on the present comparative study was minimal.

Assuming that the six most important midpoint impact categories as well as the three endpoint categories are weighted equally, the overall results of the present comparative study can be summarised as follows. At midpoint level, the laser-clad GCI, the wrought PEO-Al and the cast PEO-Al reduced the overall impacts by 55%, 35% and 41% respectively compared to the uncoated GCI. Similarly for the three endpoint categories, the laser-clad GCI, the wrought PEO-Al, and the cast PEO-Al reduced the overall impacts by 36%, 39% and 42% respectively. These results clearly demonstrate the potential reductions in damage achieved by adopting these coated rotors as a more environmentally friendly alternative to the current GCI rotor. It also demonstrated how the selection of impact assessment methods, i.e. midpoint as opposed to endpoint, can affect on the conclusion.

8.3 Recommendations for Future Work

The present study highlights the advantages of using small-scale testing to collect brake emissions data for comparative LCA. The WLTP cycle was employed during the laser-clad GCI rotor testing to maintain consistency with prior work by Limmer [1]. However, this driving cycle is representative of ICEVs and does not accurately represent BEVs. Transitioning to a BEV case study would likely reduce emissions and wear during use due to lower reliance on friction braking, thereby decreasing the overall environmental impact from each rotor. Nevertheless, the reduced usage of the friction brake system in BEVs, owing to the introduction of regenerative braking, increases the importance of corrosion as a degradation factor. As such, future LCAs for BEVs should incorporate the effects of corrosion. Given the superior corrosion resistance of coated rotors, the disparity between the coated and uncoated rotor impacts would likely be more pronounced. To enhance the inventory accuracy and better characterise corrosive particle emissions, future work could include Scanning Electron Microscopy (SEM) analysis.

The research aimed to develop an LCA methodology for evaluating the environmental and human health impacts of automotive brake systems throughout their full life cycle. The focus was on reducing weight and particulate matter (PM) emissions relative to conventional GCI brake rotors, while also enhancing overall environmental sustainability.

A key innovation in this study was the application of SADT notation to deconstruct complex processes into a hierarchical framework. Although brake pads were included within the system boundary in the defined LCA methodology, their manufacturing and end-of-life stages were assumed to be identical across all rotor types and were thus excluded from detailed analysis. However, in practice, variations in brake pad wear and maintenance requirements, resulting from different friction material and rotor pairings, can influence the use phase. Therefore, future work should involve collaboration with friction material manufacturers to obtain comprehensive inventory data for brake pad production and disposal. Incorporating these aspects would enable further optimisation of frictional performance, particularly for coated rotors whose surface characteristics differ significantly from uncoated GCI. Tailoring the pad material to suit each rotor type could improve tribological behaviour, potentially reducing emissions and wear, and thereby altering the LCA outcomes for the use phase.

List of References

[1] F. Limmer, *Tribology of novel friction pairs for environmentally friendly automotive brakes*. Thesis, 2024.

[2] D. Kay and C. Chesi, "Regulating brake emissions in a changing vehicle market for pmp workshop presentation.," 2021.

[3] D. for transport, "Transport and environmental statistics 2021 annual report," 2021.

[4] T. Grigoratos and G. Martini, "Brake wear particle emissions: a review," *Environmental Science and Pollution Research*, vol. 22, no. 4, pp. 2491–2504, 2015.

[5] G. Conway, A. Joshi, F. Leach, A. García, and P. K. Senecal, "A review of current and future powertrain technologies and trends in 2020," *Transportation Engineering*, vol. 5, p. 100080, 2021.

[6] A. Sapkota, A. P. Chelikowsky, K. E. Nachman, A. J. Cohen, and B. Ritz, "Exposure to particulate matter and adverse birth outcomes: a comprehensive review and meta-analysis," *Air Quality, Atmosphere & Health*, vol. 5, pp. 369–381, 2012.

[7] P. Peikertova and P. Filip, "Influence of the automotive brake wear debris on the environment-a review of recent research," *SAE International Journal of Materials and Manufacturing*, vol. 9, no. 1, pp. 133–146, 2016.

[8] Y. Gao, L. Chen, and M. Ehsani, "Investigation of the effectiveness of regenerative braking for ev and hev.," *Journal of Passenger Cars.*, no. 108, pp. 3184–3190, 1999.

[9] K. Chau, *Pure Electric Vehicles*, book section 21, pp. 655–684. Cambridge, England: Woodhead Publishing, 2014.

[10] R. Cai, J. Zhang, X. Nie, and J. Tjong, "Alumina-coated brake discs with intention for reduced non-exhaust emission and increased ride comfort of electrical vehicles.," in *Eurobrake Conference*.

[11] I. Ghouri, R. Barker, P. Brooks, S. Kosarieh, and D. Barton, "The effects of corrosion on particle emissions from a grey cast iron brake disc," Report 0148-7191, SAE Technical Paper, 2022.

[12] T. G. Kornberg, T. A. Stueckle, J. M. Antonini, Y. Rojanasakul, V. Castranova, Y. Yang, and L. W. Rojanasakul, "Potential toxicity and underlying mechanisms

associated with pulmonary exposure to iron oxide nanoparticles: conflicting literature and unclear risk," *Nanomaterials*, vol. 7, no. 10, p. 307, 2017.

[13] F. Del Pero, M. Delogu, and M. Pierini, "Life cycle assessment in the automotive sector: A comparative case study of internal combustion engine (ice) and electric car," *Procedia Structural Integrity*, vol. 12, pp. 521–537, 2018.

[14] W. Klöpffer and B. Grahl, *Life cycle assessment (LCA): a guide to best practice*. John Wiley Sons, 2014.

[15] F. Iraldo, C. Facheris, and B. Nucci, "Is product durability better for environment and for economic efficiency? a comparative assessment applying lca and lcc to two energy-intensive products," *Journal of Cleaner Production*, vol. 140, pp. 1353–1364, 2017.

[16] K. T. Gradin and A. H. Åström, "Comparative life cycle assessment of car disc brake systems—case study results and method discussion about comparative lcas," *The International Journal of Life Cycle Assessment*, vol. 25, no. 2, pp. 350–362, 2020.

[17] RAC, "Euro 1 to euro 6 guide - find out your vehicle's emissions standard," 2020.

[18] C. o. t. EU, "Euro 7: Council and parliament strike provisional deal on emissions limits for road vehicles," 2023.

[19] P. R. Childs, *Clutches and Brakes*, pp. 513–564. Amsterdam: Elsevier Inc., 2014.

[20] S. Murali and M. Balasubramanian, "Application of air brake system using engine exhaust gas," *Materials Today: Proceedings*, 2023.

[21] O. Aranke, W. Algenaid, S. Awe, and S. Joshi, "Coatings for automotive gray cast iron brake discs: A review," *Coatings*, vol. 9, no. 9, p. 552, 2019.

[22] J. Lange, L. Van Vo, K. Klein, and A. Stenkamp, "Friction pads for modern braking systems," *ATZ worldwide*, vol. 112, no. 5, pp. 32–36, 2010.

[23] A. J. Day and D. Bryant, *Braking of road vehicles*. Butterworth-Heinemann, 2022.

[24] D.-A. Bashar, P. B. MADAKSON, and J. MANJI, "Material selection and production of a cold-worked composite brake pad," *World Journal of Engineering and Pure Applied Sciences*, vol. 2, no. 3, p. 92, 2012.

[25] R. C. Dante, *Handbook of friction materials and their applications*. Woodhead publishing, 2015.

[26] P. Boulter, "A review of emission factors and models for road vehicle non-exhaust particulate matter," report, TRL Limited, Wokingham, 2006.

[27] J. Kukutschová, P. Moravec, V. Tomášek, V. Matějka, J. Smolík, J. Schwarz, J. Seidlerová, K. Šafářová, and P. Filip, "On airborne nano/micro-sized wear particles released from low-metallic automotive brakes," *Environmental Pollution*, vol. 159, no. 4, pp. 998–1006, 2011.

[28] A. Thorpe and R. M. Harrison, "Sources and properties of non-exhaust particulate matter from road traffic: a review," *Science of the total environment*, vol. 400, no. 1-3, pp. 270–282, 2008.

[29] R. Milczarek and N. Wittig, "Zeit für einen modellwechsel–anorganische reibmaterialien," in *International μ-Symposium Brake Conference*, pp. 1–17, Springer.

[30] D.-I. F. H. Bauer, *Tribologie*, pp. 369–373. Springer, 2002.

[31] K. Liew and U. Nirmal, "Frictional performance evaluation of newly designed brake pad materials," *Materials Design*, vol. 48, pp. 25–33, 2013.

[32] S. J. Kim and H. Jang, "Friction and wear of friction materials containing two different phenolic resins reinforced with aramid pulp," *Tribology international*, vol. 33, no. 7, pp. 477–484, 2000.

[33] J. Kukutschova, V. Roubíček, K. Malachová, Z. Pavlíčková, R. Holuša, J. Kubačková, V. Mička, D. MacCrimmon, and P. Filip, "Wear mechanism in automotive brake materials, wear debris and its potential environmental impact," *Wear*, vol. 267, no. 5-8, pp. 807–817, 2009.

[34] E. Rabinowicz, "The determination of the compatibility of metals through static friction tests," *ASLE TRANSACTIONS*, vol. 14, no. 3, pp. 198–205, 1971.

[35] "Astm international. astm g40-17, standard terminology relating to wear and erosion 2017.."

[36] F. Klocke, "Sheet metal forming," *Manufacturing Processes 4: Forming*, pp. 293–405, 2013.

[37] N. Oda, Y. Sugimoto, T. Higuchi, and K. Minesita, "Development of disk brake rotor utilizing aluminum metal matrix composite," Report 0148-7191, SAE Technical Paper, 1997.

[38] J. Preston and R. Forthofer, "Correlation of vehicle, dynamometer and other laboratory tests for brake friction materials," Report 0148-7191, SAE Technical Paper, 1971.

[39] S. o. E. T. (SETAC) and Chemistry, "Guidelines for life cycle assessment: A code of practice.," in *SETAC Workshop*, (Brussels and Pensacola, FL.), SETAC.

[40] I. O. f. S. ISO, "Iso14044:2006-2010, iso tc 207/sc. environmental management - life cycle assessment - requirements and guidelines," 2006.

[41] DIN-NAGUS, "Grundsatze produkt-bezogener okobilanzen," *DIN-Mitteilungen*, vol. 73, no. 3, pp. 208–212, 1994.

[42] H. Neitzel, "Principles of product related life cycle assessment," *International Journal Of Life Cycle Assessment*, vol. 1, pp. 49–54, 1996.

[43] K. Liu, P. Xu, F. Wang, C. Jin, M. Huang, D. Dai, and C. Fu, "Deicing efficiency analysis and economic-environment assessment of a novel induction heating asphalt pavement," *Journal of cleaner production*, vol. 273, p. 123123, 2020.

[44] I. Ghouri, R. Barker, P. Brooks, and D. Barton, "Particle emission from an aluminium metal matrix composite (al-mmc) brake rotor before and after corrosion," in *Proceedings of Eurobrake 2023*, FISITA.

[45] I. Ghouri, R. Barker, P. Brooks, S. Shestha, and D. Barton, "Wear emissions from a plasma electrolyte oxidation (peo) ceramic coated aluminium alloy brake rotor before and after corrosion," 2024.

[46] L. Stamford and A. Azapagic, "Life cycle sustainability assessment of uk electricity scenarios to 2070," *Energy for Sustainable Development*, vol. 23, pp. 194–211, 2014.

[47] G. Olivieri, A. Romani, and P. Neri, "Environmental and economic analysis of aluminium recycling through life cycle assessment," *The International Journal of Sustainable Development World Ecology*, vol. 13, no. 4, pp. 269–276, 2006.

[48] C. Pimenteira, A. Pereira, L. Oliveira, L. Rosa, M. Reis, and R. Henriques, "Energy conservation and co2 emission reductions due to recycling in brazil," *Waste Management*, vol. 24, no. 9, pp. 889–897, 2004.

[49] M. A. Huijbregts, Z. J. Steinmann, P. M. Elshout, G. Stam, F. Verones, M. Vieira, M. Zijp, A. Hollander, and R. Van Zelm, "Recipe2016: a harmonised life cycle impact assessment method at midpoint and endpoint level," *The International Journal of Life Cycle Assessment*, vol. 22, pp. 138–147, 2017.

[50] P. M. Glibert, S. Seitzinger, C. A. Heil, J. M. Burkholder, M. W. Parrow, L. A. Codispoti, and V. Kelly, "Eutrophication," *Oceanography*, vol. 18, no. 2, p. 198, 2005.

[51] D. W. Schindler, "Recent advances in the understanding and management of eutrophication," *Limnology and oceanography*, vol. 51, no. 1part2, pp. 356–363, 2006.

[52] C. Gilkeson, S. Kosarieh, A. Sanuddin, P. Brooks, D. Barton, and S. Shrestha, "Preliminary comparisons of particulate emissions generated from different disc brake rotors," in *Proceedings of Eurobrake 2021*, Leeds.

[53] F. Amato, F. R. Cassee, H. A. D. van der Gon, R. Gehrig, M. Gustafsson, W. Hafner, R. M. Harrison, M. Jozwicka, F. J. Kelly, and T. Moreno, "Urban air quality: the challenge of traffic non-exhaust emissions," *Journal of hazardous materials*, vol. 275, pp. 31–36, 2014.

[54] R. Cai, J. Zhang, X. Nie, J. Tjong, and D. Matthews, "Wear mechanism evolution on brake discs for reduced wear and particulate emissions," *Wear*, vol. 452, p. 203283, 2020.

[55] M. Riediker, R. B. Devlin, T. R. Griggs, M. C. Herbst, P. A. Bromberg, R. W. Williams, and W. E. Cascio, "Cardiovascular effects in patrol officers are associated with fine particulate matter from brake wear and engine emissions," *Particle and Fibre Toxicology*, vol. 1, no. 1, pp. 1–10, 2004.

[56] S. Yadav and P. G. Satsangi, "Characterization of particulate matter and its related metal toxicity in an urban location in south west india," *Environmental monitoring and assessment*, vol. 185, no. 9, pp. 7365–7379, 2013.

[57] TWI, "Improving brake discs with coatings applied by extreme high-speed laser application," in *Eurobrake*.

[58] G. Bolelli, R. Giovanardi, L. Lusvarghi, and T. Manfredini, "Corrosion resistance of hvof-sprayed coatings for hard chrome replacement," *Corrosion science*, vol. 48, no. 11, pp. 3375–3397, 2006.

[59] G. Balamurugan, M. Duraiselvam, and V. Anandakrishnan, "Comparison of high temperature wear behaviour of plasma sprayed wc–co coated and hard chromium plated aisi 304 austenitic stainless steel," *Materials Design*, vol. 35, pp. 640–646, 2012.

[60] A. P. Krelling, M. M. d. Souza, C. E. d. Costa, and J. C. G. Milan, "Hvof-sprayed coating over aisi 4140 steel for hard chromium replacement," *Materials research*, vol. 21, 2018.

[61] G. Bolelli, V. Cannillo, L. Lusvarghi, and S. Ricco, "Mechanical and tribological properties of electrolytic hard chrome and hvof-sprayed coatings," *Surface and Coatings Technology*, vol. 200, no. 9, pp. 2995–3009, 2006.

[62] H. J. Gibb, P. S. Lees, P. F. Pinsky, and B. C. Rooney, "Clinical findings of irritation among chromium chemical production workers," *American journal of industrial medicine*, vol. 38, no. 2, pp. 127–131, 2000.

[63] M. Leber, "Hard like diamond," 2017.

[64] M. K. Stanford and V. K. Jain, "Friction and wear characteristics of hard coatings," *Wear*, vol. 251, no. 1-12, pp. 990–996, 2001.

[65] S. Shrestha, R. Francis, and A. Smith, "Reliable: Wear resistant lightweight aluminium brakes for vehicles," in *Proceedings of Eurobrake 2020*.

[66] S. Khalili, R. Mittal, and S. G. Kalibar, "A study of the mechanical properties of steel/aluminium/grp laminates," *Materials Science and Engineering: A*, vol. 412, no. 1-2, pp. 137–140, 2005.

[67] Z. Ahmad, *Atmospheric Corrosion*, pp. 550–575. Amsterdam: Elsevier Inc., 2006.

[68] N. K. Langhelle and J. Amdahl, "Experimental and numerical analysis of aluminium columns subjected to fire," in *The Eleventh International Offshore and Polar Engineering Conference*, OnePetro.

[69] A. Belhocine and M. Bouchetara, "Investigation of temperature and thermal stress in ventilated disc brake based on 3d thermomechanical coupling model," *Ain Shams Engineering Journal*, vol. 4, no. 3, pp. 475–483, 2013.

[70] P. J. Blau, B. C. Jolly, J. Qu, W. H. Peter, and C. A. Blue, "Tribological investigation of titanium-based materials for brakes," *Wear*, vol. 263, no. 7-12, pp. 1202–1211, 2007.

[71] C. Mendis and K. Hono, "4-understanding precipitation processes in magnesium alloys," *Fundamentals of magnesium alloy metallurgy*, pp. 125–151, 2013.

[72] D. Han, J. Zhang, J. Huang, Y. Lian, and G. He, "A review on ignition mechanisms and characteristics of magnesium alloys," *Journal of Magnesium and Alloys*, vol. 8, no. 2, pp. 329–344, 2020.

[73] L. M. Manocha, "High performance carbon-carbon composites," *Sadhana*, vol. 28, pp. 349–358, 2003.

[74] T. J. Hutton, D. Johnson, and B. McEnaney, "Effects of fibre orientation on the tribology of a model carbon–carbon composite," *Wear*, vol. 249, no. 8, pp. 647–655, 2001.

[75] T. Hutton, *PhD Thesis*. Thesis, 1996.

[76] R. Renz, G. Seifert, and W. Krenkel, "Integration of cmc brake disks in automotive brake systems," *International Journal of Applied Ceramic Technology*, vol. 9, no. 4, pp. 712–724, 2012.

[77] A. Adebisi, M. Maleque, and M. M. Rahman, "Metal matrix composite brake rotor: historical development and product life cycle analysis," *International Journal of Automotive and Mechanical Engineering*, vol. 4, no. 1, pp. 471–480, 2011.

[78] R. Thornton, T. Slatter, A. H. Jones, and R. Lewis, "The effects of cryogenic processing on the wear resistance of grey cast iron brake discs," *Wear*, vol. 271, no. 9-10, pp. 2386–2395, 2011.

[79] S. A. Awe and A. Thomas, "The prospects of lightweight sicalight discs in the emerging disc brake requirements," *transport*, vol. 13, p. 14, 2021.

[80] F. Ahmad, S. J. Lo, M. Aslam, and A. Haziq, "Tribology behaviour of alumina particles reinforced aluminium matrix composites and brake disc materials," *Procedia engineering*, vol. 68, pp. 674–680, 2013.

[81] P. Wycliffe, "Friction and wear of duralcan reinforced aluminum composites in automotive braking systems," Report 0148-7191, SAE technical paper, 1993.

[82] A. Killinger, R. Gadow, G. Mauer, A. Guignard, R. Vaßen, and D. Stöver, "Review of new developments in suspension and solution precursor thermal spray processes," *Journal of Thermal Spray Technology*, vol. 20, no. 4, pp. 677–695, 2011.

[83] A. S. Alhulaifi, G. A. Buck, and W. J. Arbegast, "Numerical and experimental investigation of cold spray gas dynamic effects for polymer coating," *Journal of Thermal Spray Technology*, vol. 21, no. 5, pp. 852–862, 2012.

[84] D. Poirier, J.-G. Legoux, E. Irissou, D. Gallant, J. Jiang, T. Potter, and J. Boileau, "Performance assessment of protective thermal spray coatings for lightweight al brake rotor disks," *Journal of Thermal Spray Technology*, vol. 28, no. 1, pp. 291–304, 2019.

[85] J. Dornoff and F. Rodríguez, "Euro 7: The new emission standard for light-and heavy-duty vehicles in the european union," *International Council on Clean Transportation*, 2024.

[86] F. Limmer, D. Barton, P. Brooks, C. Gilkeson, and S. Kosarieh, "Development of a small-scale test bench for investigating the tribology and emission behaviour of novel brake friction couples," in *Proceedings of Eurobrake 2021*, Leeds.

[87] Y. Huang, R. Bird, and O. Heidrich, "Development of a life cycle assessment tool for construction and maintenance of asphalt pavements," *Journal of Cleaner Production*, vol. 17, no. 2, pp. 283–296, 2009.

[88] I. O. f. S. ISO, "Iso 14043. environmental management – life cycle assessment: Interpretation," 2000.

[89] A. Lucas, C. A. Silva, and R. C. Neto, "Life cycle analysis of energy supply infrastructure for conventional and electric vehicles," *Energy Policy*, vol. 41, pp. 537–547, 2012.

[90] R. Heijungs and J. Guinée, "Cml on actual versus potential risks," *LCA News, A SETAC—Europe Publication*, vol. 3, no. 4, p. 4, 1993.

[91] M. Finkbeiner, A. Inaba, R. Tan, K. Christiansen, and H.-J. Klüppel, "The new international standards for life cycle assessment: Iso 14040 and iso 14044," *The international journal of life cycle assessment*, vol. 11, pp. 80–85, 2006.

[92] K. R. Popper, *Logik der Forschung*. Wien: Julius Springer, 7 ed., 1934. Mohr, J.C.B. (Paul Siebeck), Tübingen, 1982.

[93] I. Muñoz, J. Rieradevall, X. Domènech, and C. Gazulla, "Using lca to assess eco-design in the automotive sector: case study of a polyolefinic door panel (12 pp)," *The International Journal of Life Cycle Assessment*, vol. 11, no. 5, pp. 323–334, 2006.

[94] V. E. Uz, M. Saltan, and Gökalp, "Feasibility of using 4th power law in design of plastic deformation resistant low volume roads," *Procedia engineering*, vol. 143, pp. 961–970, 2016.

[95] U. Olofsson, Y. Lyu, A. H. Åström, J. Wahlström, S. Dizdar, A. P. G. Nogueira, and S. Gialanella, "Laser cladding treatment for refurbishing disc brake rotors: environmental and tribological analysis," *Tribology letters*, vol. 69, no. 2, pp. 1–11, 2021.

[96] D. Silva, A. O. Nunes, A. da Silva Moris, C. Moro, and T. O. R. Piekarski, "How important is the lca software tool you choose comparative results from gabi, openlca, simapro and umberto," in *Proceedings of the VII Conferencia Internacional de Análisis de Ciclo de Vida en Latinoamérica, Medellin, Colombia*, pp. 10–15.

[97] K. Sahaf, S. Rifai, O. Bouksour, and A. Adri, "Modelling approaches of hospital supply chain: case of surgery and oncology department. state of the art," *International Journal of Management and Decision Making*, vol. 18, no. 1, pp. 93–118, 2019.

[98] F. Ahmed, S. Robinson, and A. A. Tako, "Using the structred analysis and design technique (sadt) in simulation conceptual modeling," in *Proceedings of the Winter Simulation Conference 2014*, pp. 1038–1049, IEEE, 2014.

[99] L. Storch, C. Hamatschek, D. Hesse, F. Feist, T. Bachmann, P. Eichler, and T. Grigoratos, "Comprehensive analysis of current primary measures to mitigate brake wear particle emissions from light-duty vehicles," *Atmosphere*, vol. 14, no. 4, p. 712, 2023.

[100] H. Hagino, "Brake wear and airborne particle mass emissions from passenger car brakes in dynamometer experiments based on the worldwide harmonized light-duty vehicle test procedure brake cycle," *Lubricants*, vol. 12, no. 6, p. 206, 2024.

[101] E. Weymar and M. Finkbeiner, "Statistical analysis of empirical lifetime mileage data for automotive lca," *The International Journal of Life Cycle Assessment*, vol. 21, pp. 215–223, 2016.

[102] C. Dun, G. Horton, and S. Kollamthodi, "Improvements to the definition of lifetime mileage of light duty vehicles—report for european commission—dg climate action," *Ricardo-AEA, Didcot*, 2015.

[103] I. O. f. S. ISO, "Iso 14042. environ mental management – life cycle assessment: Life cycle impact assessment.," 2000.

[104] M. Rybaczewska-Błażejowska and D. Jezierski, "Comparison of recipe 2016, ilcd 2011, cml-ia baseline and impact 2002+ lcia methods: a case study based on the electricity consumption mix in europe," *The International Journal of Life Cycle Assessment*, pp. 1–19, 2024.

[105] S. Lueddeckens, P. Saling, and E. Guenther, "Temporal issues in life cycle assessment—a systematic review," *The International Journal of Life Cycle Assessment*, vol. 25, pp. 1385–1401, 2020.

[106] D. Beloin-Saint-Pierre, A. Albers, A. Hélias, L. Tiruta-Barna, P. Fantke, A. Levasseur, E. Benetto, A. Benoist, and P. Collet, "Addressing temporal considerations in life cycle assessment," *Science of the Total Environment*, vol. 743, p. 140700, 2020.

[107] T. N. Ligthart, R. H. Jongbloed, and J. E. Tamis, "A method for improving centre for environmental studies (cml) characterisation factors for metal (eco) toxicity—the case of zinc gutters and downpipes," *The International Journal of Life Cycle Assessment*, vol. 15, pp. 745–756, 2010.

[108] Y. Huang, *Life cycle assessment of use of recycled materials in asphalt pavements*. Thesis, 2007.

[109] W. McKinney, "pandas: a foundational python library for data analysis and statistics," *Python for high performance and scientific computing*, vol. 14, no. 9, pp. 1–9, 2011.

[110] W. McKinney, "Pandas, python data analysis library," *URL http://pandas. pydata. org*, pp. 3–15, 2015.

[111] M. Summerfield, *Rapid GUI programming with Python and Qt: the definitive guide to PyQt programming*. Pearson Education, 2007.

[112] C. Koffler and K. Rohde-Brandenburger, "On the calculation of fuel savings through lightweight design in automotive life cycle assessments," *The International Journal of Life Cycle Assessment*, vol. 15, pp. 128–135, 2010.

[113] E. Scerri, *The periodic table: its story and its significance*. Oxford University Press, 2019.

[114] BP, "Bp statistical review of world energy," 2022.

[115] S. Nomura and T. Nakagawa, "The yield of coke oven gas from hard and semi-soft coking coals," *International Journal of Coal Geology*, vol. 168, pp. 179–185, 2016.

[116] J. Speight, *Production, properties and environmental impact of hydrocarbon fuel conversion*, pp. 54–82. Elsevier, 2011.

[117] "Energy dashboard (national grid eso)," 2024.

[118] Forest Research, "Typical calorific values of fuels," 2025. Accessed: 10-02-2025.

[119] HM Revenue Customs, "Gas for road fuel use manual - hcogas400350," 2025. Accessed: 10-02-2025.

[120] G. Wernet, C. Bauer, B. Steubing, J. Reinhard, E. Moreno-Ruiz, and B. Weidema, "The ecoinvent database version 3 (part i): overview and methodology," *The International Journal of Life Cycle Assessment*, vol. 21, pp. 1218–1230, 2016.

[121] B. Steubing, G. Wernet, J. Reinhard, C. Bauer, and E. Moreno-Ruiz, "The ecoinvent database version 3 (part ii): analyzing lca results and comparison to version 2," *The International Journal of Life Cycle Assessment*, vol. 21, pp. 1269–1281, 2016.

[122] "Dekati elpi+ user manual version 1.56," 2019.

[123] I. ANSYS, "Ansys edupack." https://www.ansys.com, 2025. Accessed: 13-03-2025.

[124] S. Chen and S. Hoxie, "Fine-tuning of rotor gray iron material for optimal brake performance," in *SAE 2016 Brake Colloquium & Exhibition - 34th Annual*, 2016.

[125] Green-Friction, "Sustainable friction material recycling."

[126] M. R. Factsheet, "Euric aisbl–recycling: Bridging circular economy climate policy," *URL: https://www. euric-aisbl. eu/[in English]*.

[127] H. Mzad, A. Otmani, K. Bey, and S. Łopata, "A model of water-spray cooling effect on a continuous casting process," in *MATEC Web of Conferences*, vol. 240, p. 05022, EDP Sciences.

[128] I. University of California, "Energy units and conversions," n.d. Accessed: 08-03-2025.

[129] F. Cherubini, S. Bargigli, and S. Ulgiati, "Life cycle assessment (lca) of waste management strategies: Landfilling, sorting plant and incineration," *Energy*, vol. 34, no. 12, pp. 2116–2123, 2009.

[130] L. Li, J. Yan, and Z. Xing, "Energy requirements evaluation of milling machines based on thermal equilibrium and empirical modelling," *Journal of cleaner production*, vol. 52, pp. 113–121, 2013.

[131] A. A. Tseng, Y.-T. Chen, and K.-J. Ma, "Fabrication of high-aspect-ratio microstructures using excimer laser," *Optics and Lasers in Engineering*, vol. 41, no. 6, pp. 827–847, 2004.

[132] M. Jiménez, F. Ott, F. Kern, and R. Gadow, "Manufacturing of continuous carbon fiber reinforced aluminum by spark plasma sintering," *Ceramics*, vol. 3, no. 3, pp. 265–275, 2020.

[133] T. E. Toolbox, "Metals - latent heat of melting."

[134] M.-A. WOLF, K. CHOMKHAMSRI, M. BRANDAO, R. PANT, F. ARDENTE, D. PENNINGTON, S. MANFREDI, C. C. DE, M. GORALCZYK, *et al.*, "International reference life cycle data system (ilcd) handbook-general guide for life cycle assessment-detailed guidance," 2010.

[135] I. Hore-Lacy, *Future Energy Demand and Supply*, ch. 1, p. 9. London, UK: WNUP, 2nd ed., 2011.

[136] A. T. Hamada and M. F. Orhan, "An overview of regenerative braking systems," *Journal of Energy Storage*, vol. 52, p. 105033, 2022.

[137] W. Jiang, C. He, Y. Huang, T. Wang, D. Yuan, W. Wu, and H. Fan, "Diffusion of re-suspended dust induced by vehicles: Full-scale simulation and field test," *Transportation Research Part D: Transport and Environment*, vol. 139, p. 104552, 2025.

Appendix A

Full WLTP Cycle Definition

Control inputs for the 303 braking manoeuvres of the dynamic WLTP test cycle conducted on the small-scale test rig (as designed by Limmer [1]).

Stop No.	$n_{initial}$ (rpm)	n_{final} (rpm)	t_{brake} (s)	$F_{small-scale}$ (N)	Stop No.	$n_{initial}$ (rpm)	n_{final} (rpm)	t_{brake} (s)	$F_{small-scale}$ (N)
1	679.97	0.00	6	74.87	36	1394.12	996.46	4	62.57
2	759.17	183.38	7	52.02	37	996.46	451.56	5	70.72
3	505.46	145.92	4	57.92	38	1315.24	655.65	6	70.74
4	845.94	237.28	6	65.74	39	974.76	621.14	4	55.63
5	814.06	548.51	3	56.01	40	804.53	576.45	3	46.94
6	614.24	0.00	9	42.30	41	1379.99	0.00	9	102.94
7	1069.09	0.00	6	121.34	42	721.71	388.46	4	52.57
8	904.11	388.13	5	66.73	43	1066.13	200.15	8	70.43
9	967.53	317.80	6	70.43	44	1143.36	0.00	8	95.70
10	1047.72	311.56	6	80.77	45	2501.00	0.00	13	129.77
11	481.80	0.00	5	62.83	46	750.63	0.00	5	101.43
12	1953.80	1565.67	4	59.38	47	1366.18	895.23	4	76.01
13	1565.67	1190.36	4	58.05	48	1572.90	1155.19	3	90.98
14	1256.09	839.36	4	66.41	49	1155.19	660.58	5	62.96
15	839.36	605.37	3	48.29	50	1946.24	1625.48	3	66.48
16	605.37	0.00	6	65.96	51	2396.82	2038.26	3	74.49
17	1390.17	0.00	9	103.74	52	2180.90	1887.09	3	59.33
18	1383.60	0.00	10	92.09	53	1971.22	1713.23	3	51.18
19	1029.65	409.82	3	141.45	54	2618.32	2370.85	3	46.95
20	409.82	0.00	5	52.50	55	2431.65	1722.76	6	73.86
21	1487.78	0.00	10	99.50	56	1722.76	0.00	12	95.42
22	1496.66	0.00	10	100.13	57	1982.72	0.00	10	134.71
23	1338.58	420.01	7	86.43	58	2066.20	0.00	8	178.07
24	1957.42	1534.78	4	65.67	59	1975.49	500.53	11	87.58
25	1597.55	0.00	9	120.17	60	1750.70	0.00	11	106.68
26	779.55	320.76	4	75.32	61	679.97	0.00	6	74.87
27	1232.09	0.00	9	91.23	62	759.17	183.38	7	52.02
28	1239.32	0.00	9	91.80	63	505.46	145.92	4	57.92
29	612.60	0.00	5	81.61	64	845.94	237.28	6	65.74
30	454.52	0.00	4	75.38	65	814.06	548.51	3	56.01
31	1123.64	622.46	4	82.16	66	614.24	0.00	8	48.48
32	1079.60	765.42	4	48.16	67	1532.48	307.94	5	168.68
33	840.35	608.65	3	47.72	68	1709.62	1365.20	3	72.84
34	1271.20	0.00	8	107.11	69	1638.63	1115.75	5	65.84
35	1591.63	1333.32	3	52.24	70	1609.05	782.84	7	76.06

Stop No.	$n_{initial}$ (rpm)	n_{final} (rpm)	t_{brake} (s)	$F_{small-scale}$ (N)
71	1368.15	0.00	8	115.77
72	1055.61	181.41	6	97.59
73	1660.98	1407.59	3	50.86
74	1477.59	978.71	5	62.75
75	978.71	0.00	5	134.18
76	1616.61	1088.15	5	66.71
77	1845.35	1447.36	4	61.46
78	1940.33	1683.98	3	50.86
79	1807.55	1562.06	3	48.57
80	1954.13	1312.28	5	82.41
81	1312.28	467.99	6	93.28
82	1915.68	1144.67	6	82.77
83	1299.47	986.27	3	66.32
84	1845.68	1511.12	3	70.09
85	1788.49	1327.40	4	73.12
86	1758.26	1339.56	4	65.47
87	1339.56	1050.35	3	60.39
88	1141.39	865.98	3	57.55
89	1661.31	1235.38	4	67.04
90	1235.38	737.15	5	63.28
91	1210.08	753.91	4	73.72
92	1818.07	1297.82	4	83.83
93	1297.82	509.07	6	86.54
94	1454.26	1202.19	3	51.08
95	1202.19	682.27	5	66.54
96	1051.01	816.03	3	47.98
97	1696.47	1290.27	4	63.35
98	1290.27	1065.14	3	44.96
99	1065.14	0.00	7	102.50
100	2492.45	2098.73	4	59.01
101	2380.71	1927.51	4	70.15
102	2167.09	1765.16	4	61.35
103	1802.62	0.00	10	121.90
104	2975.89	0.00	15	133.51
105	3142.84	837.06	15	99.85
106	3232.89	0.00	15	145.59
107	2721.52	2279.16	5	51.26
108	2279.16	331.28	14	91.06
109	2267.99	2029.06	3	45.78
110	2127.66	1900.23	3	43.35
111	1900.23	0.00	12	105.90
112	679.97	0.00	6	74.87
113	759.17	183.38	7	52.02
114	505.46	145.92	4	57.92
115	845.94	237.28	6	65.74
116	814.06	548.51	3	56.01
117	614.24	0.00	8	48.48
118	1372.10	0.00	10	91.27
119	1137.77	896.55	3	49.27
120	1428.30	0.00	10	95.27
121	986.92	446.63	5	70.07
122	1214.35	0.00	9	89.82
123	1354.02	969.84	4	60.22
124	969.84	591.56	3	82.97
125	591.56	0.00	5	78.59
126	967.86	727.62	3	49.47
127	727.62	266.86	4	75.81
128	555.74	0.00	5	73.45
129	471.94	114.70	3	79.15
130	1854.55	1352.38	4	80.44
131	1352.38	455.18	7	84.16
132	1851.92	1357.97	5	61.06
133	1904.51	1301.11	5	76.92
134	1301.11	733.87	4	93.74
135	876.83	0.00	10	56.04
136	3457.03	2970.63	4	73.41
137	3358.44	3011.71	3	69.12
138	3110.31	2864.48	2	74.95
139	2864.48	2376.44	4	75.25
140	2787.25	2424.75	4	52.55
141	2884.53	2266.02	6	61.66
142	2266.02	1651.12	5	77.66
143	2743.21	2342.92	3	83.72
144	2342.92	1756.94	5	73.24
145	2630.16	2169.39	4	70.88
146	2169.39	1864.41	3	62.07
147	2756.68	1397.08	7	128.97
148	2426.72	802.23	13	79.99
149	802.23	0.00	6	89.47
150	751.29	443.02	4	47.94
151	756.22	507.10	3	52.17
152	624.10	400.29	3	46.37
153	617.20	0.00	6	67.37
154	1246.23	802.55	5	55.28

Stop No.	$n_{initial}$ (rpm)	n_{final} (rpm)	t_{brake} (s)	$F_{small-scale}$ (N)
155	802.55	489.68	4	48.64
156	1487.78	851.85	5	82.76
157	1335.62	833.45	5	63.60
158	1223.55	683.58	5	69.41
159	862.70	0.00	6	96.69
160	1754.64	926.13	6	90.21
161	1398.72	623.11	6	84.67
162	1876.57	1046.08	6	90.13
163	1643.23	801.90	5	112.38
164	1912.39	982.65	7	86.12
165	982.65	697.72	3	60.28
166	1069.74	0.00	6	121.42
167	697.06	310.57	5	48.34
168	310.57	0.00	4	49.50
169	1152.89	179.77	8	80.04
170	541.28	0.00	5	71.37
171	3185.57	2408.32	8	56.79
172	2408.32	661.24	10	116.23
173	2044.84	217.56	9	137.79
174	1749.38	0.00	13	88.87
175	2748.47	0.00	15	122.82
176	783.82	0.00	7	73.75
177	2146.39	0.00	12	120.44
178	1332.33	961.62	4	57.82
179	2071.79	1714.88	3	74.93
180	1714.88	1466.09	3	49.61
181	1944.93	1485.48	5	55.77
182	1771.07	0.00	10	119.65
183	626.07	209.68	5	52.90
184	344.09	0.00	5	43.06
185	973.12	0.00	7	93.10
186	798.28	147.23	5	86.75
187	914.62	567.24	4	54.65
188	567.24	213.62	4	56.68
189	879.46	0.00	7	83.53
190	903.78	0.00	9	65.23
191	1280.08	954.06	4	49.80
192	1154.53	804.53	4	54.50
193	1376.37	1120.68	3	52.16
194	1295.85	818.66	5	60.05
195	1197.59	0.00	11	70.97
196	1830.56	0.00	11	111.83
197	1847.32	0.00	13	94.20
198	1434.21	0.00	9	107.23
199	369.40	135.73	4	35.32
200	493.63	204.42	4	45.13
201	331.93	0.00	5	41.32
202	1027.02	780.53	3	50.83
203	780.53	554.75	3	46.44
204	554.75	0.00	7	50.35
205	1314.58	349.35	7	91.38
206	513.67	205.40	4	48.55
207	513.67	287.57	3	47.21
208	431.51	0.00	5	55.61
209	760.16	492.97	3	56.55
210	595.84	447.94	2	45.87
211	636.92	377.94	3	54.87
212	377.94	0.00	4	61.61
213	1147.96	916.59	3	46.85
214	1435.53	1055.94	4	59.17
215	1055.94	406.86	5	85.80
216	406.86	0.00	4	66.81
217	481.80	0.00	5	62.83
218	454.52	0.00	4	75.38
219	406.21	0.00	3	91.21
220	614.24	0.00	8	48.48
221	605.37	0.00	6	65.96
222	1352.38	998.43	4	54.71
223	998.43	487.71	5	65.72
224	1658.35	1012.23	5	83.80
225	1012.23	0.00	8	84.00
226	406.86	0.00	4	66.81
227	481.80	0.00	4	80.28
228	614.24	0.00	8	48.48
229	605.37	0.00	6	65.96
230	454.52	0.00	4	75.38
231	406.86	0.00	4	66.81
232	481.80	0.00	4	80.28
233	3450.13	3134.96	3	61.23
234	3134.96	2708.37	4	63.34
235	3202.33	2717.25	4	73.83
236	2717.25	2449.07	3	51.72
237	2449.07	1272.85	10	74.04
238	2102.35	850.21	7	119.40

Stop No.	$n_{initial}$ (rpm)	n_{final} (rpm)	t_{brake} (s)	$F_{small-scale}$ (N)
239	1571.59	1182.47	4	60.56
240	1982.07	1195.29	6	84.53
241	1609.05	1216.98	4	61.00
242	2005.07	919.88	6	120.88
243	1418.11	819.97	6	62.97
244	1534.12	1244.91	3	59.89
245	1802.62	735.51	7	100.79
246	861.05	611.28	3	52.06
247	658.94	231.04	6	44.16
248	231.04	0.00	4	35.20
249	919.22	537.01	4	60.99
250	610.30	250.10	4	57.77
251	942.89	479.49	5	58.95
252	753.59	393.72	4	57.34
253	1513.09	0.00	10	101.30
254	1517.36	1056.27	5	57.12
255	1056.27	681.94	4	59.19
256	681.94	406.21	3	58.83
257	1396.75	583.35	6	89.29
258	745.04	0.00	8	60.15
259	819.97	563.96	3	53.68
260	1014.20	549.17	4	75.85
261	1412.52	978.05	5	53.50
262	1933.75	1599.52	3	69.78
263	1599.52	782.51	6	89.21
264	1454.26	995.80	5	56.90
265	1360.27	932.04	4	68.24
266	1690.56	1052.98	6	67.08
267	1052.98	328.65	6	79.31
268	328.65	0.00	5	40.84
269	536.02	0.00	5	70.62
270	1505.86	940.91	5	72.33
271	1342.52	836.08	5	64.21
272	1349.09	1009.93	3	72.49
273	1009.93	725.98	3	59.97
274	925.14	695.74	3	46.95
275	1235.71	978.71	3	52.84
276	1404.96	1134.82	3	55.60
277	1662.95	697.06	7	90.55
278	1640.60	828.19	6	88.54
279	1274.49	644.48	6	67.23
280	1011.90	334.56	6	73.69
281	863.35	541.61	4	50.10
282	625.09	249.11	4	60.61
283	249.11	0.00	4	38.45
284	1059.56	446.96	5	80.45
285	446.96	0.00	6	47.04
286	819.64	357.24	4	75.87
287	357.24	0.00	4	57.89
288	362.50	0.00	4	58.83
289	2133.24	839.03	8	106.99
290	3680.18	1844.03	9	134.28
291	2240.71	395.69	8	157.30
292	2657.43	1159.46	9	109.28
293	2413.58	1290.27	7	105.10
294	1290.27	0.00	12	69.87
295	4354.23	1117.40	15	142.88
296	1366.51	0.00	9	101.87
297	1087.49	207.70	6	98.19
298	1234.07	0.00	11	73.32
299	1708.30	0.00	11	103.94
300	1664.26	751.29	7	85.00
301	1567.64	769.03	7	73.27
302	1507.50	774.62	6	79.18
303	1234.72	0.00	7	119.83

Appendix B

Python Based GUI for LCA Brake Model

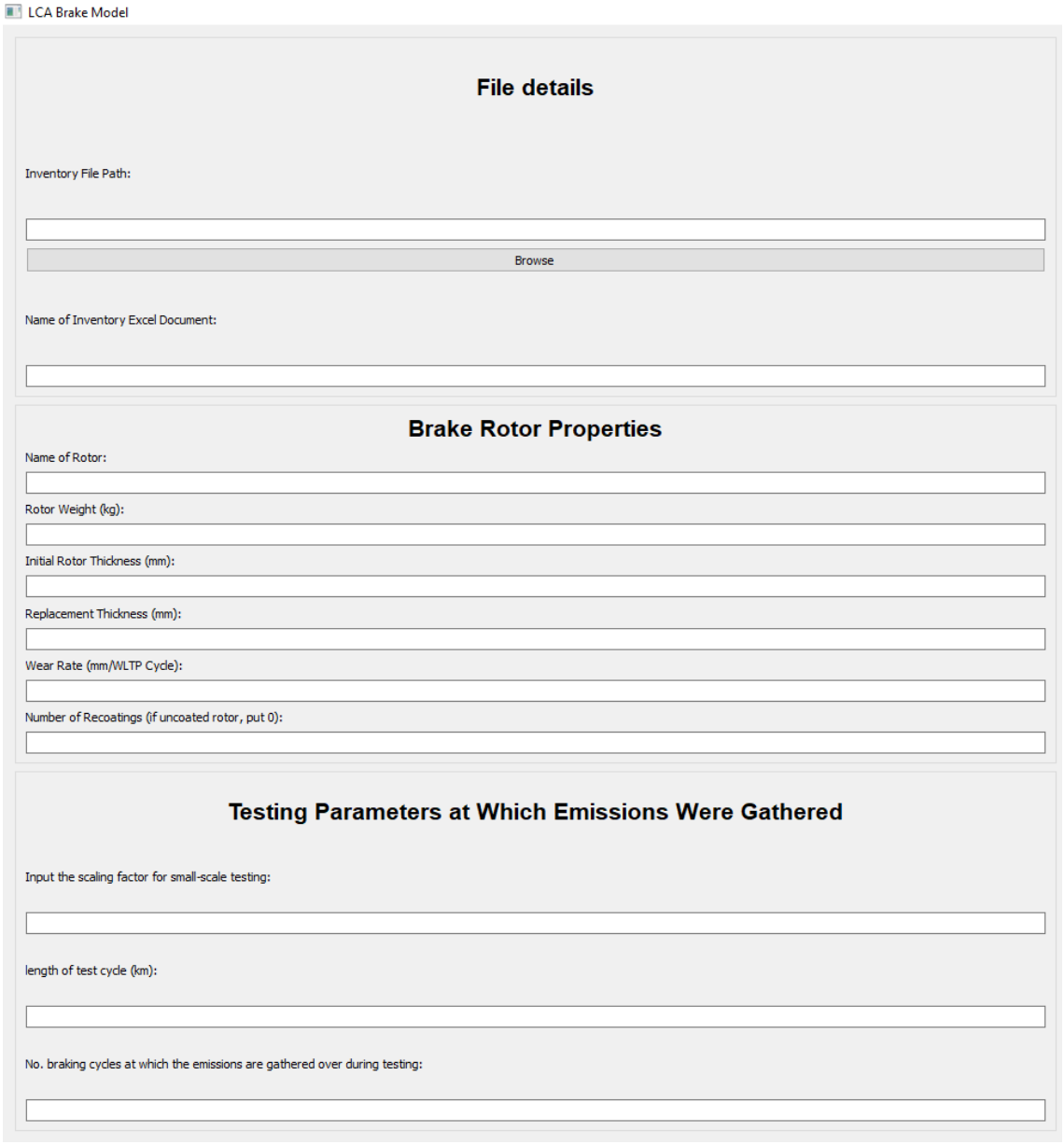

Left-hand side of the Python based GUI console for the LCA Brake model.

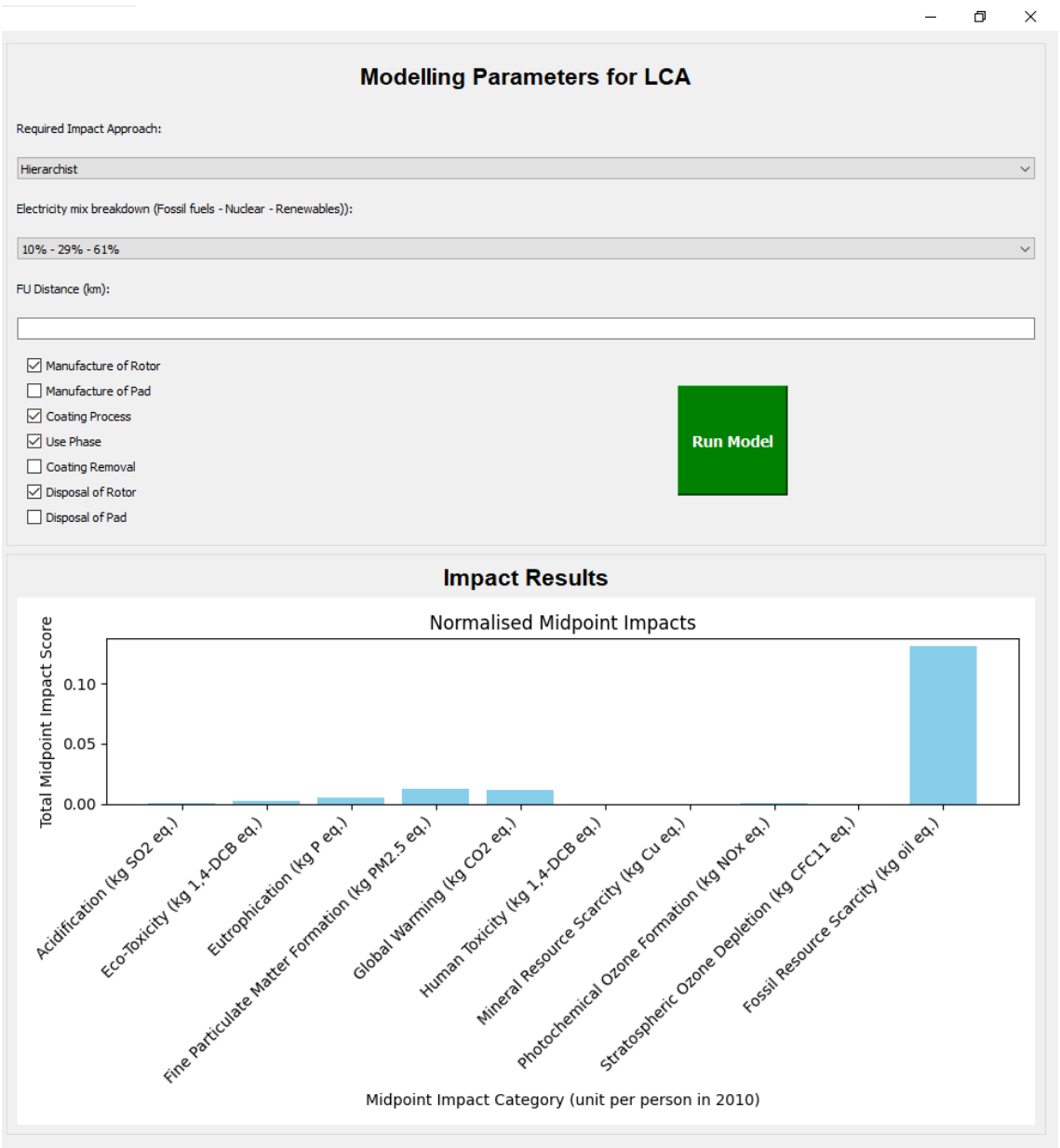

Right-hand side of the Python based GUI console for the LCA Brake model.

Appendix C

Python Code for LCA Brake Model

```
import sys
import pandas as pd
import os
import numpy as np
from PyQt5.QtWidgets import (QApplication, QWidget, QVBoxLayout, QHBoxLayout, QLabel,
                             QLineEdit, QPushButton, QCheckBox, QFileDialog, QMessageBox,
                             QComboBox, QGroupBox, QSizePolicy, QSpacerItem)
from PyQt5.QtGui import QDoubleValidator, QIntValidator, QFont
from PyQt5.QtCore import Qt
from matplotlib.backends.backend_qt5agg import FigureCanvasQTAgg as FigureCanvas
from matplotlib.figure import Figure

class LCAApp(QWidget):
    def __init__(self):
        super().__init__()
        self.initUI()

    def initUI(self):
        main_layout = QHBoxLayout()

        # Create left and right layouts\text
        left_layout = QVBoxLayout()
        right_layout = QVBoxLayout()

        # Create sections and add to respective layouts
        self.create_file_details(left_layout)
        self.create_rotor_properties(left_layout)
        self.create_brake_testing_parameters(left_layout)
        self.create_LCA_model_parameters(right_layout)
        self.create_plot(right_layout)

        # Add left and right layouts to main layout
        main_layout.addLayout(left_layout)
        main_layout.addLayout(right_layout)

        self.setLayout(main_layout)
        self.setWindowTitle('LCA Brake Model')
        self.setGeometry(100,100,600,800)
        self.show()

```

```
41      def create_file_details(self, main_layout):
42          file_group = QGroupBox()
43          file_layout = QVBoxLayout()
44
45          #Section Title
46           file_title  = QLabel('File details')
47           file_title .setAlignment(Qt.AlignCenter)
48           file_title .setFont(QFont('Arial', 16, QFont.Bold))
49          file_layout.addWidget(file_title)
50
51          # File path
52          self.file_path_label = QLabel('Inventory File Path:')
53          self.file_path_input = QLineEdit()
54          self.browse_file_path_button = QPushButton('Browse')
55          self.browse_file_path_button.clicked.connect(self.browse_file_path)
56          file_layout.addWidget(self.file_path_label)
57          file_layout.addWidget(self.file_path_input)
58          file_layout.addWidget(self.browse_file_path_button)
59
60          # Inventory Excel sheet name
61          self.inventory_doc_name_label = QLabel('Name of Inventory Excel Document:')
62          self.inventory_doc_name_input = QLineEdit()
63          file_layout.addWidget(self.inventory_doc_name_label)
64          file_layout.addWidget(self.inventory_doc_name_input)
65
66          file_group.setLayout(file_layout)
67          main_layout.addWidget(file_group)
68
69      def create_rotor_properties(self, main_layout):
70          rotor_properties_group = QGroupBox()
71          rotor_properties_layout = QVBoxLayout()
72
73          # Section title
74          rotor_properties_title = QLabel('Brake Rotor Properties')
75          rotor_properties_title.setAlignment(Qt.AlignCenter)
76          rotor_properties_title.setFont(QFont('Arial', 16, QFont.Bold))
77          rotor_properties_layout.addWidget(rotor_properties_title)
78
79          # Rotor name
80          self.rotor_name_label = QLabel('Name of Rotor:')
81          self.rotor_name_input = QLineEdit()
82          rotor_properties_layout.addWidget(self.rotor_name_label)
83          rotor_properties_layout.addWidget(self.rotor_name_input)
84
```

```
85          # Rotor weight
86          self.rotor_weight_label = QLabel('Rotor Weight (kg):')
87          rotor_properties_layout.addWidget(self.rotor_weight_label)
88          self.rotor_weight_input = QLineEdit()
89          self.rotor_weight_input.setValidator(QDoubleValidator())
90          rotor_properties_layout.addWidget(self.rotor_weight_input)
91
92          # Rotor starting thickness
93          self.rotor_thickness_label = QLabel('Initial Rotor Thickness (mm):')
94          self.rotor_thickness_input = QLineEdit()
95          self.rotor_thickness_input.setValidator(QDoubleValidator())
96          rotor_properties_layout.addWidget(self.rotor_thickness_label)
97          rotor_properties_layout.addWidget(self.rotor_thickness_input)
98
99          # Replacement thickness
100         self.replacement_thickness_label = QLabel('Replacement Thickness (mm):')
101         self.replacement_thickness_input = QLineEdit()
102         self.replacement_thickness_input.setValidator(QDoubleValidator())
103         rotor_properties_layout.addWidget(self.replacement_thickness_label)
104         rotor_properties_layout.addWidget(self.replacement_thickness_input)
105
106         # Wear rate
107         self.wear_rate_label = QLabel('Wear Rate (mm/WLTP Cycle):')
108         self.wear_rate_input = QLineEdit()
109         self.wear_rate_input.setValidator(QDoubleValidator())
110         rotor_properties_layout.addWidget(self.wear_rate_label)
111         rotor_properties_layout.addWidget(self.wear_rate_input)
112
113         # Number of recoatings
114         self.num_recoatings_label = QLabel(
115             'Number of Recoatings (if uncoated rotor, put 0):')
116         self.num_recoatings_input = QLineEdit()
117         self.num_recoatings_input.setValidator(QIntValidator())
118         rotor_properties_layout.addWidget(self.num_recoatings_label)
119         rotor_properties_layout.addWidget(self.num_recoatings_input)
120
121         rotor_properties_group.setLayout(rotor_properties_layout)
122         main_layout.addWidget(rotor_properties_group)
123
124     def create_brake_testing_parameters(self, main_layout):
125         brake_testing_parameters_group = QGroupBox()
126         brake_testing_parameters_layout = QVBoxLayout()
127
128         # Section title
```

```
129         brake_testing_parameters_title = QLabel(
130             'Testing Parameters at Which Emissions Were Gathered')
131         brake_testing_parameters_title.setAlignment(Qt.AlignCenter)
132         brake_testing_parameters_title.setFont(QFont('Arial', 16, QFont.Bold))
133         brake_testing_parameters_layout.addWidget(brake_testing_parameters_title)
134 
135         # Defining scale factor for small scale testing
136         self.test_scale_factor_label = QLabel(
137             'Input the scaling factor for  small-scale testing:')
138         self.test_scale_factor_input = QLineEdit()
139         self.test_scale_factor_input.setValidator(QDoubleValidator())
140         brake_testing_parameters_layout.addWidget(self.test_scale_factor_label)
141         brake_testing_parameters_layout.addWidget(self.test_scale_factor_input)
142 
143         # length of cycles used for gathering emissions
144         self.length_test_cycle_label = QLabel('length of test cycle (km):')
145         self.length_test_cycle_input = QLineEdit()
146         self.length_test_cycle_input.setValidator(QDoubleValidator())
147         brake_testing_parameters_layout.addWidget(self.length_test_cycle_label)
148         brake_testing_parameters_layout.addWidget(self.length_test_cycle_input)
149 
150         # Number of cycles the emissions are gathered over
151         self.number_test_cycles_label = QLabel(
152             'No. braking cycles at which the emissions are gathered over during testing:'
153             )
154         self.number_test_cycles_input = QLineEdit()
155         self.number_test_cycles_input.setValidator(QDoubleValidator())
156         brake_testing_parameters_layout.addWidget(self.number_test_cycles_label)
157         brake_testing_parameters_layout.addWidget(self.number_test_cycles_input)
158 
159         brake_testing_parameters_group.setLayout(brake_testing_parameters_layout)
160         main_layout.addWidget(brake_testing_parameters_group)
161 
162     def create_LCA_model_parameters(self, main_layout):
163         LCA_model_parameters_group = QGroupBox()
164         LCA_model_parameters_layout = QVBoxLayout()
165 
166         # Section title
167         LCA_model_parameters_title = QLabel('Modelling Parameters for LCA')
168         LCA_model_parameters_title.setAlignment(Qt.AlignCenter)
169         LCA_model_parameters_title.setFont(QFont('Arial', 16, QFont.Bold))
170         LCA_model_parameters_layout.addWidget(LCA_model_parameters_title)
171 
172         # Impact approach
```

```
173         self.impact_approach_label = QLabel('Required Impact Approach:')
174         self.impact_approach_input = QComboBox()
175         self.impact_approach_input.addItems([
176             "Individualist", "Hierarchist", "Egalitarian"])
177         LCA_model_parameters_layout.addWidget(self.impact_approach_label)
178         LCA_model_parameters_layout.addWidget(self.impact_approach_input)
179 
180         # Electricity  Mix
181         self.renewable_energy_mix_label = QLabel(
182             'Electricity  mix breakdown (Fossil fuels - Nuclear - Renewables)):')
183         self.renewable_energy_mix_input = QComboBox()
184         self.renewable_energy_mix_input.addItems([
185             "68% - 0% - 32%", "37% - 30% - 33%",
186             "10% - 29% - 61%", "0% - 0% - 100%",
187             "0% - 50% - 50%"])
188         LCA_model_parameters_layout.addWidget(self.renewable_energy_mix_label)
189         LCA_model_parameters_layout.addWidget(self.renewable_energy_mix_input)
190 
191         # Functional unit length
192         self.fu_distance_label = QLabel('FU Distance (km):')
193         self.fu_distance_input = QLineEdit()
194         self.fu_distance_input.setValidator(QIntValidator())
195         LCA_model_parameters_layout.addWidget(self.fu_distance_label)
196         LCA_model_parameters_layout.addWidget(self.fu_distance_input)
197 
198         # Checkboxes and run button postioned horizontally
199         self.processes_and_run_inputs = QHBoxLayout()
200         # Checkboxes
201         checkbox_widget = QWidget()
202         checkbox_layout = QVBoxLayout(checkbox_widget)
203         checkbox_list = [
204             'Manufacture of Rotor', 'Manufacture of Pad', 'Coating Process',
205             'Use Phase', 'Coating Removal', 'Disposal of Rotor', 'Disposal of Pad'
206         ]
207         self.checkboxes = []
208         for item in checkbox_list:
209             checkbox = QCheckBox(item)
210             self.checkboxes.append(checkbox)
211             checkbox_layout.addWidget(checkbox)
212         self.processes_and_run_inputs.addWidget(checkbox_widget)
213         # Spacer item to push run button away from right edge
214         spacer1 = QSpacerItem(40, 20, QSizePolicy.Expanding, QSizePolicy.Minimum)
215         self.processes_and_run_inputs.addItem(spacer1)
216         # Spacer item to push run button away from right edge
```

```
217         spacer2 = QSpacerItem(40, 20, QSizePolicy.Expanding, QSizePolicy.Minimum)
218         self.processes_and_run_inputs.addItem(spacer2)
219         # Run Button
220         self.run_button = QPushButton('Run Model')
221         self.run_button.setSizePolicy(QSizePolicy.Expanding, QSizePolicy.Expanding)
222         self.run_button.setFixedSize(100,100)
223         self.run_button.setStyleSheet(
224             "background-color: green; color: white; font-size: 14px; font-weight: bold;"
225             )
226         self.run_button.clicked.connect(self.run_LCA_model)
227         self.processes_and_run_inputs.addWidget(self.run_button)
228         LCA_model_parameters_layout.addLayout(self.processes_and_run_inputs)
229         # Spacer item to push run button away from right edge
230         spacer3 = QSpacerItem(10, 10, QSizePolicy.Expanding, QSizePolicy.Minimum)
231         self.processes_and_run_inputs.addItem(spacer3)
232 
233         LCA_model_parameters_group.setLayout(LCA_model_parameters_layout)
234         main_layout.addWidget(LCA_model_parameters_group)
235 
236     def create_plot(self, main_layout):
237         impact_results_group = QGroupBox()
238         impact_results_layout = QVBoxLayout()
239 
240         # Section title
241         impact_results_title = QLabel('Impact Results')
242         impact_results_title.setAlignment(Qt.AlignCenter)
243         impact_results_title.setFont(QFont('Arial', 16, QFont.Bold))
244         impact_results_layout.addWidget(impact_results_title)
245 
246         # Add figure
247         self.figure = Figure()
248         self.canvas = FigureCanvas(self.figure)
249         impact_results_layout.addWidget(self.canvas)
250 
251         impact_results_group.setLayout(impact_results_layout)
252         main_layout.addWidget(impact_results_group)
253 
254     def browse_file_path(self):
255         file_path = QFileDialog.getExistingDirectory(self, 'Select Directory')
256         self.file_path_input.setText(file_path)
257 
258     def run_LCA_model(self):
259         try:
260             # Read user inputs
```

```
261             file_path  = str(self.file_path_input.text())
262             inventory_doc_name = str(self.inventory_doc_name_input.text())
263             rotor_name = str(self.rotor_name_input.text())
264             impact_approach = str(self.impact_approach_input.currentText())
265             fu_length = float(self.fu_distance_input.text())
266             rotor_weight = float(self.rotor_weight_input.text())
267             rotor_thickness = float(self.rotor_thickness_input.text())
268             replacement_thickness = float(self.replacement_thickness_input.text())
269             wear_rate = float(self.wear_rate_input.text())
270             num_recoatings = float(self.num_recoatings_input.text())
271             test_scale_factor = float(self.test_scale_factor_input.text())
272             length_test_cycle = float(self.length_test_cycle_input.text())
273             number_test_cycles = float(self.number_test_cycles_input.text())
274             renewable_energy_mix = str(self.renewable_energy_mix_input.currentText())
275
276             # Define unit processes that are included
277             unit_processes = {
278                 'Manufacture of Rotor': self.checkboxes[0].isChecked(),
279                 'Manufacture of Pad': self.checkboxes[1].isChecked(),
280                 'Coating Process': self.checkboxes[2].isChecked(),
281                 'Use Phase': self.checkboxes[3].isChecked(),
282                 'Coating Removal': self.checkboxes[4].isChecked(),
283                 'Disposal of Rotor': self.checkboxes[5].isChecked(),
284                 'Disposal of Pad': self.checkboxes[6].isChecked(),
285             }
286
287             # Read in the CF's and normalisation factors
288             cf_midpoint = pd.read_excel(
289                 os.path.join(file_path, "Midpoint Characterisation Factors.xlsx"),
290                 sheet_name=impact_approach)
291             cf_midpoint.fillna(0, inplace=True)
292             cf_endpoint = pd.read_excel(os.path.join(
293                 file_path, "Endpoint Characterisation Factors.xlsx"),
294                 sheet_name=impact_approach)
295             cf_endpoint.fillna(0, inplace=True)
296             normalisation_factors_midpoint = pd.read_excel(os.path.join(
297                 file_path, "Normalisation Factors.xlsx"),
298                 sheet_name="Midpoint Normalisation Factors")
299             normalisation_factors_midpoint.fillna(0, inplace=True)
300             normalisation_factors_endpoint = pd.read_excel(os.path.join(
301                 file_path, "Normalisation Factors.xlsx"),
302                 sheet_name="Endpoint Normalisation Factors")
303             normalisation_factors_endpoint.fillna(0, inplace=True)
304             # Define specific fossils for endpoint and normalisation calculations
```

```
305             fossil_resource_names = [
306                 'crude oil', 'natural gas', 'hard coal', 'brown coal', 'peat']
307
308             # Add Electricity CFs to Midpoint DataFrame
309             electricity_mix = pd.read_excel(
310                 file_path + "\\" +
311                 "LCA of UK electricity Scenarios.xlsx",
312                 sheet_name = renewable_energy_mix)
313             electricity_mix.fillna (0, inplace=True)
314             #select only the columns that match those in CF_Midpoint
315              electricity_mix_filtered = electricity_mix[
316                 electricity_mix.columns.intersection(cf_midpoint.columns)]
317             #reorder columns to match CF_Midpoint
318             electricity_mix_reordered = electricity_mix_filtered.reindex(
319                 columns=cf_midpoint.columns, fill_value=0)
320             #append Electricity to end of CF_Midpoint
321             cf_midpoint = cf_midpoint._append(
322                 electricity_mix_reordered, ignore_index=True)
323             # Condensing down Midpoint CFs so one row per
324             # emission rather than new one per impact category
325             cf_midpoint = cf_midpoint.groupby([
326                 'Flow Name', 'Flow Class', 'Emission Type']).agg(
327                     lambda x: x.sum()).reset_index()
328
329             #Calculate the number of rotors per use phase
330             rotors_per_use = ((
331                 fu_length/length_test_cycle)*wear_rate)/(
332                     rotor_thickness-replacement_thickness)
333             pads_per_use = 1 # add as user input in future
334
335             # Load inventory tables
336             inventory_file_path = os.path.join(file_path, f"{inventory_doc_name}.xlsx")
337             inventory_dict = {} # Create a dictionary to store inventory DataFrames
338             included_unit_processes = []
339             # produce list of checked unit processes
340             for name, included in unit_processes.items():
341                 if included:
342                     included_unit_processes.append(name)
343                     # read specific excel sheet for unit process
344                     inventory_df = pd.read_excel(inventory_file_path, sheet_name=name)
345                     # Save DataFrame in dictionary with modified name
346                     inventory_dict[f"{name} Inventory"] = inventory_df
347
348             # Manipulate unit process DataFrames
```

```
349             if 'Manufacture of Rotor Inventory' in inventory_dict:
350                 df = inventory_dict['Manufacture of Rotor Inventory']
351                 df.iloc[:,4:] = (df.iloc[:,4:]* rotors_per_use)/(num_recoatings + 1)
352                 inventory_dict['Manufacture of Rotor Inventory'] = df
353
354             if 'Manufacture of Pad Inventory' in inventory_dict:
355                 df = inventory_dict['Manufacture of Pad Inventory']
356                 df.iloc[:, 4:] = df.iloc[:, 4:] * pads_per_use
357                 inventory_dict['Manufacture of Pad Inventory'] = df
358
359             if 'Coating Process Inventory' in inventory_dict:
360                 df = inventory_dict['Coating Process Inventory']
361                 df.iloc[:, 4:] = df.iloc[:, 4:]*rotors_per_use
362                 inventory_dict['Coating Process Inventory'] = df
363
364             if 'Use Phase Inventory' in inventory_dict:
365                 df = inventory_dict['Use Phase Inventory']
366                 df.iloc[:, 4:] = df.iloc[:, 4:] * ((
367                     test_scale_factor*2*fu_length)/(
368                         length_test_cycle*number_test_cycles))
369                 df.columns = ['Flow Name', 'Flow Class',
370                               'Emission Type', 'Unit', 'Use Phase']
371                 # Add emissions from fuel associated with the rotor
372                 # defining fuel reduction value (l per 100kg per 100km)
373                 fuel_reduction_value = 0.35
374                 # Calculate litres of petrol used associated with the rotor
375                 petrol_use = fuel_reduction_value*(rotor_weight/100)*(fu_length/100)
376                 # Calculate kg Crude oil required to make petrol
377                 crude_oil = petrol_use*0.73*3.13
378                 # CO2 emissions associated with fuel used (kg)
379                 CO2_fuel_emissions = petrol_use*0.737*0.9*3.66
380                 # Define columns to be used for effect from fuel economy
381                 fuel_economy_columns = df.columns
382                 fuel_economy_data = [
383                                 ['crude oil', 'resources', 'resources', 'kg', crude_oil],
384                                 ['CO2', 'emissions', 'to air', 'kg', CO2_fuel_emissions],
385                                 ]
386                 fuel_emissions = pd.DataFrame(
387                     fuel_economy_data, columns=fuel_economy_columns)
388                 # Select only the columns that match those in Inventory doc
389                 fuel_emissions_filtered = fuel_emissions[
390                     fuel_emissions.columns.intersection(df.columns)]
391                 # Ensure columns are in same order as Inventory Doc
392                 fuel_emissions_reordered = fuel_emissions_filtered.reindex(
```

```
393                 columns=df.columns, fill_value=0)
394             # Append weight reduction energy saving to end of Inventory Doc
395             df = df._append(fuel_emissions_reordered, ignore_index=True)
396             inventory_dict['Use Phase Inventory'] = df
397
398         if 'Coating Removal Inventory' in inventory_dict:
399             df = inventory_dict['Coating Removal Inventory']
400             df.iloc[:, 4:] = df.iloc[:, 4:]*rotors_per_use
401             inventory_dict['Coating Removal Inventory'] = df
402
403         if 'Disposal of Rotor Inventory' in inventory_dict:
404             df = inventory_dict['Disposal of Rotor Inventory']
405             df.iloc[:, 4:] = (df.iloc[:, 4:] * rotors_per_use)/(num_recoatings + 1)
406             inventory_dict['Disposal of Rotor Inventory'] = df
407
408         if 'Disposal of Pad Inventory' in inventory_dict:
409             df = inventory_dict['Disposal of Pad Inventory']
410             df.iloc[:, 4:] = df.iloc[:, 4:] * pads_per_use
411             inventory_dict['Disposal of Pad Inventory'] = df
412
413         # Initialise the results tables to store total values for each phase
414         results_midpoint_totals = pd.DataFrame(
415             columns=cf_midpoint.columns[3:]).transpose()
416         for _ in range(len(included_unit_processes)):
417             results_midpoint_totals.insert(len(
418                 results_midpoint_totals.columns), f'Blank{_ + 1}', '')
419         results_endpoint_totals = pd.DataFrame(
420             columns=cf_endpoint.columns[1:]).transpose()
421         for _ in range(len(included_unit_processes)):
422             results_endpoint_totals.insert(
423                 len(results_endpoint_totals.columns), f'Blank{_ + 1}', '')
424         results_midpoint_totals_normalised = pd.DataFrame(
425             columns=cf_midpoint.columns[3:]).transpose()
426         for _ in range(len(included_unit_processes)):
427             results_midpoint_totals_normalised.insert(
428                 len(results_midpoint_totals_normalised.columns),
429                 f'Blank{_ + 1}', '')
430         results_endpoint_totals_normalised = pd.DataFrame(
431             columns=cf_endpoint.columns[1:]).transpose()
432         for _ in range(len(included_unit_processes)):
433             results_endpoint_totals_normalised.insert(
434                 len(results_endpoint_totals_normalised.columns),
435                 f'Blank{_ + 1}', '')
436
```

```
437             # Path to excel file for results
438             output_file_path = os.path.join(
439                 file_path, f"{rotor_name} Impact Results.xlsx")
440             # Create an Excel writer object
441             with pd.ExcelWriter(output_file_path, engine='xlsxwriter') as writer:
442                 # Initialise counter for which DataFrame up to
443                 DataFrame_counter = 0
444                 # Iterate over DataFrames in dictionary of included phases of life cycle
445                 for key in inventory_dict:
446                     inventory = inventory_dict[key]
447                     current_unit_process_list = inventory.columns[4:].to_list()
448
449                     # Initialise results tables to store current phase data
450                     results_midpoint = pd.DataFrame(np.zeros((
451                         len(current_unit_process_list), len(cf_midpoint.columns[3:]))),
452                         columns=cf_midpoint.columns[3:]).T
453                     results_endpoint = pd.DataFrame(np.zeros((
454                         len(current_unit_process_list), len(cf_endpoint.columns[1:]))),
455                         columns=cf_endpoint.columns[1:]).T
456                     results_endpoint_normalised = pd.DataFrame(np.zeros((
457                         len(current_unit_process_list), len(cf_endpoint.columns[1:]))),
458                         columns=cf_endpoint.columns[1:]).T
459
460                     # Add required coal and gas for the chosen energy mix
461                     # Select the coal and gas contribution percentages
462                     if renewable_energy_mix == "68% – 0% – 32%":
463                         coal_percentage = 0.57
464                         gas_percentage = 0.11
465                     if renewable_energy_mix == "37% – 30% – 33%":
466                         coal_percentage = 0.23
467                         gas_percentage = 0.14
468                     if renewable_energy_mix == "10% – 29% – 61%":
469                         coal_percentage = 0.09
470                         gas_percentage = 0.01
471                     if renewable_energy_mix == "0% – 0% – 100%":
472                         coal_percentage = 0
473                         gas_percentage = 0
474                     if renewable_energy_mix == "0% – 50% – 50%":
475                         coal_percentage = 0
476                         gas_percentage = 0
477                     # Ensure only one energy row
478                     inventory = inventory.groupby([
479                         'Flow Name', 'Flow Class', 'Emission Type', 'Unit']).agg(
480                             lambda x: x.sum()).reset_index()
```

```
481                 # Select out energy row
482                 energy_row = inventory[inventory['Flow Name'] == 'energy']
483                 # Calculate mass of coal and Nmˆ3 of natural gas required
484                 coal_energy = energy_row.copy()
485                 coal_energy.iloc[:,4:] = (
486                     coal_energy.iloc[:,4:]*0.124*coal_percentage)
487                 coal_energy.iloc[:,:4] = [
488                     'hard coal', 'resources', 'resources', 'kg']
489                 gas_energy = energy_row.copy()
490                 gas_energy.iloc[:,4:] = gas_energy.iloc[:,4:]*0.094*(
491                     1/0.76)*gas_percentage
492                 gas_energy.iloc[:,:4] = [
493                     'natural gas', 'resources', 'resources', 'm3']
494                 # Add coal and gas required for energy back to inventory
495                 inventory = inventory._append(coal_energy, ignore_index=True)
496                 inventory = inventory._append(gas_energy, ignore_index=True)
497                 # Ensure only one per flow name and class
498                 inventory = inventory.groupby([
499                     'Flow Name', 'Flow Class', 'Emission Type', 'Unit']).agg(
500                         lambda x: x.sum()).reset_index()
501
502
503
504                 # Calculate Midpoint Impacts
505
506                 # Ensure both the CF and Inventory DataFrames are in the same order
507                 # and filtered to only include relevant CF data for the required
508                 # emissions
509                 merged = pd.merge(inventory, cf_midpoint, on=[
510                     'Flow Name', 'Emission Type'], how='inner')
511                 inventory_filtered = inventory[inventory.set_index([
512                     'Flow Name', 'Emission Type']).index.isin(merged.set_index([
513                         'Flow Name', 'Emission Type']).index)]
514                 cf_midpoint_filtered = cf_midpoint[cf_midpoint.set_index([
515                     'Flow Name', 'Emission Type']).index.isin(merged.set_index([
516                         'Flow Name', 'Emission Type']).index)]
517                 inventory_sorted = inventory_filtered.sort_values(
518                     by=['Flow Name', 'Emission Type']).reset_index(drop=True)
519                 cf_midpoint_sorted = cf_midpoint_filtered.sort_values(
520                     by=['Flow Name', 'Emission Type']).reset_index(drop=True)
521
522                 # Initialise results table to hold fossil resource scarcity data
523                 # (midpoint normalisation)
524                 fossil_data = pd.DataFrame()
```

```
525                 # Initialise results table to store impact calculation
526                 midpoint_impacts = pd.DataFrame(0, index=cf_midpoint_sorted.index,
527                                                 columns=cf_midpoint_sorted.columns)
528                 midpoint_impacts.iloc[:,0:3] = cf_midpoint_sorted.iloc[:,0:3]
529
530                 # Cycle through the unit process columns
531                 for col in range(4, inventory.shape[1]):
532                     # reset results table prior to calculations
533                     midpoint_impacts.iloc[:,3:] = 0
534                     midpoint_impacts.iloc[:,3:] = cf_midpoint_sorted.iloc[
535                         :,3:]. multiply(inventory_sorted.iloc[:,col], axis=0)
536                     # Extract any impacts associated with fossil fuels
537                     fossil_resource_midpoint_breakdown = (
538                         midpoint_impacts[midpoint_impacts['Flow Name'].isin(
539                             fossil_resource_names)][[
540                                 'Flow Name',
541                                 'Fossil Resource Scarcity (kg oil eq.)']]
542                     if fossil_data.empty:
543                         # Initialising fossil dataframe on first iteration
544                         fossil_data = fossil_resource_midpoint_breakdown
545                     else:
546                         # Save data in new column each iteration
547                         fossil_data[
548                             f'column{col-2}'] = fossil_resource_midpoint_breakdown[
549                                 'Fossil Resource Scarcity (kg oil eq.)']
550                     # Sum the columns for the results table
551                     impacts_sum = midpoint_impacts.iloc[:,3:].sum().to_frame()
552                     results_midpoint.iloc[:,col-4] = impacts_sum.iloc[:,0]
553                 # Rename column headings
554                 results_midpoint.columns = current_unit_process_list
555                 results_midpoint.index.name = 'Midpoint Impact Category'
556                 results_midpoint.reset_index(inplace=True)
557
558
559
560                 # Normalise Midpoint Impacts
561
562                 # Remove fossil resource data
563                 midpoint_data_to_normalise = results_midpoint[results_midpoint[
564                     'Midpoint Impact Category'
565                     ] != 'Fossil Resource Scarcity (kg oil eq.)']
566                 # Rename columns in fossil data
567                 fossil_data.columns = midpoint_data_to_normalise.columns
568                 # add fossil fuel data (showing fossil resource impacts broken down)
```

```
569                 midpoint_data_to_normalise = pd.concat([
570                     midpoint_data_to_normalise, fossil_data],
571                     ignore_index=True)
572                 # Select relevant normalisation factors
573                 NF_midpoint = pd.concat([
574                     normalisation_factors_midpoint.iloc[:,0:2],
575                     normalisation_factors_midpoint[impact_approach]], axis=1)
576                 merged = pd.merge(
577                     midpoint_data_to_normalise, NF_midpoint,
578                     on=['Midpoint Impact Category'], how='inner')
579                 midpoint_data_to_normalise_filtered = midpoint_data_to_normalise[
580                     midpoint_data_to_normalise.set_index([
581                         'Midpoint Impact Category']).index.isin(merged.set_index([
582                             'Midpoint Impact Category']).index)]
583                 NF_midpoint_filtered = NF_midpoint[
584                     NF_midpoint.set_index(['Midpoint Impact Category']).index.isin(
585                         merged.set_index(['Midpoint Impact Category']).index)]
586                 midpoint_data_to_normalise_sorted = (
587                     midpoint_data_to_normalise_filtered.sort_values(
588                         by=['Midpoint Impact Category']).reset_index(drop=True))
589                 NF_midpoint_sorted = NF_midpoint_filtered.sort_values(
590                     by=['Midpoint Impact Category']).reset_index(drop=True)
591                 # Calculate normalised values
592                 results_midpoint_normalised = midpoint_data_to_normalise_sorted
593                 results_midpoint_normalised.iloc[
594                     :,1:]  = results_midpoint_normalised.iloc[:,1:].div(
595                         NF_midpoint_sorted.iloc[:,-1], axis=0)
596                 # Recombine fossil scarcity into one impact category
597                 sum_values = results_midpoint_normalised[
598                     results_midpoint_normalised['Midpoint Impact Category'].isin(
599                         fossil_resource_names)].iloc[:,1:].sum()
600                 # Create row for the sum of the fossil fuel impacts
601                 new_row = pd.DataFrame([[
602                     'Fossil Resource Scarcity (kg oil eq.)', *sum_values]],
603                     columns=results_midpoint_normalised.columns)
604                 # Remove fossil fuel rows
605                 results_midpoint_normalised = results_midpoint_normalised[
606                     ~results_midpoint_normalised['Midpoint Impact Category'].isin(
607                         fossil_resource_names)]
608                 # add fossil resource scarcity row
609                 results_midpoint_normalised = pd.concat([
610                     results_midpoint_normalised, new_row],
611                     ignore_index = True)
612                 # Rename index
```

```
613                 results_midpoint_normalised.rename(columns={
614                     ('Midpoint Impact Category'):(
615                         'Midpoint Impact Category (unit per person in 2010)')},
616                         inplace=True)
617                 results_midpoint_normalised.reset_index(drop=True)
618
619
620
621                 # Endpoint Impacts and Normalisation
622
623                 # Manipulate DataFrame NF's to just have current
624                 # impact approach values
625                 # Select out relevant impact approach values
626                 normalisation_factors_endpoint = normalisation_factors_endpoint[[
627                     'Midpoint Impact Category', 'Unit', impact_approach]]
628                 # Pivot table to seperate out NF factors for each endpoint category
629                 NF_endpoint_pivot = normalisation_factors_endpoint.pivot_table(
630                     index='Midpoint Impact Category', columns='Unit',
631                     values=impact_approach).reset_index()
632                 NF_endpoint_pivot.columns = [
633                     'Midpoint Impact Category',
634                     'Damage to Human Health (DALY)',
635                     'Damage to Ecosystems (Species.year)',
636                     'Damage to Resource Availability (USD2013)']
637                 NF_endpoint_pivot.fillna(0,inplace=True)
638
639                 # Swap out fossil resource scarcity midpoint impact for the
640                 # fossil  inventory as Endpoint is calculated directly from fossils
641                 # Extracting fossil rows from inventory
642                 fossil_inventory = pd.DataFrame(inventory[inventory[
643                     'Flow Name'].isin(fossil_resource_names)])
644                 fossil_inventory.reset_index(inplace=True, drop=True)
645                 fossil_inventory.drop([
646                     'Flow Class', 'Emission Type', 'Unit'],
647                     axis=1, inplace=True)
648                 midpoint_endpoint_data = results_midpoint[
649                     results_midpoint[
650                         'Midpoint Impact Category'
651                         ] != 'Fossil Resource Scarcity (kg oil eq.)']
652                 fossil_inventory.rename(columns={
653                     'Flow Name':'Midpoint Impact Category'}, inplace=True)
654                 midpoint_endpoint_data = pd.concat([
655                     midpoint_endpoint_data, fossil_inventory], ignore_index=True)
656
```

```
657                 # Ensure the CF and Midpoint DataFrames are in the same order and
658                 #  filtered  to  only include relevant CF data for the required
659                 # emissions
660                 merged = pd.merge(midpoint_endpoint_data, cf_endpoint,
661                                   on=['Midpoint Impact Category'], how='inner')
662                 midpoint_endpoint_data_filtered = midpoint_endpoint_data[
663                     midpoint_endpoint_data.set_index([
664                         'Midpoint Impact Category']).index.isin(merged.set_index([
665                             'Midpoint Impact Category']).index)]
666                 cf_endpoint_filtered = cf_endpoint[
667                     cf_endpoint.set_index(['Midpoint Impact Category']).index.isin(
668                         merged.set_index(['Midpoint Impact Category']).index)]
669                 midpoint_endpoint_data_sorted =(
670                     midpoint_endpoint_data_filtered.sort_values(
671                     by=['Midpoint Impact Category']).reset_index(drop=True))
672                 cf_endpoint_sorted = cf_endpoint_filtered.sort_values(
673                     by=['Midpoint Impact Category']).reset_index(drop=True)
674                 # Ensure NF is in same order
675                 merged = pd.merge(merged, NF_endpoint_pivot,
676                                   on=['Midpoint Impact Category'], how='inner')
677                 nf_endpoint_filtered = NF_endpoint_pivot[
678                     NF_endpoint_pivot.set_index([
679                         'Midpoint Impact Category']).index.isin(merged.set_index([
680                             'Midpoint Impact Category']).index)]
681                 nf_endpoint_sorted = nf_endpoint_filtered.sort_values(
682                     by=['Midpoint Impact Category']).reset_index(drop=True)
683                 # as cf  and midpoint data have the fossil fuels broken down, then
684                 # the scarcity impact will have been removed from NF dataframe
685                 # and so needs to be readded
686                 nf_endpoint_sorted = pd.concat([
687                     nf_endpoint_sorted, NF_endpoint_pivot[NF_endpoint_pivot[
688                         'Midpoint Impact Category'
689                         ]=='Fossil Resource Scarcity (kg oil eq.)']],
690                         ignore_index = True)
691
692                 for  col  in  range(1, midpoint_endpoint_data_sorted.shape[1]):
693                     #  Initialise  and reset results tables prior to
694                     # calculations on each iteration
695                     endpoint_impacts = pd.DataFrame(
696                         0,  index=cf_endpoint_sorted.index,
697                         columns=cf_endpoint_sorted.columns)
698                     endpoint_impacts_normalised = pd.DataFrame(
699                         0,  index=nf_endpoint_sorted.index,
700                         columns=nf_endpoint_sorted.columns)
```

```
701                 endpoint_impacts.iloc[:,0] = cf_endpoint_sorted.iloc[:,0]
702                 endpoint_impacts_normalised.iloc[:,0
703                                                 ] = nf_endpoint_sorted.iloc[:,0]
704                 endpoint_impacts.iloc[:,1:] = 0
705                 endpoint_impacts_normalised.iloc[:,1] = 0
706                 # Calculate the endpoint impacts per midpoint category
707                 endpoint_impacts.iloc[:,1:] = cf_endpoint_sorted.iloc[
708                     :,1:]. multiply(midpoint_endpoint_data_sorted.iloc[:,col],
709                                     axis=0)
710                 # Recombine fossil scarcity into one impact category
711                 sum_values = endpoint_impacts[endpoint_impacts[
712                     'Midpoint Impact Category'].isin(
713                         fossil_resource_names)].iloc[:,1:].sum()
714                 # Create row for the sum of the fossil fuel impacts
715                 new_row = pd.DataFrame([[
716                     'Fossil Resource Scarcity (kg oil eq.)', *sum_values]],
717                     columns=endpoint_impacts.columns)
718                 # Remove fossil fuel rows
719                 endpoint_impacts = endpoint_impacts[~endpoint_impacts[
720                     'Midpoint Impact Category'].isin(fossil_resource_names)]
721                 # add fossil resource scarcity row
722                 endpoint_impacts = pd.concat([
723                     endpoint_impacts, new_row], ignore_index = True)
724                 # Normalise endpoint impacts
725                 endpoint_impacts_normalised.iloc[:,1:] = np.where(
726                     nf_endpoint_sorted.iloc[:,1:]==0, 0,
727                     endpoint_impacts.iloc[:,1:].divide(
728                         nf_endpoint_sorted.iloc[:,1:]))
729                 # Sum the column totals for the results table
730                 endpoint_impact_values = endpoint_impacts.iloc[
731                     :,1:]. sum().to_frame()
732                 results_endpoint.iloc[
733                     :, col-1] = endpoint_impact_values.iloc[:,0]
734                 endpoint_impact_values_normalised = (
735                     endpoint_impacts_normalised.iloc[:,1:].sum().to_frame())
736                 results_endpoint_normalised.iloc[
737                     :, col-1] = endpoint_impact_values_normalised.iloc[:,0]
738             # Rename column headings
739             results_endpoint.columns = current_unit_process_list
740             results_endpoint.index.name = 'Endpoint Impact Category'
741             results_endpoint.reset_index(inplace=True)
742             results_endpoint_normalised.columns = current_unit_process_list
743             results_endpoint_normalised.index.name = (
744                 'Endpoint Impact Category (per person in 2010)')
```

```
745                 results_endpoint_normalised.reset_index(inplace=True)
746
747                 # Add total columns on end of results tables
748                 results_midpoint['Total'] = results_midpoint.iloc[:,1:].sum(axis=1)
749                 results_midpoint_normalised['Total'] = (
750                     results_midpoint_normalised.iloc[:,1:].sum(axis=1))
751                 results_endpoint['Total'] = results_endpoint.iloc[:,1:].sum(axis=1)
752                 results_endpoint_normalised['Total'] = (
753                     results_endpoint_normalised.iloc[:,1:].sum(axis=1))
754                 # Save the impact results to excel file
755                 results_midpoint.to_excel(
756                     writer, sheet_name=(included_unit_processes[
757                         DataFrame_counter] + " Midpoint"), index=False)
758                 results_midpoint_normalised.to_excel(
759                     writer, sheet_name= ("Normal " + included_unit_processes[
760                         DataFrame_counter] + " Mid"), index=False)
761                 results_endpoint.to_excel(
762                     writer, sheet_name=(included_unit_processes[
763                         DataFrame_counter] + " Endpoint"), index=False)
764                 results_endpoint_normalised.to_excel(
765                     writer, sheet_name=("Normal " + included_unit_processes[
766                         DataFrame_counter] + " End"), index=False)
767                 # Store the totals columns into one dataframe
768                 results_midpoint_totals.iloc[
769                     :, DataFrame_counter] = results_midpoint.iloc[:,-1]
770                 results_midpoint_totals_normalised.iloc[
771                     :, DataFrame_counter] = results_midpoint_normalised.iloc[:,-1]
772                 results_endpoint_totals.iloc[
773                     :, DataFrame_counter] = results_endpoint.iloc[:,-1]
774                 results_endpoint_totals_normalised.iloc[
775                     :, DataFrame_counter] = results_endpoint_normalised.iloc[:,-1]
776
777                 # Step up DataFrame Counter
778                 DataFrame_counter += 1
779
780             # Edit column headings of total midpoint results
781             results_midpoint_totals.columns = included_unit_processes
782             results_midpoint_totals.index.name = "Midpoint Impact Category"
783             results_midpoint_totals.reset_index(inplace=True)
784             # Ensure Impact Category column is in correct order for totals table
785             results_midpoint_totals[
786                 'Midpoint Impact Category'] = results_midpoint[
787                     'Midpoint Impact Category']
788             # Adding total column on end of results table
```

```
789             results_midpoint_totals[
790                 'Total Midpoint Impact Score'] = results_midpoint_totals.iloc[
791                     :, 1:].sum(axis=1)
792             # Add the total midpoint sheet to the excel document
793             results_midpoint_totals.to_excel(
794                 writer, sheet_name = 'Midpoint Total Results', index=False)
795             # Edit column headings of normalised total midpoint results
796             results_midpoint_totals_normalised.columns = included_unit_processes
797             results_midpoint_totals_normalised.index.name = (
798                 'Midpoint Impact Category (unit per person in 2010)')
799             results_midpoint_totals_normalised.reset_index(inplace=True)
800             # Ensure Impact Category column is in correct order for totals table
801             results_midpoint_totals_normalised[
802                 'Midpoint Impact Category (unit per person in 2010)'
803                 ] = results_midpoint_normalised[
804                     'Midpoint Impact Category (unit per person in 2010)']
805             # Adding total column on end of results table
806             results_midpoint_totals_normalised[
807                 'Total Midpoint Impact Score'] = (
808                     results_midpoint_totals_normalised.iloc[:, 1:].sum(axis=1))
809             # Add the normalised total midpoint sheet to the excel document
810             results_midpoint_totals_normalised.to_excel(
811                 writer, sheet_name = 'Midpoint Total Normalised', index=False)
812
813             # Edit column headings of total endpoint results
814             results_endpoint_totals.columns = included_unit_processes
815             results_endpoint_totals.index.name = "Endpoint Impact Category"
816             results_endpoint_totals.reset_index(inplace=True)
817             # Ensure Impact Category column is in correct order for totals table
818             results_endpoint_totals[
819                 'Endpoint Impact Category'] = results_endpoint[
820                     'Endpoint Impact Category']
821             # Adding total column on end of results table
822             results_endpoint_totals[
823                 'Total Endpoint Impact Score'] = results_endpoint_totals.iloc[
824                     :, 1:].sum(axis=1)
825             # Add the total endpoint sheet to the excel document
826             results_endpoint_totals.to_excel(
827                 writer, sheet_name = 'Endpoint Total Results', index=False)
828             # Edit column headings of normalised total endpoint results
829             results_endpoint_totals_normalised.columns = included_unit_processes
830             results_endpoint_totals_normalised.index.name = (
831                 'Endpoint Impact Category (per person in 2010)')
832             results_endpoint_totals_normalised.reset_index(inplace=True)
```

```
                # Ensure Impact Category column is in correct order for totals table
                results_endpoint_totals_normalised[
                    'Endpoint Impact Category (per person in 2010)'
                    ] = results_endpoint_normalised[
                        'Endpoint Impact Category (per person in 2010)']
                # Adding total column on end of results table
                results_endpoint_totals_normalised[
                    'Total Endpoint Impact Score'] = (
                        results_endpoint_totals_normalised.iloc[:, 1:].sum(axis=1))
                # Add the normalised total Endpoint sheet to the excel document
                results_endpoint_totals_normalised.to_excel(
                    writer, sheet_name = 'Endpoint Total Normalised', index=False)

                # Update plot in GUI
                self.results_df = pd.DataFrame(results_midpoint_totals_normalised)
                self.update_plot()


            QMessageBox.information(
                self, 'Success', 'LCA Model run successfully! Results saved to Excel.')

        except Exception as e:
            QMessageBox.critical(self, 'Error', f'An error occured: {e}')

        print('This is number of rotors per use', rotors_per_use)

    def update_plot(self):
        if self.results_df.empty:
            return      # Do not update if DataFrame is empty

        # Clear previous plot
        self.figure.clear()
        # Create a new plot
        ax = self.figure.add_subplot(111)
        ax.clear()
        ax.bar(self.results_df[
            'Midpoint Impact Category (unit per person in 2010)'],
            self.results_df['Total Midpoint Impact Score'], color='skyblue')
        ax.set_title ('Normalised Midpoint Impacts')
        ax.set_xlabel('Midpoint Impact Category (unit per person in 2010)')
        ax.set_ylabel('Total Midpoint Impact Score')
        ax.set_xticklabels(self.results_df[
            'Midpoint Impact Category (unit per person in 2010)'],
            rotation=45, ha='right')
```

```
877             self.figure.tight_layout()       # Ensure plot fits within window
878             # Refresh the canvas
879             self.canvas.draw()
880 
881 if __name__ == '__main__':
882     app = QApplication(sys.argv)
883     ex = LCAApp()
884     sys.exit(app.exec_())
```